The positive and negative selection of B cells into the pre-immune repertoire

Jianwei Cui

Nuffield Department of Medicine
St Cross College
University of Oxford

Supervisors:
Richard Cornall
Mukta Deobagkar

DPhil in Clinical Medicine
Trinity 2024

Acknowledgements

Firstly, I am grateful to Richard Cornall and Mukta Deobagkar for their unwavering support throughout my DPhil journey at Oxford. I vivid recall the amusement shared over Richard's first "English joke" and our engrossing discussion on potential hypothesis. His passion was so intense that his mismatched boots went unnoticed. His infectious enthusiasm and unique understanding of science profoundly influenced me, showing me the pure joy of research. His mentor ship is priceless and I eager to absorb more of his wisdom and humour in the future.

Mukta has been an example of scientific rigor for me, showing me the spirits of perfection. Thanks to her incredible patience and kindness, I built my understanding of medical research methodologies from scratch. Additionally, the books "The eccentric Oxford" she gave me introduce me the quick facts of the Oxford, not only equipped me as a "qualified oxford tourist guide", but also enrich my life in this historical city. The dual role as supervisor and friend has offered me with both academic guidance and emotional support.

I would also to express my sincere gratitude to the members of the Cornall/ Bull group. Katherine's brilliant ideas on my project and the opportunity of shadowing her in the hospital gave me a glance of working in the NHS as medical profession. Tanya's endless patience and assistant in animal work were critical and instrumental for my DPhil. Rui, your dual expertise as a bioinformatician and a sincere friend, complete with Korean-style hot pot gathering, have been a source of comfort and inspiration. My sincere gratitude also goes to Jess for her festival spirit, Jie for her assistant on processing samples other routine lab works, Jenny for her contribution in animal

house, Robert for his optimism, Megan for her insightful advice on the project, Moustafa, for his invaluable assistant with single cell experiments, Racheal and Oliver for their precious project feedback, Bo for his aid with single-cell analysis and coding. I would also want to thank all the staffs in FGF, Peter, Heather, and Luke, for their care of our mice.

A special knowledge also goes to my friends, whose support help me overcoming life's adversities. Haopeng and Jinyi, your readiness to provide support is a blessing. Exploring the world with you has been a joy. To David and Daniel as thoughtful and kind friends. Discussing life and envisioning future with you has been delightful. Wish more trips with a classic motorcycle and your cigars will be on the way. Brama, your philosophy discussion and jokes has always been a treat for busy life. Zhu, Carol, Xiao,Yuyao, Jianqing, Chong, Leo, Hantao, Shuai, Jiahao and many others have contributed so much for my growth and colourful life in Oxford.

To my relatives, whose love and support have been a blessing. Uncle Xueyang's humour and wisdom of life, Aunt Xiaofeng's kindness and hospitality, Grandma Lu's delicious food, Sherry and Hao's warm welcome in London all provide strength for my DPhil.

To my parents, your unconditional love and support has been the foundation for my calmness in the life and my freedom of choosing career. Although there are always some ups and downs in the life, your wisdom always keeps me positive. Mom, like a harbour to a ship, your love provided me with the place I can hide from storms. Dad, your dedication as an outstanding surgeon always inspires me, your patience, endurance, and responsibility are life lessons for me to embody.

The DPhil voyage has been an exploration of life, science, and humanity. Though a clear stating point is set, the destination of this journey remains mystery. I am excited to see where the currents of life will guide me to.

Abstract

The mechanisms of positive and negative selection of B cells and the ontogenetic switch between early and late tissue are not fully understood. The selection of mouse B1 B cells, immune components that secrete antibodies against self-antigens and common pathogens, and have a role in housekeeping and homeostasis, is known to be strongly influenced by self-antigen and BCR signalling in early ontogeny.

The objective of this thesis is to elucidate the role of GRB2, an adaptor protein, in the positive and negative selection of B cells. Furthermore, it examines the potential role of GRB2 in preserving the ontogenetic switch between early and late hematopoietic environments. Additionally, this work aims to explore the inherent differences from fetal liver (FL) and bone marrow (BM) to give rise to B1 B cells, employing single-cell transcriptomics for in-depth analysis.

In this project, addition to a B cell specific GRB2 knock-out mouse model (*Grb2*$^{f/f}$*Mb1Cre*$^{+}$ (KO)), several transgenic mouse models were utilized to investigates GRB2's role in positive selection process of B1 B cells.

It was found that the number of B1b B cells, marginal zone B cells (MZ), and serum IgM levels were increased in the absence of GRB2. The development of B1b B cells was not restricted to early-stage tissue in the absence of GRB2, the effect of which was B cell intrinsic. Regardless of the presence of antigen, GRB2 deficiency generated more B1b B cells and MZ B cells, while intracellular membrane bound self-

antigen presentation further increased the number of B1b B cells by ten-fold. Single-cell immune profiling revealed a putative B1/MZ precursor population ($CD19^{hi}B220^{low}IgM^{hi}CD43^{hi}CD21^{hi}IgD^{low}$) in the absence of GRB2 in adult BM, suggesting a shared developmental pathway. This study also suggested GRB2 was involved in a pathway that modulates IgM receptor levels in response to self-antigens, influencing the shift from positive to negative B cell selection, which might contribute to B1b B cell ontogeny.

In conclusion, our findings suggests that GRB2 is an intrinsic negative regulator of B1b B cell development and is required to restrict the generation of these cells in adult mice. The absence of GRB2 enhanced the positive selection by self-antigen while did not alter the requirement of appropriate self-antigen form.

Table of Contents

Acknowledgements *2*

Abstract *5*

Acronyms *13*

List of Figures *22*

List of Table *26*

List of Appendices *27*

Chapter 1 . Introduction *28*

1.1 Conventional B cell development **28**

1.2 B2 B cell positive and negative selection **30**

1.3 Peripheral B2 B cell subsets and their functions **33**

1.4 A less understood pre-immune component: B1 B cells **35**

1.4.1 The functions and features of B1 B cells 35

1.4.2 The unique ontogeny of B1 B cell development: lineage and selection models 37

1.4.3 Differences between B1a and B1b B cells: origin and function 41

1.5 Functional and phenotypic similarities between B1 and MZ B cells **44**

1.6 BCR signalling and its influence on B1 B cell selection. **47**

1.7 Growth Factor Receptor Bound Protein 2 (GRB2) and B cells **50**

1.7.1 Structure and general functions of GRB2 50

1.7.2 Role of GRB2 in lymphocytes 51

1.7.3 Role of GRB2 in B cells 53

1.8 Aim and Experimental Approach adopted in this thesis. **54**

Chapter 2 Materials and Methods *56*

2.1 Animal work 56

2.1.1 Breeding and maintenance 56

2.1.2 DNA extraction 58

2.1.3 Genotyping and PCR 58

2.1.4 RNA extraction and Reverse transcription 60

2.1.5 Immunisation 62

2.1.6 Irradiation for chimera experiment 63

2.1.7 Bromodeoxyuridine (5-bromo-2'-deoxyuridine, BrdU), CellTrace Violet (CTV) and Annexin V labelling 64

2.1.8 Sample processing and long-term storage 66

2.2 Cellular Immunology assays 67

2.2.1 Magnetic beads-based pan B cell sorting 67

2.2.2 Flow cytometry staining 69

2.2.3 Activation of splenocytes by HEL and anti-μ (anti-IgM) 70

2.2.4 Signalling downstream of the BCR: Phospho Flow Cytometry assay 71

2.2.5 Signalling downstream of the BCR: Calcium Flux assay. 72

2.2.6 Single cell RNA sequencing (sc-RNASeq): Sample preparation 73

2.2.7 Flow cytometry-based cell sorting 74

2.2.8 List of Antibodies used for Flow Cytometry and single cell cellular indexing of transcriptomes and epitopes (CITE-seq) analyses. 76

2.2.9 Enzyme-linked immunosorbent assay (ELISA) 84

2.3 Protein detection and quantification 89

2.3.1 Western blot analysis: 89

2.4 Sc-RNASeq Bioinformatic analysis 96

2.4.1 Raw count generation and QC pipeline: 96

2.4.2 Dimensional reduction, data integration, and DE gene analysis: 97

2.4.3 Gene enrichment analysis: 98

2.4.4 Cell cycle analysis: 98

2.4.5 Trajectory analysis: 99

2.5.6 Data visualization: 99

2.5.7 Package version record 100

Chapter 3 Deficiency in GRB2 leads to increased B1b B cells and MZ B cells. 104

3.1 Introduction 104

3.2 Knock out of GRB2 reduces the number of FO B cells while increasing MZ B cell numbers. 105

3.3 GRB2 deficiency is associated with a raised serum IgM concentration and increased B1b B cells 109

3.4 GRB2 suppresses the development of B1b B cells from adult BM, enforcing the ontogenetic switch in B cell development. 112

3.5 The increase in B1b B cells in the absence of GRB2 is B cell intrinsic. 113

3.6 Discussion 115

Chapter 4 : The generation of B1b B cells in the absence of GRB2 is both spontaneous and driven by positive selection by self-antigen. 117

4.1 Introduction 117

4.2 Positive selection of B1b B cells by intracellular self-antigen, and in the presence of GRB2, is restricted to neonatal stage tissue but not adult BM. 119

4.3 Self-antigen independent and dependent mechanisms drive the generation of B1b B cells from GRB2 deficient neonatal liver. 122

4.4 B1b B cell generation and positive selection from adult BM in the absence of GRB2. 130

4.5 The deficiency of GRB2 is correlated with higher serum anti-self-antigen antibodies. 133

4.6 The effects of GRB2 deficiency and positively and negatively selecting self-antigens on B1 B cell development and IgM antibody production are independent but additive. 136

4.7 The absence of GRB2 in Ig^{HEL} mice is associated with HyHEL10 light chain rearrangement leading to oligoclonal B1 B cells with specificities pool of antibodies specificities identical across individual mice. 143

4.6 GRB2-deficient B1 B cells do not show increased peripheral B1 B cells proliferation or survival in comparison to WT. 146

4.7 Discussion 148

Chapter 5 : Insights into cellular and molecular pathways regulated by GRB2 during BM B cell development in the presence of self-antigen. 154

5.1 Introduction 154

5.2 Sc-RNASeq discriminates between the effects of GRB2 and antigen. 154

5.2.1 Presence of GRB2, and not self-antigen, is a dominant discriminator within the integrated immature B population. 160

5.2.2 Interaction between self-antigen and GRB2 is a distinct feature of mature B cell clusters. 167

5.4 GRB2 is required to induce the tolerogenic pathway leading to IgM modulation by self-antigen. 173

5.4 Deficiency of GRB2 alters the Calcium flux induced by BCR signal. 178

5.5 Phosphorylation of BCR related signal molecule have not been changed significantly in the absence of GRB2. 179

5.6 Discussion 181

Chapter 6 The ontogeny-related transcriptional differences in the developmental switch between FL and adult BM B cell progenitors 185

6.1 Introduction 185

6.2 Transcriptional differences between FL and BM B cell development are not GRB2-dependent. 187

6.3 Atlas of B cells subsets in FL and adult BM at the single cell transcriptomic level. 194

6.4 LIN28B related transcripts are highly expressed in FL at single cell level but not in KO BM. 206

6.5 WT FL B cell development shares a trajectory pathway with KO BM. 208

6.6 Discussion 212

Chapter 7 : Discussion 217

7.1 Summary 217

7.2 Positive selection of B1 B cells: setting the stage. 220

7.3 Positive selection of B1 B cells: the role of antigen. 222

7.4 The search for B1 B cells progenitors 225

7.5 BCR signalling in B1 B cell selection and GRB2 function 227

7.6 The pathways of B1a and B1b B cell differentiation in ontogeny 234

7.7 The potential therapeutic applications of B1 B cells 236

7.8 Human B1 B cells 237

References 239

Appendix *262*

Acronyms

ACK	Ammonium chloride potassium
ADT	Antibody-derived tag
Agbl1	ATP/GTP Binding Protein Like 1
AGM	Aorta-gonads-mesonephros
Ahnak	AHNAK Nucleoprotein
AP-1	Activator protein 1
Apoe	Apolipoprotein E
APRIL	A proliferation-inducing ligand
Arid3a	AT-Rich Interaction Domain 3A
ATA	Anti-thymocyte autoantibody
Atxn1	Ataxin 1
B. hermsii	*Borrelia hermsii*
BAFF	B-cell activating factor
BAFF-R	B-cell activating factor receptor
Bcl10	B-cell lymphoma/leukemia 10
Bcl2	B-Cell CLL/Lymphoma 2
BCR	B cell receptor
Bhlhe41	Basic Helix-Loop-Helix Family Member E41
BLNK	B Cell Linker
BM	Bone marrow
BMRC	Biomedical research computing

BrdU	Bromodeoxyuridine
BSA	Bovine Serum Albumin
BSAP/ *Pax5*	Paired Box 5
Btk	Bruton tyrosine kinase
Cacna1e	Calcium Voltage-Gated Channel Subunit Alpha1 E
CER	Cytoplasmic Extraction Reagent
CITE-seq	Cellular indexing of transcriptomes and epitopes
CLL	Chronic lymphocytic leukaemia
CLP	Common lymphoid progenitor
CLR	Centred log ratio transformation
Crip1	Cysteine Rich Protein 1
CTV	CellTrace Violet
DAG	Diacylglycerol
DE	Differential expression
DMSO	Dimethyl sulfoxide
DNase I	Deoxyribonuclease I
ECL	Enhanced chemiluminescence
EGFR	Epidermal growth factor receptor
Egr2	Early Growth Response 2
Egr3	Early Growth Response 3
ELISA	Enzyme-linked immunosorbent assay
Emid1	EMI Domain Containing 1
ERK1/2	Extracellular signal-regulated kinases 1/2

FACS	flow cytometry cell sorting
Fau	FAU Ubiquitin Like And Ribosomal Protein S30 Fusion
Fcmr	Fc Mu Receptor
Fcrl3	Fc receptor-like protein 3
Fcrl5	Fc Receptor Like 5
FCS	Fetal calf serum
FcγRIIb	Fc Gamma Receptor IIb
Fgd2	FYVE, RhoGEF and PH domain-containing protein 2
FGFR2	Fibroblast growth factor receptor 2
FhbA	Factor H-binding protein
FL	Fetal liver
FO/FOL	Follicular B cells
Foxo1	Forkhead Box O1
O/N	Over night
GADS	Grb2-related adapter downstream of Shc
GC	Germinal centre
GM-CSF	Granulocyte-macrophage colony-stimulating factor
GO	Gene ontology
GRAP	Grb2-related adapter protein
GRB2	Growth Factor Receptor Bound Protein 2
H19	H19 Imprinted Maternally Expressed Transcript
H1f0	H1 histone family, member 0
H2-Q6	Class Ib MHC antigen Qa-2

H2afz	H2A.Z Variant Histone 1
HBSS	Hank's Balanced Salt Solution
Hck	Hemopoietic Cell Kinase
HEL	Hen egg lysozyme
Hmga1	High Mobility Group AT-Hook 1
Hmgb2	High-Mobility Group (Nonhistone Chromosomal) Protein 2
Hmgn2	High Mobility Group Nucleosomal Binding Domain 2
HRP	Horseradish peroxidase
HSCs	Hematopoietic stem cells
Hspa8	Heat Shock Protein Family A (Hsp70) Member 8
HTO	Hashtag oligos
ID3	Inhibitor Of DNA Binding 3
Ifi30	Interferon Gamma-Inducible Protein 30 Preproprotein
Ighd	Immunoglobulin Heavy Constant Delta
Iglc1	Immunoglobulin Lambda Constant 1
IL-7	Interleukin-7
Il9r	Interleukin 9 Receptor
IM	Immature B cell
IRA	Innate response activator
ITAMs	Immunoreceptor tyrosine-based activation motifs
ITIMs	Immunoreceptor tyrosine-based inhibitory motifs
JNK	C-Jun N-terminal kinases
KO	B cell-specific Grb2 knock-out mice

Lars2	leucyl-tRNA synthetase 2
Lck	Lymphocyte-specific protein tyrosine kinase
LDL	low-density lipoprotein
Ltb	Lymphotoxin-Beta
Ly6a	Lymphocyte Antigen 6 Family Member A
MAPK	Mitogen-activated protein kinases
MDA	malondialdehyde
MEK	Mitogen-activated protein kinase
Mettl23	Methyltransferase 23
$mHEL^{KK}$	An ER-restricted intracellular membrane bound self-antigen
Min	Minute
Ms4a1	MS4A1 membrane spanning 4-domains A1
MSCs	Mesenchymal stem cells
Myadm	Myeloid Associated Differentiation Marker
Myl4	Myosin Light Chain 4
Myo15b	Myosin XVB Pseudogene
MZ	Marginal zone B cells
Mzb1	Marginal Zone B And B1 Cell Specific Protein
N2IC	Activated form of Notch2
NER	Nuclear Extraction Reagent
NF-κB	Nuclear factor kappa-light-chain-enhancer of activated B cells
NFAT	Nuclear factor of activated T-cells

Nfatc1	Nuclear Factor of Activated T Cells 1
Nfatc2	Nuclear Factor of Activated T Cells 2
NL	Neonatal liver
Non	No antigen
Notch2	Neurogenic locus notch homolog protein 2
OSEs	Oxidation-specific epitopes
PBS	Phosphate buffered saline
PC	phosphorylcholine
PCA	Principal Component Analysis
PGE2	Prostaglandin E2
PhIC	Phosphatase inhibitor cocktail
PI3K	Phosphoinositide 3-kinase
PIC	Protease inhibitor cocktail
Plac8	Placenta Associated 8
PLC	Phospholipase C
PLCG2	1-Phosphatidylinositol 4,5-Bisphosphate Phosphodiesterase Gamma-2
Pld4	Phospholipase D Family Member 4
PIP2	Phosphatidylinositol 4,5-bisphosphate
PKC	Protein kinase C
PMSF	Phenylmethylsulfonyl fluoride
pre-BCR	Precursor B cell receptor
PtC	Phosphatidylcholine

Raf	Rapidly Accelerated Fibrosarcoma
Rag	Recombination-activating gene
Rftn1	Raftlin, Lipid Raft Linker 1
Rpgrip1	X-linked retinitis pigmentosa GTPase regulator-interacting protein 1
Rpl18a	Ribosomal Protein L18a
Rps15a	Ribosomal Protein S15a
Rps2	Ribosomal Protein S2
Rps24	Ribosomal Protein S24
Rsph1	Radial Spoke Head Component 1
RT	Room temperature
RTKs	Receptor tyrosine kinases
S.aureus	Staphylococcus aureus Bacteria
S100a6	S100 Calcium Binding Protein A6
sc-RNASeq	Single-cell RNA sequencing
SDS-PAGE	Sodium dodecyl-sulfate polyacrylamide gel electrophoresis
SH2	Src homology 2
sHEL	soluble HEL
SHIP-1	Src homology 2 (SH2) domain containing inositol polyphosphate 5-phosphatase 1
SHP-1	Src homology region 2 domain-containing phosphatase-1
Shp2	SH2 domain-containing protein tyrosine phosphatase 2

Shisa5	Shisa Family Member 5
Siglec-g	Sialic acid binding Ig-like lectin G
SLAM	Signalling lymphocytic activation molecule
SLC	Surrogate light chain
Slc15a2	Solute carrier family 15 (H+/peptide transporter), member 2
Slc15a2	Solute Carrier Family 15 Member 2
SOCE	Store-operated Ca^{2+} entry
Sos	Son of sevenless
Sox5	SRY-box transcription factor 5
Speer2	Spermatogenesis associated glutamate (E)-rich protein 2
sRBCs	Sheep red blood cells
Sspn	Sarcospan
Stac2	SH3 And Cysteine Rich Domain 2
STAT5	Signal Transducer And Activator Of Transcription 5
TACI	Transmembrane activator and calcium-modulator and cyclophilin ligand interactor
Tagln2	Transgelin 2
TBST	Tris-buffered saline with 0.1% Tween® 20 detergent
TCR	T cell receptor
TdT	Terminal deoxynucleotidyl transferase
TI	thymus-independent
TLR	Toll-like receptors
TMB	Tetramethylbenzidine

Tnfrsf13c	TNF Receptor Superfamily Member 13C
TSLP	Stromal-derived lymphopoietin
Uba52	Ubiquitin A-52 Residue Ribosomal Protein Fusion Product 1
UMAP	Uniform Manifold Approximation and Projection
Vim	Vimentin
Vpreb1/Vpreb	V-Set Pre-B Cell Surrogate Light Chain 1
Vpreb2/Lambda 5	V-Set Pre-B Cell Surrogate Light Chain 2
WBCs	White blood cells
WT	$Mb1Cre^{+}$
Xist	X Inactive Specific Transcript
Zap70	Zeta-chain-associated protein kinase 70
Zfp318	Zinc Finger Protein 318

List of Figures

Figure 1-1 B1 B cell development models and related signal changes *40*

Figure 3-1 Loss of GRB2 expression in B cells from Grb2$^{f/f}$ Mb1Cre^{+} (KO) mice. *106*

Figure 3-2 Fewer FO and more MZ splenic B cells in GRB2 KO mice. *107*

Figure 3-3 Altered BM B cell maturation with fewer mature B cells in GRB2 KO mice. *108*

Figure 3-4 Higher serum IgM titres in GRB2 KO mice. *110*

Figure 3-5 Elevated peritoneal B1 B cell numbers, specifically B1b B cells, in GRB2 KO mice. *111*

Figure 3-6 The increase in B1b B cells in the absence of GRB2 is not affected by ontogeny. *114*

Figure 4-1 Positive selection of B1 B cells from neonatal tissue, but not BM, in the presence of intracellular antigen and GRB2. ..... *121*

Figure 4-2 GRB2 deficiency is associated with increased B1b B cells and MZ B cells, with reduced recirculating and mature FO B cells, in the MD4 transgenic mouse model. *124*

Figure 4-3 Elevated HEL-specific IgMa serum antibody titres are associated with increased HEL+ peritoneal B1b B cells in MD4 mice. *126*

Figure 4-4 Self-antigen independent and dependent mechanisms drive the generation of B1b B cells from GRB2-deficient NL. *129*

Figure 4-5 GRB2 inhibits the generation and positive selection by self-antigen of B1b B cells from adult BM. *131*

Figure 4-6 GRB2-deficient B1 B cell accumulation in the presence of self-antigen is independent of proliferation. *133*

Figure 4-7 The deficiency of GRB2 is correlated to higher serum anti-self-antigen antibodies. *135*

Figure 4-8 The effects of GRB2 deficiency and positively or negatively selecting self-antigens on B1 B cell development are independent but additive. *139*

Figure 4-9 The effects of GRB2 deficiency and various forms of self-antigen on induction of anergy in B2 B cell subsets. *140*

Figure 4-10 Modulation of surface expression of IgM^a and IgD^a BCRs by positively and negatively selecting self-antigens in the absence of GRB2. ..... *141*

Figure 4-11 The effects of GRB2 deficiency and positively and negatively selecting self-antigens on BM-derived B1 B cells and IgM antibody production are independent but additive. *142*

Figure 4-12 The absence of GRB2 in Ig^{HEL} mice is associated with HyHEL10 light chain rearrangement, leading to a pool of oligoclonal B1 B cells with identical specificities across individual mice. *145*

Figure 4-13 GRB2-deficient B1 B cells have comparable proliferation and survival when in competition with WT B1 B cells. *148*

Figure 5-1 Design of the sc-RNASeq experiment and quality control checks. . *156*

Figure 5-2 Clustering and annotation of sc-RNASeq data to identify BM B cell subsets. *158*

Figure 5-3 The cell cycle scoring and development trajectory of the cells in the integrated sc-RNASeq dataset. *160*

Figure 5-4 The distribution of CD45.2⁺ immature BM B cells across 7 clusters in the context of GRB2 expression and the presence of self-antigen. *162*

Figure 5-5 Differential expression of genes in the immature BM B cell clusters in the context of self-antigen and GRB2. ..... *166*

Figure 5-6 Identification of 11 distinct CD45.2⁺ mature BM B cell clusters using sc-RNASeq data. *168*

Figure 5-7 GRB2 and mHELKK self-antigen have distinct effects on the distribution of CD45.2+ BM B cells across the 11 clusters defined using sc-RNASeq data. *170*

Figure 5-8 Differential expression of genes in the M0 and M6 mature BM B cell clusters. *172*

Figure 5-9 GRB2 is required to induce the tolerogenic pathway leading to IgM modulation by self-antigen. *175*

Figure 5-10 Zfp318 and Egr3 transcripts are not induced by intracellular mHELKK self-antigen in mature BM B cells when GRB2 is absent. *177*

Figure 5-11 Deficiency of GRB2 alters the calcium flux, but not the phosphorylation of signalling molecules downstream of BCR stimulation. *180*

Figure 6-1 Sc-RNASeq experiment design and quality control *188*

Figure 6-2 Distinctive differences in the single cell transcriptomic profiles of FL and BM B cells. *190*

Figure 6-3 DE genes between the WT FL, WT BM and KO BM, prior to integration. *193*

Figure 6-4 Atlas of B cells subsets derived from integrated single cell transcriptomic data of FL and BM origin. *196*

Figure 6-5 Distribution of WT FL, WT BM and KO BM cells across clusters defined by transcriptomic changes at the single cell level. *198*

Figure 6-6 Expression of key B cell markers in FL and adult BM at the single cell transcriptomic level. *200*

Figure 6-7 DE genes for cells within cluster 2 of the integrated sc-RNASeq dataset. *202*

Figure 6-8 DE genes for cells within cluster 0 of the integrated sc-RNASeq dataset. *204*

Figure 6-9 DE genes for cells within cluster 1 of the integrated sc-RNASeq dataset. *205*

Figure 6-10 LIN28B related transcripts are highly expressed in FL at single cell level but not in KO BM *207*

Figure 6-11 Trajectory analysis reveals a developmental pathway shared between WT FL B cells and KO BM B cells. *209*

Figure 6-12 WT and KO BM B cells are inclined to utilise different BCR heavy chains compared to WT FL B cells. *211*

Figure 7-1 Schematic illustration summarizing the role of GRB2 in BCR signalling and its correlation with both positive and negative regulatory pathway and their association with B1 B cell generation. *228*

Figure 7-2 Schematic outlining the hypothesized role of GRB2 in self-antigen induced B cell anergy pathway and B cell metabolism pathway, and its potential connection with B1 B cell ontogeny. *234*

List of Table

Table 2-1 Primers used for PCR-based genotyping of various transgenic mice lines. *58*

Table 2-2 PCR protocols for genotyping transgenic mice *60*

Table 2-3 List of reagent and kit for B cell sorting experiment. *67*

Table 2-4 Flow Cytometry and CITE-Seq antibodies *84*

Table 2-5 The purchased reagent list for ELISA assay *85*

Table 2-6 List of Reagents for Protein assays *90*

Table 2-7 List of antibodies for western blot analyses *92*

Table 2-8 List of Seurat and R packages used for bioinformatic analyses. *103*

List of Appendices

Appendix table A Top DE genes of each cluster of total B cells in BM mixed chimera sc-RNASeq experiment *269*

Appendix table B Top DE genes of each cluster within immature B cells in BM mixed chimera sc-RNASeq experiment *273*

Appendix table C Top DE genes of each cluster within mature B cells in BM mixed chimera sc-RNASeq experiment *278*

Chapter 1 . Introduction

1.1 Conventional B cell development

As essential components of the adaptive immune response, B cells execute a multitude of critical functions ranging from antibody synthesis to antigen presentation and cytokine secretion. Emerging evidence underscores their pivotal roles in immunoregulation and the maintenance of immunological homeostasis. These functions are predominantly mediated by antibodies secreted in response to antigen-specific B cell receptor (BCR) engagement. Gaining insights on how B cells fulfil these tasks with pin-point accuracy requires comprehensive understanding of B cell development and the differentiation of B cell subsets.

B2 B cells, or conventional B cells, have been extensively characterized in mouse and originate from pluripotent hematopoietic stem cells (HSCs), which transition from the fetal liver (FL) in mid-gestation to the bone marrow (BM) postnatally[1]. Murine B cell lineage commitment ensues, following differentiation from a common lymphoid progenitor (CLP), marked by the expression of lineage-specific markers such as CD45R/B220[2]. The development of B cells is fundamentally a process of generating and selecting cells with functional, non-autoreactive BCRs[3, 4]. This developmental trajectory is divided by critical BCR rearrangement events.

According to Hardy et al. [1], the earliest B cell precursors in mouse, designated as Fraction A (Pre-pro B cells), exhibit minimal immunoglobulin gene rearrangement.

This stage is characterized by the expression of CD93 and CD43, with low levels of IL-7 receptor alpha (IL-7Rα), a critical determinant for B cell proliferation and survival[5], despite its higher expression in CLP and subsequent B cell stages[2]. As B cells initiate heavy chain rearrangement, they progress to Fractions B and C (Pro-B cells), displaying elevated CD43 and IL-7Rα expression. Concurrently, the B cell-specific molecule CD19 is expressed, enhancing proliferative and survival signals in maturing B cells[6]. The early Pre-B cell stage, or Fraction C', is marked by the assembly of the precursor B cell receptor (pre-BCR). This structure consists of two identical rearranged heavy chains of single rearranged heavy chain gene, paired with two surrogate light chains (SLC)[7], signifying a crucial checkpoint for functional BCR heavy chain rearrangement and subsequent clonal expansion[8]. This pre-BCR-mediated signalling facilitates the proliferation and expansion of heavy chain clones preceding light chain rearrangement[9]. Upon successful light chain rearrangement, Fraction D (late Pre-B) cells downregulate CD43 expression and, upon successful expression of the IgM BCR isotype, transition to Fraction E (immature) B cells. Eventually, immature B cells, supported by survival signalling from engagement with B cell activating factor (BAFF), egress from the BM to the periphery as transitional B cells that undergo further differentiation in the spleen. Mature follicular (FO) B cells, expressing both IgM and IgD BCR isotypes, and marginal zone (MZ) B cells predominantly expressing IgM, are formed in the periphery where they are poised to perform their pathogen-specific effector functions[10]. While FO B cells recirculate between secondary lymphoid organs and the BM as Fraction F cells (Fr.F), MZ B cells appear to be non-recirculating and are positioned mainly at the interface of blood circulation and the white pulp of the spleen[10].

1.2 B2 B cell positive and negative selection

The exquisite specificity of B2 B cells for antigens, coupled with their capacity to avoid self-reactivity, hinges on a series of sophisticated developmental checkpoints. The mechanisms by which the immune system maintains homeostasis and circumvents autoimmune dysregulation remain intriguing questions. Within B cell maturation, distinct checkpoints may hold the key to understanding these processes.

At the initial checkpoint, murine pre-B cells express a pre-BCR, comprising two identical functional immunoglobulin μ heavy chains of single rearranged heavy chain gene, as mentioned above, and a heterodimeric surrogate light chain (SLC) consisting of VPREB and LAMBDA5. This configuration acts as both a surrogate for light chain pairing and a sieve for functional heavy chain variable regions, while also enforcing IgH allelic exclusion[11]. The necessity for ligand-mediated pre-BCR signalling at this stage remains an area of active research; although evidence suggests that pre-B cells can proliferate and differentiate in the absence of a ligand in vitro and in vivo[12, 13], the interaction with heparan sulfate glycosaminoglycans and galectin-1 derived from BM stromal cells implies a potential role for pre-BCR ligand interactions in signalling and developmental checkpoints[14, 15]. Analysis of BCR utilization has revealed that the pre-BCR significantly influences the positive selection of the B cell repertoire, as evidenced by the enrichment and alteration in the use of VDJ combinations post-pre-B cell stage[16, 17, 18].

A subsequent checkpoint occurs at the murine immature B cell stage. Data indicate that only 10-20% of these murine cells from the BM progress to maturation in the periphery[19], with a concomitantly reduced frequency of self-reactive profiles[20]. This suggests an intermediary step that screens out self-reactive cells. Cells harbouring unproductive or autoreactive BCR may undergo BCR editing, altering light chain V region usage to evade self-reactivity[21, 22, 23, 24]. However, this editing process also has the potential to yield B cells with multiple light chains, raising the spectre of continued autoimmune reactivity[25]. When further rearrangements are exhausted, the cross-linking of IgM on immature B cells results in apoptosis in a self-antigen-specific manner, constituting a form of negative selection[26]. Yet, this stage also implicates a requirement for the functional test of the BCRs for positive and negative selection events. The attenuation of SYK signalling from the BCR prevents the maturation of immature B cells, underscoring the requirement for BCR-mediated signalling in the maturation process[27]. Observations that BCR repertoires are more restricted in mature B cells compared to their immature counterparts in vivo also suggest that selection occurs during the immature B cell stage[28].

Post-BM egress, additional checkpoints act to remove deleterious repertoires. The BAFF/BAFF-R signalling axis itself serves as a critical gatekeeper; in the periphery, autoreactive murine B cells become anergic with increased expression of pro-apoptotic factor BIM, and are therefore increasingly dependent on BAFF, rendering them less competitive and short-lived relative to non-autoreactive cells[29]. Interestingly, BAFF overexpression does not salvage autoreactive murine B cells

during BM maturation but does rescue transitional T2 stage B cells in peripheral development, indicating a developmental stage-specific effect of BAFF signaling[30, 31]. Murine immature B cells seem to be more susceptible to deletion compared to their human counterparts, with only 10% of immature B cells egressing to peripheral and a mere 30% of those progressing to maturity[32]. While the extent of immature B cells deletion in human before reaching the mature B cell compartment remains unclear, current data suggests a lower deletion rate at this stage: approximately 40-70% of immature B cells in BM exhibit autoreactivity, a figure drops to 20% in mature peripheral pool[33]. This disparity may reflect subtle differences in selection mechanism and stringency during peripheral B cell maturation between two species.

In the germinal centre (GC), additional checkpoints are present, including the censoring and deletion of auto-reactive murine B cells upon contact with self-antigen[34]. The recombination-activating genes (RAGs) are pivotal in B cell selection. It is initially upregulated during heavy chain rearrangement for pre-BCR expression and subsequently downregulated following the presentation of a productive BCR[35, 36]. Moreover, reactivation of RAG1/2 has been observed in autoreactive B cells, enabling the re-editing process to replace self-reactive BCRs[37, 38].

Hence, sophisticated intricate selection mechanisms underpin B cell development, ensuring the emergence of a repertoire capable of potent pathogen-specific responses while mitigating the risk of autoimmunity.

1.3 Peripheral B2 B cell subsets and their functions

Following egress from the BM, immature B cells transition into the bloodstream and secondary lymphoid tissues, embarking on a path toward further differentiation into either transitional B cells, FO B cells or MZ B cells. The latter two mature B cell subsets exhibit distinctive residency patterns, antigen response profiles, and dependencies on T cell cooperation.

Transitional B cells (Tr) represent an intermediary population, bridging the developmental gap between immature and mature B cell phenotypes. They express high levels of CD24, CD44 and C-type lectin transmembrane receptor CD93, while commencing the expression of mature markers including CD23, IgD, and MHC class II[39]. Hardy et al. further stratify transitional B cells into three stages: T1 ($CD93^{+}CD23^{-}IgM^{hi}$), T2 ($CD93^{+}CD23^{+}IgM^{hi}$), and T3 ($CD93^{+}CD23^{+}IgM^{low}$), based on the expression of CD93, CD23, and IgM[40]. Functionally immature, these cells lack proliferative responses to IgM cross-linking and exhibit a high turnover rate in vivo[40]. The heightened IgM and FAS expression and absence of BCL2 of this population confer susceptibility to negative selection, aligning with the substantial attrition observed during this phase[39]; from an initial cohort of $2x10^{7}$ IgM^{+} B cells, merely 10% reach the spleen, with only 1-3% achieving full maturation[41]. It is likely, of course, that many of these cells, notably in T3, are autoreactive and functionally anergic. Disruptions in CD45 and Bruton's tyrosine kinase (BTK) expression arrest development at the transitional stage, underscoring the critical role of BCR signalling in navigating the selection to maturity[41].

FO B cells, named for their localization to follicles within secondary lymphoid organs, circulate between the spleen, BM, and lymph nodes. Upon maturation in the spleen, they traverse the blood and lymphatic vessels to enter lymph nodes and Peyer's patches[42]. Upon activation by antigen, FO B cells relocate to the periarteriolar lymphoid sheaths (PALS) or paracortex in the spleen or lymph nodes respectively, where they are able to interact with T cells. In the case of thymus-dependent (TD) antigens, the survival of activated FO B cells normally requires interaction with cognate CD4 T cells that provide T cell help[43]; however, the same, to less extend, can be achieved in the case of high avidity thymus-independent (TI) antigens through Toll-like receptors (TLR) signalling alone[44]. The conjoint activation via BCR, TLR, and CD40 signalling facilitates Ig class-switching, the differentiation of FO B cells into antibody-producing cells and initiation of the GC response[42] . FO B cells can give rise to both short-lived and long-lived plasma cells, the latter migrating to the BM to sustain long-term immunity, contingent upon BCMA expression for survival[45]. Although not commonly accepted, subcategorization of FO B cells, according to one research, into Type 1 ($IgD^{hi}IgM^{low}CD21^{mid}CD23^{hi}$) and Type 2 ($IgD^{hi}IgM^{hi}CD21^{mid}CD23^{hi}$) reflects potential functional diversity, with Type 1 dependent on BTK and NOTCH2 signalling for development, whereas Type 2 differentiate independently of these signals[46].

MZ B cells are characterized by an $IgD^{low}IgM^{hi}CD21^{hi}CD23^{low}CD1d^{hi}$ phenotype and reside in the marginal zones of lymphoid organs, especially the spleen's marginal sinus. Their localization is mediated by S1P receptors, predominantly S1P1 [47]. MZ B cells, poised at the interface of innate and adaptive immunity, can rapidly

differentiate into plasma cells without BCR engagement[42]. Capable of swift responses to TI antigens through massive IgM production[48], MZ B cells can also proliferate and differentiate into plasma cells in response to low-dose polyclonal stimuli and TLR signalling via lipopolysaccharide (LPS), independent of T cell help and CD40 interactions[49]. This readiness for activation, proliferation, and differentiation into antibody-secreting cells may be attributed to their lower activation threshold[49]. In contrast, while FO B cells can also respond to TI antigens, they primarily contribute to defence against T cell-dependent antigens.

1.4 A less understood pre-immune component: B1 B cells

1.4.1 The functions and features of B1 B cells

B1 B cells, delineated from their B2 counterparts, manifest distinct ontogenic and functional attributes akin to innate immunity. First characterized in the 1980s[50, 51, 52], B1 B cells were identified as expressing CD5, a prototypic T cell surface marker that also acts as a negative regulator in certain B cell subsets[53, 54]. Their phenotypic hallmarks include low IgD and high IgM surface expression, coupled with intrinsic IgM secretion, demarcating them from the conventional B2 B cells. Predominantly residing in peritoneal and pleural cavities, B1 B cells exhibit a preferential homing influenced by a CXCL13-dependent mechanism, a chemokine secreted by omental macrophages that orchestrates their migration to the omentum[55, 56].

Contrary to B2 B cells, which rely on BM precursors for replenishment, B1 B cells exhibit a remarkable capacity for self-renewal within their serous cavity niches[57, 58]. This auto-regenerative property of peritoneal cavity-resident B1 B cells is hypothesized to act as a reservoir for steady-state B1 B cells[59], a process potentially modulated by prostaglandin E2 (PGE2) from macrophages[60]. However, evidence suggests that the bulk of natural antibody secreting B1 B cells are situated in the BM and spleen, with less than 5% residing in serous cavities[61].

More distinctive features of B1 B cells include a muted response to surface IgM crosslinking and a reduced ability to upregulate NF-κB upon activation[62]. Their BCR repertoire is narrow and skewed, with diminished TdT expression and reduced N-region diversity[63]. B1 B cells also preferentially produce IgM and IgA, particularly in the gut mucosa, as opposed to IgG and IgD[64]. Moreover, the majority of B1 B cells do not depend on BAFF signalling for survival, concomitant with low BAFF-R surface expression[65].

Functionally, B1 B cells perform housekeeping and regulatory roles, primarily via the secretion of natural antibodies — antibodies that are present in the body or spontaneously arise without explicit prior immunization[66]. These antibodies recognize oxidation-associated antigens, such as phosphorylcholine (PC) and malondialdehyde (MDA), which are prevalent on apoptotic cells and oxidative byproducts[67, 68]. Their engagement with oxidized low density lipoprotein (LDL) and other oxidation-specific epitopes (OSEs) suggests a protective role against atherosclerosis[69,70, 71]. Furthermore, natural antibodies provide a broad spectrum of

defence against pathogens[72, 73, 74, 75], including *Borrelia hermsii*, and facilitate long-lasting immunity[76, 77, 78]. They also participate in responses to *Francisella tularensis*[79, 80], *Mycobacterium tuberculosis*[81], and during *Staphylococcus aureus* infections, when B1 B cell-derived IL-10 modulates T cell responses to mitigate host damage[82]. Additionally, B1 B cells respond to influenza virus infection by secreting IgM, a process enhanced by type I interferon[83, 84]. IL-10 production by B1 B cells extends to modulating macrophage function and controlling inflammation in myocardial infarction and inflamed skin[85, 86, 87].

1.4.2 The unique ontogeny of B1 B cell development: lineage and selection models

The scientific community has proposed two primary models to explain the apparently unique origin and development of B1 B cells during ontogeny: the lineage model and the selection model[88]. As time has passed, it has become clear that these are not mutually exclusive (**Figure 1-1 A**).

The lineage model postulates that B1 and B2 B cells are derived from separate progenitors or lineages. It suggests that early-stage tissues predominantly harbour progenitors for B1 B cells, which are eventually replaced by B2 B cell progenitors, correlating with the loss of B1 B cell production in favour of B2 B cells. This theory arose from the observation that murine B1 B cells can be efficiently generated from mid-gestational embryonic tissue post 8.5 days of development up to the first week postnatally, i.e. from FL or neonatal liver (NL), a capability that declines markedly

thereafter[89, 90, 91]. It has been proposed that this decline in the potential to generate B1 B cells is correlated with dynamic changes in a $Lin^{-}CD45R^{lo/neg}CD19^{+}AA4.1^{+}$ population[90], which putatively gives rise to B1 B cells in a process influenced by IL-7Rα and negatively regulated by BTK. The discovery of an ontogenic switch in lymphoid development from FL to BM, which is governed by the *Lin28b/let-7* axis, further supports this model, with differential expression of *Lin28b/let-7* targets between progenitors of both origins, of which, LIN28B expresses dominantly in fetal/neonatal liver stage while it switch to *let-7* expression in adult stage at the cost of lower LIN28B expression(**Figure 1-1 B**)[92]. The downstream targets of the *Lin28b/let-7* axis, including ARID3A and BHLHE41, are essential for B1 B cell development. While loss of ARID3A leads to a concomitant loss of $CD5^{+}$ B1a B cells, forced over-expression of ARID3A in pre-B cells and immature B cells is characterized by the upregulation of BHLHE41 and MYC, downregulation of SIGLEC-G and CD72, and generation of B1a B cells from adult BM[93]. Similarly, BHLHE41, and to a lesser degree BHLHE40, promote B1a B cell development and maintenance via the regulation of BCR signalling, proliferation and cytokine signaling[94]. However, single-cell analysis of HSCs with cellular barcoding has shown that FL HSCs can give rise to both B1 and B2 B cells, and whilst the B1 potential wanes over time, the loss is not absolute[95]. Notably, the forced expression of LIN28B in adult HSCs can reinitiate the generation of B1 B cells from adult BM[95], albeit with distinct BCR repertoires, potentially due to TdT activity that is independent of LIN28B and activated during the generation of B1 B cells in BM[96]. Furthermore, despite the differential potential of FL and adult BM to give rise to B1 B cells, no definitive precursor population was ever proven to exist by isolation and transfer.

Critically, the lineage model does not address the role of self-antigen exposure in shaping the B1 B cell population[97, 98, 99]. Convincing support for a selection model came initially from experiments with transgenic mice demonstrating that the presence of self-antigen and a self-reactive BCR is crucial for B1 B cell generation, as evidenced by the increased numbers of B1 B cells and autoantibodies when BCRs are specific for a self-antigen[100, 101, 102, 103]. The first of these reported the generation of B1 B cells in $Ig^{Thy\text{-}1}$ transgenic mice, in which the developing B cells recognise a self-antigen (Thy-1). B1b B cells were absent when Thy-1 was removed from the system with *Thy-1*$^{-/-}$ $Ig^{Thy\text{-}1}$ double transgenic mice[100]. More recently, an experiment in which mature B2 B cells could be induced to adopt a B1 phenotype upon transfer into *Rag2*$^{-/-}$ hosts and a BCR switch to a B1 B cell-derived BCR specificity [99], was suggested as possible further evidence of positive selection by self-antigen. However, it is important to note that an intrinsic effect of differential BCR signalling via the B1 and B2 BCRs might itself have been sufficient for the B1 phenotype. Increased BCR signalling is in and of itself sufficient to either induce B1 B cells or maintain B1 B cell survival, as evidenced by increased numbers of B1 B cells in mice deficient in negatively regulators of BCR signalling such as LYN, SHP-1 and SHIP-1[104, 105, 106, 107], or conversely, in mice over-expressing positive regulators of BCR signalling, such as CD19[108].

It is now clear that elements of both models are likely required to explain B1 B cell ontogeny. An integrated model that accommodates the B1-B cell progenitor potential of developmentally early-stage tissue, the extent of BCR signalling, and the role of

antigen, seems necessary to fully capture the complexity of B1 B cell development[102, 109]. The form and location of self-antigen encounter are also pivotal for positive selection into the B1 B cell compartment[103, 110, 111], and exposure to the same antigen at different life stages can distinctly shape B1 and B2 B cell populations[98]. Further research is needed to fully unravel the intricacies of B1 B cell ontogeny and the interplay between lineage and environmental factors in their development.

Figure 1-1

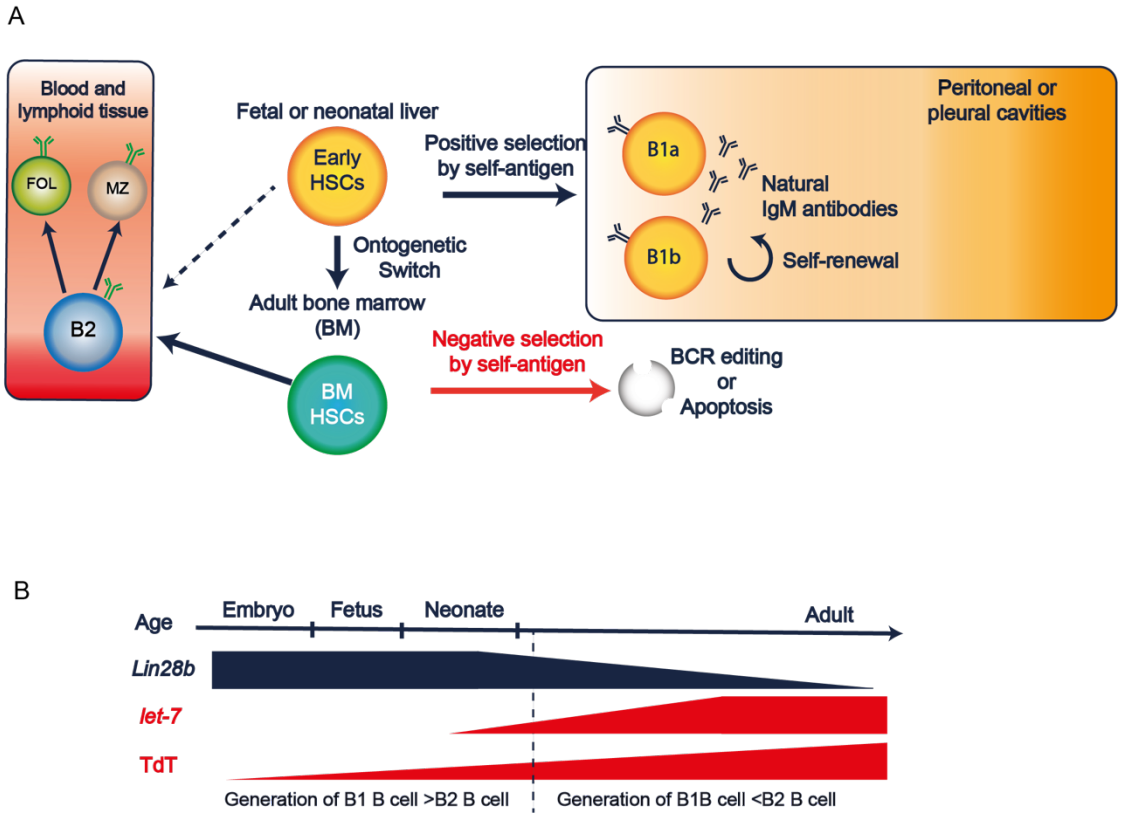

Figure 1-1 B1 B cell development models and related signal changes

The schematics plot (A) depicts overview of the major steps and requirements for B1 B cell development, highlighting distinct process divergent from B2 B cells ontogeny. Plot (B) illustrates the several key signal molecules alteration associated with B1 B cell ontogeny across the aging continuum.

1.4.3 Differences between B1a and B1b B cells: origin and function

Another persistent mystery in B1 B cell biology is that B1 B cells can be divided into two subsets based on the surface expression of the inhibitory co-receptor CD5, B1a ($CD5^+$) and B1b ($CD5^-$) B cells. Despite sharing common features such as early ontogeny, self-renewal capacity, and natural antibody secretion, it remains uncertain whether these subsets represent functionally and phenotypically distinct cell types or are merely different developmental stages of the same population. The fact that CD5 expression is induced by antigen in anergic B cells[112], might suggest that the difference is due to distinct effects of signalling during B cell development. However, mounting data indicate that B1a and B1b B cells may arise during different developmental stages and mechanisms, supporting the notion that they are more distinct populations[89, 90, 98, 108, 113].

B1a B cells appear to originate from an earlier embryonic stage, with precursors detectable as early as day 8.5 post-conception in the mouse splanchnopleure region[91], and their efficient generation persists until the first week postnatally[91]. In contrast, B1b B cells are not found in this region[91] and are marginally more effectively reconstituted from adult BM compared to B1a B cells[89, 90]. Key molecules and pathways diverge in the generation and maintenance of these subsets: Although CD19 is critical for B1a and B1b B cells, CD19 deficiency has a profound effect on B1a B cells with a 20-fold reduction compared to only a 3.5-fold reduction in B1b B cell numbers[108]. Conversely, overexpression of CD19 leads to a loss of B1b B cells

with a significant increase of B1a B cells[108]. BTK also appears more vital for B1a B cell development, as XID mice (BTK deficiency) showed a significant reduction in B1a but only a mild decrease in B1b B cells[114]. Loss of inhibitor of differentiation 3 (ID3), a transcriptional regulator that negatively regulates basic helix-loop-helix transcription factors, selectively promotes the generation of B1b but not B1a B cells[69]. Further, although both B1 B cell subsets exhibit restricted VDJ usage, favouring greater selection of a VH11 or VH12 repertoire compared to their representation in B2 B cells[88], B1a B cells display lower N-region diversity and higher sequence homology at V-D and D-J junctions, with limited deletion of joining gene sequences compared to B1b B cells[115].

While the precise mechanisms underlying these developmental differences remain elusive, both precursor differences and divergent signalling pathways likely contribute to the distinction. Functionally, B1a and B1b B cells exhibit partly divergent roles within the immune system. B1a B cells are one important source of gut IgA plasma cells[116] and generate Innate response activator (IRA)-B cells that secrete GM-CSF during bacterial sepsis[74]. B1a B cells also secrete IL-10, moderating inflammation and improving survival during bacterial infections such as with *Staphylococcus aureus*[75, 82]. In models of influenza infection, B1a B cells are thought to mount a protective virus-neutralizing IgM response by localized accumulation, albeit in an antigen-independent manner[83].

B1b B cells also play unique roles during T cell-independent immune responses. They play a pivotal role in the defence against *Borrelia hermsii*, a pathogen responsible for

tick-borne relapsing fever[76]. Studies in SCID and RAG1/RAG2-deficient mice, which lack functional B and T cells, have demonstrated that these mice are incapable of resolving *Borrelia hermsii* infection. However, mice deficient in T cell receptor (TCR) and IL-7, that can still generate functional B1 and MZ B cells, can effectively clear the infection, underscoring the essential role of B1 and MZ B cells in combating this pathogen[76]. Further research has reinforced this observation; reconstitution of RAG-deficient mice with only B1b B cells conferred long-lasting immunity to *Borrelia hermsii*, mediated by the production of unmutated IgM antibodies targeting the complement factor H-binding protein (FhbA), a surface protein of *Borrelia hermsii*, thereby establishing the sufficiency of B1b B cells for protective immunity against the bacterium[77, 78]. Beyond their role in infectious disease, B1b B cells have also been implicated in the immune response to vaccination. Unlike B1a or MZ B cells, B1b B cells proliferate and secrete protective antibodies in response to the typhoid Vi capsular polysaccharide vaccine[117]. This response is crucial for the development of effective immunity against invasive typhoidal salmonellae. Furthermore, both B1a and B1b B cells have been proposed to play a role in promoting cardiovascular health by producing IgM antibodies specific to OSEs on LDL[69, 118]. The atheroprotective function involves the secretion of natural antibodies that recognize oxidized lipids, with distinct pathway activated in B1a and B1b B cells. This process is further enhanced in B1b B cells lacking ID3, a phenomenon not observed in B1a B cells[69].

Cumulatively, these findings suggest that B1a and B1b B cells may not be merely stages of a singular developmental continuum, but more distinct entities. Future

research focusing on the ontogeny and function of B1 B cells may be expected to refine our understanding and better distinguish between B1a and B1b B cells.

1.5 Functional and phenotypic similarities between B1 and MZ B cells

MZ B cells and B1 B cells are often collectively referred to as components of the 'innate-like' immune system due to their shared functional and phenotypic characteristics[119]. Phenotypically, both express high levels of CD19, IgM and FcR homolog 3 (FCRH3), along with low CD21 [120]. Both MZ and some B1 B cells express CD9, a protein also found on plasma cells induced by TI antigens, but not on those induced by TD antigens[121].

Functionally, MZ and B1 B cells exhibit a heightened responsiveness to TI antigens rather than TD antigens, contrasting with FO B cells[122]. Upon stimulation with particulate bacterial antigens, these populations can rapidly differentiate into plasmablasts and produce a surge of IgM antibodies within three days[122]. This swift response forms a crucial link between the innate immune defences and the subsequent adaptive response. It has also been observed that MZ and B1 B cells are more prone to class-switching to IgA in response to stimuli[123], a trait that potentially equips them for a rapid response to bacterial pathogens at mucosal sites.

The shared functional similarities between B1 B cells and MZ B cells may partly stem from a similar positive selection process. B1 B cells are known to be positively

selected by self-antigens[124]. This feature that is also apparent in MZ B cells with both self-antigen and non-self-antigen within the mature B cell pool[125,126, 127], though such positive selection is atypical for B2 B cell development. Some MZ B cells, despite potentially being rendered non-functional, possess self-reactivities and can secrete self-reactive antibodies *in vitro* when stimulated[125]. This positive selection for self-reactivity aligns with observations in monoclonal B cell receptor mouse models. For instance, mice with B cell receptors specific for the self-antigen Thy-1 glycoprotein exhibited an increase in anti-Thy-1 MZ B cells, but not FO B cells, in a RAG1 knockout background[127]. This selection process is contingent on the presence of CD19 and BTK, key signalling molecules in B cell activation and development[126].

Both MZ B cells and B1 B cells exhibit a unique expression pattern of cytokine receptors, characterized by low levels of the BAFF receptor (BAFF-R) but high expression of the transmembrane activator and calcium-modulator and cyclophilin ligand interactor (TACI), which binds both BAFF and APRIL[128]. BAFF is pivotal for the survival of mature B cells and for allowing autoimmune cells to evade tolerance mechanisms[31, 129]. While MZ B cell maturation and survival are dependent on BAFF, B1 B cells appear to be less reliant on this cytokine for their maintenance[31, 128, 129]. Both MZ and B1 B cells are also reliant on BCL10, an intracellular molecule involved in NF-κB activation post antigen-receptor engagement[130]. The absence of BCL10 significantly diminishes the populations of both MZ and B1 B cells and impairs humoral immune responses[130]. Similarly, NOTCH2 signalling exerts an influence on both cell types; NOTCH2 haploinsufficiency leads to reduced numbers of B1 B cells in the peritoneal cavity and a marked decrease in MZ B cells. Conversely, the

expression of an activated form of NOTCH2 (N2IC) impedes the maturation of B2 B cells at the pre-B cell stage while promoting the development of B1 B cells[131]. Additionally, LY9 (CD229), part of the signalling lymphocytic activation molecule (SLAM) family of receptors, serves as a negative regulator for T1, MZ, and B1a B cells. Mice lacking LY9 exhibit an expansion of these cell populations without altering overall B cell development and demonstrate an enhanced response to T cell-independent antigens[132].

Although MZ B cells and B1 B cells share many functional similarities and both contribute to the early innate-like immune response, evidence suggests they originate along different developmental pathways. While B1 B cells are predominantly generated early in life, with their selection strongly influenced by BCR signalling and the recognition of self-antigens, the positive selection of MZ B cells appears to be a more complex process, involving not only BCR-mediated signals but also signals from co-receptors. Models employing self-antigen indicate that B1 B cells tend to be oligoclonal, whereas MZ B cells display more heterogeneity, pointing to differences in their selection processes[133].

Nevertheless, the close relationship between MZ and B1 B cells raises questions about their potential common origins during early development, and whether the exposure to self-antigens or developmental transitions control their generation. Understanding whether these populations arise from the same progenitors and how self-antigens influence their development requires further investigation. These

insights will be crucial in delineating the ontogeny and functional specialization of these two integral components of the immune system.

1.6 BCR signalling and its influence on B1 B cell selection.

Within the framework of the selection model, BCR signalling is central to the positive selection of B1 B cells, and yet it poses a conundrum: why does self-antigen induce positive selection in B1 B cells in early-stage tissues rather than the negative selection typical of B2 B cells in adult BM? The probable explanation lies in the divergence of signalling pathways between positive and negative selection.

One hypothesis is that an excessive activation of BCR signalling, achieved by dampening of negative signals, could lead to positive selection of B1 B cells. Upon BCR engagement, the immunoreceptor tyrosine-based activation motifs (ITAMs) of CD79a and CD79b are phosphorylated, leading to the activation of src kinases and subsequently, SYK kinase[134]. Concurrently, the phosphorylation of immunoreceptor tyrosine-based inhibitory motifs (ITIMs) on co-receptors like CD22, CD72, and CD5, in association with the BCR, facilitates the recruitment and activation of tyrosine phosphatases such as SHP-1 and SHIP-1, which transmit negative signals to modulate BCR signalling[134]. Deficiencies in these negative regulators, like SHIP-1, disrupt B cell anergy, while SHP-1 deficiency not only enhances BCR-induced calcium flux but, as already described, also leads to an increase in B1a B cells with reduced surface IgM levels[107].

Similarly, loss of CD72, another BCR-negative regulator acting from the pro-B cell stage through to mature B cells, results in an expanded B1 B cell population in the peritoneal cavity and increased calcium flux upon IgM cross-linking of splenic B cells[135, 136]. Absence of SIGLEC-G, a BCR co-receptor and negative regulator, which is highly expressed on B1 B cells, leads to a significant increase in calcium mobilization specifically in B1a B cells and an expansion of the B1 B cell population[137]. However, not every BCR-negative regulator directly affects B1 B cell selection. CD22, for instance, modulates calcium flux and proliferation in B2 B cells, and its expression is downregulated following BCR cross-linking on B2 B cells[138]. CD22 expression is low in B1a B cells and is not significantly altered by stimuli that affect B2 B cells. CD22 deficiency increases calcium influx but does not have an effect on B1a B cell numbers, indicating its limited role in B1a B cell BCR signalling[139]. Nonetheless, in SIGLEC-G × CD22 double-deficient mice, both B1 and B2 B cells exhibit increased calcium influx following BCR engagement and higher serum IgM levels, with an even greater expansion of the B1a B cell population compared to SIGLEC-G knockout mice alone[140]. This suggests that while CD22 may be dispensable for BCR signalling in B1a B cells, it collaborates with SIGLEC-G to attenuate BCR signalling and regulate B1a B cell production.

According to aforementioned research, it was initially posited that enhanced BCR signalling might drive B1 B cell selection. However, findings involving LYN, a key kinase in proximal BCR signalling, challenge this notion. LYN knockout mice exhibit a reduction in peripheral B2 B cells and an unresponsiveness to BCR cross-linking and CD40 ligand, yet paradoxically, these mice have elevated levels of IgM, IgA and

autoantibodies with increased B1a B cell numbers[105, 106]. This suggests that overly robust BCR signalling is not necessary for B1 B cell generation. LYN deficiency also leads to increased activated B1 B cells and severe haemolytic anaemia in a transgenic BCR mouse model expressing immunoglobulins specific to red blood cells[141], suggesting a role for the kinase in B1 B cell activation and tolerance maintenance. In the case of LYN, this is likely due to its non-redundant function as a Src kinase in the phosphorylation of inhibitory receptors, as has been demonstrated in the case of CD22[142].

These findings imply that the strength of BCR signalling is not the sole determinant of B1 B cell selection and development. Instead, the generation of B1 B cells may depend on a more intricate balance of BCR signalling or the nature of tonic BCR signalling, rather than a straightforward increase or decrease in signal strength. Calcium influx, another crucial signal following BCR cross-linking, is important for B cell proliferation and survival. Notably, B1 B cells stimulated by BCR cross-linking via soluble anti-IgM (sIgM) display modest calcium mobilization and a lower response to BCR stimulation compared to B2 B cells, while responding comparably to LPS[62]. Lymphocyte-specific Src tyrosine kinase (LCK) deficiency leads to increased levels of natural antibodies and increased calcium mobilization in B1a B cells, and LCK is implicated in maintaining the hyporesponsive state in $CD5^+$ B1a B cells by potentiating CD5-dependent inhibition[143].

The distinct BCR signalling observed in mature B1 B cells raises questions about the signalling dynamics in precursor B cells that give rise to the B1 lineage and whether

BCR signalling at that stage is decisive for cell fate determination. Further research is needed to elucidate the BCR signalling alterations in early-stage B cells and to better identify B1 B cell precursors, which will enhance our understanding of the molecular mechanisms regulating B1 B cell development.

1.7 Growth Factor Receptor Bound Protein 2 (GRB2) and B cells

1.7.1 Structure and general functions of GRB2

GRB2 is a member of the GRB2 family of adapters, which includes GRB2-related adapter protein (GRAP) and GRB2-related adapter downstream of Shc (GADS). These adapter proteins, particularly GRB2, are integral components in multiple signal transduction pathways. Unlike GRAP and GADS, which are primarily expressed in the hematopoietic system[144, 145], GRB2 is ubiquitously expressed in almost all tissues [145]. GRB2 is composed of a central Src homology 2 (SH2) domain flanked by two SH3 domains. Classically, it is involved in the regulation of RAS signalling through its association, via SH3 domain binding to proline-rich peptides, with Son of Sevenless (SOS), a RAS guanine-nucleotide exchange factor[146, 147]. GRB2 also binds phosphorylated tyrosine-rich residues via its SH2 domain to link receptors such as the epidermal growth factor receptor (EGFR) to downstream MAPK signalling cascade[148, 149,150]. This GRB2-dependent activation of the RAS-MAPK pathway is in turn inhibited by the DOK family of adaptor proteins. The DOK-3 protein binds and sequesters GRB2 through interactions via the GRB2 SH2 domain, thus preventing the formation of the stable GRB2-SOS complex and inhibiting RAS signalling[151].

More evidence suggested that GRB2 is essential for the function of nearly all receptor tyrosine kinases (RTKs) as it links RTKs to the Ras signalling pathway[152, 153, 154]. Beyond its role in EGFR-Ras signalling, GRB2 also regulates the fibroblast growth factor receptor 2 (FGFR2) and SH2 domain-containing protein tyrosine phosphatase 2 (SHP-2), which are part of the Ras/Raf/MEK/MAPK signalling axis that governs cell proliferation and metabolism[155]. The phosphorylation of GRB2 by FGFR2 may reduce its inhibitory function, enhancing the kinase activity of FGFR2 and the phosphatase activity of SHP-2. Conversely, SHP-2 can dephosphorylate GRB2 to provide negative feedback, thus maintaining the balance and homeostasis of EGFR2 and SHP-2 activation[156, 157]. In addition to these roles, GRB2 also interacts with AMP-activated protein kinase (AMPK), a crucial regulator of cellular glucose and fatty acid metabolism, as well as protein synthesis pathways, by mediating the phosphorylation of AMPK at Thr172[158].

1.7.2 Role of GRB2 in lymphocytes

The cell type specific function of the small adaptor protein GRB2, integral to numerous signalling pathways, remains challenging to describe precisely due to its ubiquitous involvement. Within lymphocytes, the role of GRB2 in T cell signalling has been probed, although the germline knockout of GRB2 results in embryonic lethality[159], complicating direct analyses. To solve this, researchers have employed models of haploid deficiency or conditional knockout to study GRB2 function selectively across various cell types[160, 161]. In T cells, partial loss of GRB2 appears to partly impede negative selection without affecting positive selection[162]. This partial

inhibition may be due to attenuated activation of the JNK and p38 MAPK pathways upon TCR stimulation[162]. In models where GRB2 is completely ablated in T cells, a more pronounced inhibition of negative selection is observed, alongside diminished activation of the signalling proteins LCK, ZAP70, P38, and JNK, but not ERK1/2[161, 163]. The positive selection of T cells was also attenuated in the complete absence of GRB2[163]. These findings suggest that a hemizygous expression of GRB2 suffices for positive selection in T cells, while full expression is necessary for negative selection, implicating a close regulatory relationship between GRB2 and the JNK/p38 pathways, distinct from ERK1/2 signalling.

Furthermore, GRB2 interaction with phospholipase Cγ (PLC-γ) upon TCR activation is significant[164]; deficiency in GRB2 correlates with reduced PLC-γ1 activity and consequent lower calcium influx post-TCR stimulation[163]. GRB2 also appears to interact with CD28, a co-stimulatory molecule crucial for T cell survival and activation[165]. This interaction, likely mediated via the GRB2/SOS complex, plays a regulatory role in the activation of NFAT/AP-1 transcriptional pathways[166, 167].

These insights highlight the complex role of GRB2 within T cell signalling, indicating its essential function in both the fine-tuning of T cell receptor-mediated responses and the regulation of co-stimulatory signals necessary for T cell development and activation. Further investigation is required to unravel the precise mechanisms by which GRB2 regulates these critical signalling pathways.

1.7.3 Role of GRB2 in B cells

The role of GRB2 in B cell signalling, compared to its function in T cells, is even less understood and appears to diverge significantly. Current research points to GRB2 primarily serving as a negative regulator within BCR-mediated signalling pathways.

In studies using the Chicken DT40 B cell line, GRB2 has been shown to negatively regulate calcium mobilization from both intracellular and extracellular sources[168]. The involvement of NTAL in extracellular calcium flux and the lipid raft localization of GRB2 suggest a complex regulation of Ca^{2+} flux by GRB2[168].Similarly, In B cell specific GRB2 knockout mice, an increase in Ca^{2+} influx upon BCR engagement was observed[169]. Despite close association with the RAS-MAPK pathway, the absence of GRB2 did not affect the phosphorylation of ERK and p38 in B cells following BCR stimulation. Instead, there was a notable decrease in JNK and PI3K signaling[169, 170]. This was accompanied by increased activation of SYK and reduced phosphorylation of CD22, both upstream of PLCγ2, while AKT phosphorylation downstream of PI3K was diminished[169, 170]. These findings suggest that GRB2 regulates PLCγ2 activation and calcium flux through a variety of intracellular signalling cascades.

CD19, a critical enhancer of BCR signalling, also transduce signals via GRB2. Upon stimulation, phosphorylated CD19 could recruit GRB2, SOS and Vav, activating downstream pathways[171], including Calcium flux and ERK activation when co-stimulated with the BCR[172]. In this signal cascade, phospholipase C (PLC) is activated cleaving phosphatidylinositol 4,5-bisphosphate (PIP_2) to generate diacylglycerol

(DAG) and inositol triphosphate (IP_3). This leads to the activation of protein kinase C (PKC), which in turn transduces signal through AMPK-mTOR signalling pathway [173, 174].

Moreover, the lack of GRB2 impacts B cell development, leading to a significant reduction in mature and FO B cells, compromised memory B cell responses, and impaired germinal centre formation[169, 170]. Notably, the influence of GRB2 in B cells differs from its function in T cells, as evidenced by the unchanged p38 signalling in GRB2-deficient B cells and different calcium flux responses to BCR and TCR stimulation.

The absence of the adaptor protein GRB2 in knockout models has been associated with a marked elevation in serum IgM levels, without a corresponding alteration in other antibody isotypes[169]. Speculatively, this might correlate with the increased BCR signalling or the effect of BAFF signalling on the relatively higher proportion of spleen MZ B cells in the absence of GRB2. However, there were no observable changes in the numbers of B1a B cells or in the combined population of B2 B and B1b B cells within peritoneal lavage samples.

1.8 Aim and Experimental Approach adopted in this thesis.

The primary objective of this thesis is to gain new understanding of the factors that govern the positive and negative selection of B cells during ontogeny and the early and late stages of B cell development. The experimental approach involves the study of the role GRB2 in the positive and negative selection of B cells and offers some new

perspectives on the cellular and molecular mechanisms driving B1 and MZ B cell generation and function.

This project aims to resolve key questions surrounding B1 B cell development and contribute to a deeper comprehension of B cell tolerance, immunoregulation and the maintenance of humoral homeostasis. Such insights have the potential to not only enhance our understanding of B1 B cell biology but also inform the possible mechanism of autoimmune diseases, with implications for the development of novel therapeutic interventions.

Chapter 2 Materials and Methods

2.1 Animal work

All procedures involving animals were conducted in strict accordance with the Animals (Scientific Procedures) Act of 1986, as amended in 2012. Ethical review and oversight were provided by the Clinical Medicine Animal Care and Ethical Review Body (AWERB). The research was carried out under the authority of Home Office Project Licenses P79A4C5BA and PP6163556. Every effort was made to use age- and sex-matched animals whenever feasible to ensure the rigor and reproducibility of the experiments. Animals were co-housed under controlled conditions to minimize variability and maintain a consistent experimental environment.

2.1.1 Breeding and maintenance

All mice were maintained under specific pathogen-free conditions within individually ventilated cages. The animal research protocols were conducted in accordance with the regulations outlined in Project Licenses P79A4C5BA and PP6163556, and were carried out at the Centre for Human Genetics, University of Oxford. *Grb2*$^{flox/flox}$ (*Grb2*$^{f/f}$) mice were generously provided by Dr. Lars Nitschke and were maintained on the C57BL/6 background[169], as were the previously described B6.C(Cg)-*Cd79a*$^{tm1(cre)Reth}$/EhobJ (*Mb1Cre*$^{+}$) mice[175]. Grb2$^{f/f}$Mb1Cre^{+} (KO) mice were generated through the crossbreeding of these two strains, resulting in a B-cell specific deletion of *GRB2*.

B6.SJL-*Ptprc*^{a}/BoyJ (CD45.1^{+}) mice were obtained from the Oxford University Biomedical Service facility. Intracellular hen egg lysozyme (HEL) Tg (mHEL^{KK}) , melanocyte-restricted Intracellular hen egg lysozyme Tg mice(trp2mHEL) and B6.129S7-*Rag1*^{tm1Mom}/J (Rag1$^{-/-}$)mice used in this study have been previously described[102, 176, 177] and other transgenic mouse lines including C57BL/6-Tg(MD4)4Ccg/J (Ig^{HEL}) and C57BL/6-Tg(ML5)5Ccg/J soluble HEL (sHEL) Tg mice, were kindly provided by C.C. Goodnow[111, 178]. Grb2KO, Mb1-Cre and CD45.1^{+} mice were crossed to the Ig^{HEL} strain and maintained on a C57BL/6 background. B6.SJL-*Ptprc*^{a} *Pepc*^{b}/BoyJ (CD45.1^{het}) mice were generated by crossbreeding of CD45.1^{+} and C57BL/6J (CD45.2^{+}) mice.

Transgenic mouse line	**Primer type**	**Primer sequence for confirming genotype**
Ig^{HEL}	Forward-1	5’ gcgactccatcaccagcgat 3’
	Forward-2	5’ ctggagccctagccaaggat 3’
	Reverse	5’ accacagaccagcaggcaga 3’
sHEL	Forward	5’ gagcgtgaactgcgcgaaga 3’
	Reverse	5’ tcggtacccttgcagcggtt 3’
mHEL^{KK}	Forward	5’ gagcgtgaactgcgcgaaga 3’
	Reverse	5’ tcggtacccttgcagcggtt 3’
Grb2$^{f/f}$	Forward	5’ gcacacatgtcctgccttc 3’
	Reverse	5’ acattggtggctcacaacc 3’
Mb1Cre^{+}	Forward-1	5’ ctgcgggtagaaggggtc 3’

	Forward-2	5’ acctctgatgaagtcaggaagaac 5’
	Reverse-1	5’ ccttgcgaggtcagggagcc 3’
	Reverse-2	5’ ggagatgtccttcactctgcttct 3’
Rag1$^{-/-}$	Forward-1	5’ tctggacttgcctcctctgt 3’
	Forward-2	5’ cattccatcgcaagactcct 3’
	Reverse	5’ tggatgtggaatgtgtgcgag 3’
Trp2mHEL	Forward	5' gagcgtgaactgcgcgaaga 3'
	Reverse	5’ tcggtacccttgcagcggtt 3’

Table 2-1 Primers used for PCR-based genotyping of various transgenic mice lines.

2.1.2 DNA extraction

For ear punch DNA extraction, ear punches were first dissected into small pieces. These pieces were incubated with a buffer containing 1 mg/mL of proteinase K (Sigma-Aldrich 3115887001) at 55°C for 40 minutes (min). During the incubation period, the sample mixture was intermittently vortexed every 20 min to ensure efficient lysis. Following the incubation step, DNA samples were diluted in a 1:10 ratio with PCR-grade water and heated to 100°C for 5 min to inactivate the proteinase K enzyme. The resulting DNA solution was aliquoted and stored at -20°C for use in PCR experiments.

2.1.3 Genotyping and PCR

The genotypes of each transgenic mouse were determined through PCR amplification, employing a set of specific primers as listed in **Table 2-1**. For each PCR

reaction, 0.3 µM of the primer was combined with 3.126 µM of dNTPs, 2.5 µM of MgCl2, and 0.025 U/µL of Taq DNA polymerase (Scientific Laboratory Supplies Limited, BIO21060) in a 1X PCR buffer. Additional PCR-grade water was added, and 1 µL of DNA template was introduced to bring the total reaction volume to 24 µL.

Specific PCR protocols were utilized to verify the genotypes of each transgenic mouse strain as indicated in **Table 2-2**.

Mouse genotype:	***Mb1Cre*$^{+}$**	
Step	Temperature	Duration
Initial Denaturation	94°C	3 min
Cycle	35 times	
Denaturation	94°C	60 s
Anneal primers	55°C	60 s
Extension	72°C	60 s
Last Extension	72°C	7 min
Mouse genotypes:	**Ig^{HEL}/sHEL/mHEL^{KK}/Trp2mHEL**	
Step	Temperature	Duration
Initial Denaturation	95°C	5 min
Cycle	35 times	
Denaturation	95°C	10 s
Anneal primers	60°C	30 s
Extension	72°C	30 s

Last Extension	72°C	10 min
Mouse genotype:	***Grb2$^{f/f}$***	
Step	Temperature	Duration
Initial Denaturation	95°C	5 min
Cycle	14 times	
Denaturation	95°C	10 s
Anneal primers	67°C (decrease 0.5°C each cycle)	30 s
Extension	72°C	30 s
Last Extension	72°C	10 min

Table 2-2 PCR protocols for genotyping transgenic mice

2.1.4 RNA extraction and Reverse transcription

For RNA extraction and purification from tissue, the PureLink™ RNA Mini Kit (Invitrogen™, 12183018A) was employed.

The cell suspension was centrifuged at 400 g for 5 min and discard the supernatant. Subsequently, 1 mL TRI reagent™ solution (Invitrogen™ # AM9738) was added into 5-10 X10^6 cells. Cells were homogenized with pestle, followed by a 5 min incubation in the room temperature (RT). The lysate was transferred to a 1.7 mL Eppendorf. 0.2 mL Chloroform was then added into each 1 mL of the solution. The solution was agitated at RT for 2-3 min and centrifuged at 12,000 g for 15 min at 4°C. Once the phase was

separated, the upper phase which contained the RNA was transferred into a RNase free tube from the PureLink™ RNA Mini Kit.

Subsequently, 1 mL ethanol (70%) was added to the tissue homogenate. The homogenate was shaken and mixed to disperse any visible precipitate. A volume of 700 µL of the sample was transferred to a spin cartridge. The cartridge was then subjected to centrifugation at 12,000 g for 15 s at RT.

The flow-through was discarded, and the cartridge was reinserted into the same collection tube. This step was repeated until the entire sample was processed. Subsequently, the purelink DNase mater mix solution was prepared using the PureLink™ DNase set (Invitrogen™ # 12185010). For every 10 million cells, 80ul 1X PureLink DNase was required by diluting 10ul Purelink DNase with 10X DNase I reaction buffer and Rnase-free water. The master mix was then added to each RNA sample in RT for 15 min.

To the spin cartridge, 350 µL of Wash Buffer I was added and centrifuged at 12,000 g for 15 s. After discarding the flow-through, the spin cartridge was placed into a new collection tube. Subsequently, 500 µL of Wash Buffer II with ethanol was added and centrifuged at 12,000 g for 15 s. This step was repeated once more. The cartridge was then centrifuged at 12,000 g for 1 min at RT to remove any remaining liquid. Finally, the spin cartridge was inserted into a recovery tube, and 30-100 µL of RNase-free water was added to the centre of the cartridge. The mixture was incubated at RT for 1 min before being centrifuged for 2 min at 12,000 g at RT. The purified RNA was

measured using a Nanodrop spectrophotometer and stored at -20°C for subsequent analysis.

The RNA product was reverse transcribed with SuperScript IV VILO Master Mix kit (Thermofisher, cat: 11756050). The gDNA digestion reaction mix was prepared with 1 µL of 10X ezDNase buffer, 1 µL of ezDNase enzyme, and an appropriate volume of the RNA template. The RNA mixture was adjusted to 10ul with PCR grade water and incubated at 37°C for 2 min for digestion before placing on ice. Next, 4 µL of SuperScript IV VILO master mix was mixed with 6 µL of Nuclease-free water, and the master mix was added to the RNA mixture. The cDNA reaction was incubated for 10 min at 25°C, followed by 10 min at 50°C, and finally 5 min at 85°C. After incubation, the cDNA was stored at-20°C or used for quantitative PCR (qPCR) reactions.

2.1.5 Immunisation

Sheep red blood cells (SRBC) conjugated to HEL were used to immunize mice for germinal centre assays. SRBC (Fisher Scientific UK Ltd, 12977755) were prepared by washing them with Hank's Balanced Salt Solution (HBSS). Briefly, 5 mL of SRBC were washed three times with 45 mL of HBSS and centrifuged at 2300 rpm for 5 min. After the final wash, the SRBC pellet was resuspended at 10% (volume/volume) packed cell volume (PCV) in conjugation buffer consisting of HBSS with 0.35 M mannitol and 0.01 M NaCl; hence, 10ml buffer for every ml of packed SRBC. HEL was added to the washed SRBC at a final concentration of 2 mg/ml from a stock of 20 mg/ml and allowed to mix at 4°C for 10 min on a rocker. To this mixture, 0.1 mL of a 100 mg/ml

stock of 1-Ethyl-3-(3-dimethylaminopropyl)-carbodiimide (EDCI) was added per mL of the 10% SRBC suspension. The SRBC suspension was incubated on a rocker for 30-60 min at 4°C, followed by four washes with HBSS. HEL conjugated SRBC (SRBC-HEL) were assessed by flow cytometry (FACS) and then resuspended to a concentration of 2 x 10^9 cells/mL. Finally, each mouse received an intraperitoneal injection of 200-300 µL of the conjugated SRBC-HEL on each flank.

2.1.6 Irradiation for chimera experiment

CD45.1$^+$ or CD45.1^{het} recipient mice were subjected to two doses of 4.5 Gy radiation, administered with a 3-hour interval. Each irradiated mouse received an intravenous injection via dorsal lateral tail veins within 24 hr post-irradiation, consisting of a total of 2 million NL/FL cells or 5 million BM cells from appropriate donors in a final volume of 100-200 µL.

NL samples were collected between 0 to 1 day post-birth, processed to form single cell suspensions in RPMI supplemented with 2% fetal calf serum (FCS) and 20mM HEPES (R2). Cells were centrifuged and resuspended in freezing medium (90% FCS with 10% Dimethylsulfoxide (DMSO)) and stored at -80°C for short periods. For experimental use, NL samples were thawed in a 37°C water bath, washed with RPMI supplemented with 10% FCS and 20mM HEPES (R10), counted, and resuspended in Phosphate-Buffered Saline (PBS) at 10-20 million cells/mL.

For BM chimera protocols, fresh hind limb BM samples were collected in R2 on the day of injection, or previously collected frozen BM samples were thawed as necessary. BM cells were washed, counted, and resuspended in PBS at 25-50 million cells/mL. For both NL/FL and BM chimeras, either $CD45.2^+$ donor cells were used to reconstitute the irradiated recipients, or $CD45.2^+$ and $CD45.1^+$ donor cells were mixed at required ratios and injected to generate mixed chimeras. All irradiated recipients were provided with water containing 1% Baytril (Enrofloxacin) for the first 3-4 weeks post-injection. A minimum of 7 weeks was allowed for reconstitution of the immune compartment before phenotyping and analysing various immune cell subsets.

2.1.7 Bromodeoxyuridine (5-bromo-2'-deoxyuridine, BrdU), CellTrace Violet (CTV) and Annexin V labelling

***In vivo* BrdU labelling and detection**

For *in vivo* BrdU labelling of mice, a 10X BrdU-in-water stock solution was prepared (containing 8 mg/mL BrdU and 0.1 g/mL sucrose) and stored at 4°C for up to 2 weeks. Mice were administered BrdU-labelled water at a final concentration of 0.8 mg/mL, with the duration of administration dependent on the specific experiment design. Tissue samples were collected either at the end of the labelling period or after a pre-determined waiting period.

To detect BrdU labelling of cells, single cell suspensions were prepared in R2 solution and cell surface markers were stained as necessary. Cells were washed and fixed

with BD Cytofix/Cytoperm solution (BD #554722) on ice for 15 min (using 100 µL per 1 million cells). Following fixation, cells were washed once with 1X BD Perm/Wash buffer (BD #554723) and resuspended in BD Perm Plus buffer (BD #561651) (using 100 µL per 1 million cells) for 5 min on ice. Cells were subsequently washed with 1X BD Perm/Wash buffer before DNase I treatment (final concentration 300 µg/mL, Merck 310104159001) using 100 µL per 1 million cells and incubating at 37°C for 45-60 min. Cells were washed with 1X BD Perm/Wash buffer and were incubated with anti-BrdU antibodies (diluted at 1:25, using 100 µL per million cells) for 30 min at room RT or overnight (O/N) at 4°C.

CTV Labelling of Live Cells for Proliferation Tracking in Mice

To track the *in vivo* proliferation of transferred cells, single cell suspensions were resuspended in PBS with CTV (Invitrogen C34557) at a dilution of 1:1000 and incubated at 37°C for 20 min before adding 10X volume R10 and incubating a further 5 min at 37°C. Samples were protected from light throughout the staining protocol. Cells were washed 3X with R10, counted and resuspended in PBS before intravenous injection into recipient mice. Proliferation of cells was monitored at indicated time points by flow cytometry analyses and measured as dilution of the CTV dye.

Annexin V and 7-AAD Staining (BioLegend #640930)

For Annexin V and 7-AAD staining, cell sorting buffer without NaAzide was used for washing and staining. After surface staining, cells were washed with 1X Annexin V binding buffer and resuspended at a density of 1-5 x 10^6 cells/mL in 1X Annexin V binding buffer. Then, 5 µL of fluorochrome-conjugated Annexin V was added to 100

µL of cell suspension and incubated at RT for 10 min, protected from light. After a single wash with 1X binding buffer, cells were resuspended in 200 µL of 1X binding buffer, and 5 µL of 7-AAD viability staining solution was added on ice for 5-15 min. Samples were analysed by flow cytometry within 30 min.

2.1.8 Sample processing and long-term storage

All mice were sacrificed under Schedule 1 conditions. Post scarified, the peritoneal cavity was injected with 5mL R2 via a 25G needle prior to opening peritoneal membrane. peritoneal lavage was then collected using a 3mL pipette. Subsequently, an additional 5mL R2 was applied to wash the cavity. Then, whole blood was collected by cardiac puncture and centrifuged at 15,000 g for 15 min. Serum was isolated and stored at -20°C for subsequent analysis. Spleen, lymph node and liver samples were mechanically mashed and filtered through a 70 µm cell strainer, while bone marrow was aspirated using a 25G needle to prepare single cell suspensions. All tissue samples were washed once with R2 in preparation for downstream analysis. Cell counting was performed using white blood cell (WBC) counting fluid (consisting of 1.5% acetic acid and 0.5% methyl violet in water) with the aid of a hemacytometer.

When necessary for downstream applications, tissue samples were subjected to RBC lysis by incubating them for 2 min at RT in RBC lysis buffer (Ammonium–chloride–potassium (ACK) buffer (0.15 M Ammonium chloride, 0.01 M Potassium bicarbonate and 0.0001 M Disodium EDTA, pH 7.2-7.4)). For long-term storage of cell

suspensions, cells were resuspended in freezing medium and samples were stored at -80°C or in liquid nitrogen as necessary.

2.2 Cellular Immunology assays

2.2.1 Magnetic beads-based pan B cell sorting

a) Reagents and kits

Reagent name	**Manufacturer**	**Catalogue No.**	**Additional information**
LS columns	Miltenyi Biotec	130-042-401	
B cell isolation kit, mice	Miltenyi Biotec	130-090-862	
QuadroMACS™ Separator	Miltenyi Biotec	0259014	
MojoSort™ Magnet	BioLegend	480019	
MojoSort™ mouse pan B cell isolation kit II	BioLegend	480088	
MACS buffer (PBE)	Home made		500 ml PBS + 0.5% BSA + 2 mM (final concentration) EDTA

Table 2-3 List of reagent and kit for B cell sorting experiment.

b) B cell isolation with LS columns using Miltenyi Biotec kits

Spleens were processed to prepare RBC-lysed single cell suspensions as previously described, before resuspending the cell pellet in 10ml PBE and counting total WBCs. To ensure optimal cell recovery, cell suspension was centrifuged at 1200 rpm for 5 min at 4°C and the cell pellet was resuspended in 1 mL PBE per 10^8 WBCs.

B cell sorting was performed according to manufacturer's recommendations **(Table 2-3)**. Briefly, 10 µL of a biotinylated antibody cocktail was added for every 10^7 cells. The cell suspension was gently mixed by tapping and subsequently incubated at 4°C or in the refrigerator for 5-10 min (not on ice). During the antibody incubation step, LS columns were placed on magnetic stand and washed with 4 mL PBE. Following the incubation period, 20 µL of anti-biotin-microbeads were added per 10^7 cells. The cell suspension was gently mixed and incubated at 4°C for 10 min. PBE was added to the labelled cell suspension to adjust the volume to a minimum of 1 ml and cells were loaded onto prepared LS columns in magnetic field.

The flow-through, along with a further 2 x 4 mL PBE column washes, were collected as the negative fraction of unlabelled B cells. The LS column was taken off the magnet and an additional 4ml PBE was used to collect labelled non-B cells. B cells and non-B cells were centrifuged at 1200 rpm for 5 min at 4°C. The cells were resuspended in 5 mL R10 for cell counts and for assessing sort purity. Purified B cells were resuspended at required cell density for further analyses or applications.

c) B cell isolation with MojoSort™ kits

RBC-lysed single cell suspensions of splenocytes were prepared as described earlier and cells were resuspended in PBE at 10^8 per mL. A 10 µL aliquot of the Biotin-Antibody Cocktail from MojoSort™ kit was added per 10^7 cells and incubated on ice for 15 min. Streptavidin Nanobeads were resuspended by pulse vortexing at maximum speed and 10 µL of Streptavidin Nanobeads were added per 10^7 cells. The cell suspension was mixed by vortex or by pipetting and incubated on ice for 15 min.

At the end of the incubation, 2.5 mL of PBE buffer was added to the cell suspension and the tube was placed within the MojoSort™ Magnet magnetic field for 5 min. Unlabelled cells were collected by pouring these out while the tube was still within the magnetic field. To maximise yield, the tube was removed from the magnet and a further 2.5 mL PBE was added to resuspend cells. The tube was place again in the magnetic field for 5 min and unlabelled cells were collected. Unlabelled purified B cells were centrifuged at 1200 rpm for 5 min at 4°C. Cells were resuspended in 5 mL R10 for cell counts and for assessing sort purity. Purified B cells were resuspended at required cell density for further analyses or applications.

2.2.2 Flow cytometry staining

Single cell suspensions were resuspended in an appropriate volume of R2. Cell counts were recorded, and 0.5 million cells were aliquoted per well of a 96 well U-bottom plate. The plate was centrifuged at 2000 rpm for 2 min at 4°C to pellet cells before washing 1X with flow cytometry buffer (FACS buffer, HBSS or PBS with 2% FCS,

0.05% NaAzide and 20mM HEPES). All subsequent staining steps were performed while protecting samples from light exposure.

Staining for HEL-binding B cells: To identify HEL-binding B cells, cells were first incubated with 20-25 µL of HEL at 250 ng/ml in FACS buffer, prepared from a 200X stock of 50 µg/ml HEL for 30 min on ice. Samples were washed 3X with 150-200 µL FACS buffer by centrifugation at 2000 rpm, for 2 min at 4°C. To stain for cell surface markers, cells were resuspended in 25 µL of a freshly prepared antibody cocktail mixture and incubated for 30 min on ice. Samples were washed 2X with 150-200 µL FACS buffer by centrifugation at 2000rpm, for 2 min at 4°C. The cells were resuspended in 100-200 µL FACS buffer prior to analysis on a BD FACS Canto10 or BD LSRFortessa X20 flow cytometer. Where cells had been previously incubated with HEL, a fluorophore-conjugated HyHEL9 antibody was included in the antibody cocktail.

2.2.3 Activation of splenocytes by HEL and anti-µ (anti-IgM)

HEL antigen (Sigma, #L6876-5G) (ranging from 0.1 ng/mL to 10,000 ng/mL) or anti-u (Stratech Scientific, #115-005-075-JIR-1mg) (ranging from 10 ng/mL to 10,000 ng/mL) were prepared as 10X stocks in RPMI and stored at 4°C. RBC-lysed single cell suspensions of spleen cells were prepared as described earlier and cells were resuspended at a density of 2 million cells/mL in R10. To prepare antigen at 2X final concentration, 80 µL of R10 was added per well in a 96-well U-bottom plate and 20 µL of the 10X antigen stock solution was added to the corresponding well. To achieve

a final volume of 200 µL per well and a cell density of 0.2 million cells per well, 100 µL of the cell suspension at a density of 2 million cells/mL was added to each well. The border wells of the plate were filled with 200 µL of PBS to allow for loss of volume by evaporation.

The prepared plate of cells was incubated at 37°C in a 5% CO2 environment for a duration of 16 to 18 hours. After the O/N incubation, the cells were centrifuged at 2000 rpm for 2 min, 4°C and washed twice with PBS to remove any residual culture medium. Cells were stained with a cocktail of antibodies as described previously, including antibodies specific to B220 or CD19 to identify B cells and antibodies specific to activation markers such as CD69, CD86, etc., before analysing samples using a BD FACS Canto10 flow cytometer.

2.2.4 Signalling downstream of the BCR: Phospho Flow Cytometry assay

RBC-lysed single cell splenocyte suspensions were resuspended at a concentration of 2.2 x 10^7 cells per mL in R2. Antigens were prepared in R2 at 10X concentration, including HEL at 1, 10, 100, 1000, and 10,000 ng/mL, and anti-µ at 100, 1000, and 10,000 ng/mL. 10 µL of the 10X antigen stocks were added to each well of a 96 well U-bottom plates as appropriate, and the plate was incubated at 37°C for 10 min. Then, 90 µL of the B cell suspension was added to the wells containing the 10X antigen and mixed rapidly by vortexing, before incubation for specified time (e.g., 30 s, 1 min, 3 min, 5 min, 10 min, 15 min).

At the end of the incubation, 100 µL of CytoFix (BD # 554655) was added to each well and mixed thoroughly before incubating on ice for 15 min. Fixed cells were washed twice with FACS buffer to remove excess fixative. To stain cell surface markers, 25 µL antibody cocktail was added to each well, and the plate was incubated on ice for 30 min. Cells were washed twice with FACS buffer before incubating with 100 µL of CytoFix/CytoPerm (BD # 51-2090KZ) for 15 min on ice. Cells were washed twice with 1X Perm/Wash buffer (BD # 51-2091KZ). To stain for intracellular targets, cells were incubated on ice or at 4°C for 60 min to O/N with a 25 µL cocktail of antibodies specific to phosphorylated targets prepared in 1X Perm/Wash buffer. Following intracellular staining, cells were washed twice with 1X Perm/Wash buffer and resuspended in 200 µL FACS buffer in preparation for subsequent data acquisition using a BD FACS Canto10 flow cytometer.

2.2.5 Signalling downstream of the BCR: Calcium Flux assay.

Intracellular calcium flux was assayed by ratiometric analysis of Fura Red™, AM (Invitrogen™, #F3021). To prepare the Fura Red solution, 50 µg of Fura Red was mixed with 91.8 µL of DMSO to create a 500 µM Fura Red solution. A 1 µM Fura Red solution was prepared in HBSS with 0.01% pluronic F127. While 0.5 mL of the RBC-lysed splenocytes was aliquoted as an unstained sample, the remaining cells were resuspended at 10 million cells per ml in 1 µM Fura Red. Since 0.8-1 ml of this cell suspension is required per stimulation condition, total number of cells and volume required were calculated accordingly. Cells were incubated in a 37°C water bath for 30 min prior to washing 2X with HEPES-buffered HBSS (H-HBSS, HBSS with final

concentration of 1 mM $CaCl_2$, 0.5 mM $MgCl_2$, 0.1% BSA, and 10 mM HEPES). Next, a 0.5 mL aliquot was retained as a Fura Red-labelled unstimulated compensation controls and the rest were stained in H-HBSS with an antibody cocktail specific to cell surface markers. Cells were incubated on ice for 30 min and washed twice with H-HBSS before resuspending at 10 million cells per ml in H-HBSS and incubating in a 37°C water bath for 10 min. Fura Red intensities upon excitation with both the blue (488 nm) and violet (405 nm) lasers were recorded on a BD FACS Canto10 flow cytometer to set a baseline for each sample. Pre-warmed 10X antigen (HEL, anti-μ) or 10X stimulation (Ionomycin, Merck Life Science, # I0634-1MG) were added and recording continued for various durations according to the experiment design.

2.2.6 Single cell RNA sequencing (sc-RNASeq): Sample preparation

BM or FL samples were collected and processed immediately for sc-RNASeq experiments. RBC-lysed single cell suspensions were prepared in R2 before counting WBCs. Next, 4 million cells were aliquoted from each sample into 1.7 mL Eppendorf tubes. The cells were centrifuged at 400 g at 4°C for 5 min, and supernatant was discarded. To each cell pellet containing 4 million cells, 1:100 TruStain FcX™ PLUS (anti-mouse CD16/32) antibody was added (2 μL in 200 μL FACS buffer per tube), mixed well, and incubated at 4°C for 10 min. Simultaneously, all Total-Seq (BioLegend) hashtag reagents (HTO) and Total-Seq (BioLegend) or CITE-Seq surface antibodies (ADTs) were centrifuged at 14,000 g at 2-8°C for 10 min.

Each HTO antibody was diluted in a 1:50 dilution in FACS buffer and 50 µL per million cells of the diluted HTO antibody was added to each sample before incubation for 30 min at 4°C. The samples were washed twice with FACS buffer before pooling all the HTO-labelled samples in an equal ratio into a single tube. The pooled sample was washed twice with FACS buffer and centrifuged at 400 g , 4°C for 5 min. An antibody cocktail containing Total-Seq ADTs as well as fluorophore-conjugated antibodies specific to surface markers was prepared in FACS buffer and 100 µL was added per million cells to the pooled and washed sample. After incubation at 4°C for 30 min, the HTO and ADT-labelled sample was washed twice with FACS buffer. Sample was resuspended in FACS sorting buffer (HBSS, 2% FCS, 20mM HEPES) at a concentration of 1 million cells per mL before flow cytometry-based sorting of the target population using a BD FACSAria™ Fusion Cell Sorter. The sorted samples were collected in low DNA-binding 1.7 mL tubes pre-coated with FCS O/N at 4°C and were rinsed with 0.04% BSA in PBS. The sorted pooled samples were counted using the Gibco Trypan blue dead cell exclusion dye to determine viability and live cell numbers. The cell density was readjusted to 1000 cells/µL and the samples were loaded onto the 10X Chromium chip for downstream sc-RNASeq experiment protocols.

2.2.7 Flow cytometry-based cell sorting

An RBC-lysed cell suspension was prepared in R2, and pre-determined number of cells were stained on ice for 30 min with a cocktail of antibodies specific to cell surface targets. Next, cells were washed twice, and the stained cells were resuspended in FACS sorting buffer to achieve a concentration of 1 million cells per

mL before filtering through a 70 µm strainer. Cells were sorted using a BD FACSAria Fusion Cell Sorter and sorted cells were collected in either low DNA-binding 1.7 mL tubes pre-coated with FCS or 4 mL / 15 mL polypropylene tubes. The choice of tube was dependent on factors such as cell volume and downstream application. Sorted cells were immediately mixed to collect cells that may have been deposited in the sides of the tubes and were counted to assess viability and overall quality. Sorted cells were either stored at -80°C in freezing medium or were used for downstream assays.

2.2.8 Single cell partitioning, library construction and gene sequence

Single cell partitioning and library construction were performed with the Computational and Single Cell Genomic Group in Kennedy Institute, University of Oxford, by Moustafa Attar as a collaboration. Chromium Single Cell 5' Reagent Kits (v2 - Dual Index) with Feature Barcode technology for Cell Surface Protein and Immune Receptor Mapping were utilized for this process. The resulting cDNA libraries were sequenced by Novogene (UK) company limited using Novaseq 6000 system (PE150), with a requirement of at least 90% of sequence saturation depth to ensure robust sequencing data.

2.2.9 List of Antibodies used for Flow Cytometry and single cell cellular indexing of transcriptomes and epitopes (CITE-seq) analyses.

Antibody name	**Manufacture**	**Clone**	**Catalogue**	**Dilution**
FITC anti-mouse/human CD45R/B220 Antibody	BioLegend	RA3-6B2	103205	300
PerCP/Cy5.5 anti-mouse/human CD45R/B220 Antibody	BioLegend	RA3-6B2	103236	200
APC/Cy7 anti-mouse/human CD45R/B220 Antibody	BioLegend	RA3-6B2	103224	200
APC anti-mouse/human CD45R/B220 Antibody	BioLegend	RA3-6B2	103212	300
Alexa Fluor 700 anti-mouse/human CD45R/B220 Antibody	BioLegend	RA3-6B2	103232	200
Brilliant Violet 605 anti-mouse/human CD45R/B220 Antibody	BioLegend	RA3-6B2	103244	400
Pacific Blue anti-mouse/human CD45R/B220 Antibody	BioLegend	RA3-6B2	103227	400

Alexa Fluor 700 anti-mouse CD19 Antibody	BioLegend	6D5	115528	200
Alexa Fluor 647 anti-mouse CD19 Antibody	BioLegend	6D5	115522	200
PerCP/Cy5.5 anti-mouse CD19 Antibody	BioLegend	6D5	115534	200
PE anti-mouse CD19 Antibody	BD Biosciences	1D3	557399	300
Alexa Fluor 647 anti-mouse CD19 Antibody	BioLegend	6D5	115522	200
Alexa Fluor 647 anti-mouse IgD Antibody	BioLegend	11-26c.2a	405708	300
APC/Cy7 anti-mouse IgD Antibody	BioLegend	11-26c.2a	405716	300
FITC anti-mouse IgD Antibody	BioLegend	11-26c.2a	405704	300
PE anti-mouse IgD Antibody	BioLegend	11-26c.2a	405706	300
APC anti-mouse IgD Antibody	BioLegend	11-26c.2a	405714	300
Brilliant Violet 421 anti-mouse IgD[a] Antibody	BD Biosciences	AMS 9.1(RUO)	743631	300
BUV661 anti-mouse IgD[a] Antibody	BD Biosciences	AMS 9.1(RUO)	749965	400

Brilliant Violet 605 anti-mouse IgD[a] Antibody	BD Biosciences	AMS 9.1(RUO)	743633	500
PerCP/Cy5.5 anti-mouse IgMa Antibody	BioLegend	MA-69	408612	300
FITC anti-mouse IgM[a] Antibody	BD Biosciences	DS-1	553516	300
Brilliant Violet 605 anti-mouse IgM(a) Antibody	BD Biosciences	DS-1	743887	300
FITC anti-mouse IgM Antibody	BioLegend	RMM-1	406506	300
PE-Cy7 anti-mouse IgM Antibody	BioLegend	RMM-1	406516	300
APC anti-mouse IgM Antibody	BioLegend	RMM-1	406509	300
PE anti-mouse CD5 Antibody	BioLegend	53-7.3	100608	100
PerCP-Cy5.5 anti-Mouse CD43 Antibody	BD Biosciences	S7	562865	100
PE-Cy7 anti-mouse CD43 Antibody	BD Biosciences	S7	562866	100
PE-Cy7 anti-mouse CD43 Antibody	BioLegend	S11	143210	100
Alexa Fluor 700 anti-mouse CD24 Antibody	BioLegend	M1/69	101836	300

Pacific Blue anti-mouse CD24 Antibody	BioLegend	M1/69	101820	300
Pacific Blue anti-mouse CD25 Antibody	BioLegend	PC61	102022	300
PE anti-mouse CD25 Antibody	BioLegend	PC61	102008	300
PE/Cy7 anti-mouse CD45.1 Antibody	BioLegend	A20	110730	100
Pacific Blue anti-mouse CD45.1 Antibody	BioLegend	A20	110722	100
Brilliant Violet 605 anti-mouse CD45.2 Antibody	BioLegend	104	109841	100
Brilliant Violet 510 anti-mouse CD45.1 Antibody	BioLegend	A20	110741	100
APC anti-mouse CD45.2 Antibody	BioLegend	104	109814	100
APC/Cy7 anti-mouse CD45.1 Antibody	BioLegend	A20	110716	100
APC/Cy7 anti-mouse CD45.2 Antibody	BioLegend	104	109824	100
PE/Cy7 anti-mouse CD69 Antibody	BioLegend	H1.2F3	104512	300

Brilliant Violet 605 anti-mouse CD69 Antibody	BioLegend	H1.2F3	104530	300
PerCP/Cy5.5 anti-mouse CD86 Antibody	BioLegend	GL-1	105028	200
Alexa Fluor 647 anti-mouse CD86 Antibody	BioLegend	GL-1	105020	200
APC anti-mouse CD93 Antibody	BioLegend	AA4.1	136510	200
Zombie Aqua Fixable Viability Kit	BioLegend		423102	300
Zombie NIR Fixable Viability Kit	BioLegend		423106	300
Alexa Fluor 700 anti-mouse CD3 Antibody	BioLegend	17A2	100216	300
Brilliant Violet 605 anti-mouse CD21/CD35 Antibody	BD Biosciences	7G6	747763	300
APC/Cy7 anti-mouse CD21/CD35 (CR2/CR1) Antibody	BioLegend	7E9	123418	200
APC anti-mouse CD21/CD35 (CR2/CR1) Antibody	BioLegend	7E9	123411	300

PE anti-mouse CD23 Antibody	BioLegend	B3B4	101608	300
PE/Cy7 anti-mouse CD23 Antibody	BioLegend	B3B4	101614	300
Alexa Fluor 647 anti-mouse CD1d Antibody	BioLegend	1B1	123512	300
PE anti-mouse CD1d Antibody	Life Technologies	1B1	12-0011-82	300
PE/Cy5 anti-mouse CD5 Antibody	BioLegend	53-7.3	100609	100
PE/Dazzle 594 anti-mouse CD9 Antibody	BioLegend	MZ3	124821	300
PerCP/Cy5.5 anti-mouse/rat CD29 Antibody	BioLegend	HMβ1-1	102227	200
APC/Cy7 anti-mouse Ly-6A/E (Sca-1) Antibody	BioLegend	D7	108126	100
Brilliant Violet 785 anti-mouse/human CD11b Antibody	BioLegend	M1/70	101243	200
BUV563 anti-mouse CD1d Antibody	BD Biosciences	1B1	741287	200
PE anti-mouse CD5 Antibody	BioLegend	53-7.3	100608	100

Brilliant Violet 785 anti-mouse CD45.1 Antibody	BioLegend	A20	110743	100
PE/Cy7 anti-mouse CD93 Antibody	BioLegend	AA4.1	136505	200
PE anti-mouse ApoE Antibody	BioLegend	E6D7	803404	100
PE/Cy5 anti-mouse CD3 Antibody	BioLegend	17A2	100273	300
Brilliant Violet 711 anti-mouse CD19 Antibody	BioLegend	6D5	115555	300
APC anti-mouse FCRL5/FcRH3 Antibody	Bio-Techne (R&D Systems)	Polyclonal Sheep IgG	FAB6757A	20
BUV661 anti-mouse CD21/CD35 Antibody	BD Biosciences	7G6	741522	300
BUV395 anti-mouse CD23 Antibody	BD Biosciences	B3B4	740216	300
TotalSeq-C0110 anti-mouse CD43 Antibody	BioLegend	S11	143221	100
TotalSeq-C0103 anti-mouse/human CD45R/B220 Antibody	BioLegend	RA3-6B2	103273	300

TotalSeq-C0093 anti-mouse CD19 Antibody	BioLegend	6D5	115571	200
TotalSeq-C0450 anti-mouse IgM Antibody	BioLegend	RMM-1	406541	200
TotalSeq-C0571 anti-mouse IgD Antibody	BioLegend	11-26c.2a	405747	200
TotalSeq-C0212 anti-mouse CD24 Antibody	BioLegend	M1/69	101843	300
TotalSeq-C0113 anti-mouse CD93 (AA4.1, early B lineage) Antibody	BioLegend	AA4.1	136515	200
TotalSeq-C0107 anti-mouse CD21/CD35 (CR2/CR1) Antibody	BioLegend	7E9	123441	300
TotalSeq-C0198 anti-mouse CD127 (IL-7Rα) Antibody	BioLegend	A7R34	135047	100
TotalSeq-C0097 anti-mouse CD25 Antibody	BioLegend	PC61	102065	100
Total seq-C0987 anti APC antibodies	BioLegend	APC003	408007	100
TotalSeq-C0301 anti-mouse Hashtag 1 Antibody	BioLegend	M1/42;30-F11	155861	100

TotalSeq-C0301 anti-mouse Hashtag 2 Antibody	BioLegend	M1/42;30-F11	155863	100
TotalSeq-C0301 anti-mouse Hashtag 3 Antibody	BioLegend	M1/42;30-F11	155865	100
TotalSeq-C0301 anti-mouse Hashtag 4 Antibody	BioLegend	M1/42;30-F11	155867	100
TotalSeq-C0301 anti-mouse Hashtag 5 Antibody	BioLegend	M1/42;30-F11	155869	100
TotalSeq-C0301 anti-mouse Hashtag 6 Antibody	BioLegend	M1/42;30-F11	155871	100
TotalSeq-C0301 anti-mouse Hashtag 7 Antibody	BioLegend	M1/42;30-F11	155873	100
TotalSeq-C0301 anti-mouse Hashtag 8 Antibody	BioLegend	M1/42;30-F11	155875	100
TotalSeq-C0301 anti-mouse Hashtag 9 Antibody	BioLegend	M1/42;30-F11	155877	100

Table 2-4 Flow Cytometry and CITE-Seq antibodies

2.2.10 Enzyme-linked immunosorbent assay (ELISA)

ELISA reactions were performed according to established protocols with changes to capture and detection reagents as well as buffers and development reagents, depending on the detection target. Serums samples and reference standards were

stored at -20°C and were thawed on ice just prior to dilution. Buffers and reagents were freshly prepared and were stored at 4°C for short periods.

a) Reagents and kits

Reagents	**Manufacturer**	**Catalogue No.**
96 well half area microplates	Greiner Bio	675061
Purified goat anti-mouse IgM capture antibody	Bethyl	A90-101A-22
Mouse reference serum	Bethyl	rS10-101-6
HRP-conjugated Goat anti-mouse IgM antibody	Bethyl	A90-101P-38
Tween-20	Sigma-Aldrich	P1379-1L
Purified goat anti-mouse IgM[a] capture antibody	BioLegend	B257419
Biotinylated anti-mouse IgM[a]	BD Pharmingen	DS-1
Avidin-alkaline phosphatase	Sigma-Aldrich	A7294
TMB substrate solution	ThermoFisher	N301
Sigma104 phosphatase substrate	Sigma-Aldrich	S0942-200TAB

Table 2-5 The purchased reagent list for ELISA assay

b) Buffers and other Reagents:

ELISA Coating buffer: 0.05 M Carbonate-Bicarbonate, pH 9.6.

ELISA sample/conjugate Dilution buffer: 50 mM Tris, 0.14 M NaCl, 1% BSA, 0.05% Tween-20.

ELISA Blocking solution: 50 mM Tris, 0.14 M NaCl, 1% BSA, pH 8.0.

ELISA Stop solution: 0.18 M H_2SO_4.

ELISA Wash Solution: 50 mM Tris, 0.14 M NaCl, 0.05% Tween 20, pH 8.0.

10X PBS: 80 g NaCl, 2.0 g KCl, 14.4 g Na_2HPO_4, 2.4 g KH_2PO_4, add into 800 mL distilled water, then adjust pH to 7.4, and adjust volume to 1 L.

1X PBS: 137 mM NaCl, 2.7 mM KCL, 10.1 mM Na_2HPO_4, 1.76 mM KH_2PO_4.

1% BSA/PBS: 10 mg/mL BSA in sterile 1XPBS 0.2 µm filter-sterilised.

0.1% BSA/PBS: For 200 mL, 20 mL 1% BSA/PBS in 180 mL ddH_2O.

Carbonate buffer: 10 mM Na_2CO_3, 35 mM $NaHCO_3$ pH 9.6.

ICE-T: 1% FCS, 1% milk powder (w/v), 0.1% Tween 20, 0.1%NaN_3 in 1X PBS.

Nitrophenyl phosphate (NPP) buffer: 50 mM Na_2CO_3, 0.5 mM $MgCl_2$ pH 9.8.

PBS/TW: 1X PBS, 0.05% Tween-20.

c) IgM sandwich ELISA

The ELISA plate layout was designed to include a range of dilutions for each serum sample, including, at a minimum, two technical replicates and a range of reference serum dilutions. To set up the assay, 50 µL of purified goat anti-mouse IgM capture antibody (at a 1:100 dilution, prepared in ELISA Coating buffer) was added to each well of a 96 well half-well plate and incubated for 1 hour at RT. Unbound antibody was discarded and the wells were washed five times with ELISA Wash solution. Then, 100 µL of ELISA Blocking solution was added to each well and incubated at RT for 30 min. Following the blocking procedure, 50 µL of serum samples and reference standards

diluted with ELISA Dilution buffer were added to the wells and incubated at RT for 1 hour.

Next, wells were washed five times with ELISA Wash solution and 50 µL of HRP-conjugated goat anti-mouse IgM detection antibody (diluted 1:100,000 in ELISA Dilution buffer), was added to each well and incubated for 1 hour at RT. Then, wells were washed again five times with ELISA Wash solution and 50 µL of 1X TMB was added to each well. The reaction was monitored until the top two to three standards exhibited unequivocal saturation, indicative of assay readiness. Finally, the reaction was terminated with the addition of 50 µL of ELISA Stop solution, and the absorbance at 450 nm was measured using a 96 well plate reader (Biotek ELx808).

d) IgM^a sandwich ELISA

The ELISA was performed as described previously, but with minor changes. Appropriately diluted purified goat anti-mouse IgM^a antibody (at a 1:100 dilution, prepared in ELISA Coating buffer) was used to coat wells, followed by O/N incubation at 4°C. Subsequently, the plates were washed five times with ELISA Wash solution and blocked at RT for 30 min with 100 µL of ELISA Blocking solution. Diluted serum samples and reference standards were added to the wells and incubated at RT for 1hour. On completion of the sample incubation step and following five washes, 50 µL of HRP-conjugated goat anti-mouse IgM detection antibody (diluted 1:100,000) was added to each well and the plates were incubated at RT for 1 hour. Wells were washed again five times and 50 µL of 1X TMB was to each well to allow a colorimetric reaction to develop at RT in the dark. Finally, the reaction was terminated by adding

50 µL of ELISA Stop solution, and the absorbance was recorded at 450 nm using a plate reader (Biotek ELx808).

e) HEL-specific IgM^a sandwich ELISA

The ELISA was performed as described previously, but with changes in the capture and detection protocol. Wells were coated O/N at 4°C with 50 µL of 10 µg/mL HEL solution prepared in carbonate buffer. Wells were washed and blocked with 100 µL of 1% BSA/PBS for 1 hour at RT. Plates were washed three times with PBS/TW and 50 µL of serum samples, diluted in 0.1% BSA/PBS, were added to each well and incubated at 37°C for 2 hours. Wells were washed five times with PBS/TW and 50 µL of biotinylated anti-IgM^a, diluted in ICE-T at a concentration of 0.5 µg/mL, was added to each well, and incubated at 37°C for 2 hours. Wells were washed again five times and 50 µL of avidin-alkaline phosphatase, diluted 1:3000 in 0.1% BSA/PBS, was added to each well and incubated for 1 hour at 37°C. After this final incubation, wells were washed five times with PBS/TW, once with double-distilled water and once with NPP buffer. To develop colorimetric signals, 100 µL of Sigma104 phosphatase substrate in NPP buffer was added to each well and the reaction was monitored and continually recorded at 405 nm using a plate reader (Biotek ELx808).

2.3 Protein detection and quantification

2.3.1 Western blot analysis:

a) Reagents and kits

Reagents and Kit	**Manufacturer**	**Catalogue No**
BCA protein Assay	Thermo Fisher	23225
Tris-HCl Ph 7.4	ChemCruz	D0723
NP-40 Surfact-Amps™ Detergent Solution	Thermo Fisher	85124
Sodium chloride solution, 5M in H2O	Merck	S5150-1L
MgCl2	Sigma-Aldrich	208337-100G
Tris base	Sigma-Aldrich	648311-5KG
Tween20	Sigma-Aldrich	SZBE3240V
Phenylmethylsulfonylfluoride (PMSF) Protease Inhibitor	Thermo Fisher	36978
RIPA Lysis Buffer System	Santa Cruz	sc-24948
NE-PER™ Nuclear and Cytoplasmic Extraction Reagents	Thermo Fisher	78833
Subcellular Protein Fractionation Kit for Cultured Cells	Thermo Fisher	78840
MojoSort™ Mouse Pan B Cell Isolation Kit II	BioLegend	480087
MojoSort™ Magnet	BioLegend	480019
Benzonase® Nuclease	Merck	E1014-25KU

10x reducing buffer	Invitrogen	1692328
4x LDS	Invitrogen	2064200
4–20% Mini-PROTEAN® TGX™ Precast Protein Gels, 15-well, 15 µl	Bio-Rad	4561096
4–20% Mini-PROTEAN® TGX™ Precast Protein Gels, 10-well, 50 µl	Bio-Rad	4561094
12% Mini-PROTEAN® TGX™ Precast Protein Gels, 10-well, 50 µl	Bio-Rad	4561044
10% Mini-PROTEAN® TGX™ Precast Protein Gels, 10-well, 50 µl	Bio-Rad	4561034
Ponceau S Staining Solution	Thermo Fisher	A40000279
Pierce™ BCA Protein Assay Kits	Thermo Fisher	23225
Amersham ECL Western Blotting Detection Kit	Cytiva	RPN2108
Protease Inhibitor Cocktail (PIC tablet)	Roche	4693159001
Phosphatase Inhibitor Cocktail (PhIC) tablet	Roche	4906837001
Cytiva Amersham™ Protran™ NC Nitrocellulose Membranes: Rolls	Fisher scientific	15259804
Filter papers		
Precision Plus Protein Dual Color Standards	Bio-Rad	1610374

Table 2-6 List of Reagents for Protein assays

b) Antibodies used for Western blot analyses

Antibody	**Manufacturer**	**Catalogue No**	**Dilution**
Anti-NFAT2 Rabbit Antibody [7A6]	Abcam	ab2796	1:1000
Anti-NFAT1 Rabbit Antibody	Cell Signaling Technology	4389	1:1000
Anti- Histone H3 Rabbit Antibody	Cell Signaling Technology	9715	1:5000
Anti-GAPDH (14C10) Rabbit Antibody (HRP Conjugate)	Cell Signaling Technology	3683	1:2000
Anti-β-Actin– HRP Mouse monoclonal Antibody	Sigma-Aldrich	A3854	1:5000
Anti-β-Actin Mouse monoclonal Antibody	Sigma-Aldrich	A5441-100UL	1:5000
Anti-GRB2 Mouse Antibody, clone 3F2	Sigma-Aldrich	05-372	1:500
Peroxidase AffiniPure Goat Anti-Rabbit IgG (H+L) Antibody	Jackson ImmunoResearch	111-035-144	1:10000
ZyMAX Streptavidin-HRP Antibody	Invitrogen	43-4323	1:2500

Anti- Phospho-AMPKα (Thr172) (40H9) Rabbit Antibody	Cell Signaling Technology	5256S	1:1000
Anti- AMPKα (D5A2) Rabbit Antibody	Cell Signaling Technology	4811S	1:1000

Table 2-7 List of antibodies for western blot analyses

c) Buffers and other reagents:

Laemmli Loading Buffer (5X, pH 6.8): 2.5 mL 2M Tris-HCL (pH 6.8), 2 g sodium dodecyl sulfate, 100 mg bromophenol blue, 10 mL glycerol, 1.542 g DTT. Dissolve in dH_2O and make up volume to 20 mL. Store 100 µL aliquots of the buffer at -20°C for up to 3 months.

NP-40 lysis buffer: To prepare 10 mL of NP-40-based lysis buffer (stored at 4°C) add 50 mM Tris-HCl (pH 7.4), 1% NP-40, 150 mM NaCl, 20 mM $MgCl_2$ to a final volume of 10 mL dH_2O.

10X SDS-PAGE running buffer: for 2 L total volume, 60 g Tris base (25 mM final 1X), 288 g Glycine (1.92 M), 100 mL 20% SDS (200 mL 10%SDS), add H_20 to 2 L.

10X Transfer buffer: 48.46 g Tris base, 300.28 g glycine (2 M final concentration). Add to 2 L H_2O and store at 4°C. Add 20% methanol when preparing 1X buffer.

TBS-T: 500 mL water, 10 mL Tris HCl (pH7.4), 15 mL 5 M NaCl and 250 ul Tween20.

d) Extraction of total protein from cells in suspension:

To extract total cellular protein from total splenocytes or sorted B cells in suspension, either NP-40 lysis buffer or RIPA buffer were used, depending upon the final

downstream application. To enhance buffer performance and sample stability, 1 tablet each of PIC and PhIC, and 10 µL of PMSF from a 200 mM stock solution (stored at -20°C), were added to 10 mL of buffer.

RBC-lysed single cell suspension of total splenocytes or sorted B cells were counted and defined number of cells were to a clean 1.7 mL tube. Cells were centrifuged and resuspended in 100 µL lysis buffer per 10 million cells. The sample was vortexed for 5 s at maximum speed, followed by incubation on a rotary shaker at 4°C for a minimum of 1 hour to ensure complete lysis. The lysate was clarified by centrifugation at 15,000 g for 5 min and the supernatant was collected, aliquoted and stored at -20°C until further analysis.

e) Extraction of protein from cellular fractions:

Total splenocytes or sorted B cells were washed with ice-cold PBS at 500g for 5-6 min at 4°C, and the supernatant was discarded. Reagent volumes were calculated based on the PCV for each sample. For every 10 µL PCV, 100 µL of CER I, 5.5 µL of CER II, and 50 µL of NEB were required, each containing 1% protease inhibitor.

The cell pellet was resuspended in CER I, vortexed for 15 s and incubated on ice for 10 min. Ice-cold CER II solution was added to the tube and vortexed for 5 s, placed on ice for 1 min, and vortexed again for a further 5 s. Samples were centrifuged at 16,000 g for 5 min to allow separation of the cytoplasmic and nuclear fractions. The supernatant, constituting the cytoplasmic extract, was transferred to pre-chilled tubes and stored at -20°C.

The cell pellet was washed once with ice-old PBS and centrifuged at 16,000 g for 5 min at 4°C. The supernatant was discarded and the pellet, containing the nuclear fraction, was resuspended in ice-cold NER. To extract nuclear proteins, 5X Laemmli loading buffer was added to the nuclear mixture, with 1% Benzonase Nuclease in a 5:1 ratio. Samples were vortexed until the pellet was fully dissolved and aliquots were stored at -20°C for long-term use. For protocols requiring accurate quantification of protein concentration of the nuclear extracts, SDS (to achieve final 5% concentration) and 1% Benzonase Nuclease were added to NER instead of the 5X Laemmli loading buffer. The mixture was incubated at RT for 10-30 min with vortexing and centrifuged at 16,000g for 5 min at 4°C. The supernatant, containing the nuclear fraction, was collected, and stored at -20°C. Protein concentration was quantified using the BCA assay and samples were mixed with 5X Laemmli loading buffer prior to loading onto SDS-PAGE gels.

f) Western blot protocol

Protein samples (5-10 µg) containing 5X Laemmli loading buffer were incubated at 95°C for 5 min to denature and reduce the proteins. Samples were centrifuged for 1 min at 2000 rpm and loaded on TGX™ Precast protein gel along with appropriate protein markers or ladders. Gel concentrations were chosen based on the size of the target proteins. The SDS-PAGE protocol was carried out using standard Bio-Rad apparatus at 200 V for 40 min at RT. After the electrophoretic run, the gel was rinsed and equilibrated in 1X Transfer buffer. A transfer sandwich was assembled with filter papers, nitrocellulose membrane (0.45 µm), equilibrated gel and more filter papers,

cushioned by transfer sponge pads and supported by the grid cassette. The transfer sandwich cassette was placed into the gel tank containing 1X Transfer buffer, ice pack for temperature control and a magnetic stirrer bar. The gel tank was placed on a magnetic stirrer at the lowest setting to ensure continuous mixing of buffer. Electrophoresis was performed at constant 100 V for 1 hour at RT to achieve transfer efficiency of 80-100%.

Once transfer was complete, the nitrocellulose blotting membrane was removed from the cassette with forceps and washed once for 5 min in 25 mL of TBS-T. Protein transfer efficiency was assessed using Ponceau S Staining Solution for 5 min at RT. After visualization, membrane was washed thrice for 5 min each in 25 mL of TBS-T. The membrane was blocked with 5% BSA in TBS-T at RT for 1-2 hour when antibodies specific to phosphorylated epitopes were to be used. For other antibodies, 5% skim milk in TBS-T was used for blocking at RT for 1-2 hour. After blocking, the membrane was washed three times with TBS-T and incubated O/N at 4°C with primary antibodies at indicated dilutions **(Table 2-7)**. After the O/N incubation, the membrane was washed thrice with TBS-T for 5 min each. The membrane was incubated at RT for 1 hr with appropriate secondary antibodies, either HRP-conjugated or fluorophore-conjugated, and diluted in TBS-T (Table 2-7). The membrane was washed three times with TBS-T three times for 5 min each before developing with an ECL detection kit (mixed at a 1:1 ratio between detection reagent 1 and reagent 2) in the dark for 5 min. Luminiscent or fluorescent signals on the membrane were detected using a Bio-Rad Gel-doc Imaging System.

2.4 Sc-RNASeq Bioinformatic analysis

2.4.1 Raw count generation and QC pipeline:

The raw sc-RNASeq data were processed using 10X Cell Ranger Count version 7.0.0. The reference transcriptome mm10-2020-A (dated July 8, 2020) was employed to generate gene expression matrices. An Empty Droplet algorithm was utilized to distinguish between empty droplets and actual cells based on gene expression libraries. Subsequently, a filtered gene expression matrix was constructed, containing only the barcodes associated with detected cells.

For the hashtag library, the raw data was aligned to the HTO reference library to generate the HTO feature barcode matrix. Similarly, surface ADT raw data was mapped to the ADT reference library, resulting in the ADT feature barcode matrix. The three matrices were integrated into a single Seurat object (version 4.0.0) with three distinct assays: RNA, HTO, and ADT[179]. The HTO assay count was normalized within Seurat v4.0.0 through the centred log ratio transformation (CLR) method. Subsequently, demultiplexing was performed using the "HTODemux" function, aiding in the accurate identification of doublets, singlets, and negative cells. The ADT assay was also normalized using the CLR method and subsequent scaling.

To visualise data quality, several metrics were assessed. First, violin plots were generated to visualize RNA feature number (nFeature), RNA count (nCount), and mitochondrial percentage (percent.mt). Cells exhibiting a mitochondrial percentage exceeding 5% were excluded as they were indicative of non-viable cells. Cells

displaying excessively high nFeature and nCount were also removed, as they were suspected to be doublets or mulitplets. Additionally, cells identified as doublets or negatives by the HTO markers were removed from the dataset. Finally, the filtered data objects from different batch samples were merged, to allow analyses of complete datasets.

2.4.2 Dimensional reduction, data integration, and DE gene analysis:

The RNA assay was subjected to log normalization and scaled with regression based on RNA nCount. Initially, Principal Component Analysis (PCA) was employed to reduce the dimensionality of the data, ensuring the extraction and representation of the most informative features. Data clustering was accomplished using the FindNeighbours and FindCluster functions. Initial visualization was achieved through Uniform Manifold Approximation and Projection (UMAP) to inspect potential batch effects across different experiments.

To integrate data from multiple batches, the Harmony algorithm was applied using the RunHarmony function within Seurat. This step removed batch and group variation without early stopping for convergence. Following integration, a new Harmony assay was generated and utilized for clustering and UMAP visualization. However, the log-normalized RNA assay was still utilized for subsequent differential expression (DE) gene analysis and expression profiling. RNA and ADT markers of particular interest were visualized through violin plots and dot plots. The FindAllMarkers function was employed to identify markers that exhibited differential expression across distinct clusters.

Subclusters were created by subsetting the Seurat object. The subsetted data were re-merged and re-integrated using the Harmony algorithm. These data were further normalized by log normalization for RNA assay and CLR normalization for ADT assay. The FindMarkers function was employed to identify differentially expressed genes between clusters and between experiment groups. The top 20 DE genes were selected for visualization through heatmap plots utilizing the "dittoSeq" package[180]. DE genes were also plotted in volcano plots using the ggplot2 package.

2.4.3 Gene enrichment analysis:

For the gene enrichment analysis, the R packages "clusterProfiler," "org.Hs.eg.db," "ReactomePA," and "org.Mm.eg.db" were employed[181, 182, 183, 184]. Initially, lists of differentially expressed (DE) genes were filtered to include only those with adjusted p-values less than 0.05. The mouse gene list was converted to a human gene list using the mapIds() function. Subsequently, gene enrichment analysis was conducted using the enrichGO() function, enrichKEGG() function, and enrichPathway() function. From the enriched results, the top 10 upregulated pathways and the top 10 downregulated pathways were selected. These pathways were visually represented using the ggplot2 package.

2.4.4 Cell cycle analysis:

Cell cycle markers have been previously classified and defined in hematopoietic stem cells[185], and were categorized as S phase and G2/M phase gene lists. These

gene lists were used to calculate cell cycle score with CellCycleScoring() function. Each cell was assigned a cell cycle identity after calculation. UMAPs were generated based on the assigned cell cycle identities for visualization.

2.4.5 Trajectory analysis:

Monocle3 software was employed for trajectory analysis[186]. The SeuratWrapper interface was utilized to apply Monocle3 functions to Seurat object type data. The RNA data from the Seurat object was transformed using the as.cell_data_set() function and converted to a Monocle3-compatible cell_data_set object, ensuring integration of the two analysis platforms. To enhance the downstream analyses, the estimate_size_factor() function was applied. Following size factor estimation, cells were reclustered using UMAP and the cluster_cells() function. This step enabled the identification of distinct cell populations based on their transcriptional profiles.

To unravel the temporal order of cellular states and transitions, the pseudo-time was calculated. This step was accomplished through the combined use of the learn_graph() and order_cells() functions.

2.5.6 Data visualization:

To plot data and for visual representation as figures, ggplot2, Seurat, and dittoSeq package were employed. The ggplot() function served as the foundation, complemented by geom_point() for plotting individual data points in a UMAP plot. For

added context, geom_density2d() was applied to generate contour plots. To ensure legibility and minimize label overlap, the geom_text_repel() function was integrated. The scale_colour_viridis_c() function was employed to enhance colour contrast. The dittoSeq package was used to visualise the DE genes. The dittoHeatmap() function was employed to construct heatmap visualizations.

2.5.7 Single cell BCR sequence analysis:

For single cell BCR sequence analysis, the filtered contig data (contained only confident high quality data) generated by Cell Ranger VDJ (Cellranger-7.0.0) was utilized. BCR sequence was mapping using IgBLAST (version 1.18.0) against IMGT reference (Version 3.1.37). ChangeO package (version 1.2.0) was subsequently applied to define clonotypes and germline sequences.

2.5.8 Package version record

Computing resources were provided by Biomedical Research Computing (BMRC), University of Oxford. For data analysis, Miniconda and Mamba were used to manage environments and maintain version fidelity across the software packages used **(Table 2-8)**. The version of related software and packages were as listed below:

R: version 4.1.2

R studio: version 2023.09.1+494

Package name	Version	build string
r-terra	1.5_21	r41hd904c4b_0

r-testthat	3.1.3	r41h7525677_0
r-tfisher	0.2.0	r41hc72bb7e_1
r-th.data	1.1_1	r41hc72bb7e_0
r-threejs	0.3.3	r41hc72bb7e_1
r-tibble	3.1.6	r41hcfec24a_0
r-tidygraph	1.2.0	r41h7525677_0
r-tidyr	1.2.0	r41h03ef668_0
r-tidyselect	1.1.2	r41hc72bb7e_0
r-tidyverse	1.3.1	r41hc72bb7e_0
r-timedate	3043.102	r41hc72bb7e_1002
r-tinytex	0.38	r41hc72bb7e_0
r-tmvnsim	1.0_2	r41h859d828_3
r-tsp	1.2_0	r41h06615bd_0
r-tweenr	1.0.2	r41h03ef668_0
r-tzdb	0.3.0	r41h7525677_0
r-units	0.8_0	r41h03ef668_0
r-usethis	2.1.5	r41hc72bb7e_0
r-utf8	1.2.2	r41hcfec24a_0
r-uuid	1.1_0	r41h06615bd_0
r-uwot	0.1.11	r41h03ef668_0
r-vctrs	0.4.1	r41h7525677_0
r-vipor	0.4.5	r41hc72bb7e_1003
r-viridis	0.6.2	r41hc72bb7e_0

r-viridislite	.4.0	r41hc72bb7e_0
r-vroom	1.5.7	r41h03ef668_0
r-waldo	0.4.0	r41hc72bb7e_0
r-warp	0.2.0	r41hcfec24a_1
r-webshot	0.5.3	r41hc72bb7e_0
r-whisker	0.4	r41hc72bb7e_1
r-withr	2.5.0	r41hc72bb7e_0
r-wk	0.6.0	r41h03ef668_0
r-xfun	0.30	r41h7525677_0
r-xml	3.99_0.9	r41h06615bd_0
r-xml2	1.3.3	r41h03ef668_0
r-xopen	1.0.0	r41hc72bb7e_1003
r-xtable	1.8_4	r41hc72bb7e_3
r-yaml	2.3.5	r41h06615bd_0
r-zip	2.2.0	r41hcfec24a_0
r-zoo	1.8_10	r41h06615bd_0
readline	8.1	h46c0cb4_0
sed	4.8	he412f7d_0
snappy	1.1.9	hbd366e4_1
r-shiny	1.7.1	r41h785f33e_0
sqlite	3.37.0	h9cd32fc_0
sysroot_linux-64	2.12	he073ed8_15
tiledb	2.7.2	h3f4058f_0

tk	8.6.12	h27826a3_0
tktable	2.10	hb7b940f_3
tzcode	2022a	h166bdaf_0
r-seurat	4.1.0	r41h03ef668_0
r-seuratobject	4.0.4	r41h03ef668_0
r-sf	1.0_7	r41h46eb27f_0
r-monocle3	1.0.0	r41h9f5acd7_2
r-viridis	0.6.2	r41hc72bb7e_0
r-viridislite	0.4.0	r41hc72bb7e_0
r-shinyace	0.4.1	r41hc72bb7e_1
r-shinybs	0.61.1	r41hc72bb7e_0
r-shinydashboard	0.7.2	r41hc72bb7e_0
r-sitmo	2.0.2	r41h03ef668_0
r-slam	0.1_50	r41hb699f27_1
bioconductor-s4vectors	0.32.3	r41h5c21468_0

Table 2-8 List of Seurat and R packages used for bioinformatic analyses.

Chapter 3 Deficiency in GRB2 leads to increased B1b B cells and MZ B cells.

3.1 Introduction

As mentioned in the introduction chapter, B1 B cells differ from B2 B cells in function and ontogeny. B1 B cells are mainly generated in the early stages of life with higher potential for reactivity against self or common pathogens, which may germline-encoded, and typically secrete IgM or IgA antibodies as part of the pre-immune repertoire[88].

Understanding the key elements and critical milestones involved in B1 B cell development may help us understand and explain the origin of their unique functions. To answer this question, a good starting point are mice models that have perturbed B1 B cell ontogeny with either increased or reduced production of B1 B cells. Considering the ability of B1 B cells to spontaneously secrete IgM antibodies without stimulation by antigen[187], the presence of raised serum IgM levels without a change in IgA and IgG titres might be indicative of a potential B1 B cell phenotype.

As described in the introduction to this thesis, GRB2 is a ubiquitously expressed protein in eukaryotic cells and is involved in multiple critical signalling pathways[188] as well as BCR-related signalling[170]. The systemic deletion of GRB2 leads to embryonic lethality due to its critical functions in the early stages of development[159]. Using the Cre/loxP system, B cell-specific GRB2 knock-out mice (KO) were generated by

crossing the *Mb1cre*$^{+}$ mice with *Grb2*$^{f/f}$ mice[169]. According to Nitschke and colleagues, B cell-specific deletion of GRB2 did not significantly impair the development of B2 B cells, although the total number of mature B cells in BM, and transitional and FO B cells in the spleen were reduced. However there was a significant increase of serum IgM titres, without changes in the levels of other isotypes[169]. This was associated with increased B cell signalling, notably an exaggerated Ca^{2+} flux, which has been described as due to the involvement of GRB2 in DOK3-dependent negative regulation[189, 190]. However, there were no observable changes in the numbers of B1a B cells ($CD5^{+}IgM^{+}$) or in the combined population of B2 B and B1b B cells ($CD5^{-}IgM^{+}$) within peritoneal lavage samples [169].

Since increased levels of IgM can be a strong indicator of excessive production of B1 B cells, we decided to revisit the number of B1 B cells in mice lacking GRB2 in a B cell specific manner.

3.2 Knock out of GRB2 reduces the number of FO B cells while increasing MZ B cell numbers.

Grb2$^{f/f}$ mice were created by Dr. Lars Nitschke (University of Erlangen, Germany) and given to us as a gift. *Grb2*$^{f/f}$ mice were crossed with *Mb1Cre*$^{+}$ mice, which express the *Cre* recombinase gene under the *Cd79a* promoter, to generate *Grb2*$^{f/f}$*Mb1Cre*$^{+}$ (KO) mice. The *Cd79a* promoter allows *Cre* expression as early as from the pro B cell stage, and this system shows a high efficiency of gene deletion throughout B cell development and differentiation.

To control for unforeseeable effects of either the *Grb2* floxed allele or the *Cre* cassette in the *Cd79a* gene on B cell development, both *Mb1Cre*$^{+}$ (WT) and *Grb2*$^{f/f}$ mice were used as controls. To validate the knockout efficiency, B cells were sorted from the spleens of adult KO, WT and *Grb2*$^{f/f}$ mice before lysing cells to extract the total cellular proteins. Western blotting confirmed loss of GRB2 protein in B cells from KO mice (**Figure 3-1**).

Figure 3-1

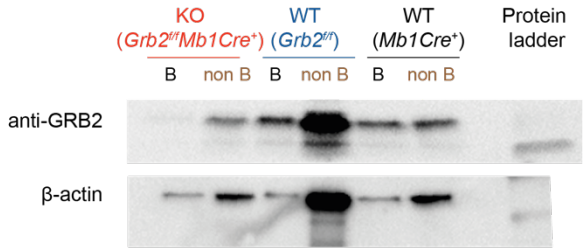

Figure 3-1 Loss of GRB2 expression in B cells from Grb2$^{f/f}$ Mb1Cre^{+} (KO) mice.

Representative western blot analysis confirming B cell-specific loss of GRB2 expression in splenic B cells. Splenocytes from KO (Grb2$^{f/f}$ Mb1Cre^{+}) and WT (Grb2$^{f/f}$ or Mb1Cre^{+}) mice were fractionated into B cells and non-B cells. The samples were probed with antibodies specific against mouse GRB2 or β-actin. This panel is representative of data from three independent experiments.

Flow cytometry confirmed the published findings. GRB2-deficiency resulted in loss of FO B cells in the spleen, and an approximately three-fold increase in the number of MZ B cells (**Figure 3-2A and Figure 3-2B**). In terms of B2 B cell development in the BM, KO mice have similar proportions of Fr.A or pre-pro B cells (B220^{+}CD43^{hi}BP-1^{low}CD24^{low}), Fr.B or early pro B cells (B220^{+}CD43^{hi}BP-1^{low}CD24^{hi}) and Fr.C or late pro B/ large pre B cells (B220^{+}CD43^{hi}BP-1^{hi}CD24$^{-/low}$) compared to the two control groups.

Interestingly, a significantly higher proportion of Fr.D or small pre B cells ($B220^{+}CD43^{low}IgM^{low}IgD^{low}$) were observed in KO mice, alongside decreased Fr.F or mature B cell ($B220^{+}CD43^{-}IgD^{+}$) numbers (**Figure 3-3A and Figure 3-3B**). However, no significant reduction in the number of Fr.D cells was recorded in these mice. Speculatively, this might suggest a block during development from Fr.D to Fr.E in the absence of GRB2, especially since subtle changes in this population may not be detected by flow cytometry analysis.

Figure 3-2

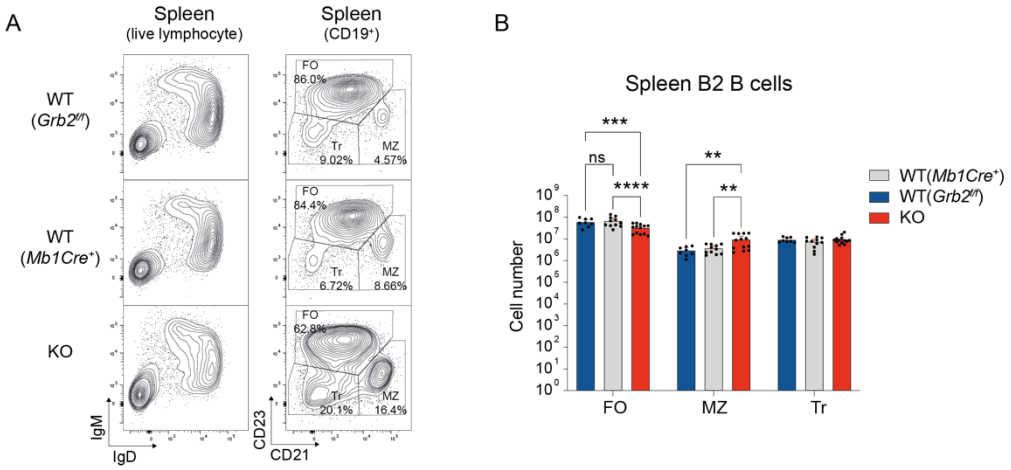

Figure 3-2 Fewer FO and more MZ splenic B cells in GRB2 KO mice.

*(A) Representative flow cytometry plots for live lymphocytes (left panel) and B cells (right panel) from indicated groups: $Grb2^{f/f}$, $Mb1Cre^{+}$ and KO mice. FO are gated as live $CD19^{+}CD23^{hi}CD21^{-/int}$, MZ gated as live $CD19^{+}CD23^{int}CD21^{hi}$, and Tr (transitional B cell) gated as live $CD19^{+}CD23^{-/low}CD21^{-/low}$. (B) Absolute numbers of Tr, FO and MZ spleen B cells within the three indicated groups. The bars represent the means, dots indicate data from individual mice and error bars depict 95% confidence limits. Statistical testing was performed using two-way ANOVA with **P<0.01, ***P<0.001 and ****P<0.0001.*

Figure 3-3

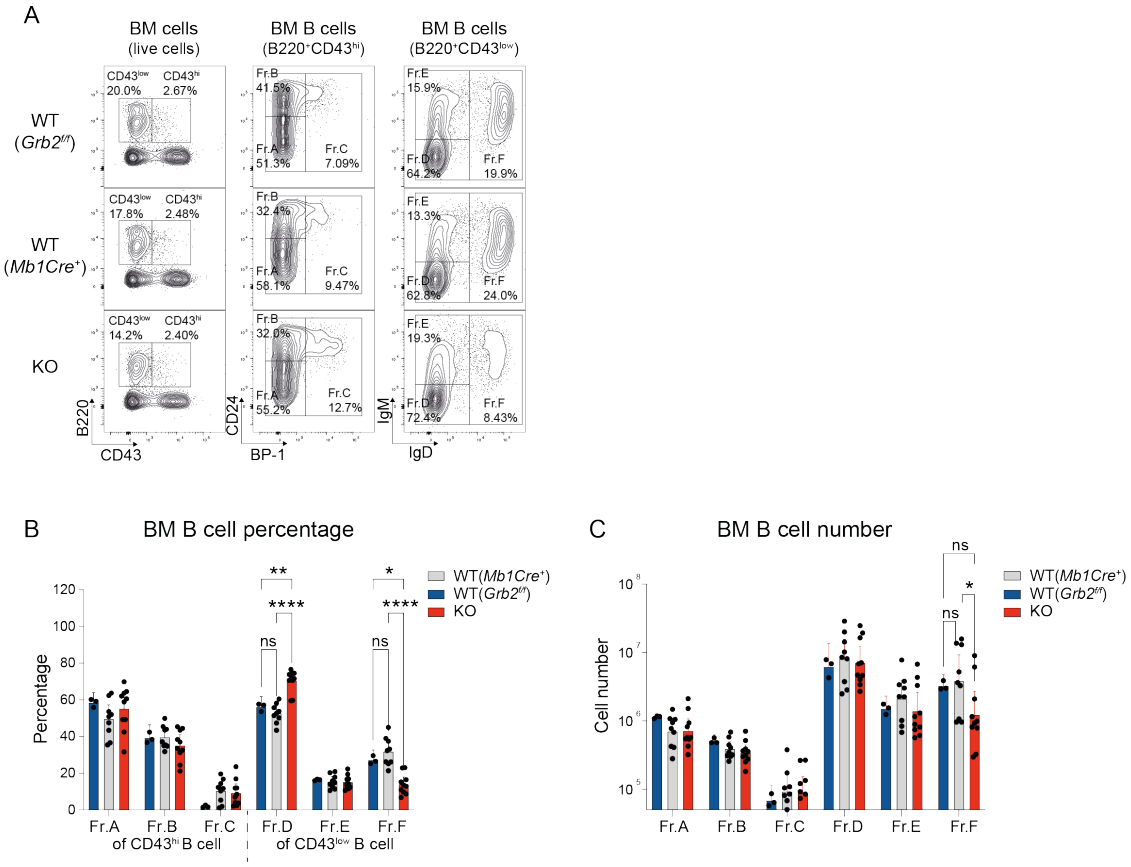

Figure 3-3 Altered BM B cell maturation with fewer mature B cells in GRB2 KO mice.

*(A) Representative flow cytometry plots for total live (left panel), CD43^{hi} (middle panel) and CD43^{low} (right panel) BM B cell populations from indicated groups: Grb2$^{f/f}$, Mb1Cre^{+} and KO. B220^{+} BM B cell subsets were further defined as follows: Fr.A as CD43^{hi}BP-1^{low}CD24^{low}; Fr.B as CD43^{hi}BP-1^{low}CD24^{hi}, Fr.C as CD43^{hi}BP-1^{hi}CD24$^{-/low}$, Fr.D as CD43^{low}IgM^{low}IgD^{low}, Fr.E as CD43^{low}IgM^{hi}IgD^{low} and Fr.F as CD43^{low}IgM^{+}IgD^{hi}. The proportions of cells within each subset in this representative example are indicated on the plots. (B) Pooled data for the percentage of Fr.A, Fr.B and Fr.C B cells within CD43^{hi} B cells (B220^{+}CD43^{hi}), and the percentage of Fr.D, Fr.E and Fr.F B cells within CD43^{low} B cells (B220^{+}CD43^{low}) in the BM of mice from indicated groups: Grb2$^{f/f}$, Mb1Cre^{+} and KO mice. (C) The absolute numbers of Fr. A, Fr.B, Fr.C, Fr.D, Fr.E and Fr.F B cells in BM across three mouse groups: Grb2$^{f/f}$, Mb1Cre^{+} and KO mice. For both (A) and (B), bars represent means with error bars showing the 95% confidence limits, and symbols indicate individual data points. Statistical analysis was performed using a two-way ANOVA: *P<0.05, **P<0.01, and ****P<0.00001.*

3.3 GRB2 deficiency is associated with a raised serum IgM concentration and increased B1b B cells

Since one of the most interesting results reported by the Nitschke group was an increase in serum IgM levels in unimmunised mice kept in SPF conditions, serum was collected from the KO and control mice that had not been exposed to any known antigens. As previously reported, KO mice had almost ten times higher IgM than mice from both control groups (**Figure 3-4A**).

It was first considered whether the higher IgM titre might be due to the increased MZ B cells in KO mice, since MZ B cells are capable of differentiating into IgM-producing plasma cells on a large scale[48]. However, the secretion of IgM antibodies by MZ B cells is typically a result of activation by commensal antigens and often results in additional secretion of other isoforms, such as IgG and IgA[191]. The absence of any obvious exposure to pathogens and the absence of other forms of antibodies[6] make this scenario less likely. Comparison of MZ B cell numbers and serum IgM titres in individual mice did not show a strong correlation (**Figure 3-4C**).

In contrast, B1 B cells were increased three-fold in the peritoneal cavity, and the majority of these were $CD5^-$ B1b B cells (Five-fold increase) (**Figure 3-5**). As previously reported, B1a B cells in the KO mice remained at a similar level as those in control groups[169]. B1b B cell numbers also showed stronger correlation with serum IgM titres (**Figure 3-4B**)**.** These observations, alongside evidence of similarly higher IgM titres in other mice strains with elevated B1b B cells, were highly consistent with the

increased B1b B cells in the GRB2 KO mice being the origin of the high IgM antibody levels. Interestingly, the correlation between MZ B cells numbers and B1b B cells number were also strong in the mice (**Figure 3-4D**), suggesting that these two populations might have a closer relationship during ontogeny.

Since there weren't significant differences between the two control groups, *Mb1Cre*$^{+}$ was used as the WT control for all subsequent experiments.

Figure 3-4

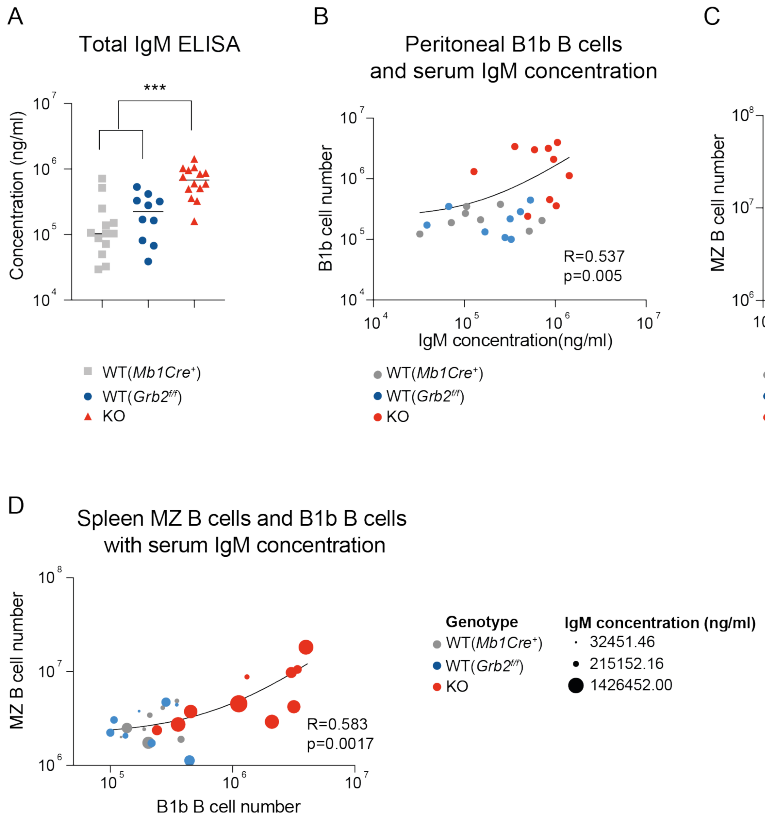

Figure 3-4 Higher serum IgM titres in GRB2 KO mice.

*(A) The serum IgM concentration for Grb2$^{f/f}$, Mb1Cre^{+} and KO mice. Each dot indicates data from an individual mouse. Statistical analysis was performed using unpaired t-test: ***P < 0.001. (B) The scatter plot shows the correlation between B1b B cell numbers and serum IgM concentration of individual Grb2$^{f/f}$, Mb1Cre^{+} and KO mice. (C) The scatter plot shows the correlation between MZ B cell numbers and serum IgM concentration of individual Grb2$^{f/f}$, Mb1Cre^{+} and KO mice. For (B) and (C), The curve line indicates the linear correlation between these two factors. Spearman correlation analysis was performed with an R value reported*

for the Spearman correlation coefficient. Statistical testing was performed with a two tailed t-test and p values are reported. (D) The scatter plot depicts the MZ and B1b B cell numbers from individual Grb2$^{f/f}$, Mb1Cre^{+} and KO mice with the serum IgM titres represented by the size of each dot. Spearman correlation analysis was performed with an R value reported for the Spearman correlation coefficient. Statistical testing was performed with a two tailed t-test. Data are pooled from three independent experiments.

Figure 3-5

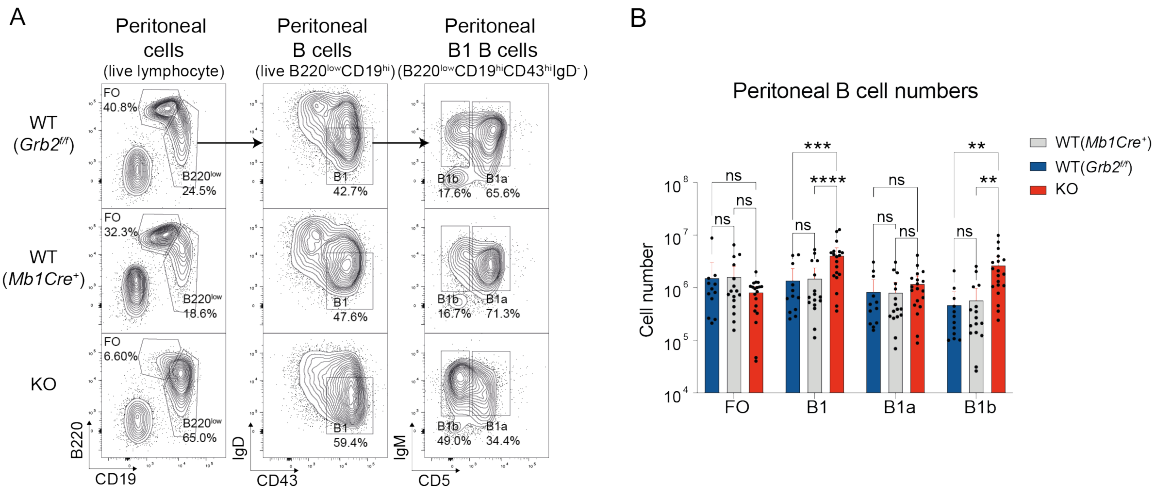

Figure 3-5 Elevated peritoneal B1 B cell numbers, specifically B1b B cells, in GRB2 KO mice.

*(A) Representative flow cytometry plots of peritoneal lavage cells with live lymphocytes (left panel), peritoneal B220^{low}CD19^{hi} B cells (middle panel) and B1 B cells (right panel) isolated from Grb2$^{f/f}$, Mb1Cre^{+} and KO mice. Peritoneal cell populations were defined as FO B cells (live CD19$^{med/low}$B220^{hi}), B1 B cells (live CD19^{hi}B220^{low}CD43^{hi}IgD^{low}), B1a B cells (CD19^{hi}B220^{low}CD43^{hi}IgD^{low}CD5^{hi}), B1b B cells (CD19^{hi}B220^{low}CD43^{hi}IgD^{low}CD5^{low}). The proportion of each population is indicated on the representative plots. (B) The absolute numbers of FO, B1, B1a and B1b B cells in the peritoneal cavity of mice. The bars represent means with error bars indicating 95% confidence limits, and symbols indicating individual data points. Statistical analysis was performed using a two-way ANOVA: **P<0.01, ***P<0.001, ****P<0.0001.*

3.4 GRB2 suppresses the development of B1b B cells from adult BM, enforcing the ontogenetic switch in B cell development.

Under normal circumstances B1 B cells (both B1a and B1b B cells) can only be efficiently generated from fetal liver during early stages of ontogeny[192]. To establish whether the increased number of B1b B cells in the absence of GRB2 might be due to sustained B1b B cell development during later life, lethally irradiated WT CD45.1$^{+/-}$/CD45.2$^{+/-}$ recipient mice (CD45.1^{het}) were reconstituted with CD45.1^{+} WT BM mixed at a 50:50 ratio with either CD45.2^{+} KO or CD45.2^{+} WT BM. After 8 weeks of reconstitution, there were on average five times more B1b B cells derived from KO donor BM compared to WT donor BM in the mixed chimeras (**Figure 3-6**).

This result indicates that there is a failure to turn off B1b B cell development in the absence of GRB2. Hypothetically, this could be due to the loss of a function required to establish the ontogenetic switch, perhaps involving the well-described *Lin28b/let-7* pathway, or a gain of function that restores B1b B cell development or selection via an independent mechanism.

Whilst previous studies have shown that BM has limited ability to reconstitute B1 B cell, and the B1b B cells were generated more in comparison with B1a B cells from BM[90]. Our data only showed that slightly more B1b B cells were generated from WT adult BM, compared to the proportion of B1b B cells in unmanipulated adult mice (**Figure 3-6E**). Given the significant increase in the proportion of KO B1b B cells it is likely that GRB2 specifically inhibits the production of B1b B cells.

3.5 The increase in B1b B cells in the absence of GRB2 is B cell intrinsic.

The lethally irradiated WT mice reconstituted with 50:50 mixtures of CD45.1$^+$ WT BM and CD45.2$^+$ KO or WT also provided a useful test for whether the B cell-specific effects of GRB2 deficiency operated *in cis* or *in trans*. Excessive B1b B cells were exclusively generated from CD45.2$^+$ KO BM (**Figure 3-6**) despite recipients being reconstituted with WT and KO mixtures, indicating that the effects of GRB2-deficiency on B1 B cell development are B cell-intrinsic.

Figure 3-6

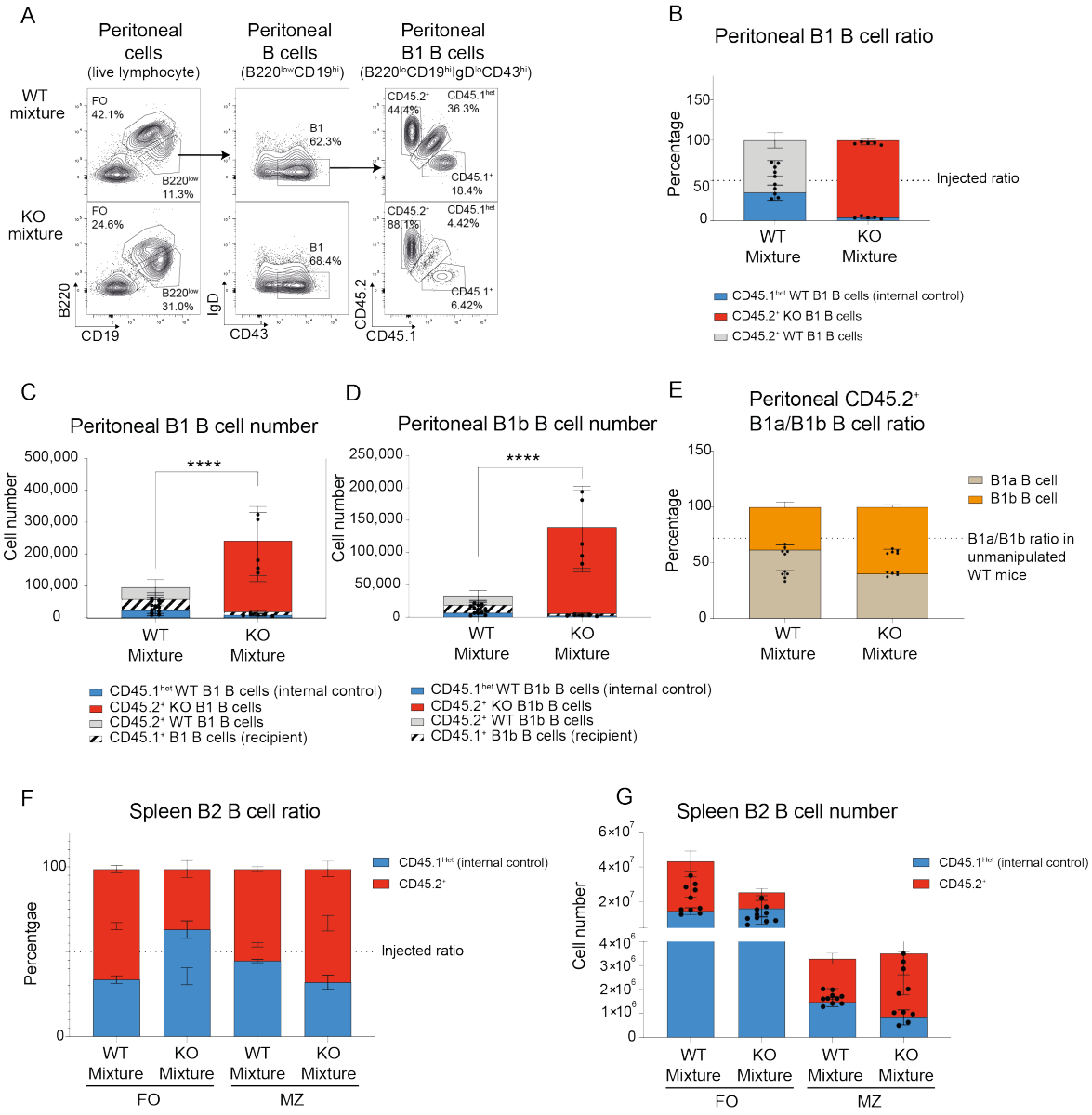

Figure 3-6 The increase in B1b B cells in the absence of GRB2 is not affected by ontogeny.

Irradiated CD45.1^{het} WT mice were reconstituted for 8 weeks with 50:50 mixtures consisting of CD45.1^{+} WT BM and either CD45.2^{+} Mb1Cre^{+} BM (WT mixture) or CD45.2^{+} KO BM (KO mixture), and peritoneal lavage, BM, and spleen. (A) Representative flow cytometry plots for live lymphocytes (left panel), total B cells (middle panel) and B1b B cells from the peritoneal cavity of the two groups of irradiated mice that had received either a WT or KO BM mixture. Percentages indicate the proportion of each subset within the representative sample. (B) The ratio of CD45.2^{+} and CD45.1^{+} B1 B cells recovered from the peritoneal cavity of reconstituted mice with the dotted line indicating the input ratio of CD45.2^{+} and CD45.1^{+} B cells in the WT and KO BM mixtures at the time of injection. (C) The absolute numbers of B1 B cells and (D) the absolute numbers of B1b B cells in peritoneal cavity of in the peritoneal cavity of mice reconstituted with WT or KO mixture. (E) The ratio between B1a and B1b CD45.2^{+} B cells recovered from the peritoneal cavity of mice reconstituted with WT and KO BM mixtures. The dotted line indicates the ratio of B1a and B1b B cells observed in WT unmanipulated mice.

*(F) Ratio of FO and MZ B2 B cells and (G) absolute numbers of FO and MZ B2 B cells from spleens of mice reconstituted with WT or KO mixtures. The dotted line indicates the input ratio of CD45.2$^+$ and CD45.1$^+$ B cells in the WT and KO BM mixtures at the time of injection. For B-G, bars represent means with error bars indicating 95% confidence intervals, and symbols indicating individual data points. Statistical analysis was performed using a two-way ANOVA: ****P<0.0001.*

3.6 Discussion

In this chapter, previously published results including the elevated serum IgM titre, the loss of FO B cells and an increase in MZ B cells in the spleen upon B cell-specific deletion of GRB2 were confirmed[169]**.** The ten-fold increase in IgM levels correlate with an approximately five-fold increase of B1b B cells, but not B1a B cells, in the absence of GRB2. The correlation between IgM titres and B1b B cell numbers suggests that B1b B cell derived plasma cells are likely to be the source of the elevated IgM.

Further, B1b B cells are produced from adult BM in the absence of GRB2, while B1a B cell development from adult-origin tissue remains suppressed. These findings additionally show that GRB2 negatively regulates the development of B1b B cells during ontogeny without affecting the development of B1a B cells, which may be consistent with qualitatively or quantitatively distinct origins and/or signalling pathways regulating B1b vs B1a B cell development.

Under the lineage and selection models for the origin of B1 B cells, development in early ontogeny can occur through entirely intrinsic mechanisms or through positive selection by self-antigens. However, the mechanisms by which these intrinsic

mechanisms or self-antigens cause positive and negative selection during early and late ontogeny might additionally be affected by GRB2-mediated pathways.

Chapter 4 : The generation of B1b B cells in the absence of GRB2 is both spontaneous and driven by positive selection by self-antigen.

4.1 Introduction

As described in the introduction, the B1 B cells appear to arise from a different development pathway than B2 B cells. However, although the development of B1 B cells is increasingly better understood, the key elements underlying their selection remain unclear. Current evidence suggests that B1 B cells are primarily generated from developmentally early-stage tissue and have BCRs that are germline encoded, often reactive to common pathogens, possibly hyper-excitable and weakly self-reactive.

Historically, two theories have been proposed to explain B1 B cell development: a lineage model and a selection model[88]. The lineage model proposes that unique B1 B cell progenitors exist predominantly present in early-stage tissue and can only give rise to B1 B cells. The evidence in support of this theory arises from the apparent failure to generate B1 B cells from BM progenitors[55] and the identification of a possible B1 B cell progenitor, which mainly exists in early stage life[193]. According to the selection theory, B1 B cell populations are shaped and positively selected by antigen exposure[97, 194], and the interaction between specific BCR and self-antigen

determines the fate of the B1 B cell. On balance, most evidence suggests that a combination of early stage tissue and encounter with antigen may be required to generate B1 B cells[102, 109]. How this is explained mechanistically is not clear.

Animal models with defined BCRs provide a useful way to investigate effects of BCR and antigen interactions on B1 B cell generation. There are several commonly used immunoglobulin transgenic mouse models, including the MD4 Ig^{HEL} transgenic mouse, which expresses BCR heavy and light chain specific to HEL[195], a foreign protein not expressed in mice; the 3-83 Ig mouse, which carriers a productive BCR recognizing MHC class I antigens H-$2K^k$ and H-$2K^b$, but not H-$2K^d$ [196]; the anti Thy-1 (CD90) transgenic mouse, in which the presence of an anti Thy-1 transgenic heavy μ chain leads to the generation of anti-thymocyte autoantibody (ATA), a type of antibody typically secreted from B-1 B cells[197]; and transgenic mice expressing BCRs specific to phosphatidylcholine (PtC)[198], the ubiquitous self-membrane phospholipid. The latter three mouse models express transgenic BCRs against naturally occurring self-antigens.

Since HEL is not naturally present in mice, the introduction of HEL as a transgene and the comparison of such mice with non-transgenic controls enables us to test for positive and negative selection as well as the timing of these events in ontogeny and cell development. A variety of HEL transgenic mice express HEL as a neo self-antigen with differing avidity and concentrations, and in different forms and locations have been described[103, 195, 199]; four distinct HEL-transgenic mouse models were used in this study to investigate the role of GRB2 in the positive selection of B1 B cells. Since

the Ig^{HEL} transgene was derived from a BALB/c hybridoma, its heavy chain is characterised by the IgM^a and IgD^a BCR allotype, rather than the IgM^b and IgD^b BCR allotype of C57BL/6 mice. This provides an additional way to identify Ig^{HEL} B cells expressing the transgenic BCR heavy chains[195].

In previous studies of mice co-expressing the Ig^{HEL} transgene and an ER-restricted intracellular membrane bound self-antigen ($mHEL^{KK}$), anti-HEL specific B1 B cells were positively selected by the antigen from fetal or neonatal stage tissue in the presence of intracellular membrane-bound self-antigen, whereas the same antigen induced negative selection from adult tissue[102]. In this chapter, I investigated the role of GRB2 during the positive selection of B1 B cells by the $mHEL^{KK}$ self-antigen and other forms of self-antigen.

4.2 Positive selection of B1b B cells by intracellular self-antigen, and in the presence of GRB2, is restricted to neonatal stage tissue but not adult BM.

To establish a model for the positive selection of B1 B cells by self-antigen, previously published experiments were repeated wherein Ig^{HEL} B cells are positively selected into the B1b B cell compartment from fetal and neonatal stage liver tissue, but negatively selected from adult BM tissue, by an intracellular self-antigen ($mHEL^{KK}$)[102]. Here, *Mb1Cre*$^+$ mice were crossed with Ig^{HEL} mice to generate Ig^{HEL} *Mb1Cre*$^+$ double

transgenic mice (Ig^{HEL}WT) that had an expected WT phenotype and were used as controls for further experiments.

To confirm that B1 B cells are preferentially generated from early-stage tissue in the presence of the intracellular self-antigen, allotype-marked CD45.2^{+} Ig^{HEL}WT BM was mixed with CD45.1^{+} Ig^{HEL}WT NL at a B cell ratio of 80:20 and injected the mixture into lethally irradiated CD45.1^{het} mice expressing either the $mHEL^{KK}$ or no antigen (Non). 8 weeks later, cells originating from the BM and NL donor tissues were distinguished by their surface CD45 isotype (**Figure 4-1A**).

On an important technical note, the meaningful reconstitution of these mixed chimeras depends upon using an appropriate ratio of NL and BM tissues. The NL and BM have different capacity to generate B cells and it is difficult to estimate equivalent progenitor proportions from NL and BM, and to adjust their ratio in the donor mixture to ensure that the injected BM and NL tissues contribute equivalently to reconstitution of the B cell pool. Hence, I chose to calculate the ratio based on the minimal cell number required to reconstitute irradiated mice. In previous experiments at 28 days, 70% of lethally irradiated mice that received 1 million BM cells and 100% that received 10 million BM cells survived[200], whist close to 100% NL chimeras with both 1 and 10 million survived with complete reconstitution of the immune compartment. In our laboratory, we typically use 5 million BM cells and 1-2 million NL cells for efficient reconstitution of irradiated recipient mice. Therefore, I chose 1:4 as the ratio for NL and BM mixtures for subsequent experiments.

As expected, B220^{lo}CD19^{+}CD43^{+}IgD^{-} IgM^{a+}HEL^{+} B1 B cells were predominantly derived from NL in the presence of mHEL^{KK} self-antigen (**Figure 4-1B-D**). It would be important to mention here that, despite stringent gating strategies, the CD45.2^{+} IgM^{a+}HEL^{+} B1 B cells of BM origin in the Non and mHEL^{KK} recipients, and to a smaller degree the CD45.1^{+} IgM^{a+}HEL^{+} B1 B cells of NL origin in the Non recipients, are more susceptible to contamination from the significantly larger IgM^{a+}HEL^{+} B2 population(**Figure 4-1B**). For B2 B cells, prior observations indicate that mature populations, including FO and MZ B cells, can be effectively reconstituted from both BM and NL tissues without apparent defects in B2 B cell development[201]. In summary, Ig^{HEL}WT B1 B cells are efficiently derived primarily from early-stage tissue and are positive selected by self-antigen.

Figure 4-1

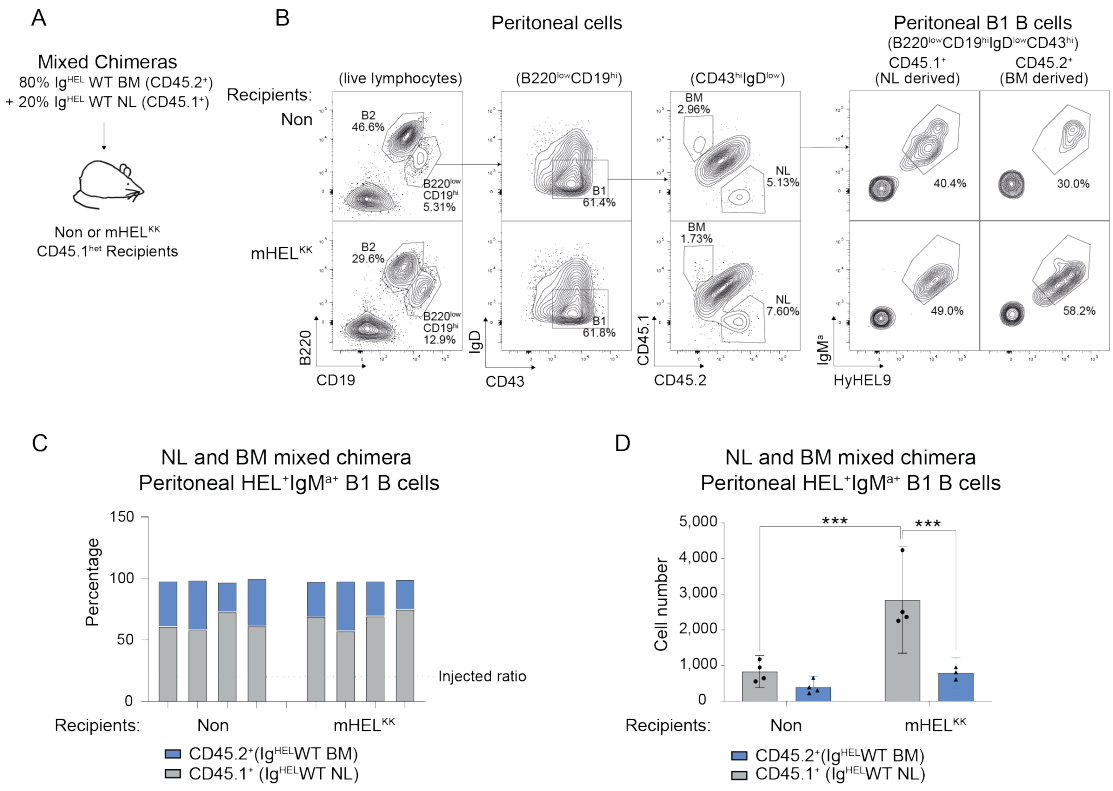

Figure 4-1 Positive selection of B1 B cells from neonatal tissue, but not BM, in the presence of intracellular antigen and GRB2.

*(A) Schematic depicting design of the NL mixed chimera experiment. CD45.2$^+$ Ig^{HEL}WT BM and CD45.1$^+$ Ig^{HEL}WT NL were mixed in an 80:20 ratio before injecting into either Non (no antigen) or mHEL^{KK} (intracellular antigen) CD45.1^{het} recipients. (B) Representative flow cytometry plots illustrating the gating strategy for identification of peritoneal B220^{low}CD19^{hi}IgDa^{low}CD43^{hi} B1 B cells (left panel), and the HEL binding specificity and IgM^a expression of CD45.1$^+$ and CD45.2$^+$ B1 B cells of NL and adult BM origin, respectively (right panel), recovered from Non and mHEL^{KK} recipients after 8 weeks of reconstitution. (C) The proportion of CD45.2$^+$ and CD45.1$^+$ HEL$^+$IgM^{a+} peritoneal B1 B cells recovered from Non or mHEL^{KK} recipients. Dotted line represents the CD45.2$^+$:CD45.1$^+$ ratio of total B cells in the BM:NL donor mixture at the time of injection. (D) The absolute numbers of CD45.2$^+$ and CD45.1$^+$ HEL$^+$IgM^{a+} B1 B cells recovered from the peritoneal cavity of Non or mHEL^{KK} recipients. Bars show means with 95% confidence limits and symbols indicate data from individual samples. Statistical testing by two-way ANOVA with *P<0.05 and **P<0.001. Data are representative of two independent experiments.*

4.3 Self-antigen independent and dependent mechanisms drive the generation of B1b B cells from GRB2 deficient neonatal liver.

To investigate the role of self-antigen during B cell development in GRB2 deficient mice, Ig^{HEL} mice were crossed with *Grb2$^{f/f}$ Mb1Cre$^+$* mice to generate Ig^{HEL} transgenic mice with a B-cell specific deletion of GRB2 (Ig^{HEL}KO). Similar to the observations from nonMD4 mice in the previous chapter, the absence of GRB2 in MD4 mice results in a depletion of FO B cells in the spleen with a corresponding a roughly two-fold increase in the MZ B cell population (**Figure 4-2 A and B**). Although, the proportion of Fr.E B cells increased and that of Fr.F B cells increased in the Ig^{HEL}KO BM (**Figure 4-2C and D**), the absolute numbers for these two populations remained statistically unchanged (**Figure 4-2E**). B cells in MD4 mice are characterized by rapid expression of pre-rearranged BCRs earlier during development. This leads to a postulated overlap of Fr. D and Fr. E BM B cell populations, with some Fr.E B cells still retaining Fr.D B cell characteristics but defined as immature B cells by their IgM expression. The postulated subtle developmental block at Fr.D in nonMD4 mice in the absence

of GRB2 may present as an accumulation of cells at the Fr.E B cell stage in MD4 counterparts. However, higher resolution phenotyping of the BM B cell populations might be required to detect any subtle changes in KO B cell development.

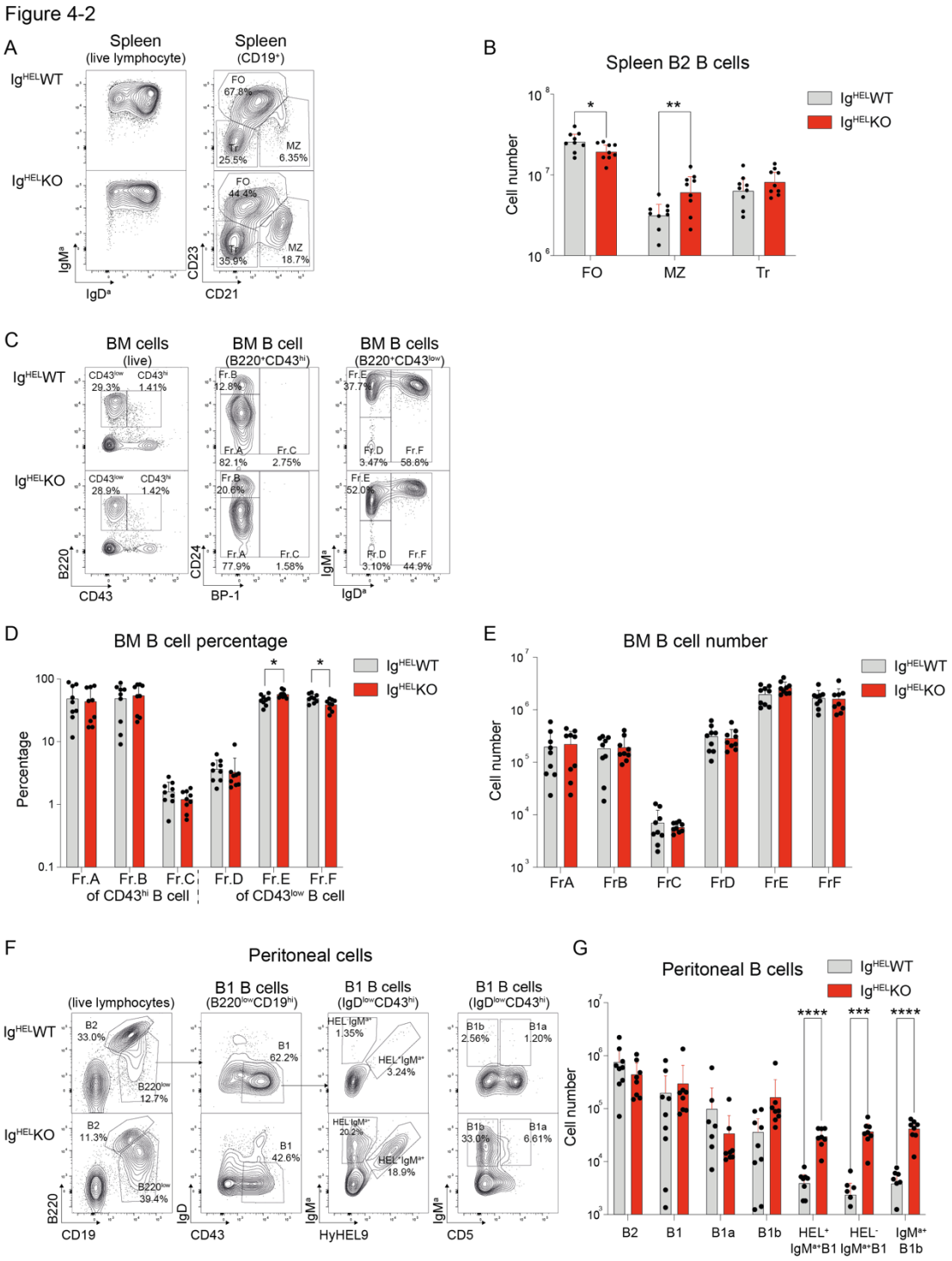

Figure 4-2 GRB2 deficiency is associated with increased B1b B cells and MZ B cells, with reduced recirculating and mature FO B cells, in the MD4 transgenic mouse model.

(A) Representative flow cytometry plots illustrating IgM^a and IgD^a profiles of spleen lymphocytes (left panel) and B cells (right panel) from Ig^{HEL}WT and Ig^{HEL}KO mice. The representative proportion of FO (CD19$^+$CD23^{hi}CD21$^{low/int}$), MZ (CD19$^+$CD23$^{low/int}$CD21^{hi}), and Tr (CD19$^+$CD23^{low}CD21^{low}) cells from Ig^{HEL}WT and Ig^{HEL}KO mice are depicted. (B) The absolute numbers of T, FO, MZ spleen B cells from Ig^{HEL}WT and Ig^{HEL} O mice. (C) Representative flow

*cytometry plots for BM B cell populations from Ig^{HEL}WT and Ig^{HEL}KO mice. Live cells were gated as $B220^{+}CD43^{hi}$ and $B220^{+}CD43^{low}$ (left panel). $CD43^{hi}$ cells (middle panel) were gated as Fr.A, pre-pro B cells ($B220^{+}CD43^{hi}BP\text{-}1^{low}CD24^{low}$); Fr.B, early pro B cells ($B220^{+}CD43^{hi}BP\text{-}1^{low}CD24^{hi}$) and Fr.C, late pro B/large pre B cells ($B220^{+}CD43^{hi}BP\text{-}1^{hi}$). $CD43^{low}$ cells (right panel) were gated as Fr.D, small pre B cells ($B220^{+}CD43^{low}IgM^{alow}IgD^{alow}$); Fr.E, immature B cells ($B220^{+}CD43^{low}IgM^{ahi}IgD^{alow}$) and Fr.F, mature B cells ($B220^{+}CD43^{low}IgM^{a+}IgD^{ahi}$). (D) The percentage of Fr.A, Fr.B and Fr.C from $CD43^{hi}$ and of Fr.D, Fr.E and Fr.F from $CD43^{low}$ BM B cells from Ig^{HEL}WT and Ig^{HEL}KO mice. (E) The absolute numbers of Fr.A, Fr.B, Fr.C, Fr.D, Fr.E and Fr.F B cells in BM from Ig^{HEL}WT and Ig^{HEL}KO mice. (F) Representative flow cytometry plots for live $B220^{low}CD19^{hi}IgD^{low}CD43^{hi}$ peritoneal B1 B cells from Ig^{HEL}WT and Ig^{HEL}KO mice (left and middle left panels). Representative proportions of $HEL^{+}IgM^{a+}$ and $HEL^{-}IgM^{a+}$ B1 B cells (middle right panel), and of B1a and B1b B cells (right panel) are indicated. (G) The absolute numbers of indicated peritoneal B cell subsets from Ig^{HEL}WT and Ig^{HEL}KO unmanipulated mice. Bars show means with 95% confidence limits and symbols indicate data from individual samples. Statistical testing by two-way ANOVA with *P<0.05, **P<0.01 and ****P<0.0001. Data are pooled from three independent experiments with nine mice per group.*

The proportion and number of peritoneal B1 B cells was significantly increased in Ig^{HEL}KO mice, with B1b B cells dominating this population (**Figure 4-2F**). In addition to the seven-fold increase in $HEL^{+}IgM^{a+}$ B1 B cells in the Ig^{HEL}KO mice (**Figure 4-2F and G**), serum titres of HEL-specific IgM^{a} were also elevated (**Figure 4-3A**). Consistent with data from the nonMD4 mice, Ig^{HEL} B1b B cells numbers have a stronger correlation with serum IgM titres, compared to Ig^{HEL} MZ B cells, supporting the hypothesis that the B1b B cells might be a major source of the elevated anti-HEL IgM^{a} antibodies in Ig^{HEL}KO mice (**Figure 4-3B-D**).

Figure 4-3

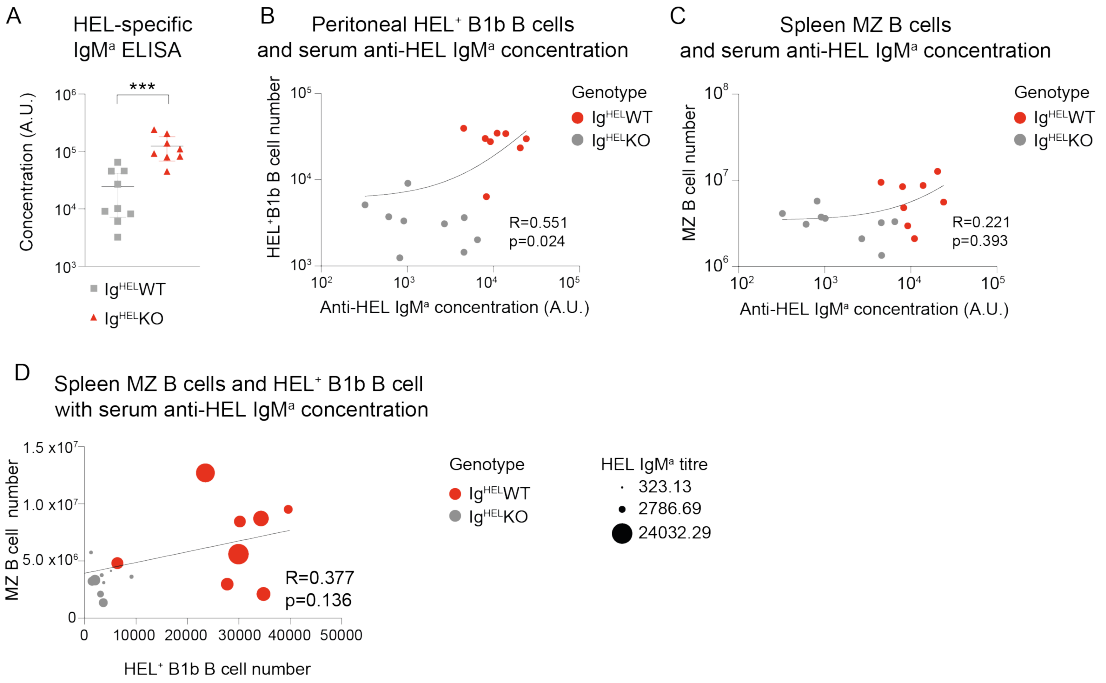

Figure 4-3 Elevated HEL-specific IgMa serum antibody titres are associated with increased HEL+ peritoneal B1b B cells in MD4 mice.

*(A) Concentration of HEL-specific IgM^a antibodies from the sera of Ig^{HEL}WT and Ig^{HEL}KO mice. Statistical analysis using unpaired t-test with ***P < 0.001. (B-D) Scatter plots for correlation analyses between (B) HEL$^+$ peritoneal B1b B cell numbers and HEL-specific IgM^a concentration, (C) MZ B cells numbers and HEL-specific IgM^a concentration, and (D) MZ B cells numbers and HEL$^+$ peritoneal B1b B cell numbers, from Ig^{HEL}WT or Ig^{HEL}KO unmanipulated mice. Filled circles indicate data from individual animals and the lines show the linear correlation between the two factors for each plot. For D, size of the filled circle represents the concentration of HEL-specific IgM^a. Correlation analysis was carried out with Spearman R analysis and p value from two-tailed t tests is reported. R stands for Spearman correlation coefficient value. Data are pooled from three independent experiments with nine mice per group.*

Next, Ig^{HEL}WT NL or Ig^{HEL}KO NL were transferred into lethally irradiated Non and mHEL^{KK} recipients and allowed to reconstitute for 8 weeks (**Figure 4-4A**). Consistent with data from nonMD4 mice and independent of self-antigen, no differences were observed in BM B cell development, while Ig^{HEL}KO MZ B cells were increased in the spleen. While a few HEL$^+$IgM^{a+} WT peritoneal B1 B cells were detected in the absence of self-antigen, Ig^{HEL}KO NL gave rise to six-fold more HEL$^+$IgM^{a+} B1 B cells even in the

absence of self-antigen, and the majority of these were B1b B cells (**Figure 4-4B, D and E**). Hence, the increased generation of B1b B cells in the absence of GRB2 does not depend on positive selection by self-antigen.

At the same time, however, It was noticed that a significant number of $HEL^{-}IgM^{a+}$ B1b B cells were also generated from the Ig^{HEL} KO NL (**Figure 4-4B, D and E**), and were also observed in the Ig^{HEL} KO unmanipulated mice (**Figure 4-2F and G**), presumably due to re-editing or replacement of the transgenic light chain. This was a surprising observation because the MD4 transgene exists as a concatemer at the genomic insertion site and its allelic exclusion is very strongly reinforced – one of the reasons it is such an effective BCR transgenic model. As a result, successful re-editing is rarely observed in the pre-immune repertoire, and then only under strong negative selection. Whilst the Ig^{HEL} KO NL-derived $HEL^{-}IgM^{a+}$ B1b B cell population seen in the presence of $mHEL^{KK}$ was less obvious on the flow cytometry contour plots (**Figure 4-4C, third panel**), the absolute numbers were equivalent to the elevated number of $HEL^{-}IgM^{a+}$ Ig^{HEL} KO B1 B cells recovered in the absence of antigen (**Figure 4-4D**). This might be consistent with a situation in which strong positive selection for B1b B cells, analogous to the sort generated by $mHEL^{KK}$, was being exerted by endogenous self-antigens in the absence of GRB2.

I turned next to B cell development in the presence of the self-antigen $mHEL^{KK}$. Although Ig^{HEL}WT NL B1 B cells were positively selected in the presence of self-antigens, $HEL^{+}IgM^{a+}$ B1 B cells were increased almost ten-fold in the absence of GRB2, with B1b B cells still the major population (**Figure 4-4C and D**). In conclusion, these

data indicate that GRB2 deficiency not only promotes the generation of B1b B cells in the absence of self-antigen, it also promotes the positive selection of B1b B cells in response to self-antigens.

Figure 4-4

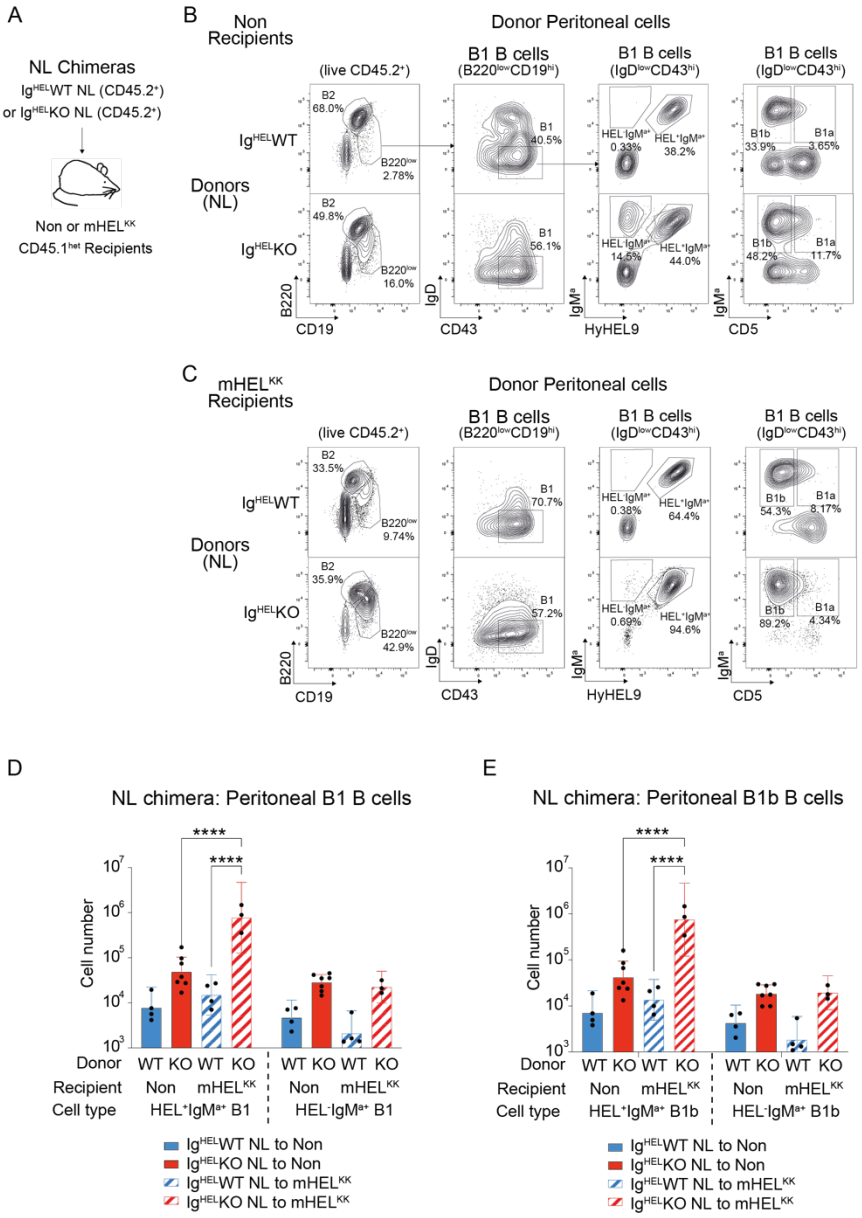

Figure 4-4 Self-antigen independent and dependent mechanisms drive the generation of B1b B cells from GRB2-deficient NL.

(A) Schematic depicting design of the NL chimera experiment. Either Ig^{HEL}WT or Ig^{HEL}KO NL was transplanted into lethally irradiated CD45.1^{het} (B) Non or (C) mHEL^{KK} recipients and allowed to reconstitute for 8 weeks. (B and C) Representative flow cytometry plots for live CD45.2^{+}B220^{low}CD19^{hi}IgD^{low}CD43^{hi} peritoneal B1 B cells of either Ig^{HEL}WT or Ig^{HEL}KO NL origin (left and middle left panels). Representative proportions of HEL^{+}IgM^{a+} and HEL^{-}IgM^{a+} B1 B cells (middle right panel), and of B1a and B1b B cells (right panel) are indicated. The absolute numbers of peritoneal (D) HEL^{+}IgM^{a+} and HEL^{-}IgM^{a+} B1 B cells and (E) HEL^{+}IgM^{a+} and HEL^{-}IgM^{a+} B1b B cells from non and mHEL^{KK} recipients reconstituted with either Ig^{HEL}WT or Ig^{HEL}KO NL donors. Bars show means with 95% confidence limits and symbols indicate data from

*individual samples. Statistical testing by two-way ANOVA with ****P<0.0001. Data are representative of two independent experiments.*

4.4 B1b B cell generation and positive selection from adult BM in the absence of GRB2.

To assess the effects of GRB2 on B cell development later during ontogeny, and to distinguish between *cis* and *trans* effects, Non and mHEL^{KK} recipients were reconstituted using a 50:50 ratio of Ig^{HEL}WT CD45.1^{+} BM mixed with either Ig^{HEL}WT or Ig^{HEL}KO CD45.2^{+} BM (**Figure 4-5 A**). In the absence of self-antigen, numbers of Ig^{HEL}KO BM-derived IgM^{a+}HEL^{+} and IgM^{a+}HEL^{-} B1b B cells are increased five-fold and ten-fold respectively, relative to WT (**Figure 4-5B and D**). There was a hundred-fold increase in the number of Ig^{HEL}KO BM-derived HEL^{+}IgM^{a+} B1b B cells, relative to WT, in the presence of the mHEL^{KK} self-antigen; however, the increase in IgM^{a+}HEL^{-} B1b B cells remains unchanged (**Figure 4-5C and D**). The positive selection of HEL^{+} B1b B cells derived from Ig^{HEL}KO adult BM by self-antigen was comparable to the large numbers generated from Ig^{HEL}KO NL in the presence of self-antigen (**Figure 4-4B and D**). Hence, in the absence of GRB2, the self-antigen dependent and independent selection of B1b B cells from adult BM was maintained and was comparable to selection from NL, suggesting that GRB2 is required for the normal switch away from B1b B cell selection during ontogeny.

Figure 4-5

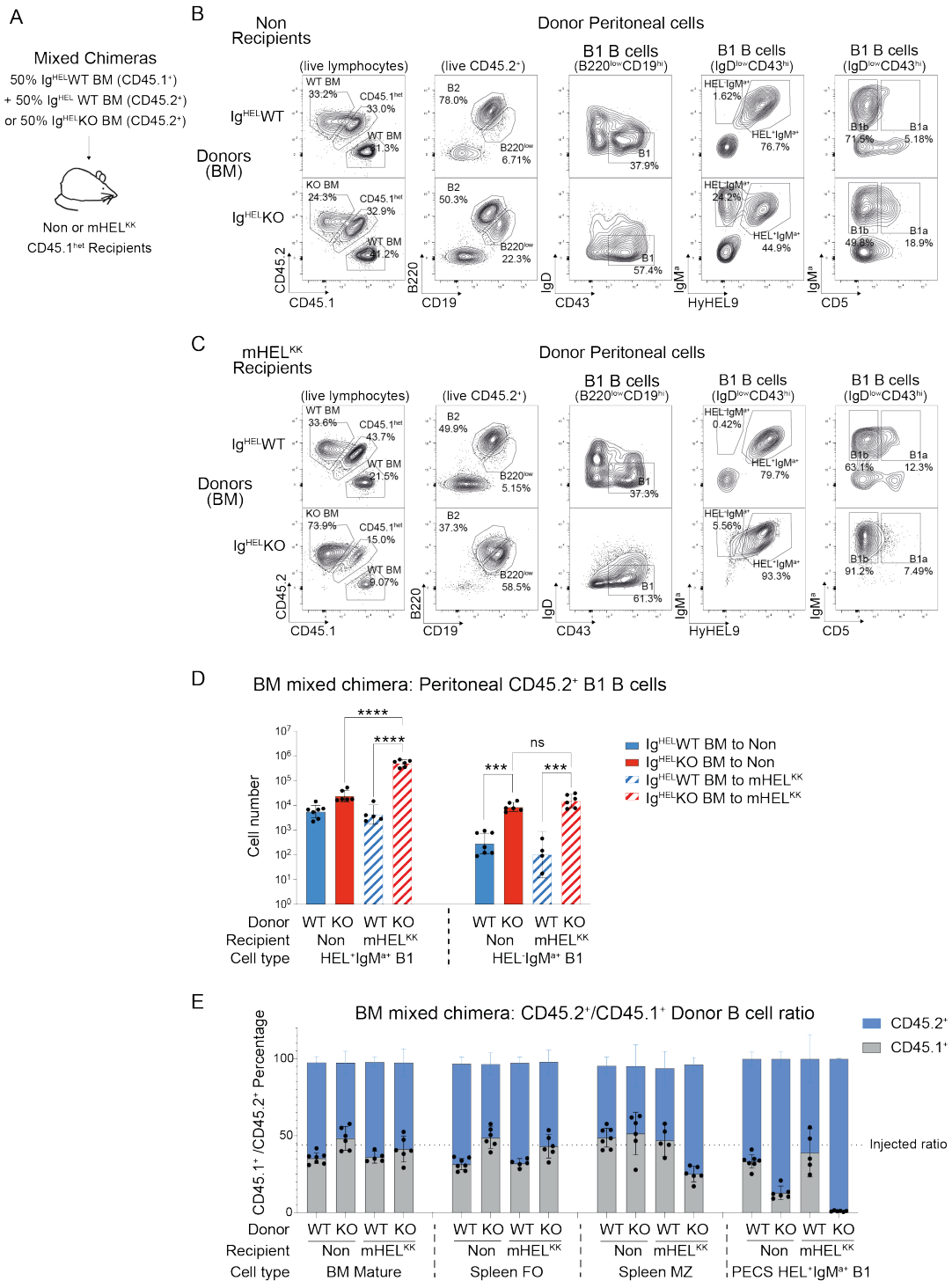

Figure 4-5 GRB2 inhibits the generation and positive selection by self-antigen of B1b B cells from adult BM.

(A) Schematic depicting design of the BM mixed chimera experiment. CD45.2+ IgHELWT or IgHELKO BM was mixed with CD45.1+ IgHELWT BM in 50:50 ratio before transferring into lethally irradiated CD45.1het (B) Non or (C) mHELKK recipients and allowed to reconstitute for 8 weeks. (B and C) Representative flow cytometry plots depicting the gating strategy for live peritoneal

*CD45.2^{+}B220^{low}CD19^{hi}IgD^{low}CD43^{hi} B1 B cells of either Ig^{HEL}WT or Ig^{HEL}KO BM origin (1st, 2nd and 3rd panels). Representative proportions of HEL^{+}IgM^{a+} and HEL^{-}IgM^{a+} B1 B cells (4th panel), and of B1a and B1b B cells (5th panel) are indicated in each plot. (D) The absolute numbers of HEL^{+}IgM^{a+} and HEL^{-}IgM^{a+} CD45.2^{+} B1 B cells of either Ig^{HEL}WT or Ig^{HEL}KO BM origin from Non and mHEL^{KK} recipients. Bars show means with 95% confidence limits and symbols indicate data from individual samples. Statistical testing by two-way ANOVA with *P<0.05 and ****P<0.0001. (E) The ratio of Ig^{HEL}WT or Ig^{HEL}KO CD45.2^{+} and Ig^{HEL}WT CD45.1^{+} cells recovered from Non and mHEL^{KK} chimeric mice across four distinct cell populations: BM mature B cells (B220^{+}CD19^{+}IgD^{a+}), spleen FO B cells (B220^{+}CD19^{+}CD21$^{low/int}$CD23^{hi}), spleen MZ cells (B220^{+}CD19^{+}CD21^{hi}CD23$^{low/int}$) and peritoneal HEL^{+}IgM^{a+} B1 B cells (B220^{low}CD19^{hi}IgDa^{low}CD43^{hi}HEL^{+}IgM^{a+}). Bars show means with 95% confidence limits and symbols indicate data from individual samples. Data are representative of three independent experiments.*

Additionally, the mixed BM chimera experiment allowed us to conclude that the effects of GRB2 deficiency on the reduction of mature BM B cells and FO B cells, the increased MZ B cells and the positive selection of B1b B cells by antigen in the absence of GRB2, are cell-intrinsic or in *cis* (**Figure 4-5E**). Next, BrdU incorporation was measured by the CD45.2^{+} HEL^{+}IgM^{a+} B1 B cells to evaluate their rate of proliferation. While the proportion of proliferating BrdU^{+} B1 B cells remained unchanged, regardless of the presence of self-antigen and GRB2 (**Figure 4-6A**), more total BrdU^{+} Ig^{HEL}KO B1 B cells were recovered in the presence of self-antigen (**Figure 4-6B**), possibly leaded to the higher number of total Ig^{HEL}KO B1 B cells in these mice. These findings suggest that the expanded B1 B cell population in the absence of GRB2 is likely not due to enhanced proliferation of B1 B cells but is perhaps due to the enhanced generation or survival of B1 B cells.

Figure 4-6

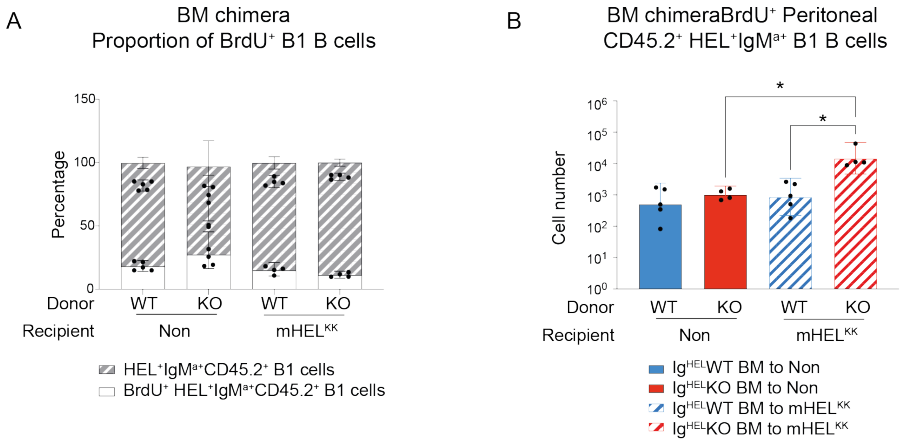

Figure 4-6 GRB2-deficient B1 B cell accumulation in the presence of self-antigen is independent of proliferation.

*(A) BrdU+ HEL+IgMa+CD45.2+ B1 B cells as a proportion of total HEL+IgMa+CD45.2+ B1 B cells of either IgHELWT or IgHELKO donor BM origin, recovered from Non or mHELKK chimeric recipients. (B) The absolute numbers of IgHELWT or IgHELKO BrdU+ HEL+IgMa+CD45.2+ B1 B cells from Non and mHELKK recipients. Data are representative of three independent experiments with 4-5 mice per group. Bars show means with 95% confidence limits and symbols indicate data from individual samples. Statistical testing by two-way ANOVA with *P<0.05.*

4.5 The deficiency of GRB2 is correlated with higher serum anti-self-antigen antibodies.

Since plasma cells and the titre of anti-HEL IgM antibodies correlate closely with B1b B cell selection in the Ig^{HEL} model[102], serum anti-HEL IgM^a concentration was measured in the sera from Non and $mHEL^{KK}$ mice reconstituted with NL or BM from both Ig^{HEL}WT or Ig^{HEL}KO to assess the effects of GRB2 deficiency and positive selection by self-antigen.

As expected from the number of HEL-binding B1b B cells, in chimeras reconstituted from Ig^{HEL} NL, $mHEL^{KK}$ and GRB2 deficiency acted individually and additively to

increase anti-HEL IgM^{a} titres (**Figure 4-7A**)**.** Anti-HEL IgM^{a} titres were increased twelve-fold in mHEL^{KK} mice reconstituted with Ig^{HEL} KO BM compared to non-transgenic chimeras reconstituted with Ig^{HEL} KO BM (**Figure 4-7B**). Intriguingly, the number of HEL^{+}IgM^{a+} B1b B cells and the number of MZ B cells demonstrated a significant correlation with HEL-specific IgM^{a} in serum from the BM chimeric mice (**Figure 4-7C, D and E**). Notably, this correlation was more pronounced in the presence of self-antigen (**Figure 4-7 C, D and E**), suggesting a potentially pivotal role for the two populations in the generation of HEL-specific IgM^{a} antibodies.

Figure 4-7

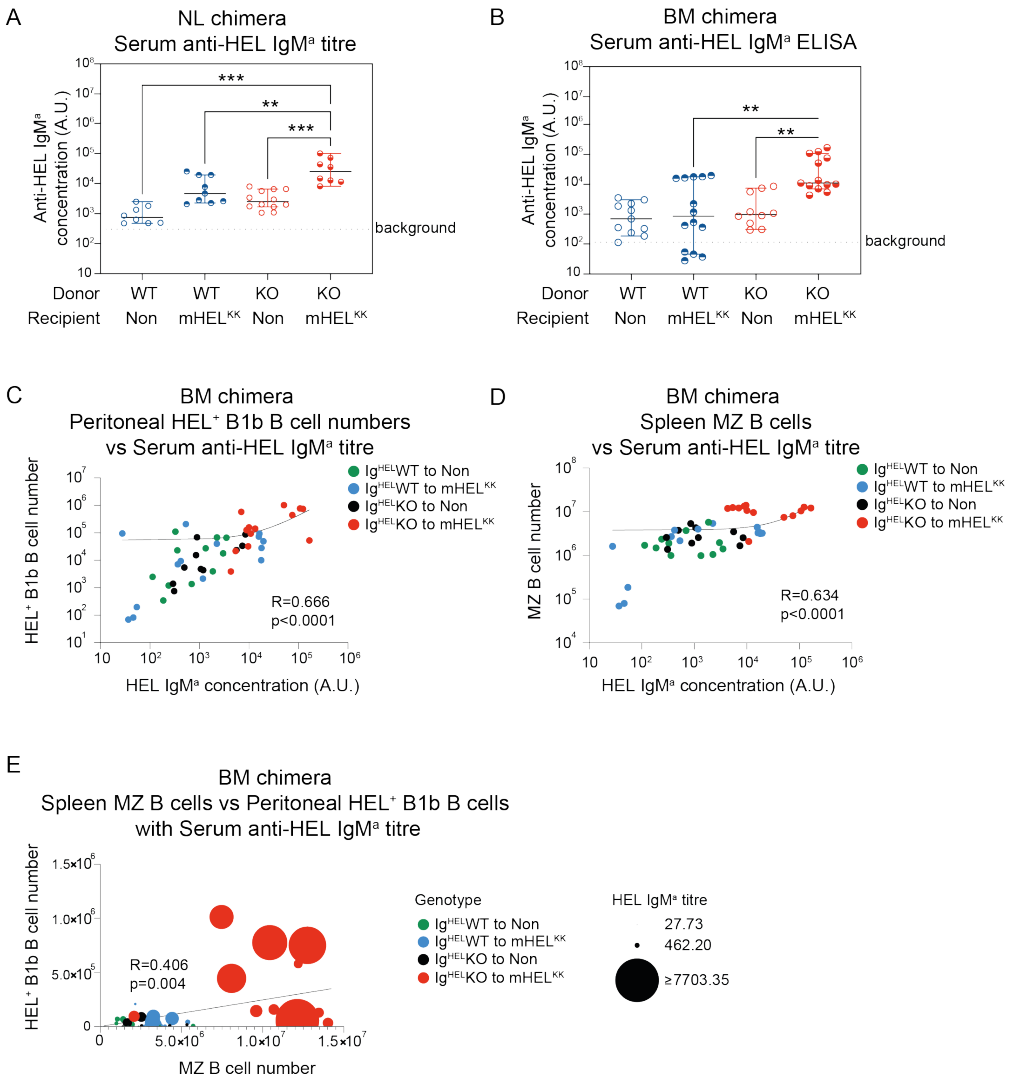

Figure 4-7 The deficiency of GRB2 is correlated to higher serum anti-self-antigen antibodies.

*(A) Ig^{HEL}WT or Ig^{HEL}KO NL was transferred to lethally irradiated Non or $mHEL^{KK}$ mice to establish NL chimeras and the serum anti-HEL IgM^a titres for samples from the four indicated groups were measured by ELISA. (B) Ig^{HEL}WT or Ig^{HEL}KO BM was transferred to lethally irradiated Non or $mHEL^{KK}$ mice to establish BM chimeras and the serum anti-HEL IgM^a titres for samples from the four indicated groups were measured by ELISA. Statistical analysis was performed using unpaired t-test with ***P < 0.001, **P < 0.01. (C-E) Scatter plots for correlation analyses between (C) HEL^+ peritoneal B1b B cell numbers and HEL-specific IgM^a concentration, (D) splenic MZ B cells numbers and HEL-specific IgM^a concentration, and (E) splenic MZ B cells numbers and HEL^+ peritoneal B1b B cell numbers, from Ig^{HEL}WT or Ig^{HEL}KO into Non or $mHEL^{KK}$ BM chimeras. Filled circles indicate data from individual animals and the lines show the linear correlation between the X- and Y-axes parameters for each plot. For E, size of the filled circle represents the concentration of HEL-specific IgM^a. Correlation analysis was carried out with Spearman R analysis and p value from two-tailed t tests is reported. R*

stands for Spearman correlation coefficient value. Data are pooled from three independent experiments with three to five mice per group.

4.6 The effects of GRB2 deficiency and positively and negatively selecting self-antigens on B1 B cell development and IgM antibody production are additive.

According to previous research, the positive selection of B1 B cells is strictly restricted to certain forms of self-antigen[103, 110]. In the Ig^{HEL} mouse model, only a ubiquitously expressed form of intracellular ER-restricted, membrane-bound HEL ($mHEL^{KK}$) has been shown to positively select B cells. Soluble HEL (sHEL) at ~20ng/ml leads to B cell anergy; whilst $mHEL^{KK}$ expressed exclusively in melanocytes under the Trp2 promoter, does not affect B cell selection at all[177].

To investigate whether GRB2 deficiency qualitatively or quantitatively affects negative selection or the threshold for positive selection by self-antigens, irradiated Non, $mHEL^{KK}$, sHEL, or Trp2mHEL transgenic mice were reconstituted with Ig^{HEL}WT or Ig^{HEL}KO BM (**Figure 4-8, Figure 4-9, Figure 4-10 and Figure 4-11**). The number of B1 B cells in these mice, and particularly the serum anti-HEL IgM^a titres, show the cumulative effects of positive and negative selection by self-antigens and GRB2 deficiency, indicating the deficiency of GRB2 could independently generate B1 B cells. Consistent with previous results, more B1b B cells and higher serum anti-HEL IgM^a titres are detected when Ig^{HEL}KO BM is transferred to Non mice, while these effects are further increased by $mHEL^{KK}$ in the absence of GRB2 (**Figure 4-8A, Figure**

4-11B and C). In contrast, B1 B cells are negatively selected by the sHEL antigen, even when GRB2 is absent. Serum anti-HEL IgM^{a} titres are also lower in the sHEL recipients, and although they are slightly elevated in the absence of GRB2, they are still five-fold lower than IgM levels in Non recipients from Ig^{HEL}WT donors. The B1 B cells in the Trp2mHEL chimeras, where the self-antigen is sequestered in melanocytes, are functionally equivalent to those without antigen, without significant positive or negative selection of Ig^{HEL} B cells (**Figure 4-8B, Figure 4-11B and C**).

While BM B cell reconstitution was comparable across the groups, MZ B cell numbers were elevated, as previously, in mice reconstituted with GRB2 deficient BM. Similar to the observation with B1 B cells, B2 B cells from reconstituted Trp2mHEL mice were phenotypically equivalent to those from Non mice. As expected, sHEL exerted strong negative selection on B2 B cells regardless of the presence of GRB2 and characterized by the downregulation of surface IgM in mature B cells **(Figure 4-9, Figure 4-10 and Figure 4-11)**. In sHEL mice reconstituted with Ig^{HEL}WT BM, mature B cells from the BM and spleen had an anergic phenotype with downregulated IgM, independent of GRB2 deficiency. Similar downregulation of IgM on the surface of mature BM B cells was observed in the presence of mHEL^{KK}; however, GRB2-deficient B cells did not modulate the surface IgM BCR in response to the intracellular self-antigen (**Figure 4-9 and Figure 4-10**). The Ig^{HEL}KO MZ B cell population was also enlarged in the presence of the mHEL^{KK} antigen (**Figure 4-5E and Figure 4-11A**), again suggesting a potential GRB2-regulated link between the elevated B1b B cells and MZ B cells.

As described earlier, a significantly high number of $IgM^{a+}HEL^{-}$ B1b B cells were generated from the Ig^{HEL} KO NL and Ig^{HEL} KO BM in Non recipients **(Figure 4-4D and Figure 4-5D)**. This observation posits the question of whether light chain replacement or editing is exclusive to Ig^{HEL}KO B1 B cells, especially in the context of the similarities between B1 B cells and MZ B cells[119], and the statistically significant increase of both populations in the absence of GRB2. The majority of IgM^{a+} Ig^{HEL}KO FO B cells retained HEL-reactivity independent of the form of antigen. On the other hand, a small proportion of $IgM^{a+}HEL^{-}$ Ig^{HEL}KO MZ B cells were detected in Non and Trp2mHEL recipients, and this population was even bigger in sHEL recipients **(Figure 4-10)**. These findings imply potential shared developmental pathways or regulatory mechanisms between B1 B cells and MZ B cells, under the influence of GRB2. This change is consistent with the previous observation wherein B1b B cells, in the absence of GRB2, demonstrated a strong association with MZ B cells in unmanipulated mice **(Figure 4-3D)**

Collectively, these results are consistent with GRB2-dependent pathways exerting quantitative effects on B cell development in the naïve repertoire and influencing the positive and negative selection of B cells by self-antigens, such that the effects are additive.

Figure 4-8

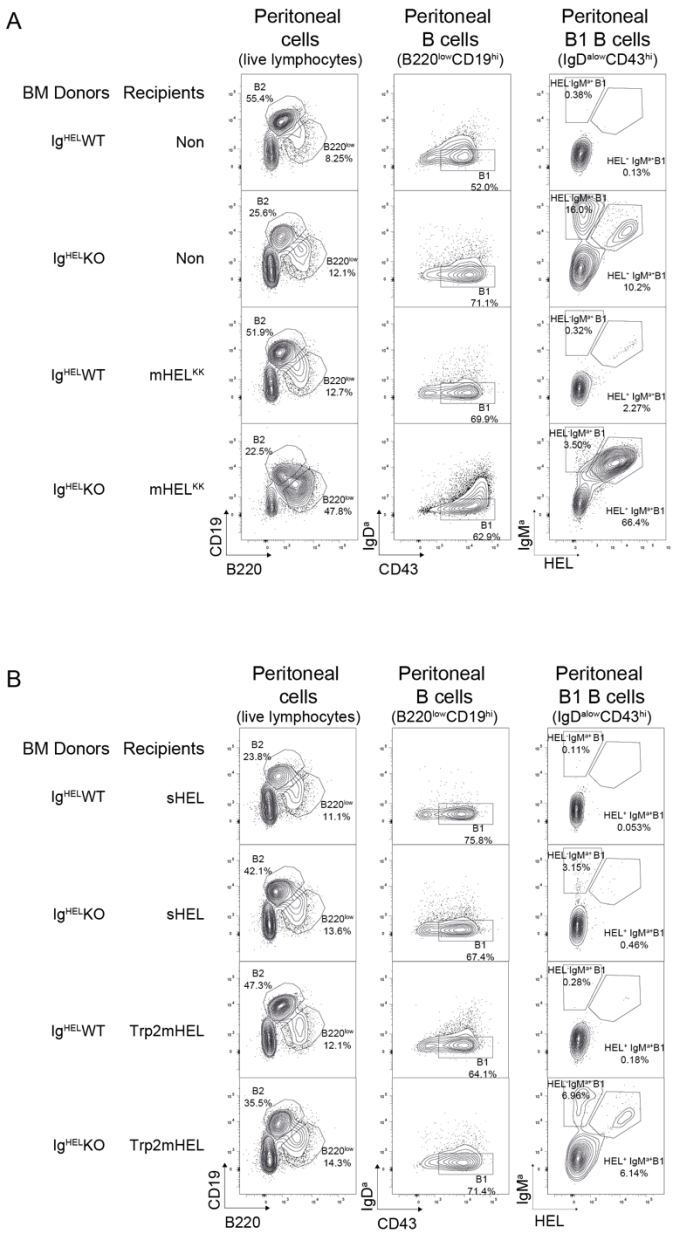

Figure 4-8 <u>The GRB2 deficiency independently affects positively or negatively selecting self-antigens on B1 B cell development with the effect of self-antigens being additive in adult tissue</u>.

Ig^{HEL}WT or Ig^{HEL}KO BM was transferred to lethally irradiated Non or $mHEL^{KK}$ or sHEL or Trp2mHEL mice to establish BM chimeras. (A and B) Representative flow cytometry plots illustrating the phenotypes and proportions of Ig^{HEL}WT and Ig^{HEL}KO peritoneal live lymphocytes (left panel) and peritoneal $B220^{low}CD19^{hi}IgD^{a\ lo}CD43^{hi}$ B1 B cells (middle and right panels) from (A) Non and $mHEL^{KK}$ recipients, and (B) sHEL and Trp2mHEL recipients. Data are representative of 4-5 mice per group.

Figure 4-9

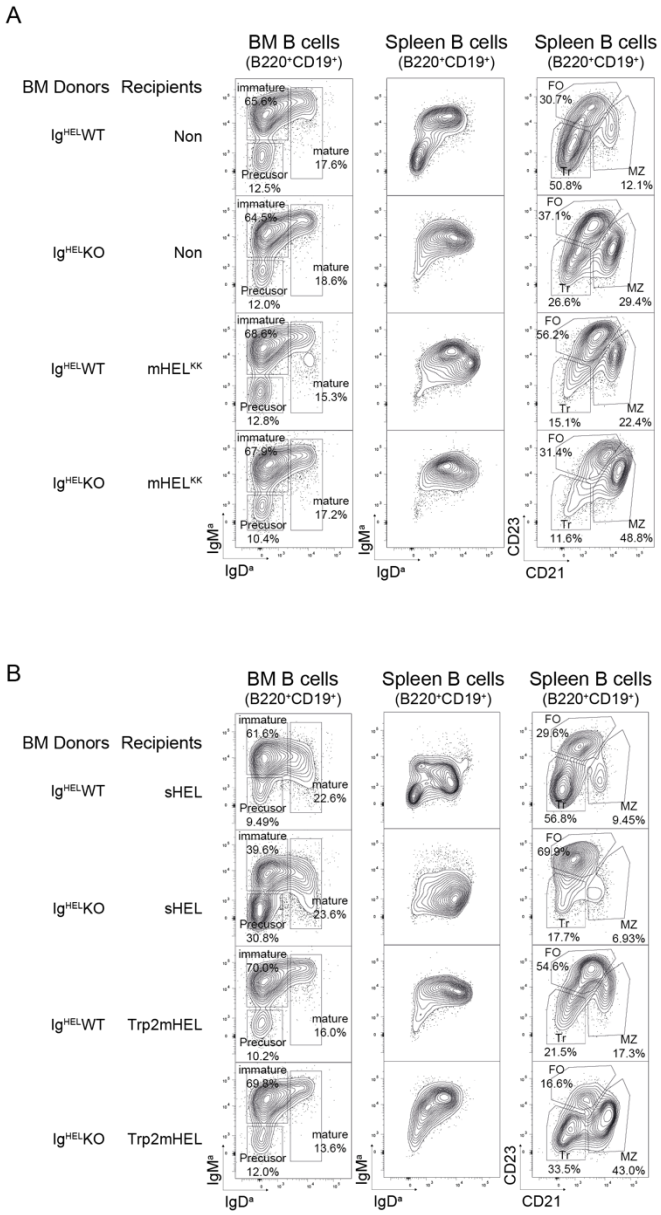

Figure 4-9 The effects of GRB2 deficiency and various forms of self-antigen on induction of anergy in B2 B cell subsets.

Ig^{HEL}WT or Ig^{HEL}KO BM was transferred to lethally irradiated Non or $mHEL^{KK}$ or sHEL or Trp2mHEL mice to establish BM chimeras. (A and B) Representative flow cytometry plots illustrating the phenotypes and proportions of Ig^{HEL}WT and Ig^{HEL}KO BM B cells (left panel), and spleen B cells (middle and right panels) from (A) Non and $mHEL^{KK}$ recipients, and (B) sHEL and Trp2mHEL recipients. BM B cell subsets are identified as follows: precursor ($B220^{+}IgM^{alow}IgD^{alow}$); immature ($B220^{+}CD43^{low}IgM^{ahi}IgD^{alow}$) and mature ($B220^{+}IgM^{a+}IgD^{ahi}$) B cells. Spleen B cell subsets are identified as follows: FO (live $B220^{+}CD19^{+}CD23^{hi}CD21^{low/int}$), MZ (live $B220^{+}CD19^{+}CD23^{low/int}CD21^{hi}$), and T B cell (Live $B220^{+}CD19^{+}CD23^{low}CD21^{low}$). Data are representative of 4-5 mice per group.

Figure 4-10

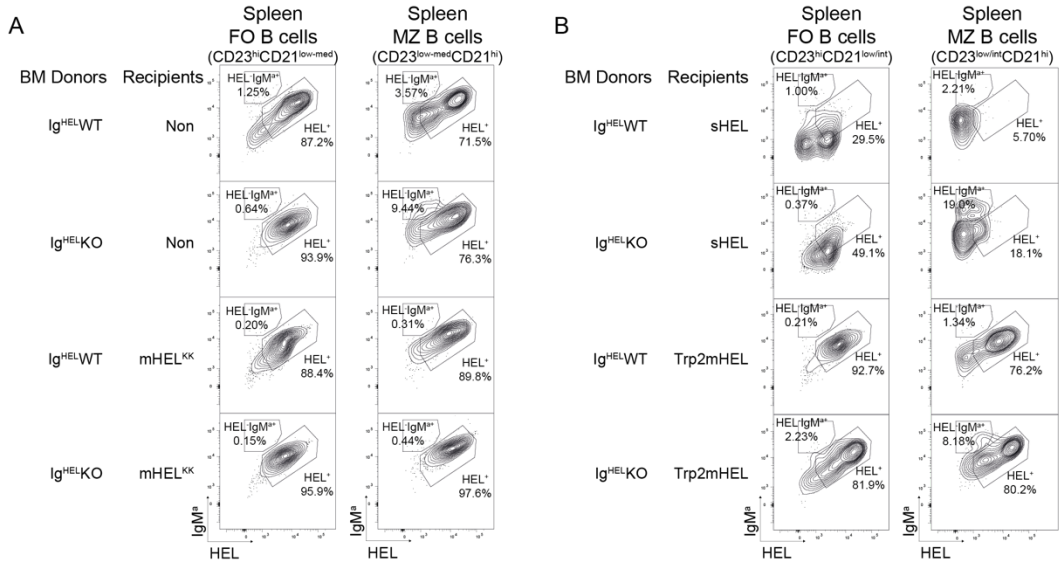

Figure 4-10 Modulation of surface expression of IgM^a and IgD^a BCRs by positively and negatively selecting self-antigens in the absence of GRB2.

Ig^{HEL}WT or Ig^{HEL}KO BM was transferred to lethally irradiated Non or mHEL^{KK} or sHEL or Trp2mHEL mice to establish BM chimeras. (A and B) Representative flow cytometry plots illustrating the HEL-specificity and IgM^a expression on splenic Ig^{HEL}WT and Ig^{HEL}KO FO (left panel) and MZ B cells (right panel) from (A) Non and mHEL^{KK} recipients, and (B) sHEL and Trp2mHEL recipients. Data are representative of 4-5 mice per group.

Figure 4-11

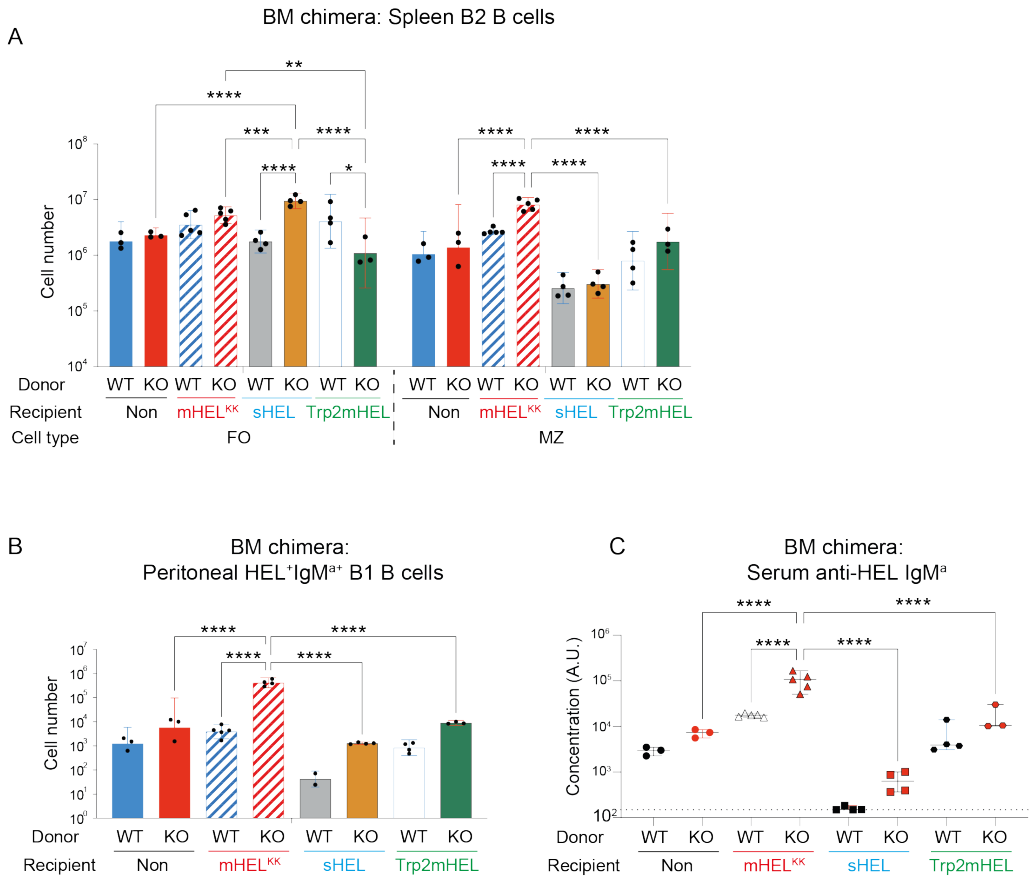

Figure 4-11 The GRB2 deficiency independently affects positively or negatively selecting self-antigens on B1 B cell development and IgM antibody production with the effect of self-antigens being additive in adult tissue.

*Ig^{HEL}WT or Ig^{HEL}KO BM was transferred to lethally irradiated Non or $mHEL^{KK}$ or sHEL or Trp2mHEL mice to establish BM chimeras. (A) The absolute numbers of Ig^{HEL}WT or Ig^{HEL}KO splenic B2 B cells (FO and MZ) from Non, $mHEL^{KK}$, sHEL and Trp2mHEL recipients in BM chimera experiment. (B) The absolute numbers of Ig^{HEL}WT or Ig^{HEL}KO peritoneal $HEL^{+}IgM^{a+}$ B1 B cells from Non, $mHEL^{KK}$, sHEL and Trp2mHEL recipients in BM chimera experiment. Bars show means with 95% confidence limits and symbols indicate data from individual samples. Statistical testing by one-way ANOVA with *P<0.05, **P<0.01, ***P<0.001 and ***P<0.0001. (C) Serum anti-HEL IgM^{a} titres from the eight indicated groups in BM chimera experiment, consisting of Ig^{HEL}WT or Ig^{HEL}KO BM transferred to either Non, $mHEL^{KK}$, sHEL or Trp2mHEL recipients. Statistical analysis using unpaired t-test with ****P < 0.0001.*

4.7 The absence of GRB2 in Ig^{HEL} mice is associated with HyHEL10 light chain rearrangement leading to oligoclonal B1 B cells with specificities pool of antibodies specificities identical across individual mice.

Since HEL^{-} IgM^{a+} B1 B cells retain the HyHEL10 heavy chain but without HEL-specificity, I hypothesized that this might be a consequence of either increased positive signalling by unknown endogenous antigens that promotes selection of HyHEL10 heavy chains paired with alternative light chains, or the negative selection of B cells that have re-edited or swapped light chains to escape and undergo increased spontaneous, antigen-independent development into B1b B cells in the absence of GRB2. While the former would result in a positively selected oligoclonal pool of B1 cells, the latter would result in a more diverse pool of clonotypes with little or no clonal enrichment.

To address the light chain usage of the HEL^{-} IgM^{a+} B1 B cells that accumulate in peritoneal cavity of Ig^{HEL}KO mice, HEL^{-} IgM^{a+} B1 B cells from 5 naïve Ig^{HEL}KO mice were sorted that had no previous exposure to self or foreign antigen. The sorted cells from each mouse were labelled with a hashtag (HTO) before sequencing their BCRs at a single cell resolution (**Figure 4-12A and B**). While cluster calling from BCR sequence information mainly relies on heavy chain VDJ sequences to define clonotypes, this was not practical for my experiment since I had sorted B1 B cells based on their shared IgM^{a} heavy chain expression. Hence, clonotypes were defined by combining

heavy chain VDJ usage with light chain V and J usage, and the CDR3 amino acid sequences (**Figure 4-12C**). Using this more stringent definition, several clonotypes were identified; however, the majority of unique BCR sequences clustered into less than ten clonotypes. Although the B1 B cells were sorted from five independent Ig^{HEL} mice, the top ten clonotypes were shared across the five donors at similar distribution frequencies.

the sequences of the top six clonotypes were then interrogated and compared their light chain sequences with the HyHEL10 light chain sequence **(Figure 4-12D).** The light chain variable region usage was distinct and different across the clonotypes, but with limited usage of light chain junction regions. This difference in variable region usage also leads to greater diversity in the CDR1, CDR2 and CDR3 regions, suggesting that these clonotypes likely have different antigen-binding specificities. However, the enrichment of a few clonotypes within a mouse, and this shared oligoclonality across independent mice is consistent with increased positive selection of $HEL^{-}IgMa^{+}$ B1 B cells by unknown self-antigen(s) in the absence of GRB2, occurring independently of and in parallel with the selection of $HEL^{+}IgM^{a+}$ in the presence of the $mHEL^{KK}$ self-antigen.

Figure 4-12

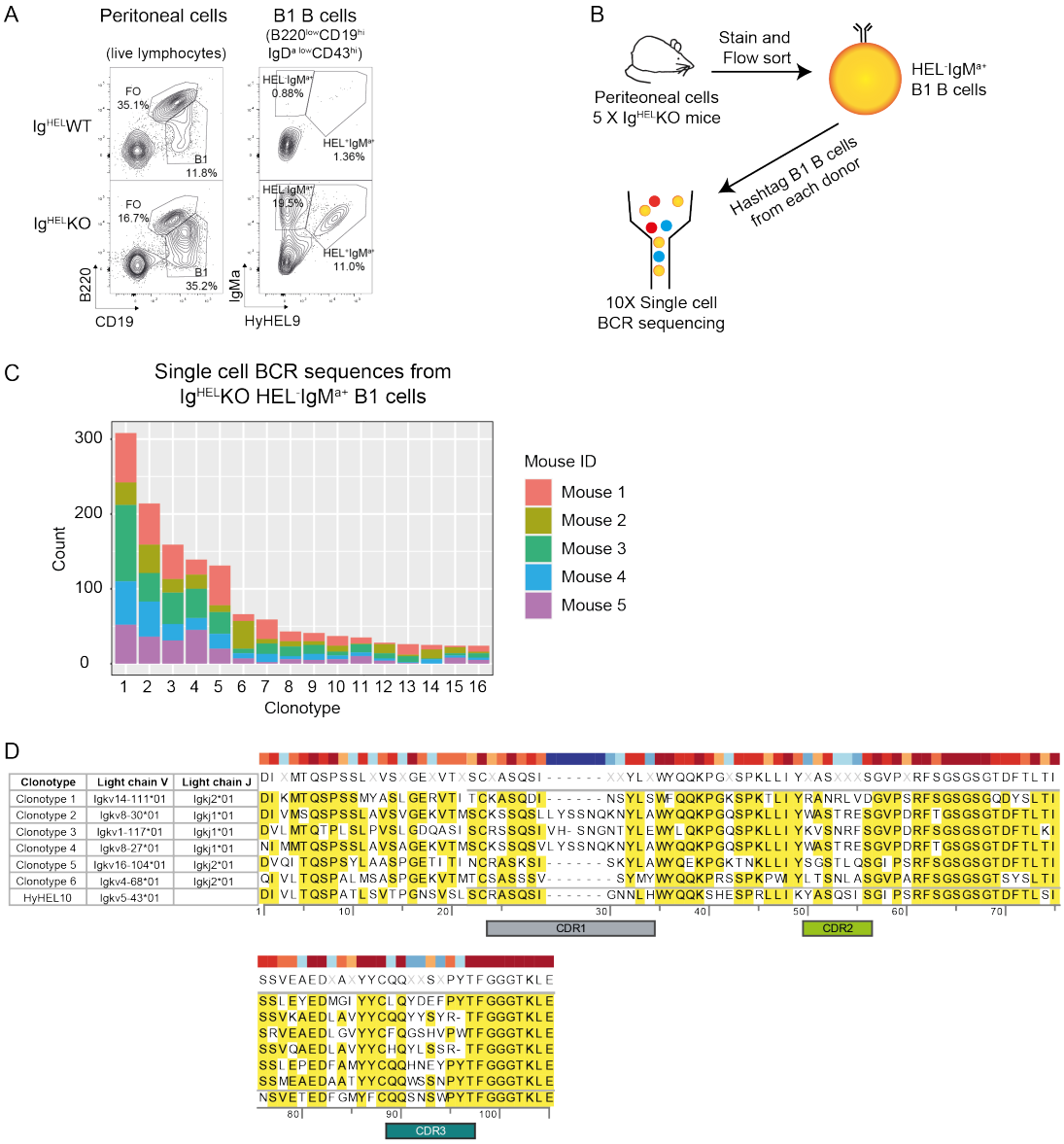

Figure 4-12 The absence of GRB2 in Ig^{HEL} mice is associated with HyHEL10 light chain rearrangement, leading to a pool of oligoclonal B1 B cells with identical specificities across individual mice.

(A) Representative flow cytometry plots illustrating the phenotypes of peritoneal live lymphocytes (left panel) and peritoneal B220^{low}CD19^{hi}IgD$^{a\ low}$CD43^{hi} B1 B cells (right panel) from Ig^{HEL}WT and Ig^{HEL}KO unmanipulated mice. (B) Schematic for the single cell BCR sequencing experiment. HEL^{-}IgM^{a+} peritoneal B1 B cells were flow sorted from 5 Ig^{HEL}KO mice and were labelled with individual hashtag antibodies (HTOs) before pooling and barcoding for sequencing on the 10X platform. (C) The absolute numbers of the various B1 B cell clone types identified from sequencing the BCRs of single cells. Clone type was defined by a combination of BCR heavy chain sequence, BCR light chain V usage, J usage and CDR3 amino acid sequence. Each colour represents sequences isolated from the B1 B cells of a single mouse. (D) Light chain V and J usage, and the amino acid sequence alignment for the HyHEL10 light chain and the top 6 clone types defined as above. Heavy chain sequences for

all six clone types are identical to the heavy chain of the HyHEL10 antibody (sequence not shown here).

4.6 GRB2-deficient B1 B cells do not show increased peripheral B1 B cells proliferation or survival in comparison to WT.

The findings reported in this chapter have shown that the generation of B1b B cells in the Ig^{HEL} model is a quantitative trait, driven by independent and additive effects of GRB2 deficiency and the presence of self-antigen.

Hypothetically, the self-antigen independent expansion of B1b B cells in the absence of GRB2 might be due to an increase in production of these cells or could be due to increased cell division and survival. While the effects on BCR selection are strongly in favour of the enhanced production, the other possibilities cannot be excluded. To explore these further, $CD45.2^+$ WT or KO and $CD45.1^+$ WT peritoneal cells was mixed at a B1 B cell ratio of 50:50 and transferred into the peritoneal cavity of *Rag1*$^{-/-}$ mice (**Figure 4-13A**). *Rag1*$^{-/-}$ mice cannot generate mature B cells and T cells due to incompetent VDJ recombination[176], which gives a relatively 'empty' peritoneal space for B1 B cells. After three weeks, the ratio between $CD45.2^+$ and $CD45.1^+$ B1 B cells in *Rag1*$^{-/-}$ recipients was maintained at 50:50 irrespective of genotype (**Figure 4-13B**).

One drawback to the use of *Rag1*$^{-/-}$ mice is that the combination of unrestricted space and BAFF availability[202] in these animals might mask the effects of normal competition for limited resources between cells. To account for this possibility, I set

up a similar transfer experiment with WT C57BL/6 mice as recipients (**Figure 4-13A**). At two weeks, there was no effect of GRB2 on the ratio of $CD45.1^+$ and $CD45.2^+$ donor B1 B cells recovered from the peritoneal cavity (**Figure 4-13B**), and the proportion of proliferating $BrdU^+$ B1 B cells was comparable in both groups (**Figure 4-13C**). These results suggested that the deficiency of GRB2 did not alter mature B1 B cell survival or proliferation and was unlikely to change the life span of mature B1 B cells.

Hypothetically, the effect of self-antigen might also be to increase selection into the B1b B cell pool or increase the division and expansion of mature B1b B cells or their survival. To address the last two possibilities, I transferred a 50:50 mixture of HEL^+IgM^{a+} B1 B cells from $CD45.2^+$ $Ig^{HEL}KO$ and $CD45.1^+$ $Ig^{HEL}WT$ mice into non or $mHEL^{KK}$ recipients. Despite some variability across experiments, which were challenging due to the low number of $Ig^{HEL}WT$ cells available for the transfer, no increase of transferred HEL^+IgM^{a+} B1 B cells was observed in the presence of $mHEL^{KK}$ in any situation at two weeks (**Figure 4-13E**) or three weeks (**Figure 4-13F**). Numbers of both $Ig^{HEL}WT$ and $Ig^{HEL}KO$ B1 B cells decreased in the presence of self-antigen (**Figure 4-13 E and F**). These results imply that self-antigen does not increase the rate of proliferation of mature B1 B cells in the absence of GRB2.

Figure 4-13

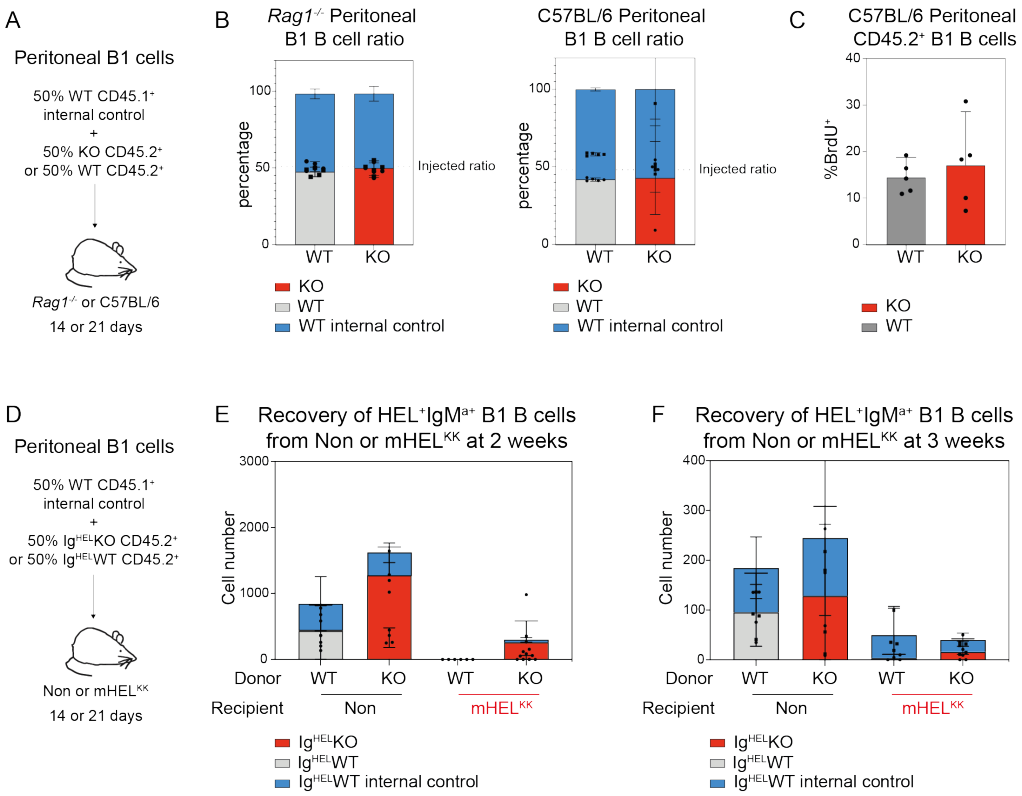

Figure 4-13 GRB2-deficient B1 B cells have comparable proliferation and survival when in competition with WT B1 B cells.

(A) CD45.2+ WT or KO peritoneal B1 B cells were mixed with the WT CD45.1+ peritoneal B1 B cells in a 50:50 ratio before intraperitoneal transfer into either Rag1-/- or B6 WT mice. The B6 mice were treated with BrdU in water for the entire duration. (B) The percentage of donor-origin peritoneal B1 B cells recovered from Rag1-/- recipients at 3 weeks (left panel) and B6 WT recipients at 2 weeks (right panel). Dotted line indicates the CD45.2+:CD45.1+ ratio of the B1 B cell mixture. (C) The proportion of BrdU labelling in B1 B cells recovered from B6 WT mice at 2 weeks post-transfer. (D) CD45.2+ IgHELWT or IgHELKO peritoneal B1 B cells were mixed with the IgHELWT CD45.1+ peritoneal B1 B cells in a 50:50 ratio before intraperitoneal transfer into either Non or mHELKK mice. (D) The absolute numbers of CD45.2+ and CD45.1+ HEL+IgMa+ peritoneal B1 B cells recovered from Non or mHELKK recipients at 2 weeks (left panel) and at 3 weeks (right panel). Bars show means with 95% confidence limits and symbols indicate data from individual samples.

4.7 Discussion

The regulatory function of GRB2 during the development and maturation of B2 B cells has been extensively investigated in WT mice[169]. Notably, the absence of GRB2

significantly reduces the mature B cell population in BM and FO B cells within the spleen while increase the MZ B cell population (**Figure 3-2 and Figure 3-3**). This phenotype persists in the MD4 mouse model, which has limited BCR diversity, and suggests that the changes in the naïve B2 B cell populations are independent of antigen stimulation. The absence of GRB2 in MD4 mice mirrors the phenotype observed in nonMD4 mice: a reduction of mature B cells in BM, FO B cells in spleen and an increase of MZ B cells were observed **(Figure 4-2)**. Beyond the B2 B cells, more intriguing findings come from the B1 B cell compartment.

In WT mice, there is an ontogeny switch between early-stage tissue and mature tissue to control the generation of B1 B cells. This switch is partially controlled by the *Lin28b*/*let-7* axis[109]. Using the Ig^{HEL} model, my data confirms that in the presence of GRB2, intracellular self-antigen can positively select B1 B cells only from early-stage tissue. Since this self-antigen is intracellularly retained and is likely only exposed to the immune system during cell death, this suggests that self-antigen exposure by cell death or apoptosis in early life may be key to the positive selection of B1 B cells.

In the absence of GRB2, both NL and BM can generate $HEL^{+}IgM^{a+}$ B1 B cells in the absence of HEL as a self-antigen. Considering the absence of HEL antigen in these recipients, the absence of GRB2 may activate an alternative pathway in both NL and BM, permitting more B1 B cell progenitors to become mature B1 B cells. Due to the lack of self-antigen for these B1 B cells, the enlargement of this population is independent of antigen and selection events.

Interestingly, consistent with the $HEL^{-}IgM^{a+}$ B1 B cells detected in unmanipulated $Ig^{HEL}KO$ mice, the $Ig^{HEL}KO$ NL and BM also produced more $HEL^{-}IgM^{a+}$ B1 B cells in non-transgenic recipients (**Figure 4-2G, Figure 4-4B, Figure 4-5B**). According to the single-cell BCR sequencing result, these B1 B cells are oligoclonal and share clonotypes across different individual mice. This result strongly supports the idea that there is strong positive selection of B1 B cells by unknown self-antigen(s) in the absence of GRB2. Under normal circumstances, there is strong allelic exclusion enforced by the MD4 transgene, which is probably due to its insertion as a concatemer of heavy and light chains. No light chain preference has been reported in mice expressing the HyHEL10 heavy chain alone as a transgene[111] or as a gene targeted allele[203] . The putative self-antigenic targets of these B1 B cell BCRs remain unknown. Unveiling the identities of these antigens will help us to gain insights into endogenous antigens that can induce positive selection of B1 B cells. To answer these questions, I plan to use the sequences of the shared clonotypes acquired from single-cell BCR sequencing to generate oligoclonal antibodies (**Figure 4-12C**). The next step would be to confirm their auto-reactivity against cell lines and then identify their targets in mice with libraries of self-antigens.

In the absence of GRB2, both BM and NL can generate B1 B cells in the absence of self-antigen. It is hard to tell whether GRB2 suppresses the positive selection of B1 B cells or inhibits B1 B cell generation independently of self-antigen. However, in the absence of GRB2 and the presence of intracellular membrane-bound self-antigen, there is a significant increase in the number of positive selection of B1b B cells, which is evidenced by the large expansion of $HEL^{+}IgM^{a+}$ B1 B cells in the peritoneal cavity.

The increase in this population is due to an interaction between the BCR and self-antigen leading to positive selection.

The form of self-antigen matters in the context of positive antigen. Abundant high avidity soluble self-antigen cannot positively select B1 B cells in the absence of GRB2 while it instead negatively selects B2 B cells (**Figure 4-11**). It remains unknown at which developmental stage can B cells be positively selected into B1 B cells in the absence of GRB2.

Another interesting question is whether the deficiency of GRB2 provides additional help in positive selection in early-stage tissue when comparing the ability to generate B1 B cells in KO NL and KO BM. I could not directly compare the KO NL and KO BM by setting up a mixed NL chimera experiment because all our Ig^{HEL}KO mice are maintained as $CD45.2^{+}$ lines. The current data suggests that KO NL generates slightly more $HEL^{+}IgM^{a+}$ B1b B cells than KO BM, however these results do not reach statistical significance (data not shown).

I found a strong correlation between $HEL^{+}IgM^{a+}$ B1 B cells and anti-HEL IgM^{a} antibodies in the serum. This result indicates the source of the rising antibodies could be B1b B cells in the peritoneal cavity. However, peritoneal B1 B cells mainly serve as a "steady state" reservoir and produce only a small amount of antibody[59, 204]. The majority of native antibodies are secreted by B1 B cells in bone marrow and spleen[59, 204]. MZ B cells are also capable of secreting IgM antibodies, which further complicates this issue[205]. The role of MZ B cells in generating the excess IgM is harder

to determine. Data from both nonMD4 and MD4 unmanipulated mice, however, suggests the correlation between MZ B cell number and serum IgM titres is weak (**Figure 3-4 and Figure 4-3**). Hence, there might be an unidentified population of B1 B cells or B1 B cell-derived plasma cells in the spleen or BM that produce the native antibodies. To identify the source of increased serum antibodies, an ELISPOT assay may provide further insights into this issue.

My results show that GRB2 deficiency and self-antigens operate independently to determine the level of antibodies. In the absence of GRB2, the serum antibody level was higher compared to WT regardless of the form of antigen, and an increase relative to the levels in WT mice was seen with $mHEL^{KK}$. As expected, the tolerising antigen, sHEL, led to a reduction in autoreactive antibodies. sHEL mice reconstituted with Ig^{HEL}KO donors generated more autoantibodies compared to Ig^{HEL}WT donors. In Trp2mHEL recipients, the antibody level for both type of donors was comparable to that in Non recipients, implying that this antigen is neither positively nor negatively selecting, perhaps due to very low level of antigen exposure in Trp2mHEL mice.

How GRB2 and antigens of different forms regulate the secretion of antibodies remains unknown. However, it seems likely that the differences reflect B1 B cell number in these recipients (**Figure 4-11 B and C**)**.** This correlation is powerful evidence in support of this hypothesis. We have noted that Ig^{HEL}KO B cells also showed a lower surface IgM^a modulation on encountering $mHEL^{KK}$ self-antigen (**Figure 4-9, Figure 4-10**). The absence of GRB2 may also alter the function of B2 B cells via their regulation of surface BCR, however this requires further evidence.

In this chapter I have also explored whether higher B1 B cell proliferation, life span or a larger B1 B cell progenitor pool could underlie the increased B1 B cell number in the absence of GRB2 and the presence or absence of cognate self-antigen. Transfer experiments revealed no difference in the rate of cell proliferation or survival after three weeks. Therefore, it seems most likely that an expansion of the B1 B cell progenitor pool underlies the increase in B1 cells in the absence of GRB2. However, the nature of the B1 B cell progenitors is unclear. Importantly, a deficiency in GRB2 leads to the generation of more B1 B progenitors in both the NL and adult BM stage.

The technical difficulties of transferring enough $HEL^{+}IgM^{a+}$ B1 B cells into antigen-presenting mice pose some variations in results (**Figure 4-13E and F**). In the transfer experiments there was a trend towards greater cell loss in the presence of self-antigen. This would not be surprising in the case of WT B cells, which undergo arrest and relocation to the T cell zone where their survival depends on finding T cell help. However, in the case of GRB2 deficiency, it raises the question of how $mHEL^{KK}$ might inhibit the proliferation of mature B1 B cells in the peritoneal cavity, yet promote the positive selection of B1 B cells? Hypothetically, this could be due to difference in the form, location or stage of antigen exposure, or coincidental signals from elsewhere. The B1 B cells used in peritoneal transfer experiments had not been exposed to self-antigen before, therefore the sudden strong BCR-antigen reaction signal might have rendered these B1 B cells anergic or susceptible to deletion. This could be tested by a secondary transfer experiment in the future.

Chapter 5 : Insights into cellular and molecular pathways regulated by GRB2 during BM B cell development in the presence of self-antigen.

5.1 Introduction

The role of GRB2 in B cells has been described predominantly as a negative regulator of signalling downstream of the BCR. Spleen B cells from mice with B cell specific GRB2 knockout exhibit an augmented Ca^{2+} influx upon BCR stimulation, concomitant with a decrease in JNK and PI3K signalling[169, 170]. Nevertheless, the precise molecular effects on B cell development and the generation of B1 B cells in mice with B cell specific GRB2 knockout remains elusive. This is a question that might be addressed at the level of single cells in MD4 mice, where BCR specificity and the presence or absence of self-antigen is controlled. Single-cell RNA sequencing (sc-RNASeq) technology may provide valuable insights into unravelling this complex issue.

5.2 Sc-RNASeq discriminates between the effects of GRB2 and antigen.

As demonstrated in Chapter 4, the absence of GRB2 augments the number of MZ B cells, and significantly enhances the generation of B1b B cells from neonatal tissue and adult BM, with positive selection by self-antigen (**Figure 4-4, Figure 4-5 and Figure 4-11**). Further, the peritoneal transfer experiments suggest that the increased

B1b B cell population in the absence of GRB2 is not attributable to heightened proliferation or extended lifespan of mature B1b B cells **(Figure 4-6 and Figure 4-13)**. Consequently, the potential expansion of B1b B cell progenitors in the presence of self-antigen, facilitated by the absence of GRB2, may be the primary driver for the larger mature B1b B cell population.

To identify the cellular and transcriptomic changes associated with the positive selection of B1b B cells and the expansion of MZ B cells in the absence of GRB2, a BM mixed chimera with four groups, namely, Ig^{HEL}WT into Non, Ig^{HEL}WT into $mHEL^{KK}$, Ig^{HEL}KO into Non, and Ig^{HEL}KO into $mHEL^{KK}$ was established (as described in Chapter 4 and **Figure 4-5**). BM tissue was collected 8 weeks after reconstitution from 4 mice per groups. 16 mice from 4 experimental groups were divided into 2 batches, each containing the 4 groups with 2 mice per group. Cells from individual mice in each batch were labelled with 8 distinct hashtags (HTOs), pooled, and further labelled with CITE-Seq reagents (ADTs). After flow cytometry sorting into $CD45.1^+$ and $CD45.2^+$ subsets, 2 samples per batch were generated, resulting in a total of 4 samples. The 4 post-sort samples were counted and processed on separate lanes of the 10X sc-RNASeq Chromium platform as 2 batches of $CD45.1^+$ and 2 batches of $CD45.2^+$ cells (**Figure 5-1A**). A total of 44,689 cells were successfully captured: 27,655 from the $CD45.2^+$ samples and 17,044 from the $CD45.1^+$ samples (**Figure 5-1B**). The median gene count per cell averaged ~1,800 across all samples, accompanied by an average of 54,000 reads per cell. Subsequently, cells were filtered based on the number of genes detected per cell (nCounts_RNA) and the percentage of mitochondrial genes (percent.mt) to eliminate non-singlets and non-viable cells (**Figure 5-1C**).

Figure 5-1

A

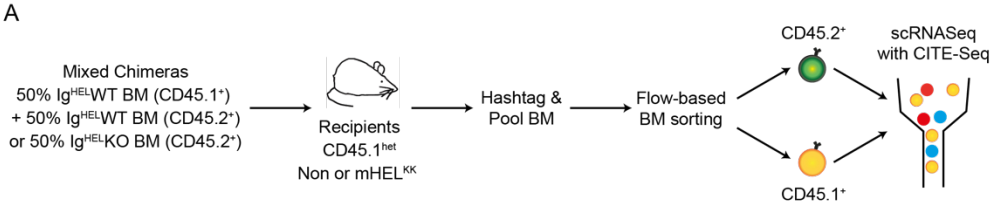

B

Sample	Batch 1 CD45.2+	Batch 1 CD45.1+	Batch 2 CD45.2+	Batch 2 CD45.1+
Cell capture number	13784	9227	13871	7817

C

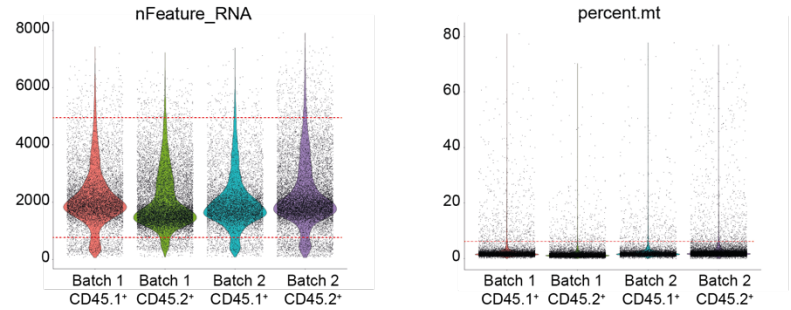

Figure 5-1 Design of the sc-RNASeq experiment and quality control checks.

(A) Schematic of the design of the sc-RNASeq experiment. CD45.2+ IgHELWT BM or IgHELKO BM and CD45.1+ IgHELWT BM were mixed at a 50:50 ratio and transplanted into lethally irradiated Non or mHELKK recipients. BM B cells from 4 recipients of each experiment group were collected 8 weeks later and labelled with CITE-Seq antibodies (ADTs) and individual hashtags (HTOs) before pooling the samples. Live CD19+B220+ BM B cells were sorted by flow cytometry into CD45.1+ and CD45.2+ populations and processed for 10X sc-RNASeq partitioning, library preparation and sequencing. (B) The table shows the number of cells recovered from each sample of two batches. (C) The violin plot depicts the number of genes detected per cell (left panel) and the percentage of mitochondrial genes (right panel) in the unfiltered RNA assay from each sample. Each dot represents a single cell. The dotted line denotes the filtering threshold set for the RNA assay.

The use of HTOs allowed us to perform quality control checks to annotate singlets, doublets, and negative droplets, as well as to interrogate data as pooled samples or as from 4 individual mice per group. The data were filtered to retain singlets based on HTO demultiplexing to yield a total of 15,216 CD45.2+ single cells and 10,569 CD45.1+ single cells in the final dataset. Harmony integration algorithm was employed to integrate the RNA assays and mitigate any variations in the two batches. Following

integration, principal component analysis (PCA) was applied to reduce the dimensionality of the data, resulting in the clustering of all cells into 16 distinct clusters based on their RNA expression features (**Figure 5-2A**). The BM B cell clusters were classified according to classic Hardy fraction markers based on their ADT expression features (**Figure 5-2B**), supported by RNA expression of selected markers (**Figure 5-2C**). UMAP visualization indicated successful BM reconstitution and cell sorting, with B cells spanning all Hardy fractions (A to F), except for minor contamination from NK cells and neutrophils (GN). Cluster annotation was further confirmed using the top10 differentially expressed (DE) genes detected using the Seurat FindMarkers function (**Appendix table A**). This outcome confirmed the effectiveness of the FACS sorting procedure, demonstrating that no major B cell subset was excluded.

Figure 5-2

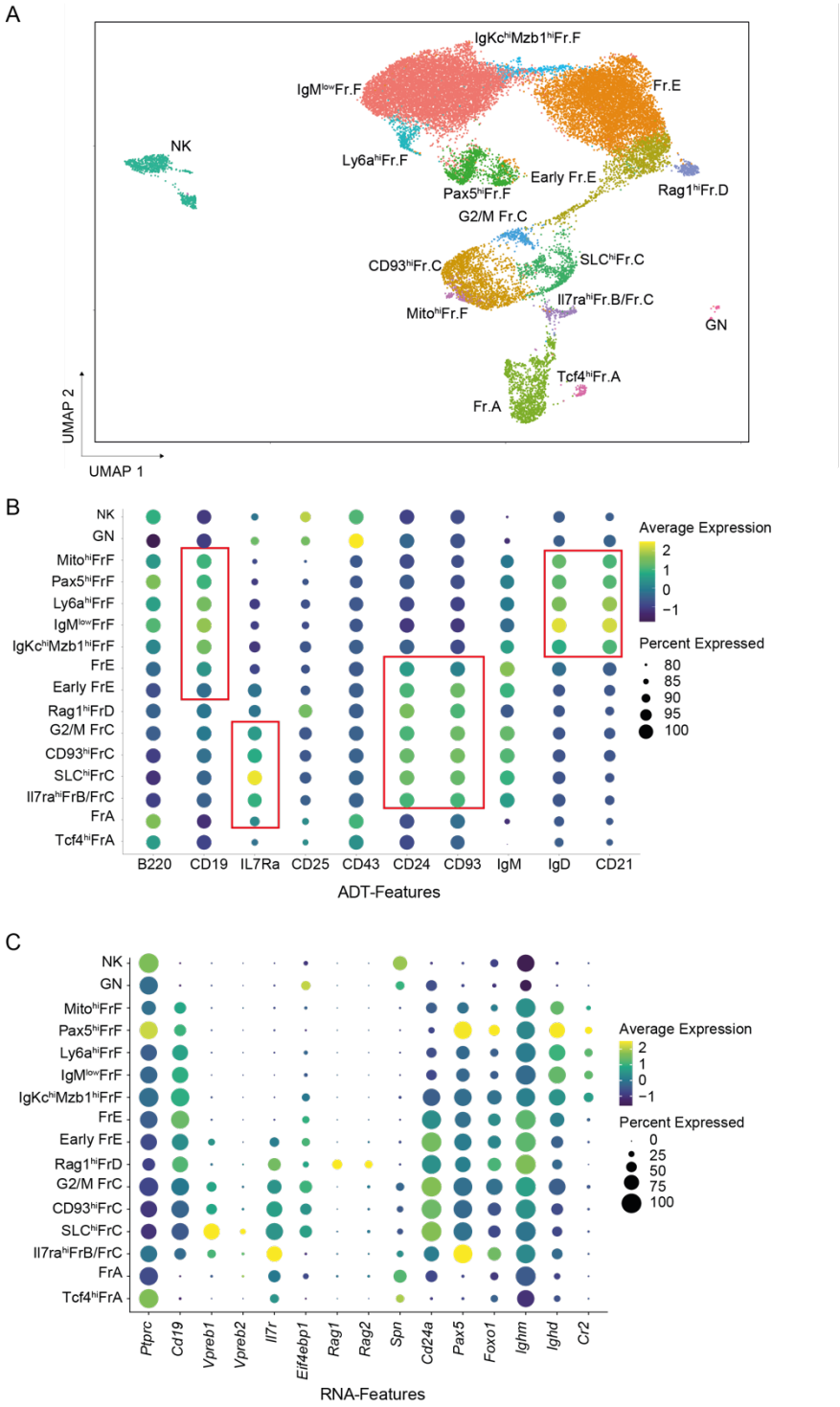

Figure 5-2 Clustering and annotation of sc-RNASeq data to identify BM B cell subsets.

(A) The UMAP depicts the distribution of individual cells from the integrated sc-RNASeq dataset after batch effect correction using harmony algorithm. Cells were clustered at a resolution of 0.4 into 16 clusters, labelled on the plot and indicated with individual colours. (B) The dot plot visualises the expression of indicated protein markers from the ADT assay in the integrated dataset. The colour of each dot correlates with the average expression for the

marker within a cluster, and the size of dot indicates the percentage of cells within each cluster that express the marker. Fr.A, Fr.B, Fr.C, Fr.D, Fr.E and Fr.F B cells were classified according to Hardy nomenclature and red boxes highlight markers that are characteristic for a developmental stage. Mito^{hi}FrF denotes a Fr.F cell cluster with higher mitochondrial gene expression. GN stands for bone marrow neutrophils and granulocytes, and NK stands for NK cells. (C) The dot plot visualises the expression of indicated genes from the RNA assay in the integrated dataset. The colour of each dot correlates with the average expression for the marker within a cluster, and the size of dot indicates the percentage of cells within each cluster.

Early-stage populations clustered in lower right of the UMAP, while Fr.F and Fr.E B cells were located towards the top. To validate the annotation accuracy before proceeding with further analysis, cell cycling score analysis (**Figure 5-3A**) and trajectory analysis (**Figure 5-3B**) was performed. Fr.B and Fr.C B cell clusters had the highest proportion of cells in the S and G2/M phases, aligning with the biological features of these being proliferative stages during B cell development. The trajectory analysis along pseudotime was consistent with the annotated populations, with Fr.A having the least Pseudotime score and Fr.F having the highest score.
Notably, GN and NK clusters showed no connection with the B cell populations in the trajectory analysis, indicating substantial differences in RNA expression profiles between B cells and other cell types.

Next, to investigate the impact of GRB2 and self-antigen on these populations, the data was sub-setted into groups which aimed to approximate CD45.2$^+$ mature B cells (predominantly Fr.F clusters), CD45.2$^+$ immature B cells (predominantly Fr.E clusters) and CD45.2$^+$ early precursor B cells (predominantly Fr.A to Fr.D clusters), allowing for a focused analysis of these smaller populations without the influence of the CD45.1$^+$ internal control.

Figure 5-3

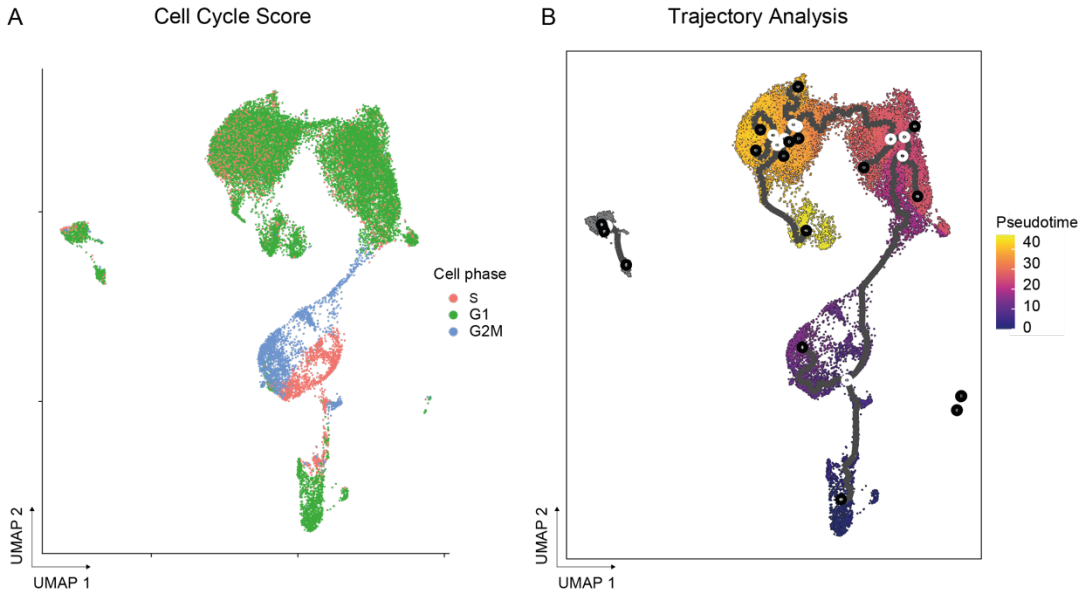

Figure 5-3 The cell cycle scoring and development trajectory of the cells in the integrated sc-RNASeq dataset.

(A) The UMAP depicts the distribution of individual cells from the integrated sc-RNASeq dataset, coloured by the calculated cell cycle score assigned to each cell. The three distinct cell cycle phases, S, G1 and G2/M, are represented by three distinct colours. The score was determined by CellCycleScoring function from the Seurat package. The reference genes for cell cycle phases, originally defined for human data, were converted to mouse analogues for analysis. (B) UMAP for the trajectory analysis of the integrated sc-RNASeq dataset using the "monocle3" package. The trajectory was calculated on the basis of the relatedness of transcriptional profiles of individual cells, and data were aligned along a continuum of gene expression indicating developmental progression. The trajectory is indicated by the black line. The spectrum of colours represents the pesudotimes, with lower values corresponding to earlier development stages.

5.2.1 Presence of GRB2, and not self-antigen, is a dominant discriminator within the integrated immature B population.

The immature B cells (Fr.D and Fr.E in this data) were clustered into 7 clusters following the reintegration, normalization and filtering (**Figure 5-4A**). Cells from two additional clusters, IM7 and IM8, were excluded from the dataset prior to further analysis since they were enriched for markers suggesting they were a mix of non-

immune cells and dead cells. The IM1, IM4 and IM5 clusters at the bottom of the UMAP have higher surface CD93 and lower IgM, IgD and CD21 expression, while the IM2 and IM6 clusters towards the top of the UMAP have comparatively higher IgD and CD21 expression (data not shown). Cluster annotation was confirmed using the top10 differentially expressed (DE) genes detected using the Seurat FindMarkers function (**Appendix table B**). Trajectory analysis further confirmed that clusters IM1, IM4 and IM5 had lower Pseudotime values, suggesting they were at a developmentally earlier stage within the immature B cell pool (**Figure 5-4 B**).

In these broadly defined immature B cell populations, the primary differences among the four experiment groups arise from the absence of GRB2, with antigen presentation exerting a lesser impact on population distribution and transcriptomic changes. (**Figure 5-5A-C**). A relative accumulation of GRB2 deficient cells was observed in IM1 and IM5, with a reduction in IM2 (**Figure 5-4C**), and a redistribution of cells in IM1 and IM0, particularly apparent with GRB2 deficiency **(Figure 5-4A)**. This change coincided with previous findings in the GRB2 deficient mice where Fr.D B cells (**Figure 3-3**, nonMD4 mouse model) and Fr.E B cells (**Figure 4-2**, MD4 mouse model) accumulated in the BM. These observations, supported by the trajectory analysis, were consistent with a developmental progression from IM4/IM5 to IM1, IM0 and IM2, showing the possible arrest of development at this stage in the absence of GRB2. Flow cytometry analyses lack the sensitivity to pick up such subtle distinctions, demonstrating the power of sc-RNASeq-based deep-immunophenotyping to distinguish such differences.

Cluster IM6 was the possible exception to the absence of an effect of self-antigen. IM6 appears to be at the interface between immature and mature populations and was enriched in the absence of GRB2 and the presence of antigen. This subset will be further discussed later in this chapter.

Figure 5-4

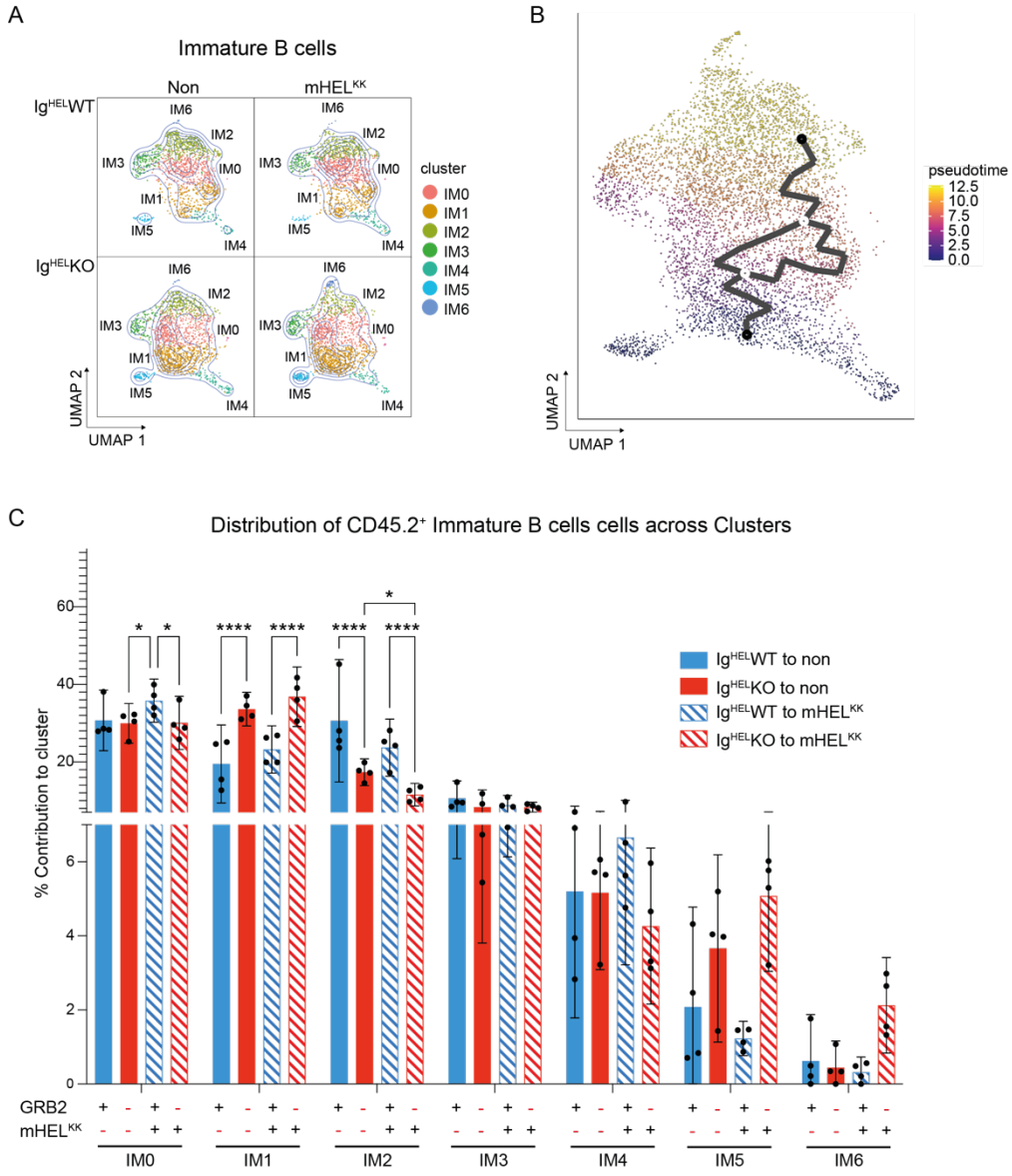

Figure 5-4 The distribution of CD45.2⁺ immature BM B cells across 7 clusters in the context of GRB2 expression and the presence of self-antigen.

Immature B cells identified from the sc-RNASeq integrated data of CD45.2⁺ Ig^{HEL}WT and Ig^{HEL}KO BM B cells reconstituted in either Non and mHEL^{KK} mice, were reclustered and 7 distinct populations were identified at a resolution of 0.4. (A) Contour plots for the UMAPs of the integrated CD45.2⁺ immature B cells. Plots are split by the indicated groups to allow

*quantitative comparison. Colours indicate distinct clusters, and each dot represents a cell. (B) UMAP for the trajectory analysis of the integrated immature B cells data using the "monocle3" package. The trajectory was calculated on the basis of the relatedness of transcriptional profiles of individual cells, and data were aligned along a continuum of gene expression indicating developmental progression. The trajectory is indicated by the black line. The spectrum of colours represents the pesudotimes, with lower values corresponding to earlier development stages. (C) Normalized distribution of cells across the 7 CD45.2^{+} immature BM B cell clusters. The number of Ig^{HEL}WT and Ig^{HEL}KO B cells, reconstituted in either Non or mHEL^{KK} mice, from each cluster was normalized to the total number of cells of that group in the entire experiment on a per mouse basis. Bars show means with 95% confidence limits and symbols indicate data from individual mice. Statistical testing by two-way ANOVA with *P<0.05, **P<0.01 and ****P<0.0001.*

In the immature IM1 cluster, the cells express *Myl4*, *Rsph1*, *Cd72*, *Lrmp*, *Emid1*, *Vpreb3*, *Cd93* (**Appendix table B**). While *Cd72* is a BCR co-receptor expressed on all B cells, *Lrmp* is highly expressed in germinal centre B cells[206], *Vpreb3* is the gene for pre-B cell receptor and *Cd93* is highly expressed in B cell precursors. These observations suggest that IM1 may represent an early-stage immature B cell stage, with no further distinct features identified through RNA and ADT analysis. To gain insight into this population, the RNA expression differences were compared within cluster IM1 between Ig^{HEL}WT and Ig^{HEL}KO donors (**Figure 5-5B**). *Slc16a2*, *Rpgrip1*, and *Dynlt1b* were highly expressed in Ig^{HEL}KO donors, while *Tnfrsf13c*, *Ifi30*, and *Bcl11a* were downregulated.

Similarly, IM0 also shows many features of early-stage immature B cells. This cluster was characterized by high expression of *Ifi30*, *Fgd2*, *Lars2*, *Ms4a1*, *Hck*, *Cd52*, and *Pld4* genes (**Appendix table B**). Of these genes, *Fgd2* expression is suppressed upon BCR activation[207]; *Ms4a1* encodes CD20, which is expressed in all B cells from pro B cell stage and increases during maturity. While *Hck* is highly expressed in B cell progenitors[208]. *Cd52* is highly expressed in plasma cells and binds to SIGLEC10

(SIGLECG). Upon analysis of DE genes in IM0 cluster, the absence of GRB2 had a significant influence on the pattern of DE genes, independent of antigen presence (**Figure 5-5 A**). This included *Cd36*, which is linked to autophagy in B cells[209], and other genes that also differentially expressed in the IM1 comparison. However, clear connections between these DE genes were not identified for both IM0 and IM1 and gene set enrichment analysis and pathway analysis did not produce any relevant results (data not shown).

The IM2 cluster, characterised by comparatively lower CD93 surface expression and higher CD21 and IgD surface expression amongst the immature cells, was most like a late-stage immature B cell population. This cluster highly expressed *Ltb*, *Shisa5*, *Iglc2*, *Tagln2*, *Fcer2a*, *Sell* and *Ms4a4c* genes (**Appendix table B**). Among these, *Ltb* has been identified as a pro-inflammatory inducer that is essential for lymphoid architecture[210] and *Shisa5* has been noted to cooperate with p53 to promote apoptosis[211]. *Tagln2*, a constitutively-expressed small actin protein in immune cells, is upregulated under stimulation by LPS[212]. *Fcer2a*, encoding the Fc receptor CD23, plays an essential role in B cell proliferation and differentiation and is highly expressed in mature B cells. *Sell*, coding for CD62L, is expressed in murine memory cells[213] and is essential for B cell migration[214]. Collectively, these markers suggest that IM2 represents a relatively more mature stage of immature B cells. Analysis of DE genes between the four experiment groups also revealed a dominant effect of GRB2 on transcriptional profiles, regardless of the presence of self-antigen (**Figure 5-5C**).

IM5, characterized by elevated expression of surface CD24, CD25 and CD93, and lower levels of IgM, CD21 and IgD, was most likely a very early-stage immature B cell subset. Gene expression profiles displayed the heightened expression of *Iglv1*, *Atp1b1*, *Rag1*, *Il7r*, *Smarca4*, *Coq7*, *Cecr2* (**Appendix table B**). Notably, *Il7r*, encoding interleukin 7 receptor, is predominantly expressed in early-stage B cells, while *Iglv1* is associated with more mature stage cells. Additionally, *Rag1*, which is crucial for BCR recombination and re-editing, is also highly expressed, suggesting that cells in IM5 might represent populations undergoing BCR re-editing within the immature B cell population. The expansion of IM5 in the absence of GRB2 implied a development impediment between IM1 and IM0 stage, which may redirect cells to IM5 for BCR re-editing before full maturation.

Figure 5-5

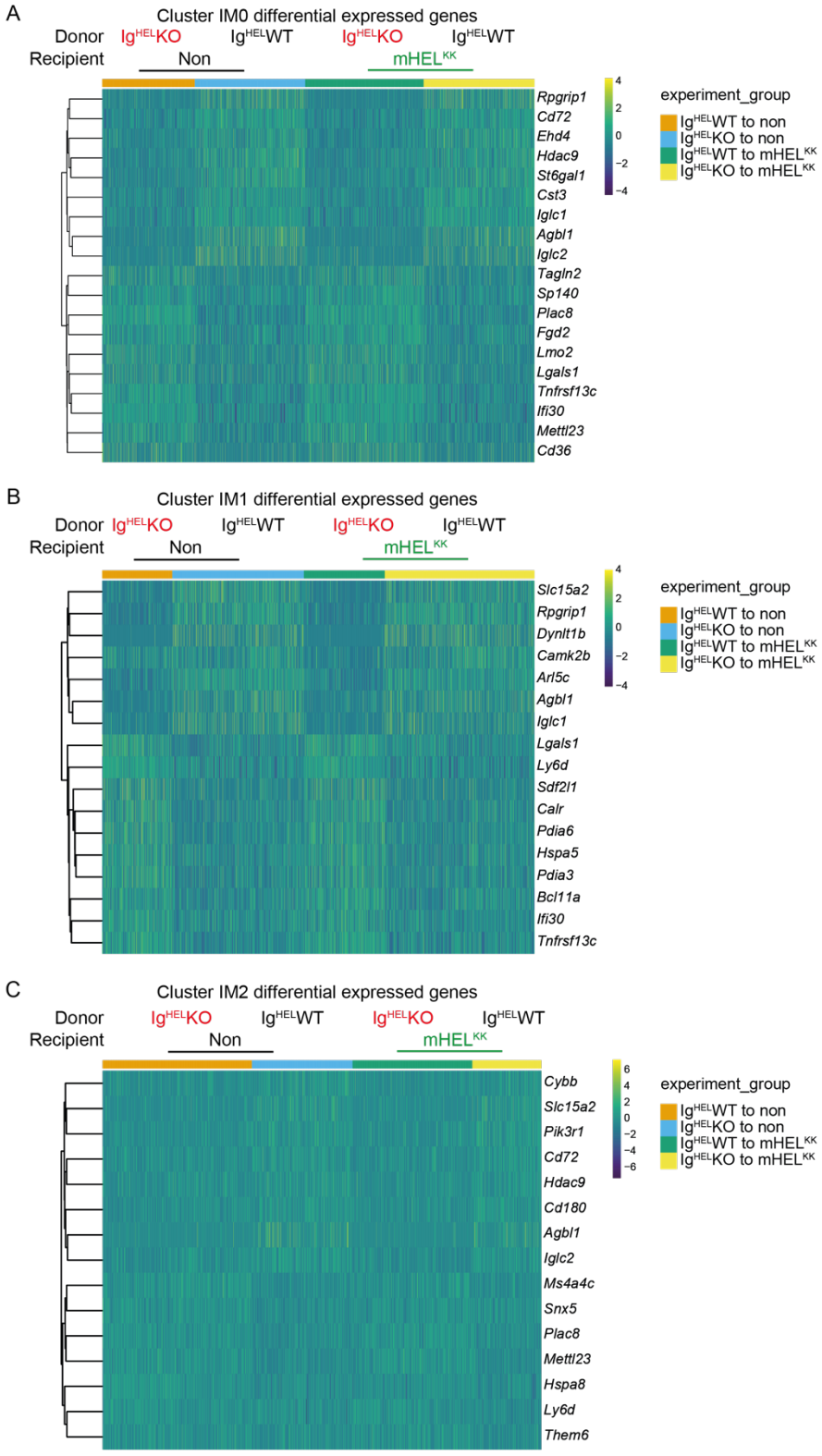

Figure 5-5 Differential expression of genes in the immature BM B cell clusters in the context of self-antigen and GRB2.

Immature B cells defined by the sc-RNASeq data from CD45.2⁺ Ig^{HEL}WT and Ig^{HEL}KO BM B cells, reconstituted in either Non and mHEL^{KK} mice were re-clustered and DE genes were analysed.

Heatmap depicts DE genes within indicated groups for (A) cluster IM0, (B) cluster IM1 and (C) cluster IM2. The coloured horizontal bars on the top of each heatmap indicate the 4 experiment groups. Each column represents data from a single cell and rows indicate genes, as listed on the right of each heatmap. The colours allow visualization of the relative expression of indicated genes with the scale indicated for each heatmap.

5.2.2 Interaction between self-antigen and GRB2 is a distinct feature of mature B cell clusters.

Next, the mature B cell population was sub-clustered into 11 distinct populations as visualized on the UMAP (**Figure 5-6A**). Notably, for Ig^{HEL}WT donors, the presence of self-antigen resulted in a population shift from the upper right to the lower left on the UMAP, with this effect most pronounced in cluster M0. In contrast, for Ig^{HEL}KO donors, the presence of self-antigen shifted the cell population from the right to the top left, indicating distinct effects of self-antigen in the absence of GRB2. Considering the potential influence of self-antigen on both surface protein and RNA expression, the ADT and RNA features of the 'Ig^{HEL}WT to Non' group were utilized to annotate each subcluster (**Figure 5-6B**). Together with trajectory analysis on integrated data (**Figure 5-6 C**), clusters M0, M1, and M2 were identified as the most mature populations, while M4, M7, and M9 were the least mature with higher surface CD93 and CD24 expression. Intriguingly, M6 demonstrated high surface CD21, IgM, and CD43 expression, alongside lower IgD expression, making it challenging to classify this population based on expression of known surface protein features.

Figure 5-6

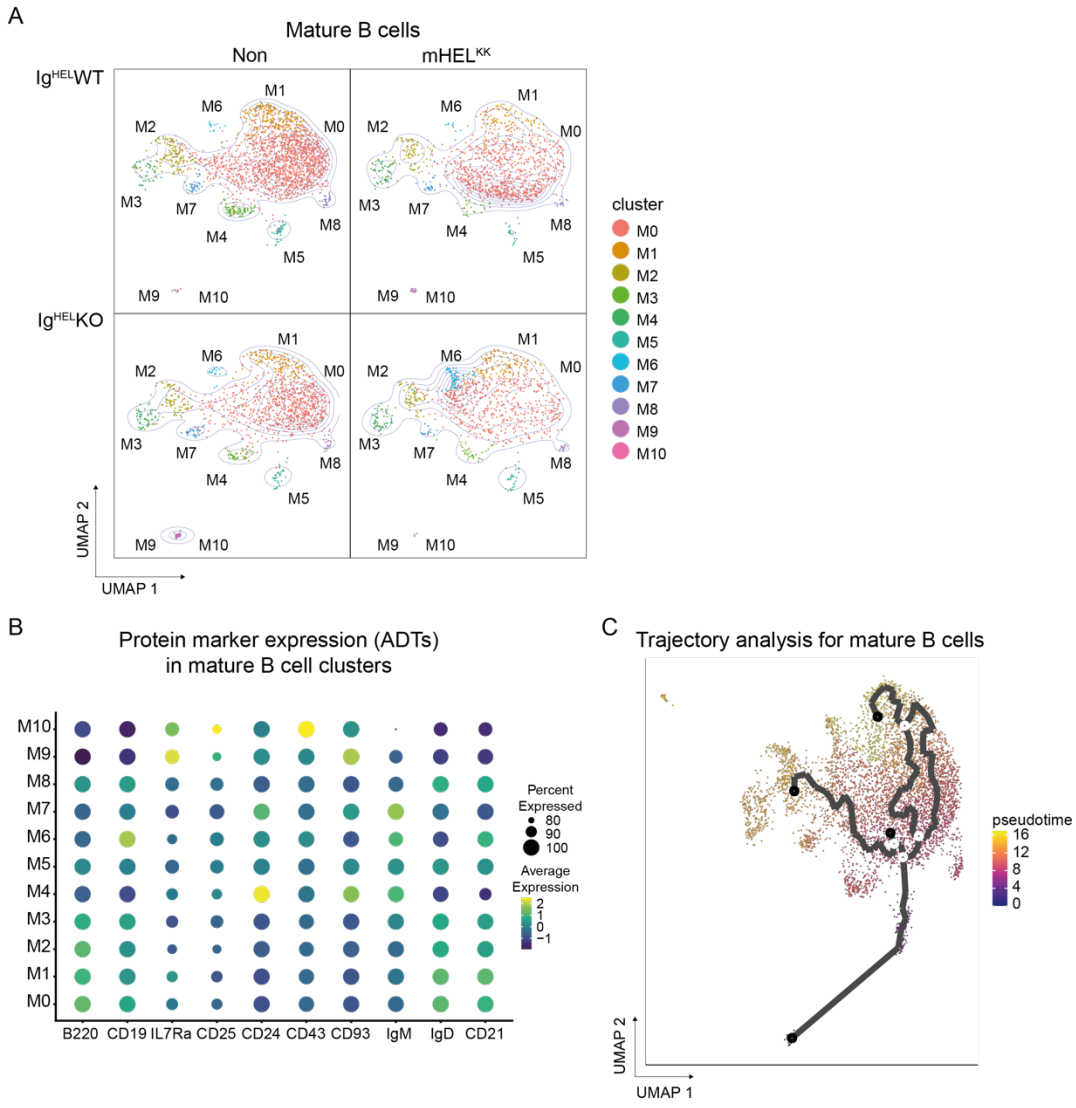

Figure 5-6 Identification of 11 distinct CD45.2⁺ mature BM B cell clusters using sc-RNASeq data.

Mature B cells identified from the sc-RNASeq integrated data of CD45.2⁺ Ig^{HEL}WT and Ig^{HEL}KO BM B cells, reconstituted in either Non and mHEL^{KK} mice, were reclustered and 11 distinct populations were identified at a resolution of 0.3. (A) Contour plots for the UMAPs of the integrated CD45.2⁺ mature B cells. Plots are split by the indicated groups to allow quantitative comparison. Colours indicate distinct clusters, and each dot represents a cell. (B) Dot plot to visualise the expression of indicated protein markers in the mature B cell clusters in the integrated data. The colour of each dot correlates with the average expression for the marker within a cluster, and the size of dot indicates the percentage of cells within each cluster that express the marker. (C) UMAP for the trajectory analysis of the integrated mature B cells data using the "monocle3" package. The trajectory was calculated on the basis of the relatedness of transcriptional profiles of individual cells, and data were aligned along a continuum of gene expression indicating developmental progression. The trajectory is indicated by the black line. The spectrum of colours represents the pesudotimes, with lower values corresponding to earlier development stages.

When comparing different experimental groups, the absence of GRB2 led to a reduction in the percentage of the M0 population, with a more pronounced reduction observed in the presence of self-antigen **(Figure 5-7)**. While the presence of self-antigen did not alter the total number of cells for Ig^{HEL}WT donors, it did shift the distribution of cells within clusters. In cluster M1, the presence of self-antigen reduced the cell number, but the absence of GRB2 mitigated this reduction. Remarkably, the absence of GRB2 increased the cell number in the M6 cluster, and the presence of self-antigen further expanded this population. The characteristics of M0, M1, and M6 clusters drew were also interesting. M0 exhibited high expression of *Rps24*, *Uba52*, *Rps2*, *Rps15a*, *Fau*, and *Rpl18a* (**Appendix table C**), most of which are related to ribosomal proteins, suggesting a state of high metabolism in this mature B cell population. On the other hand, M1 cluster displayed high expression of *Tagln2*, *Vim*, *Myadm*, *Ahnak*, *Jund*, *Cd2*, *Cd69*, and *Cd83* genes (**Appendix table C**), indicative of distinctive activation-like molecular features within this cluster. *Tagln2* is expressed in most B cells while it is upregulated in germinal centre cells and activated B cells[215]. *Vim* encodes vimentin, an important part of antigen presentation and antibody response in B cells[216]. *Ahnak* encodes AHNAK-1 protein that mediates the TCR induced intracellular calcium mobilization[217], while its role in B cells remains unknown. Although CD69 is typically recognized as an activation marker in T cells, its role in B cells is less understood. Intriguingly, the deficiency of CD69 has been associated with augmented B cell development in a previous study[218]. Similarly, CD83 is highly expressed in activated B cells and light zone B cells[219]. According to these gene features, cluster M1 seems to be an activated mature B cell population.

Figure 5-7

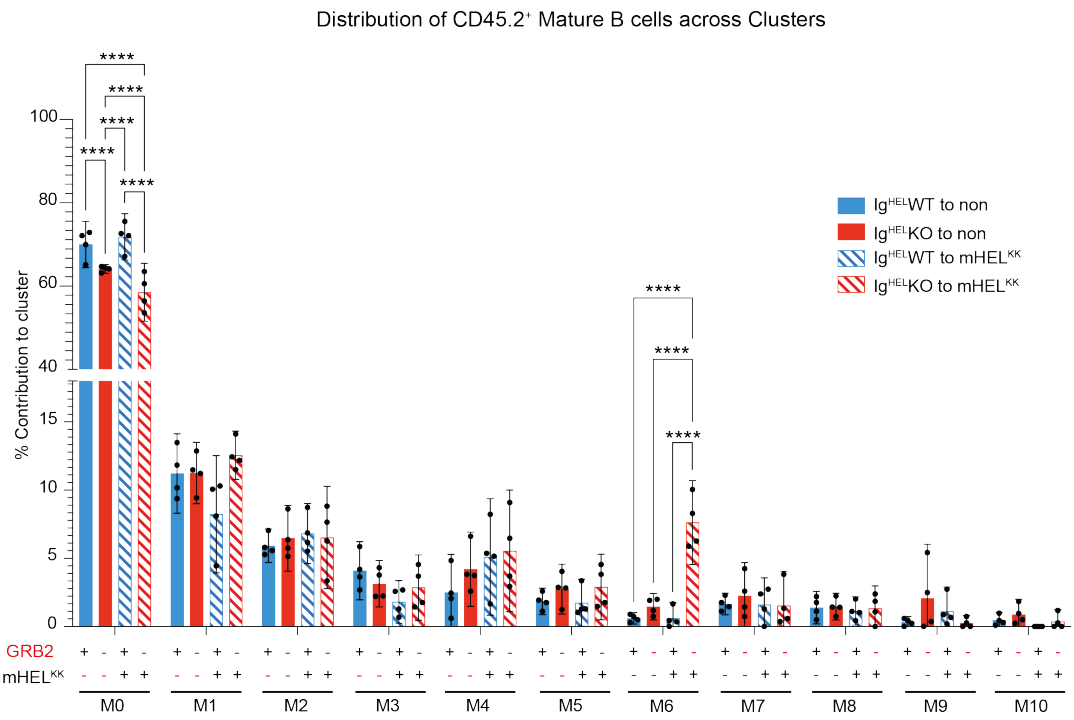

Figure 5-7 GRB2 and mHELKK self-antigen have distinct effects on the distribution of CD45.2+ BM B cells across the 11 clusters defined using sc-RNASeq data.

*Normalized distribution of cells across the 11 CD45.2^{+} mature BM B cell clusters defined using the RNA and ADT assays from the sc-RNASeq experiment. The proportion of Ig^{HEL}WT and Ig^{HEL}KO B cells reconstituted in either Non and mHEL^{KK} mice within each cluster was quantified and normalized to the total number of cells in the assay from individual mice in each group. Bars show means with 95% confidence limits and symbols indicate data from individual mice. Statistical testing by two-way ANOVA with **P<0.01 and ****P<0.0001.*

As both GRB2 and self-antigen influenced cell distribution in the M0 cluster, the gene expression changes within this cluster across different experiment groups is of interest. Hence, the differential gene expression was compared within M0 between the four experiment groups. The presence of self-antigen resulted in alterations in several BCR-related genes, including upregulation of *Fcmr*, *Ighd*, *Bcl2*, and *Zfp318*, and downregulation of *Crip1* and *Hspa8* (**Figure 5-8A**). In the absence of self-antigen, the deficiency of GRB2 did not induce substantial changes in the RNA expression

profile. However, in the presence of self-antigen, the absence of GRB2 revealed more pronounced differences: upregulation of *S100a6*, *Sox5*, *Ly6a*, and *Crip1*, and downregulation of *Fcmr*, *Ighd*, *Zfp318*, *Cd72*, and *Mettl23* (**Figure 5-8A**). While no clear pattern emerged from these changes, the presence of self-antigen appeared to induce alterations in BCR-related signalling, with the deficiency of GRB2 mitigating some of these effects.

Examining the M6 cluster revealed high expression levels of *Apoe*, *S100a6*, *Cd9*, *Plac8*, *Cacna1e*, *Nfatc1*, *Atxn1*, and *Rftn1* genes (**Figure 5-8B**). Notably, *Apoe*, *S100a6*, and *Nfatc1* are genes that are highly expressed in B1 B cells, while *Cd9*, *Plac8*, and *Atxn1* are genes expressed in both MZ B cells and B1 B cells, as indicated by the Immgen database[220]. The distinctive transcriptomic profile observed in this subpopulation suggests a potential close relationship between this population and the ontogeny of B1 B cells or MZ B cells. Given the increased prevalence of this population, particularly in the absence of GRB2 and reaching the highest levels in the 'Ig^{HEL}KO to $mHEL^{KK}$' group, I hypothesize that this subpopulation may represent positively selected progenitors, perhaps most likely MZ B cells given the high expression of CD21. Further experiments are required to confirm the existence of this population and to elucidate its function, as well as to establish whether similar intriguing populations exist in the periphery.

Figure 5-8

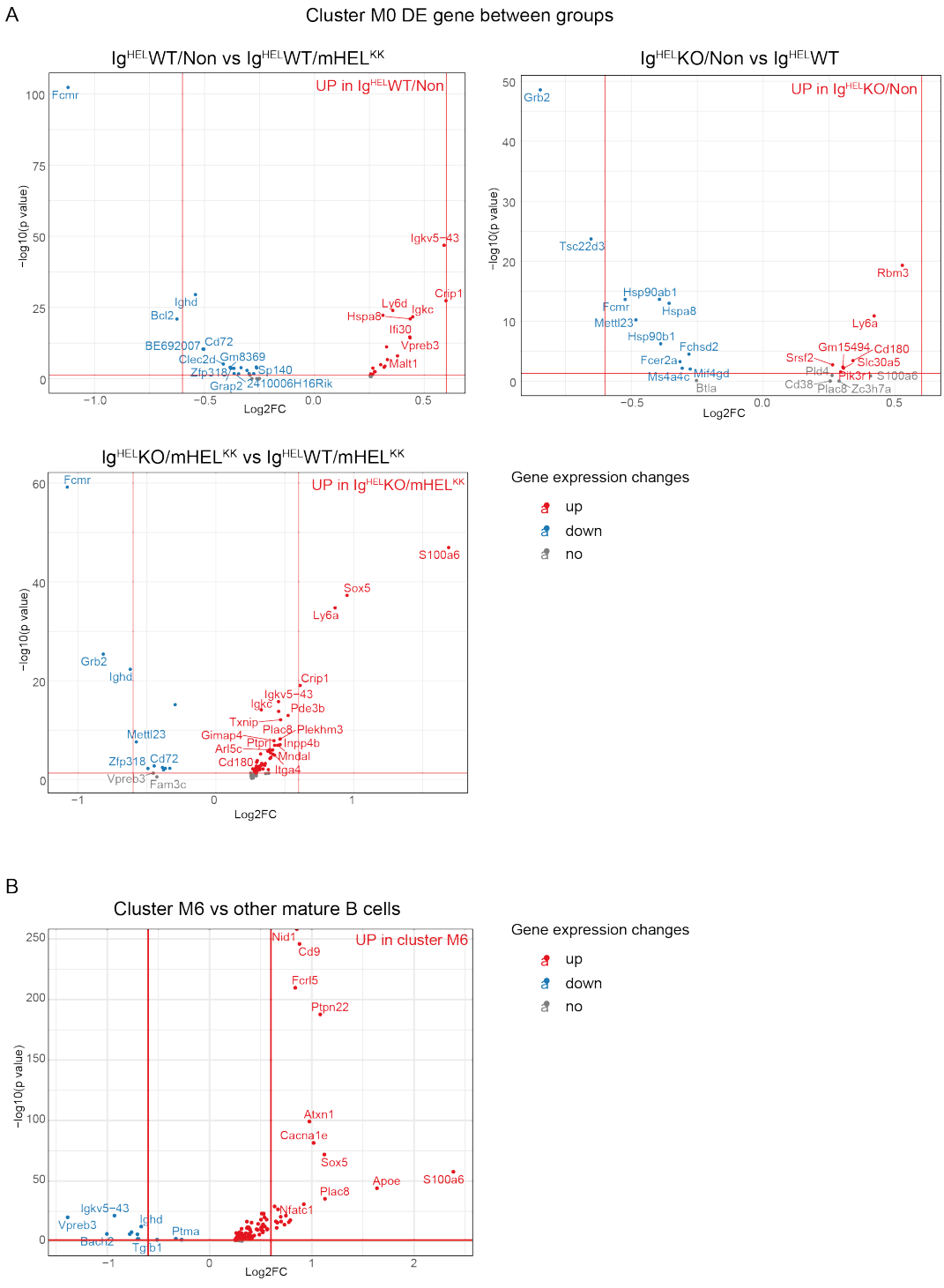

Figure 5-8 Differential expression of genes in the M0 and M6 mature BM B cell clusters.

(A) Volcano plots comparing the DE genes of the CD45.2⁺ mature BM B cell cluster M0, identified using the RNA and ADT assays from the sc-RNASeq experiment. The first and second groups for every comparison are indicated for each violin plot. The vertical red lines represent the log2 fold change (Log2FC) threshold at -0.6 and 0.6, and the horizonal red line represents the p value threshold corresponding to an adjusted -log10 p value of 0.05.

Genes upregulated in the first group in every comparison are indicated in red and genes downregulated in the first group are in blue. (B) Volcano plot, constructed as above, and comparing the DE genes of CD45.2⁺ mature BM B cell cluster M6 with all other CD45.2⁺ mature BM B cells clusters. Genes upregulated in M6 are indicated in red and downregulated genes are in red.

5.4 GRB2 is required to induce the tolerogenic pathway leading to IgM modulation by self-antigen.

When developing B cells encounter self-antigen at levels sufficient to induce anergy, surface IgM is downregulated and IgD is upregulated in equal measure[221,111]. The continuous BCR signalling in anergic cells leads to an elevated cytosolic calcium concentration[222], with enhanced translocation of NFAT from cytoplasm to nucleus[222] leading to increased *Egr2*/*Egr3* and *Zfp318* expression[221, 223]. As NFAT target genes, *Egr2*/*Egr3* are also subject to co-regulation by NFAT-interacting protein NIP45[224]. The elevated level of *Egr2*/*Egr3* could further induce the expression of the suppressor of cytokine signaling-1 (SOCS1) and SOCS3, which function as the inhibitors of STAT1 and STAT3 signalling pathways, and attenuate BATF activity in B and T cells[225]. While no direct interaction has been demonstrated yet, the *Egr2*/*Egr3* knockouts have been associated with reduced expression of *Zfp318* in B cells[221], a factor that induces preferential splicing to *Ighd* at the expense of *Ighm*[226]. Coincidentally, *Zbtb32*, *Zbtb20*, *Mzb1* and related genes, downregulated by *Egr2*/*Egr3*, exert an inhibitory role on plasma cell differentiation[221].

The same phenomenon of IgM modulation can be observed upon exposure to self-antigen at lower concentrations that are not sufficient to induce anergy, or when

mutations in key signalling components increase BCR signalling[227]. Since antigen-induced IgM modulation was observed on Ig^{HEL}WT mature BM B cells in the presence of the $mHEL^{KK}$ self-antigen, but not Ig^{HEL}KO BM cells (**Figure5-9 A-D**), it was speculated that a defect in the *Egr2/3*-dependent pathways for enforcing tolerance might explain why GRB2-deficiency leads to an increase in positive selection.

Figure 5-9

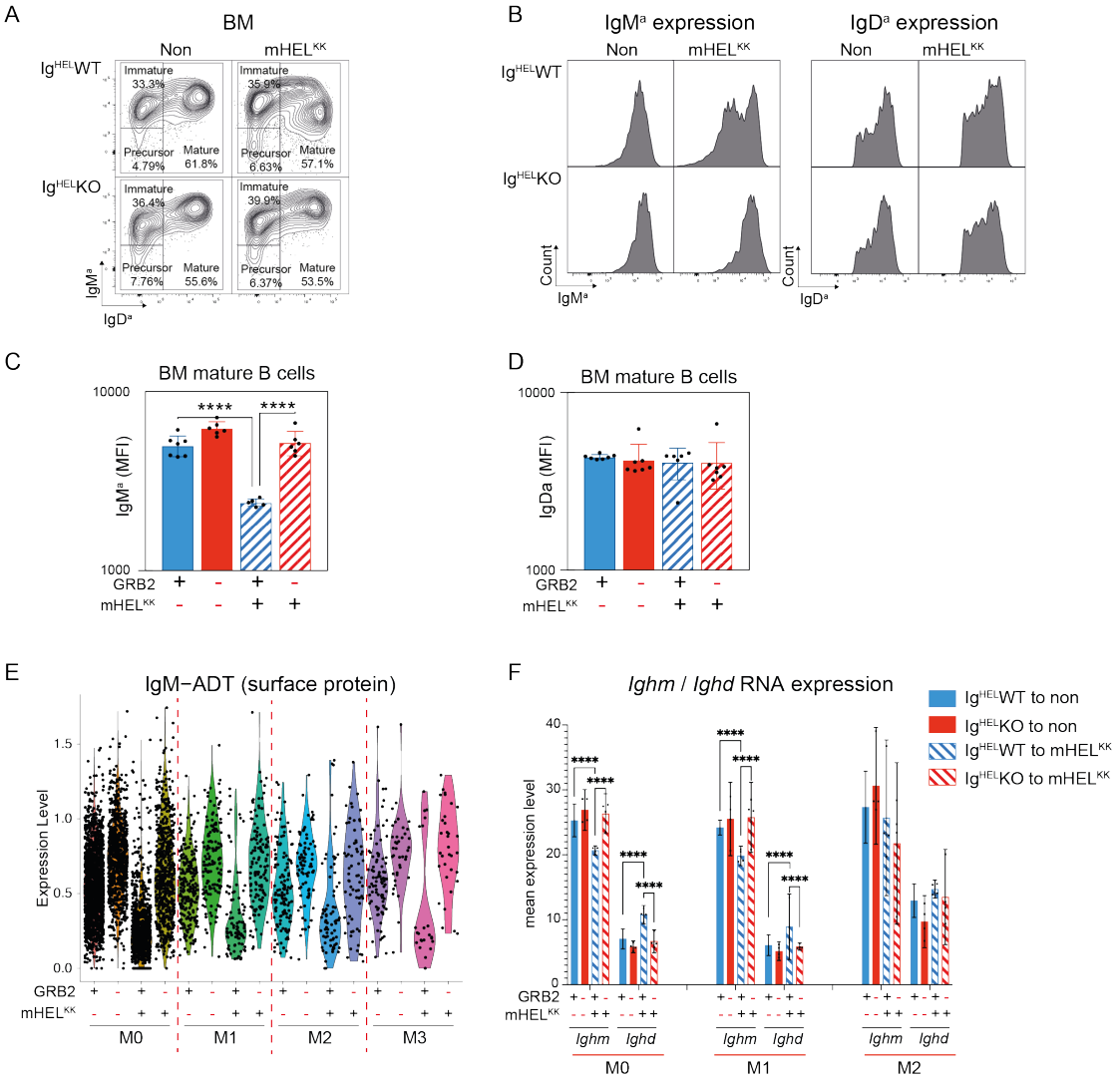

Figure 5-9 GRB2 is required to induce the tolerogenic pathway leading to IgM modulation by self-antigen.

*(A-D) Ig^{HEL}WT or Ig^{HEL}KO BM was transplanted into irradiated Non and $mHEL^{KK}$ mice and reconstitution was assessed 8 weeks later. (A) Representative flow cytometry contour plots for $B220^+CD19^+$ BM B cells from indicated groups. BM B cells were gated as precursor B cells ($B220^+IgM^{a-}IgD^{a-}$), immature B cells ($B220^+ IgM^{a+} IgD^{alow}$) and mature B cells ($B220^+ IgM^{a+} IgD^{ahi}$). The percentages of each subset in the representative sample are indicated on the plots. (B) Representative histograms for expression of IgM^a (left) and IgD^a (right) on the surface of mature BM B cells from the indicated groups. (C) The IgM^a MFI and (D) the IgD^a MFI of mature BM B cells as defined in (A) and represented in (B). Bars show geometric means with error bars indicating 95% confidence limits and dots show the individual data points. Data are representative of at least 3 independent experiments with 4-7 mice per group. Statistical testing by one-way ANOVA with ****P<0.0001. (E-F) BM chimeras were generated with $CD45.2^+$ Ig^{HEL}WT or Ig^{HEL}KO BM and $CD45.1^+$ Ig^{HEL}WT BM transplanted into irradiated Non and $mHEL^{KK}$ mice. Sc-RNASeq data with HTO and ADT assays was generated from sorted $CD45.2^+$ and $CD45.1^+$ BM B cells. Mature $CD45.2^+$ B cell subclusters were identified from the sc-RNASeq data using the RNA and the ADT assays. (E) Violin plot compares the CLR-normalized*

*expression level of surface IgM protein on CD45.2$^+$ mature BM B cells from the indicated groups. Each dot represents data from an individual cell. (F) The mean expression level of Ighm and Ighd in CD45.2$^+$ mature BM B cells from the indicated groups, as measured from the RNA assay in the sc-RNASeq data. The bars represent the geometric means, each dot is average data pooled from the single cells of individual mice, and error bars indicate 95% confidence limits. Statistical testing by two-way ANOVA with ****P<0.0001.*

As already described, antigen exposure induced changes in the distribution of mature B cell clusters on the UMAP and their total numbers within clusters (**Figure 5-6A and Figure 5-7**). Focusing on the surface IgM expression of B cells within the same clusters across four different experiment groups, we observed that for clusters M0, M1, M2 and M3, the IgM-ADT expression was downregulated in the presence of self-antigen for Ig^{HEL}WT donors, while Ig^{HEL}KO donors did not exhibit this change (**Figure 5-9E**).

Similarly, *Ighm* mRNA was suppressed and *Ighd* mRNA elevated by mHEL^{KK} in Ig^{HEL}WT M0 and M1 B cells, but not in the absence of GRB2 **(Figure 5-9 F)**. Mature Ig^{HEL}WT and Ig^{HEL}KO B cells from M0 and M1 were induced by mHEL^{KK} to expressed increased *Nfatc1*. However, only WT Ig^{HEL} B cells showed elevated *Egr3* and *Zfp318* expression in M0 and M1 in response to antigen (**Figure 5-10A and B**); neither *Egr3* nor *Zfp318* were elevated in the absence of GRB2 (**Figure 5-10A and B**). Whilst IgM is normally modulated in anergic B cells exposed to sHEL in the absence GRB2, the implication here is that GRB2 may be required to induce the *Zfp318*-dependent pathway in response to mHEL^{KK}.

Figure 5-10

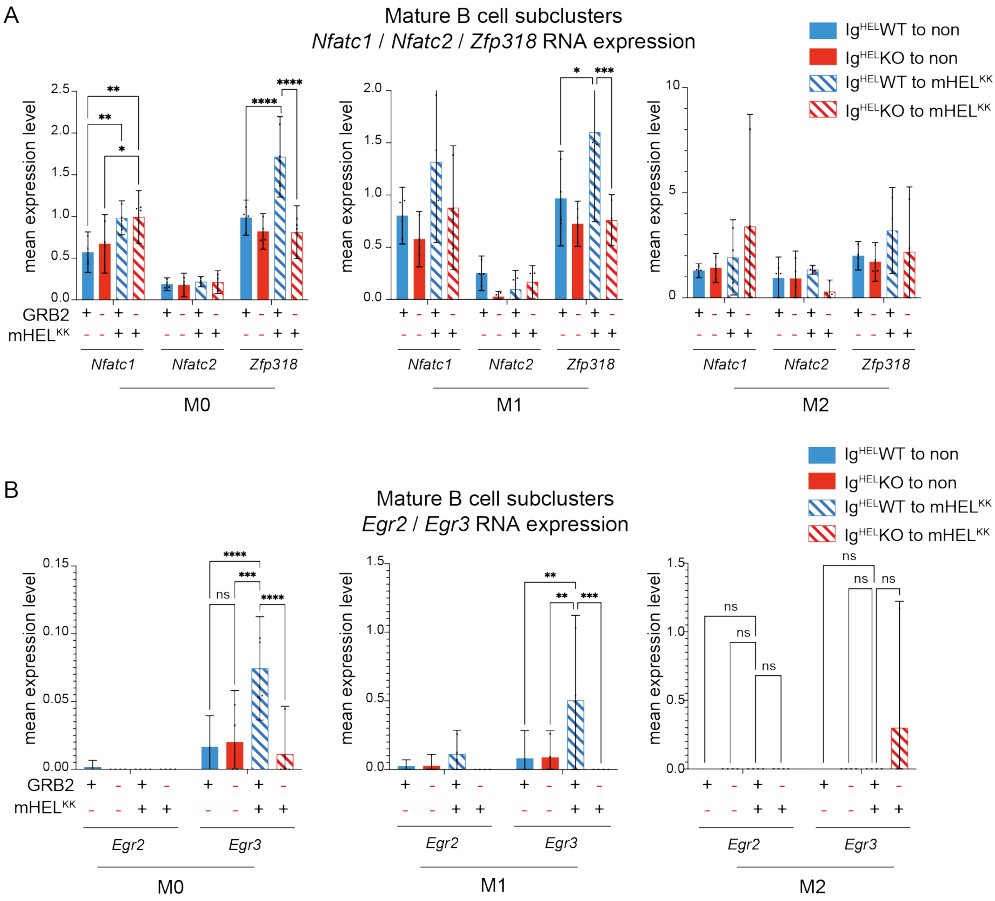

Figure 5-10 Zfp318 and Egr3 transcripts are not induced by intracellular mHELKK self-antigen in mature BM B cells when GRB2 is absent.

*Mature CD45.2^{+} B cell subclusters were identified from the sc-RNASeq data generated from Ig^{HEL} BM mixed chimeras. (A) The mean expression level of Nfatc1, Nfatc2 and Zfp318, and of (B) Egr2 and Egr3 in Ig^{HEL}WT and Ig^{HEL}KO B cells in the presence or absence of mHEL^{KK}. Data are pooled from 4 mice per group with each dot representing a mouse. The bars represent the geometric means and error bars indicate 95% confidence limits. Statistical testing by two-way ANOVA with ****P<0.0001, ***P<0.001 and **P<0.01.*

5.4 Deficiency of GRB2 alters the Calcium flux induced by BCR signal.

Given the role of BCR-related signals in the positive selection of B1 B cells and the induction of tolerance by upregulation of NFAT-dependent signalling, it is noteworthy that BCR-dependent calcium signalling has been reported to be elevated in the absence of GRB2[169]. This alternation of calcium flux signalling may be mediated by DOK3, an adaptor that sequesters GRB2 and negatively regulates the B cell activation and calcium flux upon IgM aggregation[151, 228]. Another potential mediator is CD22, which recruits GRB2 upon BCR activation and act as a negatively regulator of calcium flux [229]. Correspondingly, signals downstream of the calcium signal play a pivotal role in determining the activation, proliferation, or survival of B cells[230]. It is possible that the enhanced calcium signalling observed might be one main factors of increased positive selection in the absence of GRB2.

Nitschke and colleagues described how GRB2 deficiency enhances the calcium flux induced by BCR stimulation, affecting both intracellular and extracellular Ca^{2+} mobilization[169]. Similar enhancements were encountered when splenic Ig^{HEL}KO B cells were stimulated with anti-IgM or sHEL (**Figure 5-11A**). Similar effects were seen in BCR activated immature and mature B cells in BM (**Figure 5-11B**). If changes in calcium flux are crucial for B1 B cell selection in the absence of GRB2, B1 B cell progenitors should experience similar Ca^{2+} flux alterations in Ig^{HEL}KO mice when generating B1 B cells. However, the lack of a clear definition and markers for B1 B cell progenitors makes direct testing of Ca^{2+} flux on B1 B cell progenitors challenging.

Calcium flux in peritoneal $FSC^{hi}B220^{low}CD19^{hi}CD43^{+}$ peritoneal B1 B cells was evaluated (**Figure 5-11C**). GRB2 was found to negatively regulate calcium flux in mature B1 B cells, with BCR-induced calcium flux being weaker in B1 B cells compared to that in B2 B cells, potentially attributable to a lower surface BCR expression rate in B1 B cells.

5.5 Phosphorylation of BCR related signal molecule have not been changed significantly in the absence of GRB2.

Nitschke and colleagues also observed that BCR-induced phosphorylation of SYK was increased in KO mice, whilst the phosphorylation of AKT, a downstream component of the PI3K pathway, was reduced[169]. To assess BCR signalling in the Ig^{HEL}KO B cells, the phosphorylation of SYK, BLNK (B cell linker protein), BTK, PLCG2, and ERK with various concentrations of anti-IgM stimulation were measured **(Figure 5-11 C)**. The absence of GRB2 did not exhibit significant differences in these BCR proximal signal pathways.

Further experiments are warranted to identify potential targets of GRB2 within the broader BCR signalling cascade.

Figure 5-11

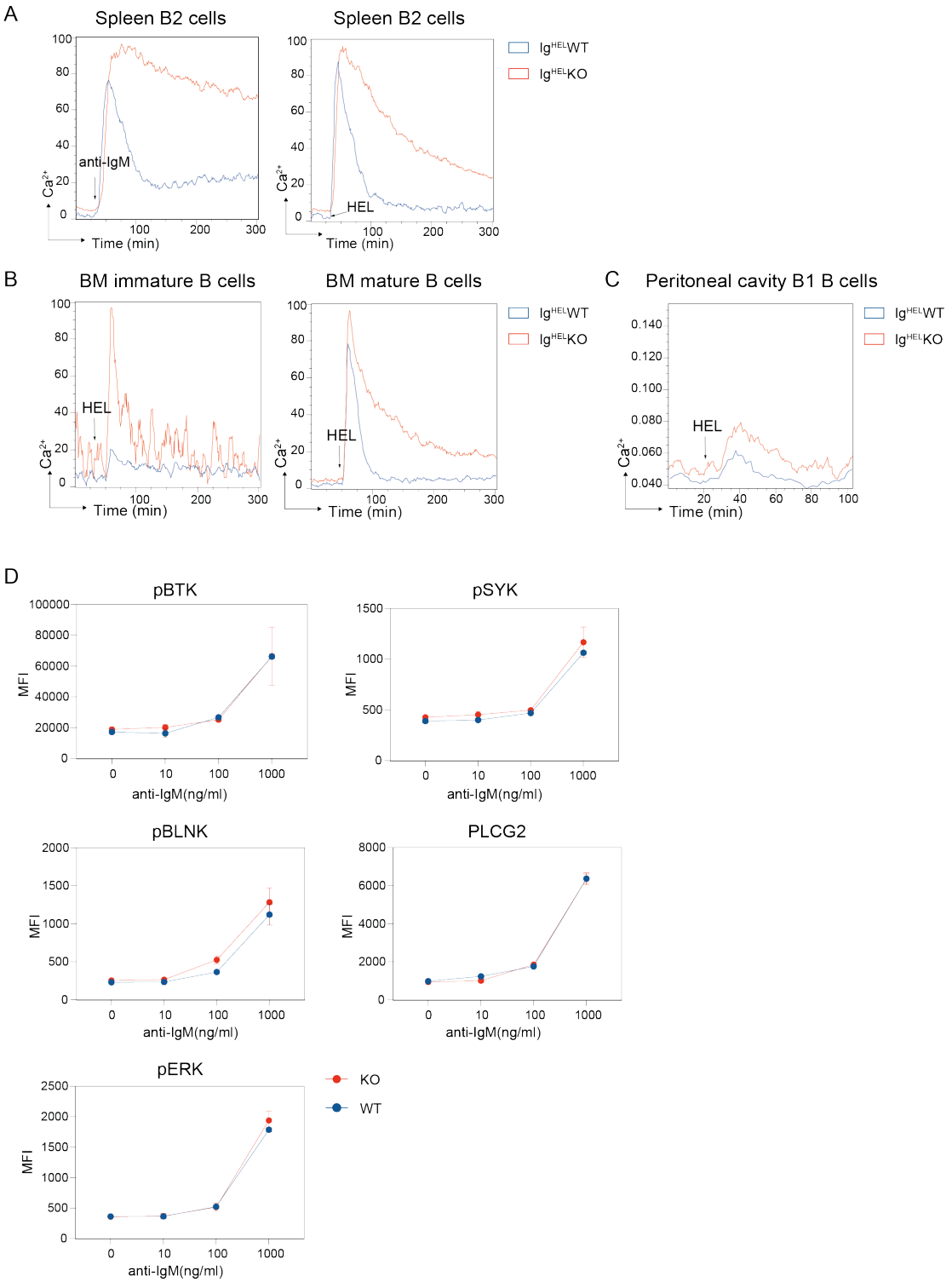

Figure 5-11 Deficiency of GRB2 alters the calcium flux, but not the phosphorylation of signalling molecules downstream of BCR stimulation.

(A) Ratiometric analysis of FuraRed by flow cytometry to measure calcium flux in Ig^{HEL}WT and Ig^{HEL}KO spleen B2 B cells stimulated with 1 μg/ml anti-IgM (left panel) or 1 μg/ml HEL (right panel) for 5 min. (B) Calcium flux measured for 5 min in immature (left panel) and mature (right panel) BM B cells from Ig^{HEL}WT and Ig^{HEL}KO mice upon stimulation with 1 μg/ml HEL. (C) Calcium flux measured for 2 min in peritoneal B1 B cells from Ig^{HEL}WT and Ig^{HEL}KO mice upon

stimulation with 1 μg/ml HEL. (D) Ig^{HEL}WT and Ig^{HEL}KO B cells were stimulated with indicated doses of anti-IgM at 37°C for 5 min and the phosphorylation of indicated signalling molecules was measured by intracellular flow cytometry. Data are representative of results from three independent experiments. The filled circles are average MFIs for each marker and error bars indicate 95% confidence intervals.

5.6 Discussion

Single-cell RNA sequencing empowers researchers to explore rare populations without prior knowledge in a high-throughput manner. Although one study has reported a potential population of B1 B cell progenitors[193], there is no clear validation using cell transfers to test for B1 B cell development. We have shown that the absence of GRB2 does not alter the proliferation rate or lifespan of B1 B cells, leaving increased development of B1 B cell progenitors as the most likely cause for the increased number of mature B1 B cells in the BM chimera experiment. Therefore, the current situation in which B1 B cell selection is increased by GRB2 deficiency, is an opportunity to search again for a progenitor population.

Interestingly, a small population (M6) was identified in the mature BM B cell subset, exhibiting both B1 B cell and MZ B cell RNA features, characterized by high surface expression of CD19, CD21, CD43, IgM, and low IgD. Categorizing this population into any classical B cell precursor definition proves challenging. Remarkably, the absence of GRB2 slightly increased the number of cells in this cluster, and the presence of self-antigen further significantly enlarged this population. These features suggest that this population might be a potential B1 B cell or MZ B cell progenitor. The expression of CD43 decreases with B cell maturation, while CD21 increases during

the same period. The unusual co-expression of CD43 and CD21 raises questions about whether this is a heterogeneous population comprising two distinct subpopulations. Despite potential concerns about false positives due to technical noise or over-clustering in the computing process, this cluster was robustly maintained as one unique population (data not shown). Although the small number of cells in this population does complicate this issue, present data suggests that this cluster is more likely to be one unique population rather than a mixture of two populations.

In future experiments this population will be identified by flow cytometry, isolated and transferred into *Rag1*$^{-/-}$ mice to investigate whether B1 B cells or MZ B cells can be generated.

In addition to identifying this unique population with B1 and MZ B cell markers, sc-RNASeq data also revealed distinctive features of both mature and immature B cells. Notably, for immature B cells, the primary differences between groups were associated with GRB2, with self-antigen exerting a comparatively lesser influence on UMAP distribution and RNA expression. This observed pattern may be attributed to the relatively low expression of surface BCR. In the absence of GRB2, key genes such as *Rpgrip1*, *Slc15a2*, *Agbl1*, and *Iglc1* were upregulated, while *Lgals1*, *Ifi30*, and *Tnfrsf13c* were downregulated. The function of *Rpgrip1*, *Slc15a2* and *Agbl1* in B cells is not fully understood. *Lgals1* seems to be important for regulatory function of B cells[231], *Ifi30* functions for MHC class II antigen processing in B cells[232] and *Tnfrsf13c* encodes BAFF-R, a critical element for B cell survival[233]. This suggests that the

absence of GRB2 may have altered immature B cells in terms of survival and function. However, no specific biological pathways can be pinpointed with these changes in gene sets. Currently, it remains unknown whether these alterations are related to B1 B cell positive selection or changes in B2 cells. Additionally, comparison of the RNA expression profile of early-stage B cells (Fr.A to Fr.D) in the BM chimera showed no remarkable changes even after further sub-clustering of this population (data not shown). Based on current evidence, GRB2 appears to exert significant influence mainly from the immature B cell stage and onwards.

In mature B cells, both GRB2 and self-antigen exerted effects on RNA expression. Apart from cluster M6, the primary changes in the mature B cell subset were associated with the proposed *Ighd*/*Ighm* signalling pathway[221]. The KO mice failed to simultaneously downregulate IgM and upregulate *Zfp318* in the presence of self-antigen. *Nfatc1* was upregulated in KO donors in the presence of self-antigen, without concurrent upregulation of *Egr2*/*Egr3* and *Zfp318*. GRB2 may regulate key proteins within the NFATC1 to ZFP318 signalling pathway. However, it is uncertain whether this regulation is a result of direct interaction, interactions between GRB2 and any protein within this pathway has not been previously reported. Additionally, the involvement of this pathway in B1 B cell ontogeny is not clear. One hypothesis is that the failure to downregulate IgM in response to self-antigen in the absence of GRB2 shifts negative selection into positive selection, leading to an increase in B1 B cells. This hypothesis is supported by a similar phenomenon observed in 3-week-old Ig^{HEL}/$mHEL^{KK}$ double transgenic mice (data not shown), where BM B cells have not yet downregulated their surface IgM and can still give rise to B1 B cells at that point in

time. To identify the targets of GRB2 within this signalling pathway, I will conduct follow-up experiments to assess NFATC1/NFATC2 translocation in the absence of GRB2 using western blot analysis.

Nitschke and colleagues reported increased SYK phosphorylation and reduced AKT levels in KO splenic B cells[169]. SYK is a key protein in proximal BCR signalling, and AKT is situated downstream of PLCR2 and the PI3K signal. However, no obvious differences were observed in the phosphorylation of SYK, ERK, PLCG2, BLNK, or BTK in Ig^{HEL} B cells in the absence of GRB2. This difference could stem from variations in sensitivity of measurements and the subtle nature of changes in signals without GRB2. Hence, loss of GRB2 does not significantly alter proximal BCR signalling, suggesting that molecules other than these proximal signals may be involved in BCR signalling changes in the absence of GRB2.

Chapter 6 The ontogeny-related transcriptional differences in the developmental switch between FL and adult BM B cell progenitors

6.1 Introduction

Developmental haematopoiesis unfolds in distinct waves. In its earliest stages, it initiates in the dorsolateral plate of the aorta-gonads-mesonephros (AGM) region around embryonic day 10.5 (E.10.5)[234], and transitions to the FL by E.11 and E.12[235]. Subsequently, from near birth throughout life, haematopoiesis primarily occurs in the BM[235].

Fetal B cell development is distinct from that in the BM in that FL HSCs do not show the same dependence on the presence of IL-7 or stromal-derived lymphopoietin (TSLP)[236]. Additionally, the PAX5/BSAP transcription factor appears indispensable for B cell development in the FL, whereas it is dispensable for BM B cell development[237].

As already discussed, a further distinction between FL and BM, is the former's ability to generate B1 B cells. Single-cell tracing experiments reveal that FL HSCs are able to give rise to both B1a B cells and B2 B cells, whereas BM retains the potential for generating primarily B2 B cells with a significantly lower contribution to B1a B cells[95, 238, 239]. FL HSCs demonstrate the ability to produce both B1a and mast cells within a narrow time window, with this capability diminishing after E.14.5[240].

The variance between FL and BM in generating B1 B cells is attributed, in part, to the *Lin28b*/*let7* switch and its related downstream signalling pathways, which regulate the balance of positive and negative selection in B1 B cell generation[109]. The overexpression of LIN28B in BM partially restores its capacity to generate B1 B cells[109]. Furthermore, FL B cells exhibit little or no expression of TdT during HC rearrangement, resulting in fewer non-templated nucleotide additions at the junction of BCR sequences[241]. The forced expression of TdT in FL reduces the secretion of anti-PC antibodies, typical of natural antibodies secreted by B1 B cells[242]. This suggests that TdT expression may play a crucial role in B1 B cell generation and may be a key reason for the diminished ability of adult BM to generate B1 B cells.

Despite these insights, there remains no detailed understanding of the switch in haematopoiesis that occurs in ontogeny from FL to BM. Our discovery that GRB2 was required to suppress antigen-independent and antigen-driven B1b B cell generation from FL and BM tissue created an opportunity to explore these mechanisms further. The following chapter discusses work using single cell sequencing technology to construct a comprehensive atlas of FL and adult BM B cells, with the aim to uncover clues regarding B1 B cell generation.

6.2 Transcriptional differences between FL and BM B cell development are not GRB2-dependent.

To obtain an unbiased RNA profile of FL and BM B cells, while minimizing technological bias and biological variation, three E.18 FL samples were collected on the same day as adult BM samples from three WT and three KO mice of same gender and similar age. The experiment was designed to identify the common features of WT FL and KO BM vs WT BM that might be associated with B1b B cell development. Each donor tissue was individually processed and labelled with a unique HTO reagent. The nine samples were then pooled post labelling and subject to flow cytometric sorting. IgD^{low} B cells (live, $B220^{+}CD19^{+}$ IgD^{low}) were isolated to exclude mature B cells and enrich for precursor cells, with the aim to improve the sensitivity for the detection of rare progenitor populations. The sorted samples were further processed for single-cell partitioning and sequencing (**Figure 6-1A**). Due to the limitations in cells captured and recovery per gel bead, the sorted pool was divided into two identical samples, loaded them separately as two batches for single cell partitioning (labelled as batch 1 and batch 2). 12773 cells from batch 1 sample and 13501 cells from batch 2 sample (**Figure 6-1 B**) were successfully recovered and merged together for subsequent analysis.

The raw data were demultiplexed into singlets and doublets using the HTO stain information. Subsequently, the data were filtered to retain singlets with a specified range of RNA features per cell (nFeature RNA) and a low percentage of mitochondrial genes (percent.mt) (**Figure 6-1C**).

Figure 6-1

A

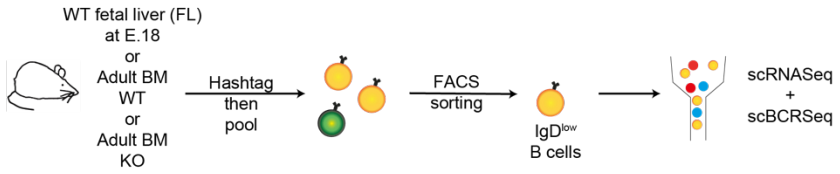

B

Sample	Batch 1	Batch 2
Cell capture number	12773	13501

C

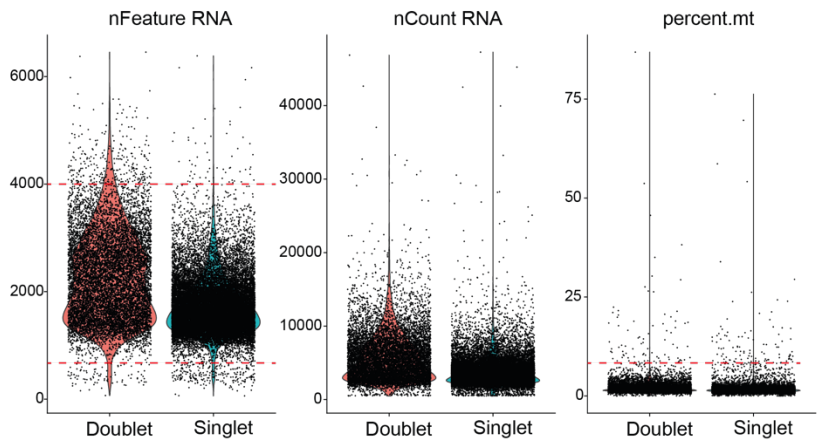

Figure 6-1 Sc-RNASeq experiment design and quality control

(A) Schematic of the design of a sc-RNASeq experiment to characterize differences between B cells from WT FL, WT BM and KO BM. Three E.18 FL samples were collected, processed and HTO labelled. Three BM samples each were collected from gender and age matched WT and KO mice, processed and HTO labelled. The HTO labelled samples were pooled and labelled with fluorescent antibodies before sorting live B cells ($B220^{+}CD19^{+}IgD^{low}$). Sorted single cells were partitioned on the 10X platform and sequenced to collect transcriptomic and BCR sequence information. (B) Table shows the number of cells recovered from sc-RNASeq experiment of two batches of samples. (C) Violin plots illustrate the number of genes detected per cell (left panel) and the percentage of mitochondrial genes (right panel) detected for each sample prior to filtering. Cells were classified as doublets or singlets using HTO demultiplexing. Dotted red lines represent the filtering threshold.

UMAP analysis of the pooled merged data from all nine donors revealed distinct differences between FL and BM cells with minimal overlap on the UMAP plot. In contrast, KO BM did not show significant differences from WT BM both on UMAP or in the cell cluster distribution (**Figure 6-2A, B and C**). The comparison of total B cells in

WT FL and WT BM identified DE genes, with FL exhibiting higher expression of early-stage B cell genes such as *Vpreb1*, *Vpreb2*, *Igll1*, and *Plac8*, while BM expressed more mature B cell genes, including *Iglc2*, *Iglv1*, *H2-q6*, and *H2-q7* (**Figure 6-3 A**). This phenomenon could arise from varying proportions of early-stage B cell precursors and late-stage B cells in FL and BM, or intrinsic tissue specific differences in gene expression within similar B cell subsets. Notably, *Xist* was highly expressed in FL, a gene primarily expressed in female mice. This is likely to be due to gender differences which were the result of not being able to confirm the sex of the FL donors at E.18. To elucidate the patterns of these differentially expressed genes, gene enrichment analysis using GO and Reactome pathway analysis was conducted, revealing no particularly informative pathways that adequately explained the observed distinctions (**Figure 6-3B**).

Figure 6-2

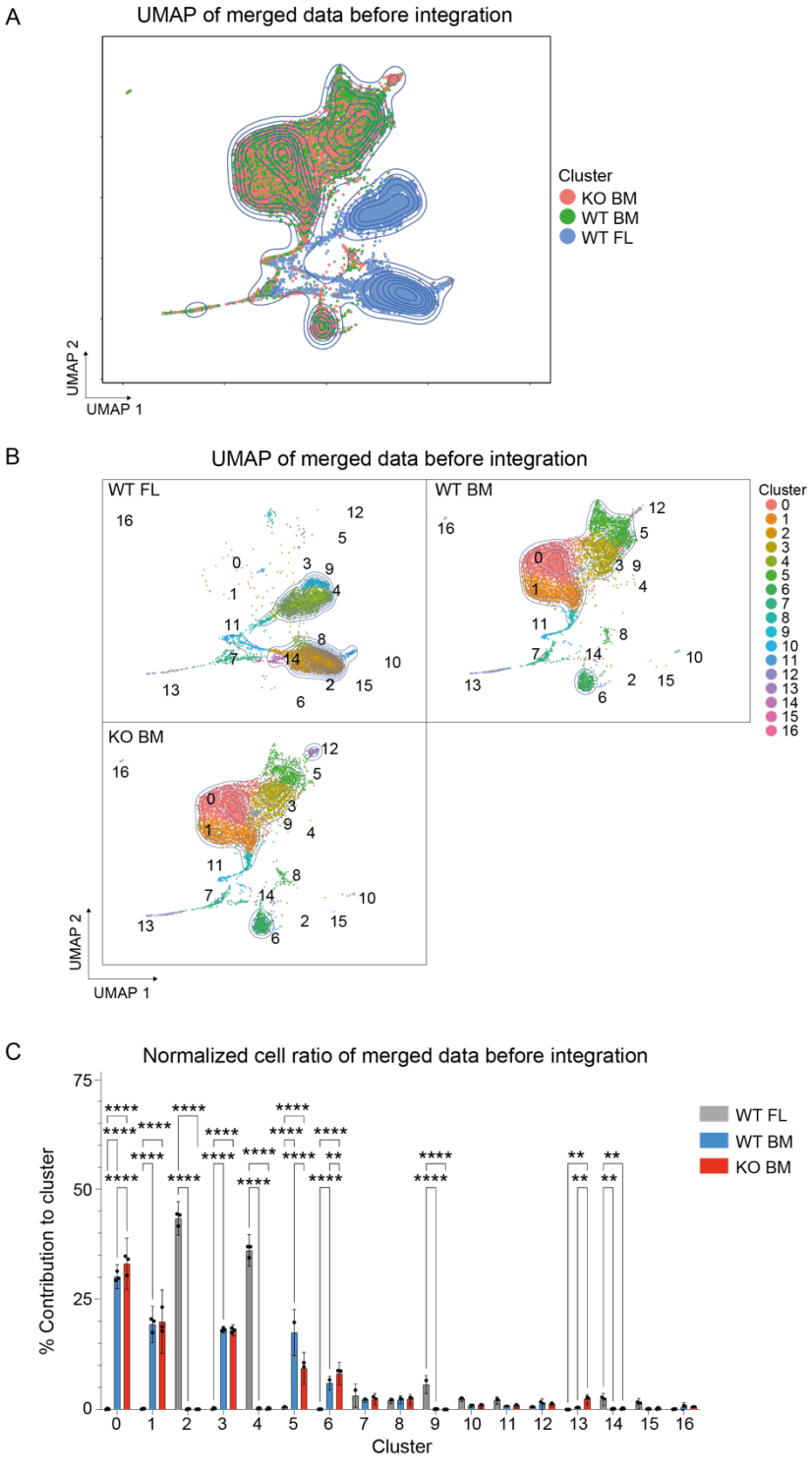

Figure 6-2 Distinctive differences in the single cell transcriptomic profiles of FL and BM B cells.

(A) The UMAP visualises the log normalized merged sc-RNASeq data from BM B cells, sorted from three samples each of WT FL, WT BM and KO BM origin, prior to batch effect correction.

*Each dot denotes an individual cell. (B) The data from (A) was subjected to dimensional reduction by PCA (27 dimensions) and clustering at a resolution of 0.7 to obtain 17 clusters. The contour plot UMAPs visualise the merged data, split by sample identity (WT FL, WT BM, and KO BM), prior to batch effect correction. Each dot denotes an individual cell. (C) The normalized distribution of the 3 samples each of WT FL, WT BM, and KO BM origin across the 17 clusters. Bars show means with 95% confidence limits and symbols indicate data from individual mice. Statistical testing by two-way ANOVA. **P<0.01, ****P<0.0001. The percentage of cell of each cluster was normalized by total cell number of each mouse.*

Figure 6-3

A

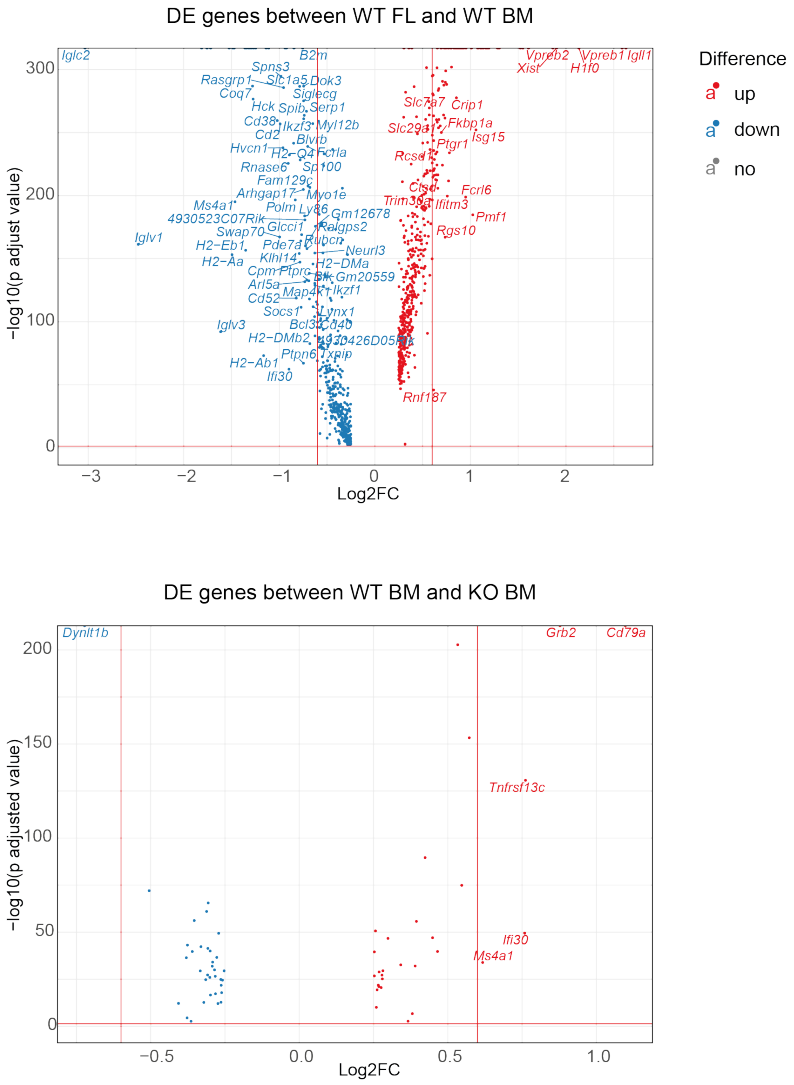
DE genes between WT FL and WT BM
Difference
up
down
no
−log10(p adjust value)
Log2FC
DE genes between WT BM and KO BM
−log10(p adjusted value)
Log2FC

Figure 6-3

B

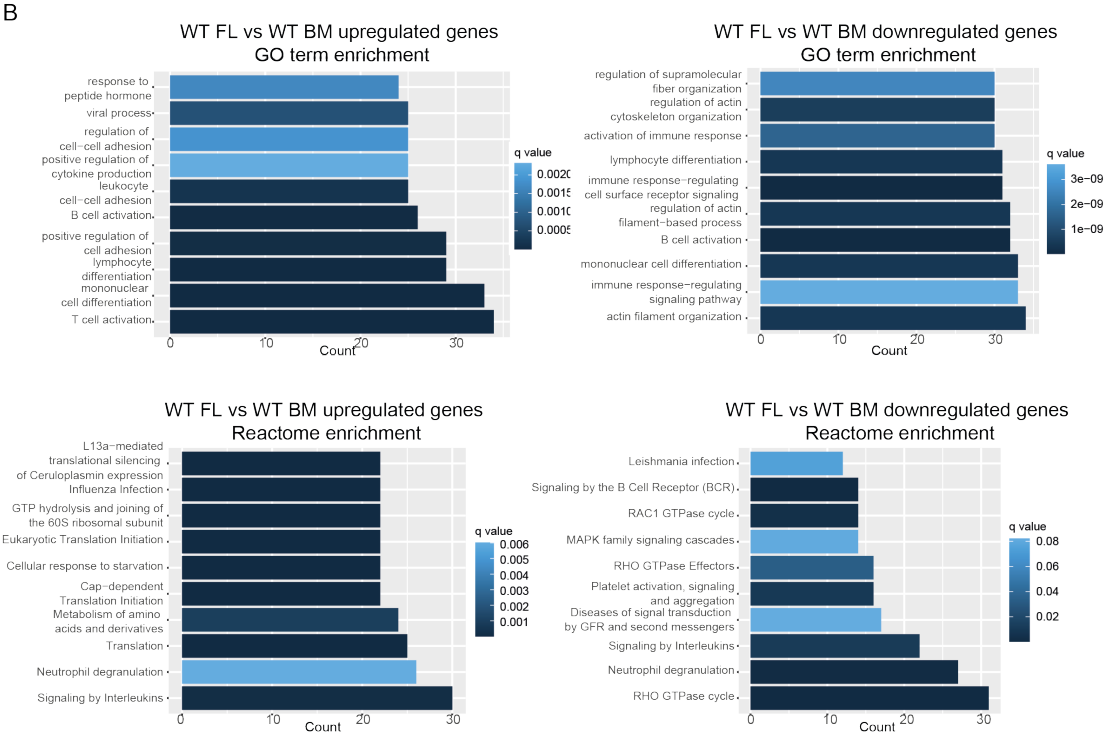

Figure 6-3 DE genes between the WT FL, WT BM and KO BM, prior to integration.

(A) The volcano plots compare DE genes between the two sample groups indicated for each plot, WT FL vs WT BM (upper panel) and WT BM vs KO BM (lower panel). Genes upregulated in the first group in each comparison are indicated in red and downregulated genes are in blue. Vertical red lines denote the log2 fold change (Log2FC) threshold at -0.6 and 0.6, and the horizonal red lines denote an adjusted -log10 p value threshold corresponding to of 0.05. (B) Gene enrichment analysis results of DE genes between WT FL and WT BM. The analysis utilized reference datasets from the GO database (upper left and right panels), and the Reactome pathway database (lower left and right panels). The bar length correlates with the number of gene associated with the enriched pathway, while colour intensity indicates q value significance of the pathway enriched.

6.3 Atlas of B cells subsets in FL and adult BM at the single cell transcriptomic level.

Given the differences observed between FL and BM on UMAP at the RNA transcriptomic level and the unclear patterns of DE genes between these samples, an integration approach using the Harmony algorithm was employed to allow the identification of B cell clusters with shared or distinctive features, independent of tissue of origin. Each sample type was treated as an individual dataset, and the data were integrated using Harmony integration, which projects cells from different datasets into a shared cell type space to preserve biological features and reduce noise[243].

To enhance the precision of cell categorization and annotation, a publicly available sc-RNASeq and CITE-Seq dataset of BM B cells from 6 to 12 week-old C57BL/6J WT mice was incorporated into the analysis and only used for annotation of clusters[244]. This dataset contained RNA profiles and surface protein information (ADTs) for the WT BM B cells. Integrating this published external dataset with the three-sample datasets, allowed clusters to be annotated using RNA features from the integrated dataset and ADT features from the reference dataset (**Figure 6-4A, B and C**). This annotation revealed dynamic changes in cell surface marker expression and RNA expression during B cell development. For example, surface CD25 expression was low in very early precursors, increased with maturity with the highest level in a PreB population, before dropping in the immature B cell stage. CD93 expression reduced gradually along with maturation, and surface IgM levels were highest in the immature

B cell stage (**Figure 6-4B**). With regards to RNA expression, *Vpreb1*, *Vpreb2*, *Rag1*, and *Rag2* were mainly expressed in early-stage B cells, while *Pax5*, *Foxo1*, and *Ighm* were expressed in later stages of B cell development (**Figure 6-4C**).

Cell cycle scores were calculated for the integrated data, showing high DNA synthesis and proliferation scores in clusters 3 and 4, annotated as Fr.C' and Fr.D B cells, representing highly proliferative populations of B cells (**Figure 6-4D**). Trajectory analysis supported the annotation, indicating that B cell development progressed from cluster 2 (Fr.A to Fr.C B cells) to cluster 6 (early Fr.C' B cells), then to cluster 3 (Fr.C' B cells) and cluster 4 (Fr.D B cells), and finally, cluster 0 (Fr.D to Fr.E B cells) transitions to cluster 1 (Fr.E B cells) (**Figure 6-4E**).

Figure 6-4

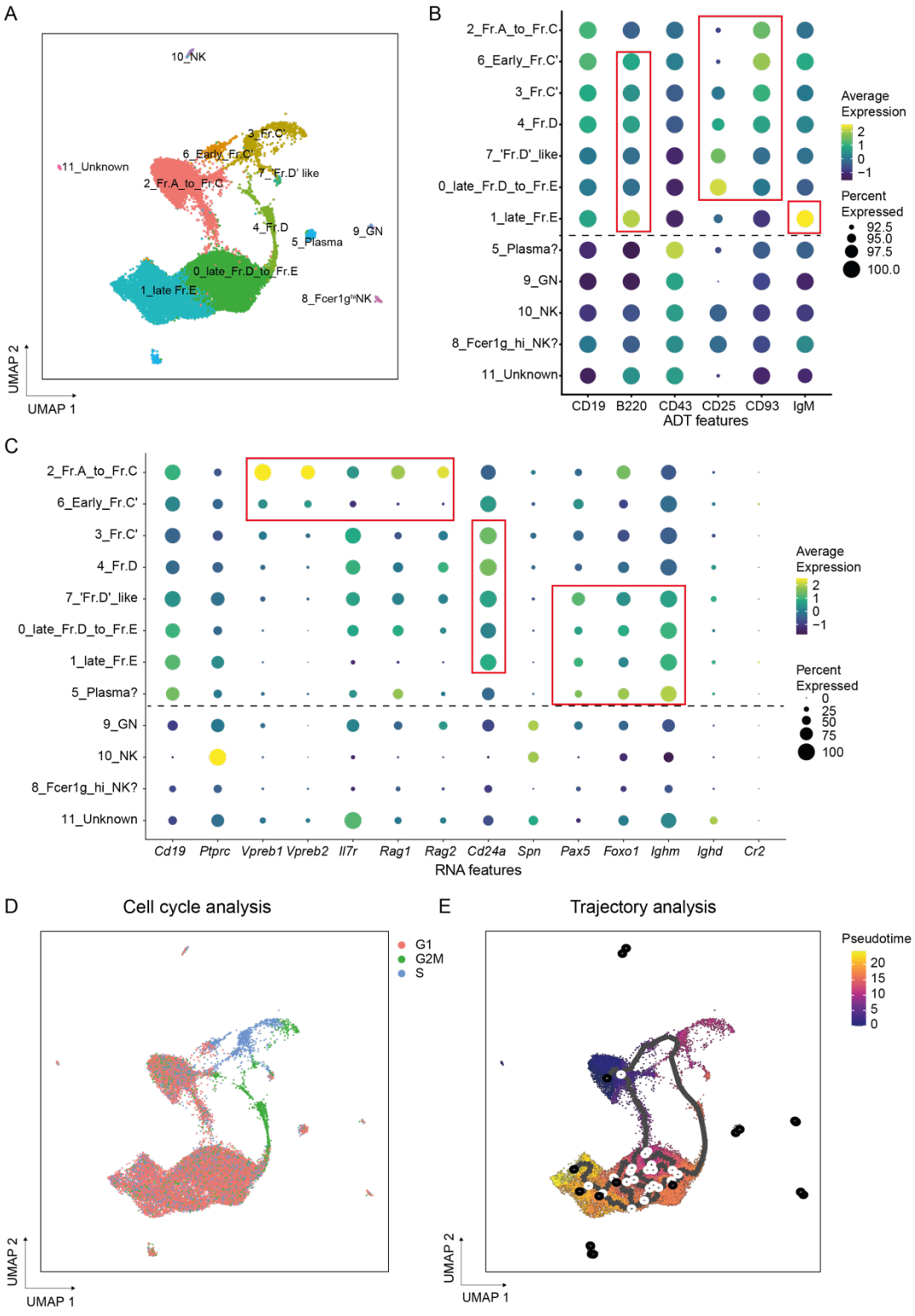

Figure 6-4 Atlas of B cells subsets derived from integrated single cell transcriptomic data of FL and BM origin.

(A) The UMAP visualises the data from three samples each of WT FL, WT BM, and KO BM origin, integrated using Harmony algorithm with a previously published BM B cell reference dataset

that included ADT markers (WT BM (RF)). The data were log normalized and subjected to dimensional reduction by PCA (27 dimensions), with clustering at 0.7 resolution. (B) Surface ADT information from the reference dataset was used to inform cluster annotation within the integrated data. The colour of the filled circles correlates with the mean expression rate of the marker within a cluster, and the size of the circle indicates the percentage of cells within the cluster that express the marker. Fr.A to Fr.C, early Fr.C, Fr.C', Fr.D, 'Fr.D' like, late Fr.D to Fr.E and late Fr.E are B cells classified according to classical Hardy fraction nomenclature, on the basis of RNA information with confirmation from the reference ADT data. GN stands for bone marrow neutrophil, NK stands for NK cells. The main annotation features of different clusters are highlight with red frames. (C) The dot plot visualises RNA expression of integrated WT FL, WT BM, and KO BM data across various cell clusters, not including the reference sc-RNASeq dataset. The colour of the filled circles correlates with the mean expression rate of the marker within a cluster, and the size of the circle indicates the percentage of cells within the cluster that express the marker. The red frames indicate features that are characteristic for a set of BM B cell subsets. (D) UMAP for the cell cycle score for individual cells within the integrated dataset. The three distinct cell phases: S phase, G1 and G2/M phase are represented by three distinct colours. The score was determined by CellCycleScoring function from the Seurat R package. The cell cycling reference genes were originally defined for human datasets but were subsequently converted into mouse analogues for analysis. (E) UMAP for the trajectory analysis of the integrated data calculated using the "monocle3" package. Pseudotime was quantified by the transcriptional similarity between individual cells and data were subsequently aligned along a continuum of developmental progression, denoted by the black line. The indicated spectrum of colours represents different pesudotime values, with cells at earlier stage of development assigned a lower pseudotime value and more mature cells having a higher value.

The distribution of cells in each cluster on UMAP was then examined in the context of the sample type, revealing a broadly similar distribution across clusters (**Figure 6-5A**). However, comparison of the normalized distribution of WT FL, WT BM and KO BM cells across the 12-cluster revealed that FL cells were enriched in cluster 2 with fewer FL cells in clusters 0 and 1 (**Figure 6-5B**). This may reflect the higher proportion of precursor B cells and lower number of more mature B cells at this developmental stage.

Figure 6-5

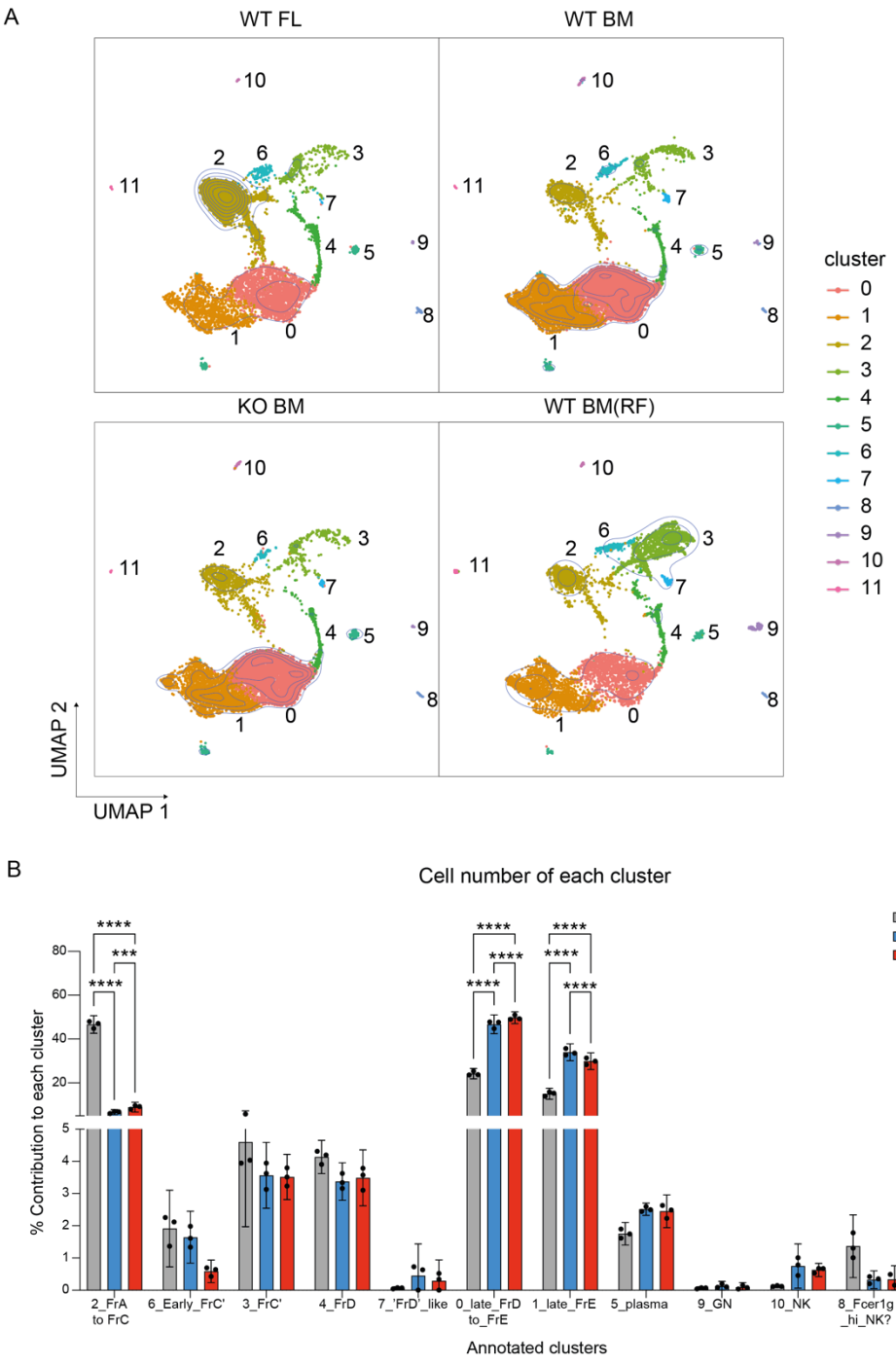

Figure 6-5 Distribution of WT FL, WT BM and KO BM cells across clusters defined by transcriptomic changes at the single cell level.

*(A) UMAP for the integrated sc-RNASeq data split by sample type: WT FL, WT BM, KO BM and WT BM (RF). Integrated data was clustered into 12 clusters at a resolution of 0.7 and with dimensionality set to 27. (B) Normalized distribution of cells from the three experiment groups: WT FL, WT BM and KO BM across the 12 clusters. Bars indicate means, errors bars indicate 95% confidence intervals and data from individual mice are denoted by the dots. Statistical testing by two-way ANOVA with ***P<0.001 and ****P<0.0001.*

To explore whether cells that clustered together expressed different levels of key RNA markers across sample types, cells within a cluster were compared by sample type to inspect their RNA expression features (**Figure 6-6**). Except for *Vpreb1*, *Vpreb2*, and *Il7r*, which showed higher expression in FL in clusters 6 (early Fr.C B cells), 3 (Fr.C B cells), and 4 (Fr.D B cells), expression of these key B cell genes were at similar levels in the three sample types. This is consistent with the fact that these cells were clustered together mainly based on a similar expression of key B cell RNA markers.

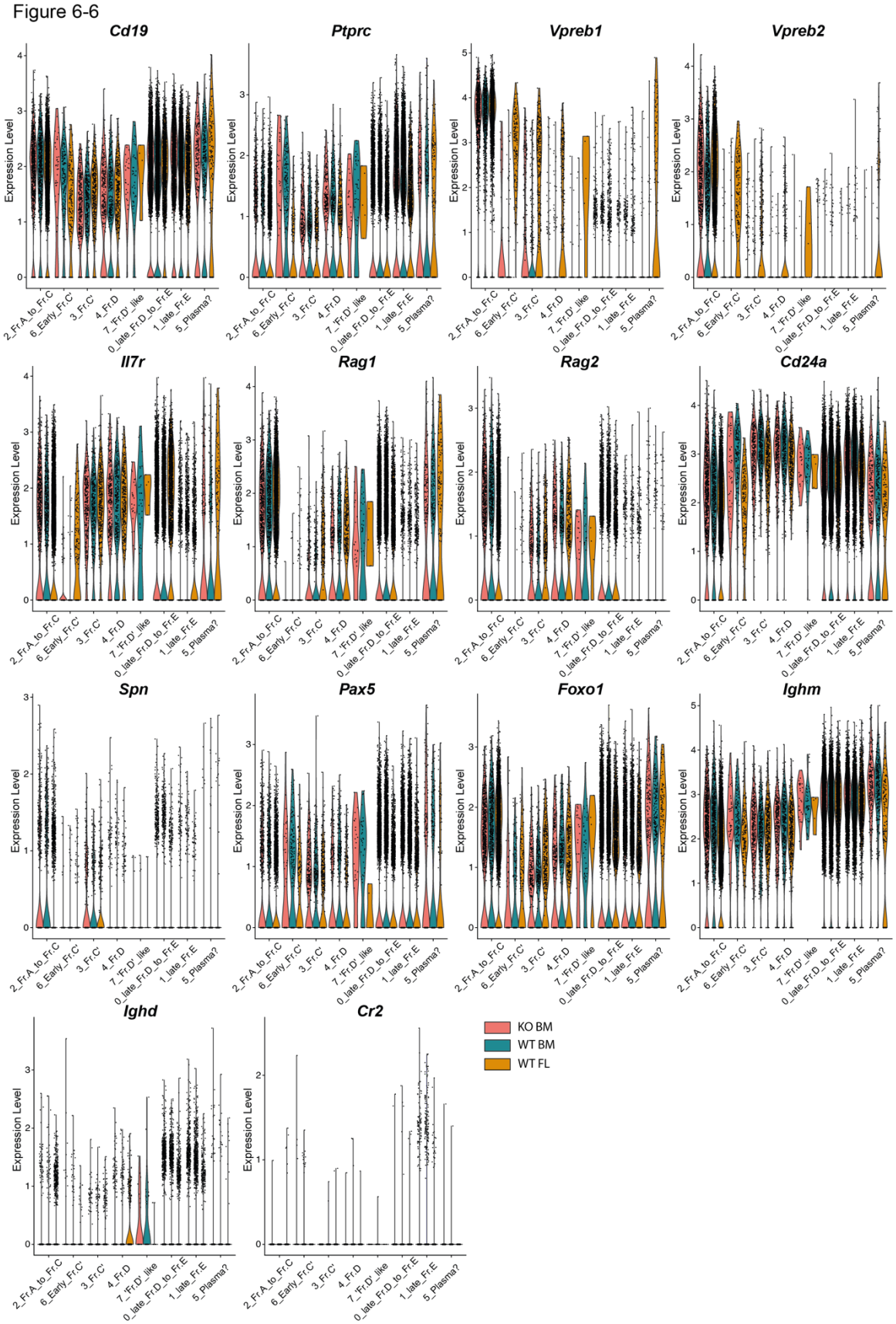

Figure 6-6 Expression of key B cell markers in FL and adult BM at the single cell transcriptomic level.

Violin plots comparing the expression level of indicated B cell markers in the 12 clusters from the WT FL, WT BM and KO BM single cell transcriptomic data. Each dot represents data from a single cell. The red represents cells from KO BM, green represents cells from WT BM and orange denotes cells from WT FL.

Based on the annotation, it was evident that FL has significantly fewer cells in cluster 0 (Fr.D to Fr.E B cells) and cluster 1 (Fr.E to Fr.F B cells) compared to BM. KO BM was enriched in cluster 0, and WT BM enriched in cluster 1, which may be consistent with the findings in Chapter 5. Both BM samples showed slightly fewer cells in cluster 3 (Fr.C' B cells), indicating that FL had a higher proportion of early-stage precursor cells and fewer late-stage cells. Since the primary differences among the three sample types are in the number of cells in clusters 0, 1, and 2, DE genes within these clusters were compared (**Figure 6-7A, Figure 6-8A and Figure 6-9A**).

Figure 6-7

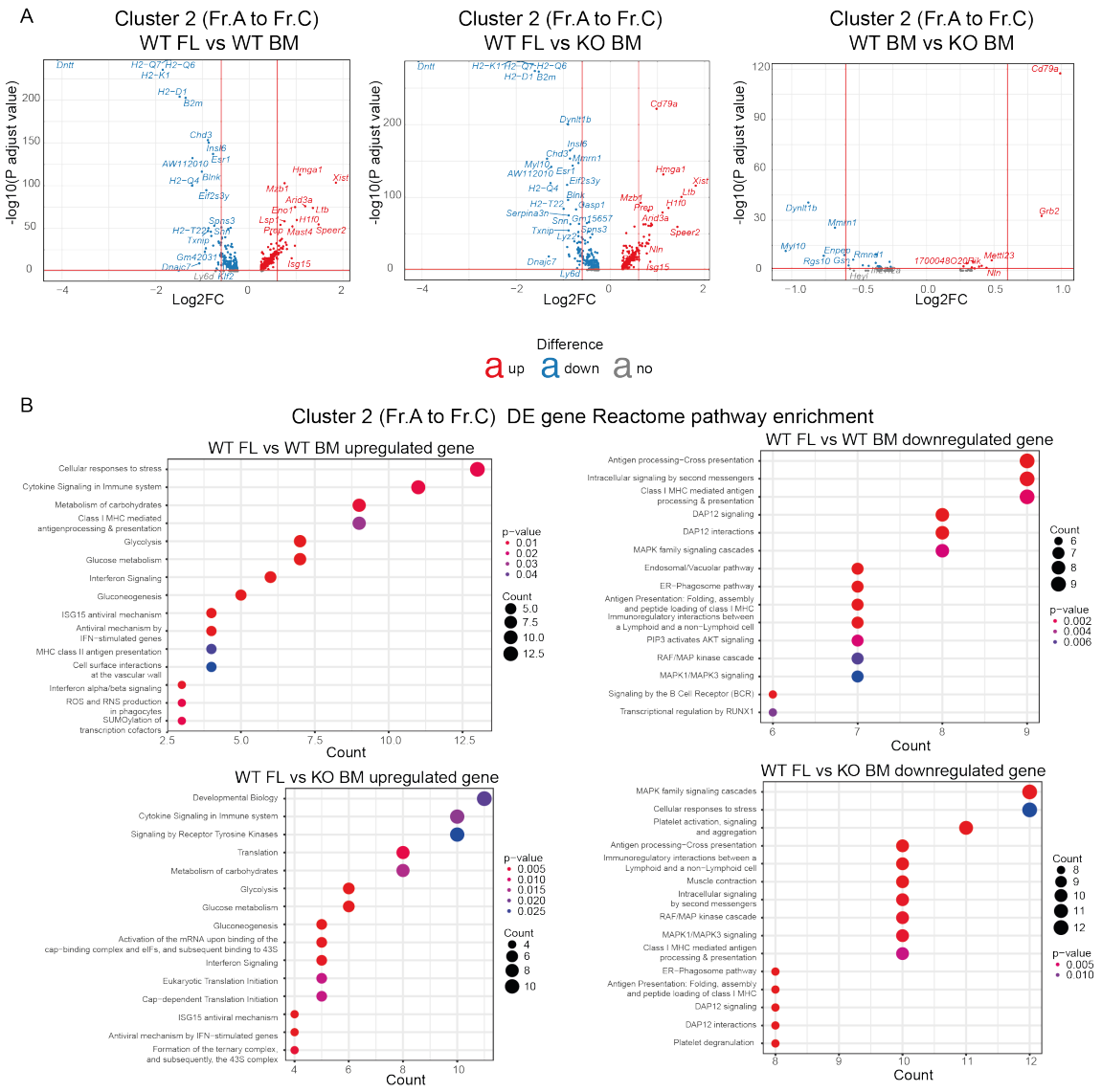

Figure 6-7 DE genes for cells within cluster 2 of the integrated sc-RNASeq dataset.

(A) Volcano plots depict DE genes for cells in cluster 2 from the indicated pairwise comparison between the WT FL, WT BM and KO BM samples in the sc-RNASeq integrated data. Genes are color-coded based on their upregulation (red) or downregulation (blue). Vertical red lines represent log2 fold change (Log2FC) threshold at -0.6 and 0.6 and the horizonal red line represents an adjusted -log10 p value threshold of 0.05. (B) The dot plots depict results of gene enrichment analysis for DE genes within cluster 2 B cells when comparing WT FL with WT BM and KO BM, utilizing the Reactome pathway database as a reference. The dot size corresponds to the number of genes associated with the enriched pathway, while colour intensity indicates p-value significance of the enriched pathway.

In cluster 2 (Fr.A to Fr.C B cells), the absence of GRB2 had no effect on DE in BM except the higher expression of *CD79a* (Mb1) and *Grb2* itself in the WT BM. Comparison of FL and BM showed increased FL expression of *Arid3a*, *H1f0*, *Mzb1*, and *Speer2*, and BM expression of *H2-q7*, *H2-q6*, *H2-d1*, and histone-related genes (**Figure 6-7A**). Gene enrichment analysis suggested an enrichment of metabolism, glycolysis, and mRNA translation signatures in FL Fr.A to Fr.C B cells (**Figure 6-7B**).

In cluster 0 (later Fr.D to Fr.E B cells), WT BM and KO BM expressed many shared DE genes compared to WT FL (**Figure 6-8A**). WT FL highly expressed *Arid3a*, *Mzb1*, *Hmga1*, *Plac8*, and *Ltb* genes, while expressing lower levels of *Iglc2*, *Iglv1*, *H2-q6* and *H2-d1* (and a few other mature B cell genes) (**Figure 6-8A**). In contrast, comparison of WT BM with KO BM showed differences only in *CD79a* and *Grb2* (as previously), with higher expression of *Id3* and *Mettl23*, and suppression of *Dynlt1b* in WT BM. Intriguingly, Id3, an inhibitor of E protein activity, is a negative regulator of B1b B cells[71]. The elevated level of the *Id3* gene suggested a potential correlation between Id3 function and B1 B cells in the context of GRB2. In terms of gene enrichment, WT FL seemed to have enriched genes related to translocation and protein synthesis, while both WT and KO BM showed enrichment in antigen presentation and the MAPK signalling pathway (**Figure 6-8B**).

Figure 6-8

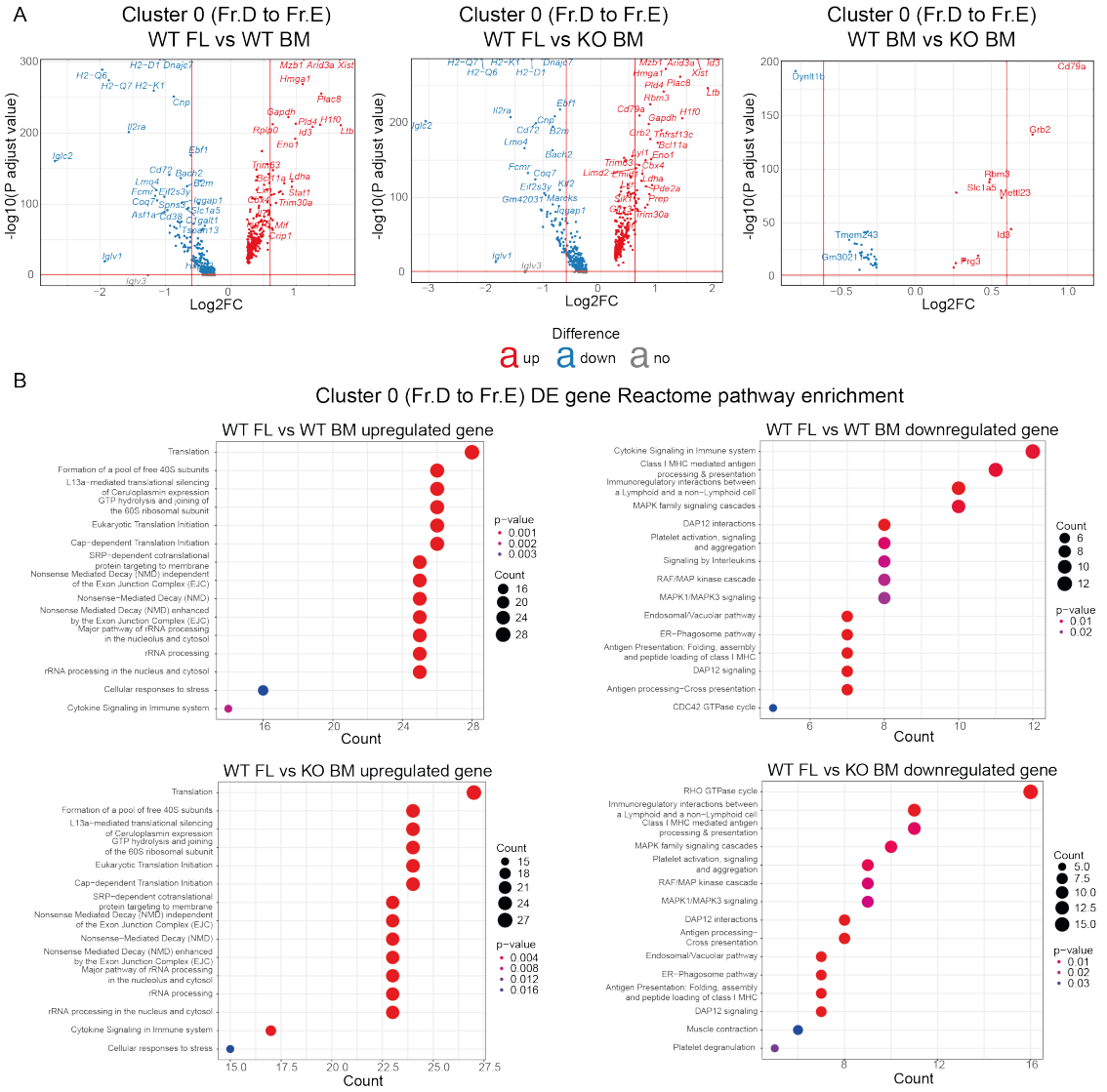

Figure 6-8 DE genes for cells within cluster 0 of the integrated sc-RNASeq dataset.

(A) Volcano plots depict DE genes for cells in cluster 2 from the indicated pairwise comparison between the WT FL, WT BM and KO BM samples in the sc-RNASeq integrated data. Genes are color-coded based on their upregulation (red) or downregulation (blue). Vertical red lines represent log2 fold change (Log2FC) threshold at -0.6 and 0.6 and the horizonal red line represents an adjusted -log10 p value threshold of 0.05. (B) The dot plots depict results of gene enrichment analysis for DE genes within cluster 2 B cells when comparing WT FL with WT BM and KO BM, utilizing the Reactome pathway database as a reference. The dot size corresponds to the number of genes associated with the enriched pathway, while colour intensity indicates p-value significance of the enriched pathway.

In cluster 1 (Fr.E to Fr.F B cells) FL still expressed high levels *Arid3a*, *Plac8*, *Mzb1*, and *H1f0* genes, and lower levels of *Iglc2*, *Fcmr*, and *Cd72*. KO BM and WT BM

differentially expressed *Rpgrip1*, *Tnfrsf13c*, *Rbm3*, and *Ifi30* (**Figure 6-9A**). Gene enrichment showed a pattern similar to that observed for cluster 0 (**Figure 6-9B**).

Figure 6-9

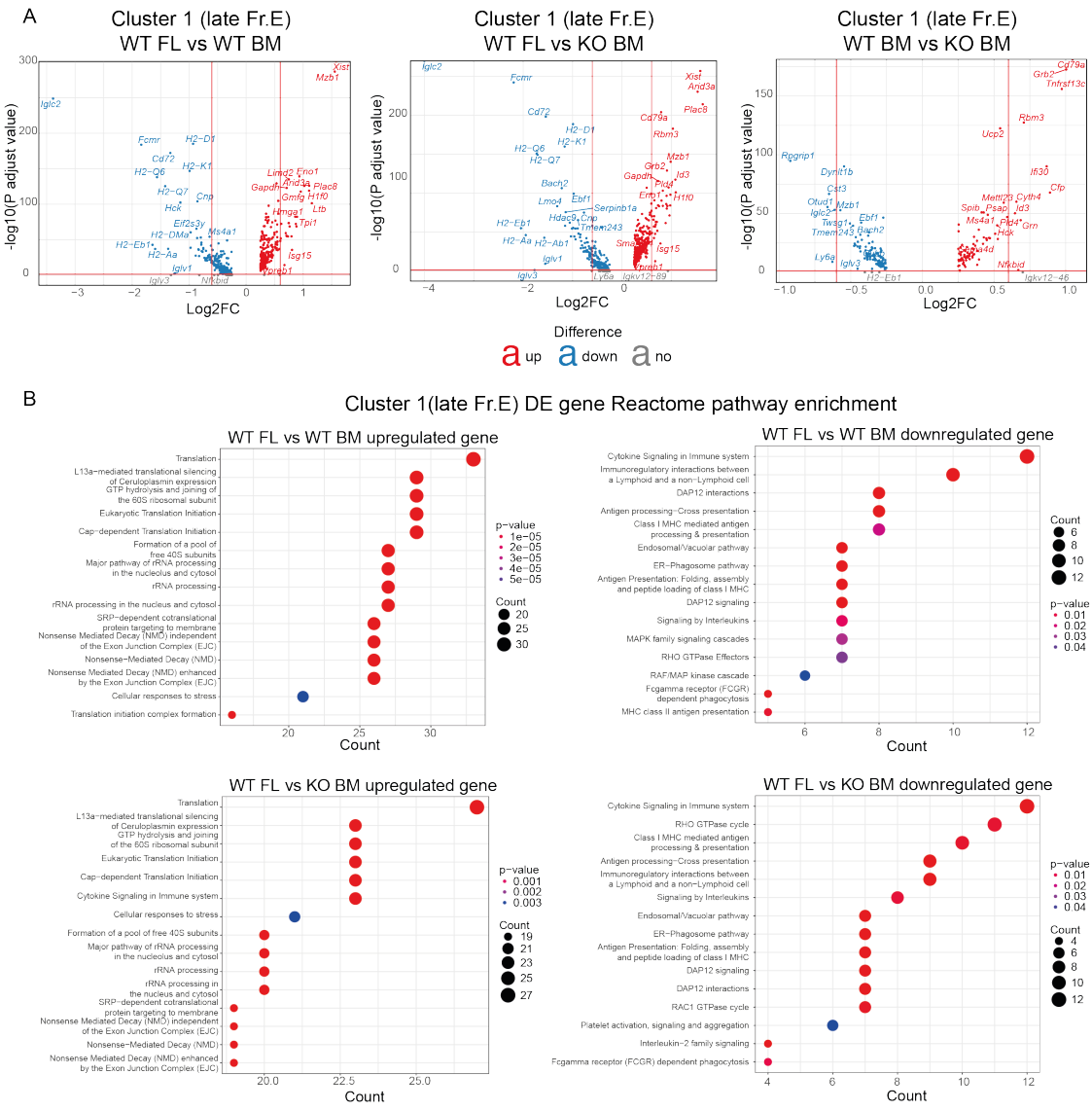

Figure 6-9 DE genes for cells within cluster 1 of the integrated sc-RNASeq dataset.

(A) Volcano plots depict DE genes for cells in cluster 2 from the indicated pairwise comparison between the WT FL, WT BM and KO BM samples in the sc-RNASeq integrated data. Genes are color-coded based on their upregulation (red) or downregulation (blue). Vertical red lines represent log2 fold change (Log2FC) threshold at -0.6 and 0.6 and the horizonal red line represents an adjusted -log10 p value threshold of 0.05. (B) The dot plots depict results of gene enrichment analysis for DE genes within cluster 2 B cells when comparing WT FL with WT BM and KO BM, utilizing the Reactome pathway database as a reference. The dot size corresponds to the number of genes associated with the enriched pathway, while colour intensity indicates p-value significance of the enriched pathway.

6.4 LIN28B related transcripts are highly expressed in FL at single cell level but not in KO BM.

In the context of previous research on the *Lin28b*/*let-7* axis and its role in the ontogeny switch between FL and BM, and the differential ability of FL and BM to generate B1 B cells, a number of genes including *Arid3a*, *Stac2*, *Plag1*, *Myo15b*, *Plaur*, *Lst1*, *Bhlhe41*, *Sspn*, and others have been implicated in B1 B cell generation[109]. As this research was initially conducted using bulk RNA sequencing, these findings were validated using the single-cell level data to investigate whether the continued generation of B1b B cells from BM in the absence of GRB2 was associated with the *Lin28b/let-7* signature.

As expected, most *Lin28b/let-7* -dependent genes exhibited much higher expression in FL than in both types of BM (**Figure 6-10**). This trend extended from early-stage B cells (cluster 2) to immature cell populations. In immature stage B cells, FL not only had higher *Lin28b* expression but also elevated expression of *Myc*, *Arid3a*, *Plag1* and *Lst1*. Both types of BM showed similar but lower expression levels for these genes compared to FL. There was no evidence of a *Lin28b/let-7* signature in the KO BM suggesting that the increased generation of B1b B cells is not due to a loss of the *Lin28b*/*let-7* switch but is likely due to a separate pathway.

Figure 6-10

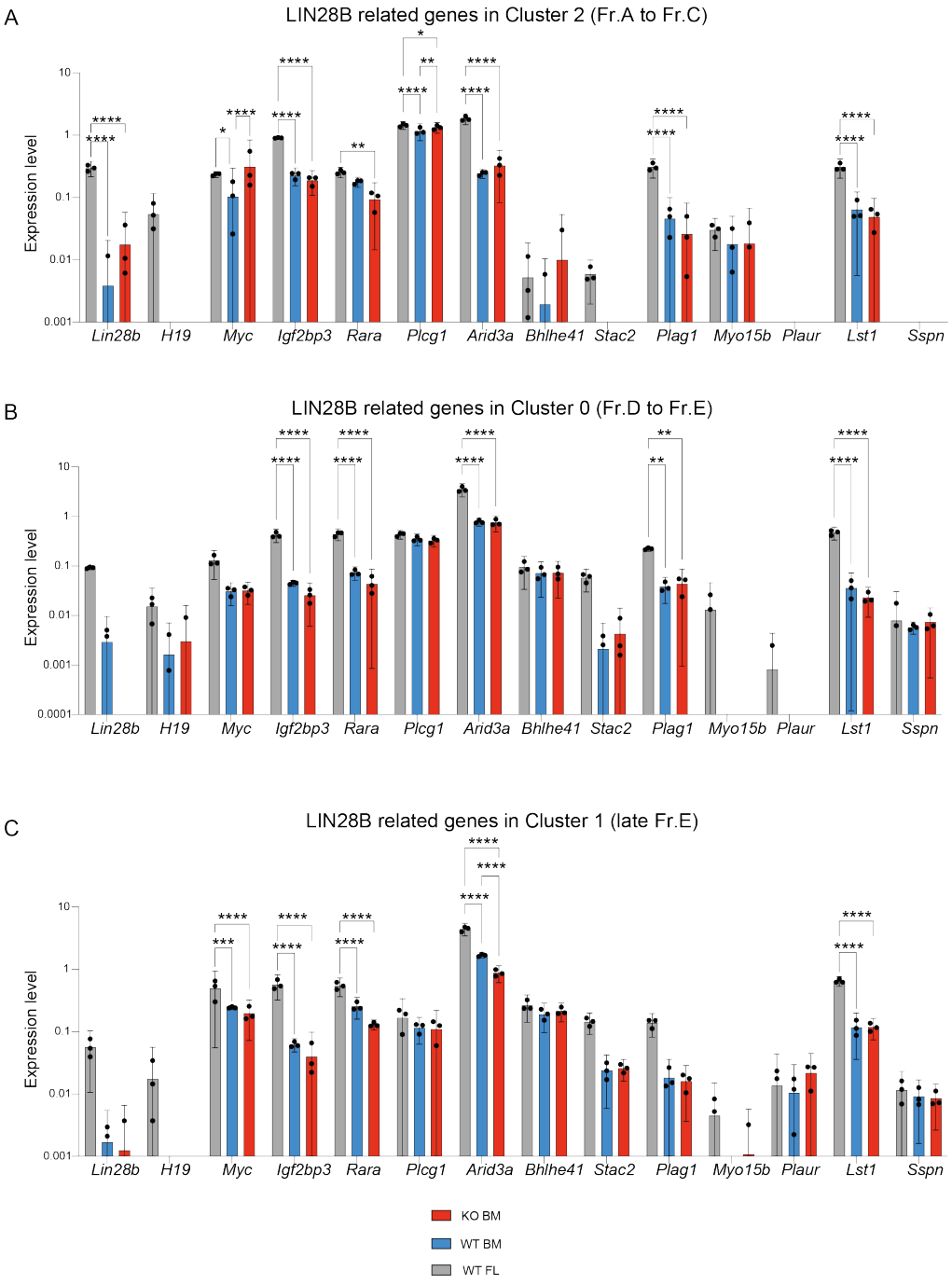

Figure 6-10 LIN28B related transcripts are highly expressed in FL at single cell level but not in KO BM

*The average expression of RNA transcripts related to the Lin28b/let7 module in (A) cluster 2, Fr.A to Fr.C, (B) cluster 0, Fr.D to Fr.E, and (C) cluster 1, late Fr.E, from the WT FL, WT BM, and KO BM samples in the integrated sc-RNASeq dataset. RNA expression is plotted on a log scale. Each dot represents data from an individual mouse, and error bars represent 95% confidence intervals. Statistical analysis conducted using two-way ANOVA, with **P<0.01 and ****P<0.0001.*

6.5 WT FL B cell development shares a trajectory pathway with KO BM.

Trajectory analysis was employed to investigate other similarities in FL and KO BM B cell development. This revealed the possibility of alternative pathways, one common to FL and KO BM and the other to WT BM (**Figure 6-11A**). This raised the possibility that the first pathway might consist of cells capable of bypassing the pre-B cell stage and associated proliferation (**Figure 6-4D and Figure 6-11B**), as proposed by independent research[245].

When DE gene analysis was applied to these trajectories, pathway A, which is shared by WT FL and KO BM, was enriched for genes such as *Vpreb1*, *Vpreb3*, *Btg1*, *Malat1*, *Igll1*, etc, that are associated with cytokine signalling and BCR signalling. In contrast, pathway B, unique to WT BM, was enriched for genes like *Hmgn2*, *Hmgb2*, *H2afz* and *Stmn1*, and gene enrichment analysis suggesting that these are linked to cell cycle progression (**Figure 6-11B, C and D**). Despite these insights, these analyses did not conclusively determine the precise mechanisms underlying the different pathways.

Figure 6-11

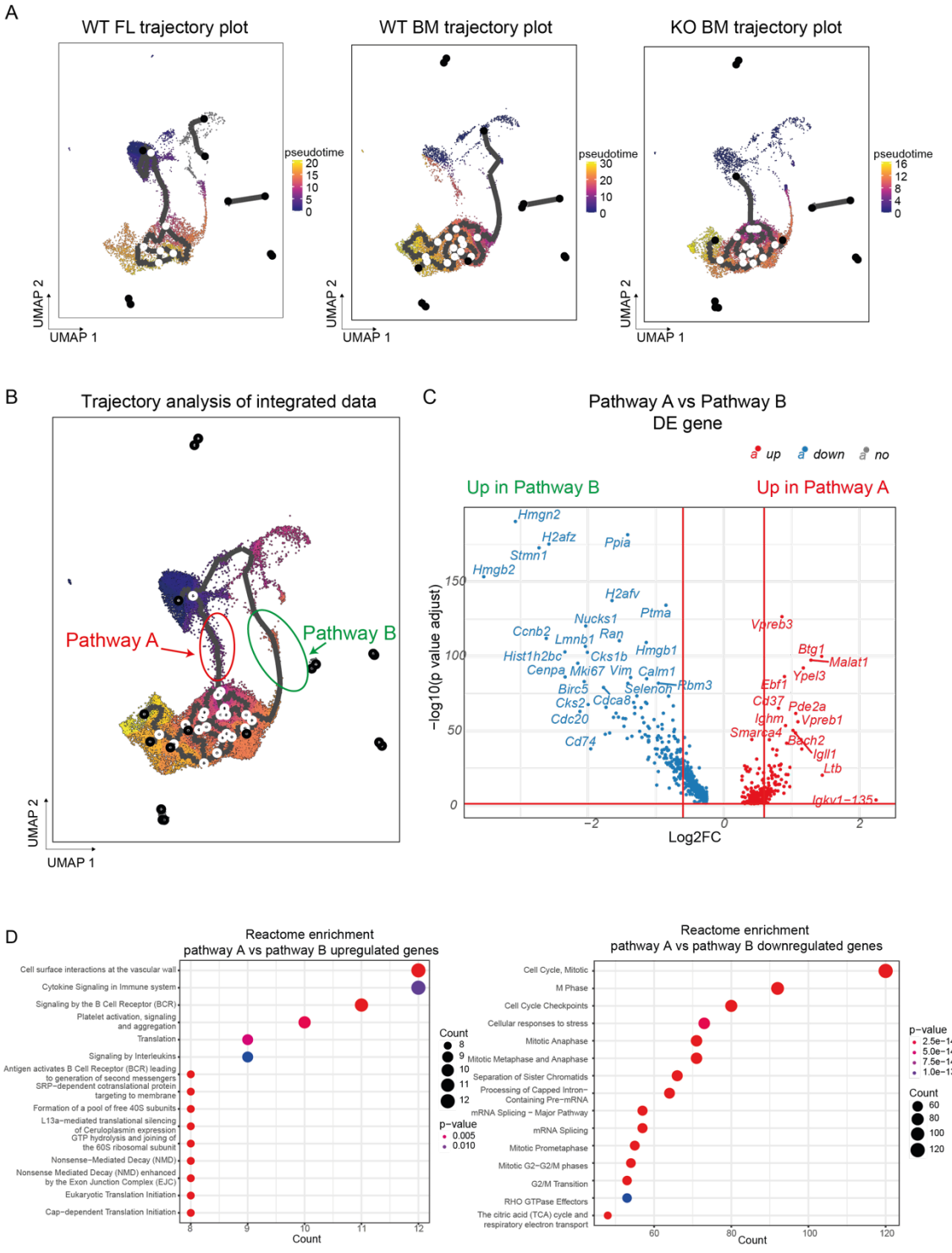

Figure 6-11 Trajectory analysis reveals a developmental pathway shared between WT FL B cells and KO BM B cells.

(A) UMAPs for trajectory analysis of the integrated data, split by the three sample types to visualize the separate trajectories for B cells from WT FL, WT BM and KO BM. (B) UMAP for

trajectory analysis of the integrated sc-RNASeq dataset consisting of FL and BM samples. Pathway A (highlighted in red) and pathway B (highlighted in green) are two possible trajectories from the earliest precursor B cell stages (purple) to more mature B cell clusters (yellow). The pseudotimes were calculated using the "monocle3" package by measuring the transcriptional similarity across individual cells and data was aligned along a continuum of developmental progression indicated by the black line. A spectrum of colours represents different pesudotimes with lower pseudotime values corresponding to earlier development stages. (C) Volcano plot depicting DE genes between single cells from pathway A and pathway B, as defined in (B). Genes upregulated in pathway A are in red while genes upregulated in pathway B are in blue. Vertical red lines denote the log2 fold change (Log2FC) threshold at -0.6 and 0.6 and the horizonal red line denotes an adjusted -log10 p value threshold of 0.05. (D) The dot plots depict results of gene enrichment analysis for DE genes of B cells between pathway A and pathway B, utilizing the Reactome pathway database as a reference. The dot size corresponds to the number of genes associated with the enriched pathway, while colour intensity indicates p-value significance of the enriched pathway.

WT and KO BM samples showed higher usage of *Ighv1-26*, *Ighv1-8*, *Ighv3-6*, and *Ighv9-3* genes, whereas the FL samples were more enriched for *Ighv2-2* and *Ighv5-2* genes (**Figure 6-12A and B**). However, only a minority of cells demonstrated productive BCR sequences, making it challenging to compare the diversity between the two developmental pathways. Most clonotypes consisted of singular occurrences, with only a few presenting as duplicates (data not shown). This pattern suggests a high degree of diversity. The scant presence of identical clonotypes is likely because of our focus on early B cell stages, before the point where proliferation of identical clones predominantly occurs. With mature B cells excluded from the analysis, discerning BCR diversity is inherently problematic.

In conclusion, the current data does not substantiate the existence of an alternative pathway shared between KO BM and WT FL. The complexity of discerning the cellular and molecular differences between the pathways and their association with B1 B cell generation warrants further investigation to clarify these developmental processes. The predominant conclusion is that the mechanism by which GRB2 induces the

increased production of B1b B cells is not inherently the same as the one that regulates production of B1 B cell of fetal origin.

Figure 6-12

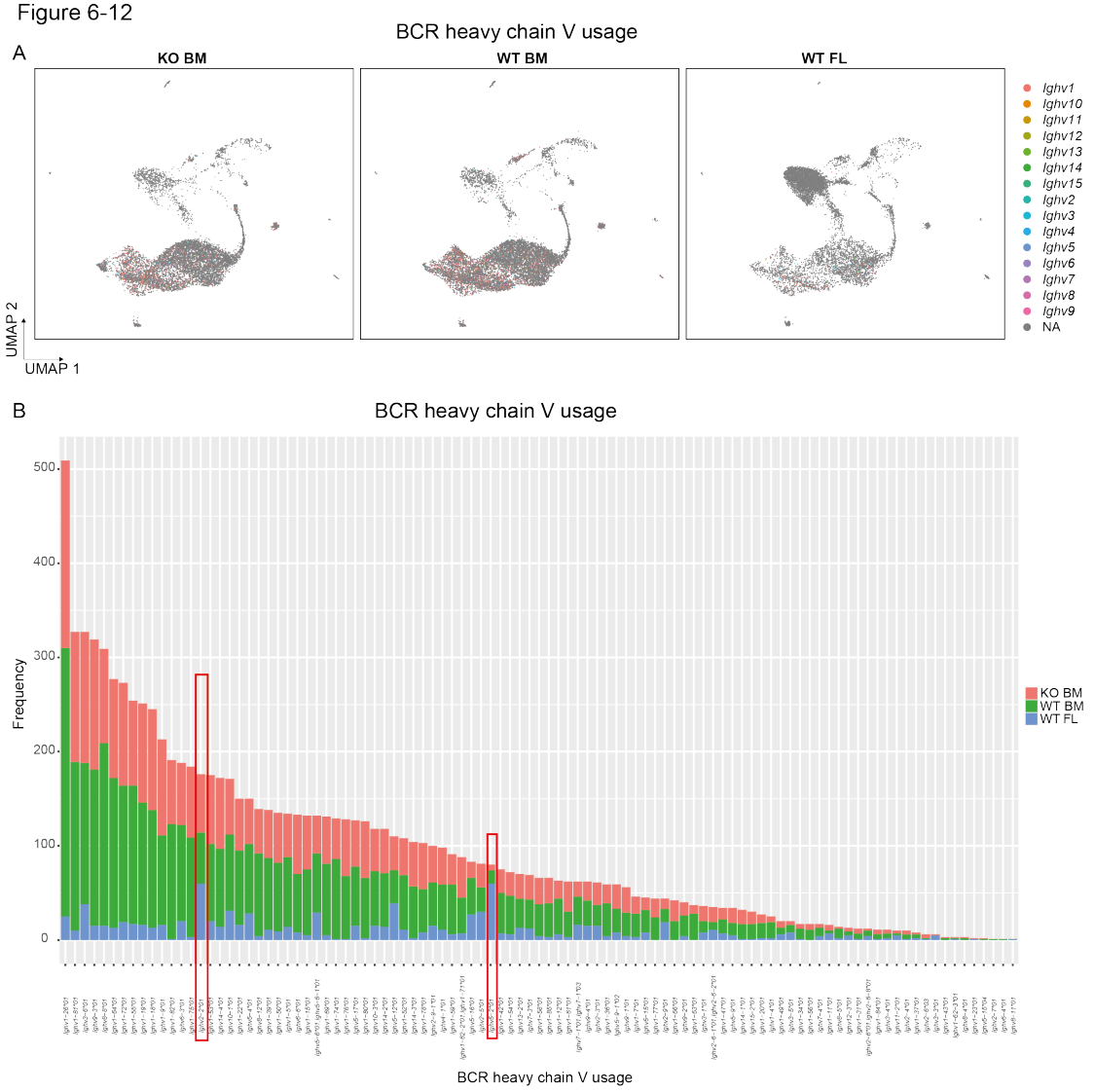

Figure 6-12 WT and KO BM B cells are inclined to utilise different BCR heavy chains compared to WT FL B cells.

(A) The UMAP visualises the BCR heavy chain usage by single cells across the three WT FL, WT BM and KO BM samples. Individual heavy chain V genes are denoted in a distinct colour. (B) The bar chart depicts BCR heavy chain V region usage among B cells from the three WT FL, WT BM and KO BM samples. The x-axis indicates the various heavy chain V genes used, while the colours indicate the sample types.

6.6 Discussion

Based on the analysis presented previously (**Figure 6-2A, B and C**), it was evident that FL cells exhibited distinctive transcriptomic differences compared to BM B cells. Almost no overlap was found between the two types of samples, suggesting intrinsic differences between B cells of FL and adult BM origin. These observations were not due to technical factors, since samples were processed on the same day, partitioned and sequenced together as a single pooled HTO-labelled sample. When examining the genes contributing to these differences, the majority of genes upregulated in FL were early-stage B cell genes such as *Igll1*, *Vpreb1*, *H1f0*, *Vpreb2*, and *Mzb1* - genes highly expressed in pre-B cell stages. In contrast, BM samples had elevated expression of *Iglv1*, *Iglc2*, *Cd74*, *H2-q7* - genes typically expressed in late-stage B cells. This difference indicates that, although FL and BM have B cells that can be classified into similar Hardy fraction subsets, the proportion of early-stage B cells is higher in FL, and even FL B cells that have been categorized as being more mature, still express a greater proportion of early-stage B cell genes. This delay in downregulating genes related to B cell development may contribute to the unique features of FL origin precursor B cells that might also be critical for the ability of FL to generate B1 B cells.

To analyse and compare differences under one framework and temporally remove the influence of less important genes, the data was merged and integrated. After integration, the main biological differences appeared to have been preserved, as integrated B cells were mainly clustered based on their B cell development-related

gene signatures (**Figure 6-4A, B and C**). This suggested that the un-supervised integration primarily removed less important differences between the two types of samples and treated the differences in B cell development gene signatures as the main distinctions across the cells—these differences were preserved post-integration.

It is worth noting that the UMAP for the reference WT BM mice was not identical to the UMAP for the WT BM samples in this experiment. This discrepancy may arise from slight differences in the background of C57BL/6 mice, age variations, or differences in experimental preparation methods and sequencing depth. Given that this dataset was only used for integration and annotation with the ADT assay, and they were removed prior to subsequent analysis, this difference should not significantly impact the main analysis results.

In the integrated dataset, one of the most distinctive differences among the three datasets was the distribution of cells. While each sample type included B cells from Fr.A to Fr.E B cells, FL had a much higher proportion of cells falling into Fr.A to Fr.C B cells, whereas BM had a higher proportion of immature stage B cells. This finding aligned with the previously established understanding of FL B cells being characterized by more B cell precursors and fewer mature B cells. Although integration better aligned B cells from FL and BM, causing them to overlap and cluster together on the UMAP, the differences in gene signatures were preserved within each cluster. The primary source of difference in each cluster still originated from the

sample type, as evidenced by comparing the DE genes between FL and BM in clusters 0, 1, and 2.

In clusters 0, 1, and 2, FL highly expressed genes such as *Arid3a*, *Mzb1*, *Plac8*, *H1f0*, and *Ltb*, while BM highly expressed genes like *Iglc2*, *H2-d1*, *H2-k1*, and *H2-q7* in all three clusters. Gene enrichment analysis revealed that FL highly expressed genes were focused on protein translation indicating higher metabolic activity, while BM highly expressed genes were enriched in the antigen processing pathway. This suggested that FL B cells still retained more features associated with precursor B cells even in the immature B cell stages (clusters 0 and 1), exhibiting higher metabolic signals. In contrast, BM B cells showed more markers associated with B cell activation and function. The delay in downregulating metabolic features in FL B cells may contribute to the generation of B1 B cells.

As discussed in the introduction section, the *Lin28b*/*let-7* axis plays a role in the ontogeny switch between FL and BM, and regulates the positive and negative selection of B cells[109]. The overexpression of LIN28B has been shown to restore the positive selection of B1 B cells from the BM, partially through LIN28B-dependent genes. However, our evidence suggested that GRB2 does not directly modulate this pathway.

The trajectory analysis of each sample type suggested the intriguing possibility that WT FL and KO BM might share a trajectory pathway, which is largely absent from WT BM **(Figure 6-11 A and B)**. This raises the question of whether such a pathway could

be a key factor in the generation of B1 B cells. Hypothetically, within this pathway, cells might move directly from Fr.A / Fr.B to Fr.D / Fr.E B cells, bypassing Fr.C B cells. The existence of such a pathway, which could potentially skip certain negative selection checkpoints, has been previously speculated about and discussed. An example of this concept is the bypassing of the pre-BCR, leading to an increased number of B1a B cells[246].

Attempts to identify key markers in the trajectories through regression analysis and graph-autocorrelation analysis had not yielded significant insights. Additionally, the analysis did not pinpoint any crucial pathways responsible for the divergence. It's worth noting that the diverse trajectories could potentially be attributed to differences in cell density among the samples. The monocle3 algorithm used for trajectory analysis first places each cell in the expression space before reducing dimensions and calculating pseudotime[247]. The bias introduced by sampling from different cell densities in high-dimensional space might impact the calculation of pseudotime and, consequently, the trajectory pathway. FL, with higher cell density on the left side of the UMAP, may lead to an alternative trajectory pathway. However, this explanation did not entirely account for why WT BM and KO BM, which share similar cell densities, had distinct, albeit not altogether dissimilar, trajectory pathways. Alternative analysis tools and traditional biochemistry approaches could be considered to further investigate and validate this intriguing trajectory-related observation.

In the present analysis, it was observed that both FL and KO BM can generate B1 B cells, yet FL and KO BM exhibit limited similarities at the transcriptomic level. This discrepancy may be attributed in part to potential differences in the ontogeny of B1a and B1b B cells. B1a cells predominantly originate from FL, while B1b cells can be partially renewed by WT BM B cells[193], and the KO BM model primarily generates B1b B cells. This biased generation of B1b B cells suggested that KO BM might not employ the same pathway as FL to generate B1 B cells. Moreover, it is possible that the *Lin28b*/*let7*-related pathway might be crucial for B1a B cell generation in FL but less critical for the ontogeny of B1b B cells. Further investigations into the distinct pathways and molecular mechanisms involved in the generation of these B1 B cell subtypes in FL and KO BM could provide valuable insights into their developmental processes.

Chapter 7 : Discussion

The primary objective of this thesis is to investigate the cellular and molecular mechanisms underpinning the positive and negative selection processes that govern the differentiation of B cells into B1 B cells. A comprehensive understanding of the pathways and critical factors involved in the generation of B1 B cells is fundamental, particularly considering the potential for leveraging the unique housekeeping and immunoregulatory functions of B1 B cells in therapeutic applications. To this end, the thesis details the use of GRB2 knockout mice (KO) models to delineate the generation of B1 B cells and to determine the regulatory function of GRB2 in this process. The characterisation of these models seeks to shed light on the specific role GRB2 plays within the selection and generation of B1 B cells.

This chapter will analyse the implications of the findings presented in this research, setting the stage for future investigations. The goal is to deepen our understanding of B1 B cell biology, which may open new avenues for the development of innovative treatments targeting a variety of immune-related conditions and infections.

7.1 Summary

B1 B cells, with their distinct ontogeny and unique characteristics such as the secretion of natural IgM antibodies, self-renewal capabilities, larger size, and self-reactive nature, stand apart from B2 B cells[88]. Emerging evidence supports that B1 B cell generation is contingent upon both early-stage tissue environments and positive

selection processes driven by BCR signalling, either intrinsic or driven by self-antigen. The switch from LIN28B to *let-7* between FL and adult BM, and the expression of related downstream genes, have been implicated in influencing the balance between positive and negative selection of B1 B cells[92, 109]. Yet, despite various studies highlighting the influence of BCR signalling strength and antigen characteristics on B1 B cell development[102, 103, 105, 106, 107, 109, 110, 111, 137], the potential "driving factors" for B1 B cell ontogeny have not been identified.

This gap in knowledge has propelled the exploration of potential pathways and key elements that regulate B1 B cell ontogeny, particularly concerning the mechanisms of positive and negative selection. Our research using B cell-specific GRB2 knockout mice models reveals that GRB2 acts as a negative regulator of B1 B cell generation, predominantly impacting B1b B cells (**Figure 7-1**). The ablation of GRB2 seemingly circumvents the developmental switch between fetal liver and bone marrow, enhancing the positive selection of B1b B cells without notably affecting B1a B cells. Yet, self-antigen remains a critical determinant for positive selection, even in the absence of GRB2's negative regulation. At a cellular and molecular level, it appears that the deficiency of GRB2 expands the differentiation of B1 B cells and MZ B cells, rather than increasing B1 B cell proliferation or longevity. Interestingly, the absence of GRB2 does not directly modify *Lin28b*/*let-7* signalling, suggesting alternative pathways might regulate the switch during ontogeny. Furthermore, sc-RNASeq data suggest that GRB2 might be pivotal in the pathway by which self-antigens induce the downregulation of IgM and upregulation of IgD in anergic B cells. This might explain

why there is a swing away from negative selection to B1 B cell positive selection in the presence of self-antigens.

In conclusion, the findings presented indicate that GRB2 negatively regulates B1b B cell generation by potentially enforcing a developmental switch during ontogeny or by modulating the positive selection of B1 B cells, possibly through its influence on the generation of a shared B1 B cell/MZ B cell progenitor pool. This research offers a novel perspective on B1 B cell ontogeny and the mechanisms underlying their positive selection.

Figure 7-1

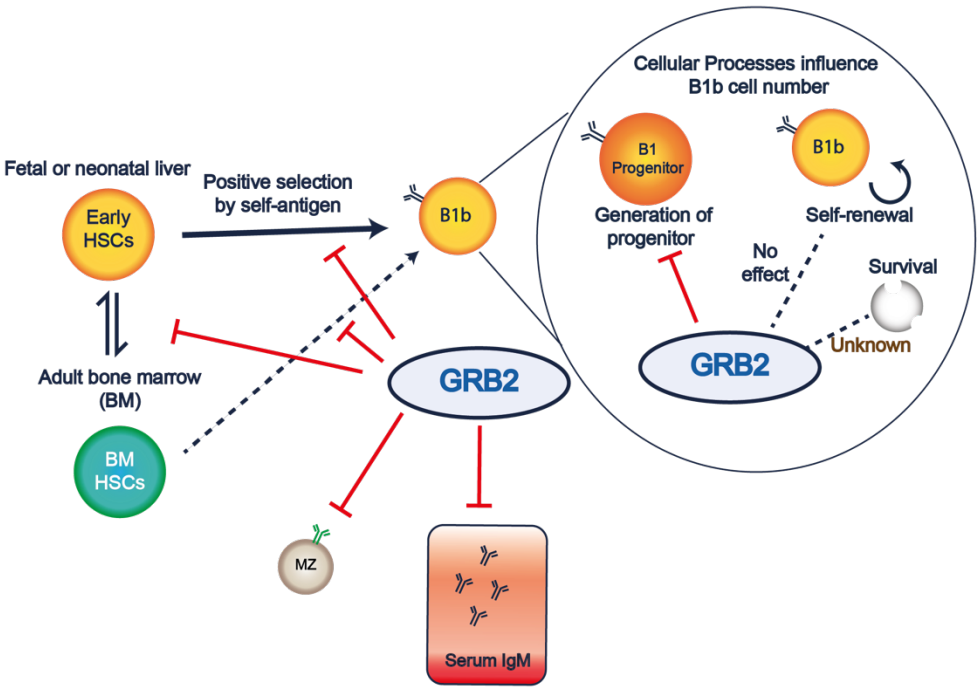

Figure 7-1Schematic illustration summarizing the potential cellular functions of GRB2 in the differentiation of B1b and MZ B cells, highlighting the associated cellular pathways involved in B1b B cell generation and maintenance.

7.2 Positive selection of B1 B cells: setting the stage.

The question of how B1 B cells undergo positive selection is a focal point of increasing research efforts. Key considerations include the timing of selection, the necessity and duration of antigen exposure, and the specific signalling alterations that underpin the process.

The consensus among researchers is that positive selection likely begins at the immature B cell stage or later, or even at the circulating B cell stage, when a complete BCR is expressed and capable of recognizing specific self-antigens. In its most extreme example, support for this theory comes from a BCR switch experiment demonstrating the potential for mature B2 B cells to be positively selected into "B1-like cells"[99]. This aligns with the idea that a fully formed BCR is essential for specific antigen recognition. Our single cell transcriptomic data from BM mixed chimera experiments seem to support this concept, showing no significant changes in the B cell populations from Fr.A to Fr.D B cells, even in the presence of a strongly positively selecting antigen. Further sc-RNASeq-based comparison of peripheral B cell populations in the presence and absence of GRB2 may provide more information on the stage and timing of selection.

However, the dichotomy between B1a and B1b B cells presents a challenge to this model. The differentiation of B1a and B1b B cells and their respective points of origin during B cell development present a complex picture. B1a B cells are hypothesized to arise from an earlier developmental stage compared to B1b B cells, and it is

postulated that B1a B cells may undergo positive selection as early as the pre-B cell stage, when the pre-BCR is expressed on the cell surface. The signalling initiated by an antigen binding to a single heavy chain paired with a SLC may be potent enough to drive this positive selection. Challenging this idea, experimental evidence has shown that B1a B cell development may proceed independently of the pre-BCR and SLC[246]. Specifically, experiments in which the SLC was deleted demonstrated that while the development of B1b and B2 B cells was hindered, the generation of B1a B cells remained unaffected[246]. This suggests that B1a B cells might bypass the need for pre-BCR signalling, potentially due to upregulated *Igk* expression in early pro-B cells caused by reduced IL7R/STAT5 signalling in NL[246].

Despite these insights, the precise phase at which B1a B cells are positively selected remains uncertain. Investigating the single cell BCR sequence at various stages of B cell maturation, including mature B1 B cells, may yield valuable information. If B1 B cells are selected at the pre-BCR stage, a bias towards certain heavy chains would be expected. However, a diverse light chain repertoire is seen among mature B1 B cells, implying that if the heavy chain plays a dominant role in positive selection, it does so without a preference for specific light chain pairings. However, the light chain pairing preference in the absence of selection pressure would also have to be taken into consideration for any analysis. One study has explored BCR usage in B1 B cells across mice of different ages but did not focus on elucidating the stage of positive selection from this perspective, and these data also suffered from low capture number and sequencing quality[248]. Arguably, comprehensive single cell BCR sequencing of B1 B cells would provide deeper insights into the selection process,

and might clarify whether the pre-BCR stage is indeed a critical juncture for positive selection.

7.3 Positive selection of B1 B cells: the role of antigen.

The properties of self-antigen are pivotal in the positive selection of B1 B cells, with factors such as the form of antigen, antigen abundance, exposure time and duration playing significant roles. Research has indicated that highly abundant soluble forms of self-antigen (sHEL) invariably trigger strong negative selection across various developmental stages[249]. Membrane-bound forms of self-antigen (mHEL) have similar effects[249]. Conversely, intracellular antigen forms ($mHEL^{KK}$) do not elicit deletion or anergy. Instead, they positively select B1 B cells[103], although this positive selection is confined to early B cell ontogeny[102]. This selection is accompanied by an increase in anti-self-antigen IgM antibodies[102]. The concentration of these antigens in serum also varies, with HEL present at 15-20ng/ml in the serum of sHEL transgenic mice and at more than 200ng/ml in mHEL transgenic mice, compared to serum HEL amounts of 2-10ng/ml in $mHEL^{KK}$ transgenic mice[103], underscoring the importance of both antigen form and abundance in B1 B cell selection. Notably, these are the serum levels of antigen detected in transgenic mice in the absence of MD4 HEL-specific B cells or anti-HEL IgM antibody, which could mask the free antigen.

Interestingly, the absence of GRB2 increases positive selection in the presence of intracellular self-antigens but does not change the requirements of antigenic form for positive selection. Low-abundance intracellular antigens, such as Trp2mHEL, do not

strongly select for B1 B cells, even in the absence of GRB2 (**Figure 4-8 and Figure 4-11**). This suggests that GRB2 may not directly regulate the signals from antigen-BCR interactions and that neither overly abundant nor sparse signals are simply conducive to B1 B cell positive selection. Given the increase in circulating natural IgM antibodies observed alongside heightened positive selection, it's plausible that these antibodies could influence B1 B cell selection by masking self-antigens, thereby allowing self-reactive B1 B cells to evade negative selection. However, altering natural antibody levels *in vivo* poses challenges. BM mixed chimera experiments have shown that elevated circulating IgM is itself not sufficient to promote B1 B cell positive selection from WT adult BM, implying that increased natural antibodies are likely a result, rather than a driver, of positive selection (**Figure 4-4**).

Additionally, the discovery of increased non-HEL binding IgM^{a+} B1 B cells in Ig^{HEL}KO mice is intriguing (**Figure 4-2 and Figure 4-12**). Given the MD4 mouse model's design, in which the allelic exclusion is strongly reinforced due to the concatemerized multiple HC and LC transgenes that are resistant to gene editing, the presence of B cells with the IgM^{a} heavy chain and a non-HEL specific light chain implies a significant selection pressure. On this basis, and the recurrence of single oligoclonal specificities in multiple mice, it seems highly likely that these B1b B cells are positively selected by an alternative self-antigen. Whilst the absence of GRB2 might reduce negative selection pressure and allow a broader array of B1 B cells to persist, regardless of BCR specificity, the oligoclonality of the B1 B cell population argues against this. Although monoclonal antibodies were generated based on the sequences of these $HEL^{-}IgM^{a+}$ B1 B cells as a first step towards identifying their

antigenic targets, these were negative in an antinuclear antibody test (data not shown). More experiments might be required using protein arrays to identify the antigen targets of these antibodies. Identifying the antigens could significantly advance our knowledge of the forces driving B1 B cell positive selection and could inform the design of antigens that effectively induce B1 B cell responses. Such insights would be invaluable for harnessing the therapeutic potential of B1 B cells, particularly in the context of designing vaccines or treatments that leverage their natural antibody production.

The heightened positive selection of B1 B cells in KO mice exposed to intracellular antigens opens questions about the specific cellular changes that underlie this process. The observed increase in the B1 B cell population could be due to an expansion of progenitor cells destined to become B1 B cells, an increase in the proliferation rate of mature B1 B cells, or an extension of the lifespan of mature B1 B cells.

Research to date has been limited in distinguishing which of these cellular processes might be most critical for B1 B cells. For instance, CD19 deficiency has been shown to increase the number of B1b B cells while significantly reducing B1a B cells[108]. Inhibition of CD19 expression with rat anti-mouse CD19 monoclonal antibodies in the peritoneal cavity impedes B1a B cell proliferation and reduces their numbers, but specific cellular changes associated with the increase in B1b B cells have not been well documented[57, 108]. Using BrdU labelling, our results suggest that GRB2 deficiency does not alter the rate of BrdU incorporation in B1 B cells in BM chimeras **(Figure 4-**

6), implying that the proliferation rate of mature B1 B cells is not influenced by GRB2. Despite the consistent proportion of $BrdU^+$ B1 B cells, the larger population of BrdU-labelled B1 B cells in the absence of GRB2, suggests a steady state production of mature B1 B cells from an expanded pool of B1 B cell precursors. It remains to be clarified whether GRB2 also influences the lifespan of B1 B cells.

7.4 The search for B1 B cells progenitors

The quest to pinpoint a definitive B1 B cell progenitor is a key aspect of the lineage model of B cell development. The population characterized as $Lin^-CD45R^{lo-neg}CD19^+AA4.1^+$ was described as a candidate, with its peak presence in the fetal liver correlating with the emergence of B1 B cells and a decline over time[90]. Yet, the capacity of this population to give rise to B1 B cells in adult BM is poorly defined and uncertain. Instead it may be possible that B1a and B1b B cell generation are separated over time during ontogeny[90]. Adding another layer of complexity to this scenario is the IL7-Rα dependence of the $Lin^-CD45R^{lo-neg}CD19^+AA4.1^+$ population[250], which contradicts the notion that the development of B1 B cells and MZ B cells is IL7-independent[251]. This contradiction highlights the possibility that there might be additional, as yet unidentified, progenitor populations that contribute to the B1 B cell repertoire. At the same time, the alternative possibility that there perhaps is no unique B1 B cell progenitor, but that a switch in tissue-, environment- and developmental stage-dependent signalling modules governs the choice between B1 and B2 B cell development from common HSC precursors, needs further consideration and research.

In the KO bone marrow chimera model, where B1 B cells are positively selected on a large scale in the presence of self-antigen, a mature B cell population expressing both B1 B cell and MZ B cell markers was identified (M6) (**Figure 5-6 and Figure 5-8 B**). This population, which expresses markers such as *Apoe*, *Plac8*, *Sox5*, *Atxn1*, as well as *Cd9*, *Mzb1*, *Fcrl5*, and *Il9r*, exhibits features of both B1 B cells and MZ B cells. The expansion of this population in the absence of GRB2, along with the observation that MZ B cells also increase (**Figure 4-5 and Figure 4-7**), supports the hypothesis that there might be a common progenitor for MZ B cells and possibly B1 B cells. The notion of a shared progenitor is further bolstered by the observation that tissues like the yolk sac and intra-embryonic para-aortic splanchnopleure of ES.9 can give rise to B1 B cells and MZ B cells but not to FO B cell or other B cell types[252]. This suggests that there may be a common progenitor early in development that diverges as B2 B cells emerge. Furthermore, selectively reducing *Rag2* expression in mice shows that while FO B cells decrease over time, MZ and B1 B cells remain stable[253]; however, direct evidence that these cells share a unique progenitor, to the exclusion of other B cell types, has not been found. Furthermore, the mature B cells features found on this population (M6) may indicate that they could firstly be generated in peripheral immune system, like spleen tissue before recirculating back to BM. To validate this potential M6 progenitor population, the next step involves using flow cytometry to identify and sort this population for transfer experiments to either WT recipients or *Rag1*$^{-/-}$ recipients to ascertain its differentiation potential. However, the rarity and complex marker expression of this population pose significant challenges to this

approach. Alternatively, Sc-Seq of spleen B cell tissue may offer deeper insights into the development of this population, provided it is first generated in these tissues.

7.5 BCR signalling in B1 B cell selection and GRB2 function

The generation of B1 B cells through positive selection, facilitated by antigen-BCR interaction signalling, is a crucial aspect of B1 B cell ontogeny. The hypothesis that excessive activation of BCR signalling leads to B1 B cell generation is supported by evidence from various mouse models where the negative regulatory signals associated with BCR are diminished (**Figure 7-2**). Examples include the knockout of SHP-1, where an increase in B1 B cell numbers is observed[104, 107, 134]. Similarly, reductions in the expression of negative co-receptors like SIGLEC-G and CD72 also lead to B1 B cell expansion[135, 137, 254]. The expansion of B1a B cell population in the deficiency of *Siglecg* is partly attributable to a reduced apoptosis rate of B1a B cells, concomitant with the increased expression of NFATC1[255]. Intriguingly, the augmented B1a B cell number observed in SIGLEC-G deficiency mice could be offset by the introduction of an IgM hypomorphic transgene[256]. Whilst the dampening of CD22 alone does not seem to significantly affect the B1 B cell population[139, 257], a double knockout of SIGLEC-G and CD22 results in an even larger expansion of B1 B cells[140]. These findings suggest that negative regulatory phosphatases might play a central role in the generation of B1 B cells. Many of the inhibitory receptors that modulate B1 B cell generation also transduce their negative signals through SHP-1 phosphatase activity[258, 259, 260]. The heightened BCR signal in these knockout models is often characterized by increased calcium mobilization, further supporting a role

for SHP-1 in this process[258, 259, 260]. Further, SHIP-1 is also a negative regulator of BCR signalling and Ca^{2+} signalling and transduces CD22 signals via binding to GRB2; however, direct evidence for its role in B1 B cell generation remains to be established[261]. FCγRIIB is another receptor known for its inhibitory role in B cell survival and its function as a negative regulator for B1 B cells. Deletion of FCγRIIB leads to an expansion of B1 B cells, possibly by decreasing cell death and increasing survival rates[262]. LYN is a kinase involved in the early transduction of BCR signalling that acts as a negative regulator of BCR signalling through its phosphorylation of inhibitory co-receptors such as CD22. LYN deficiency also leads to a reduction in SHP-1 recruitment and an increase in B1a B cells[227, 263, 264].

Figure 7-2

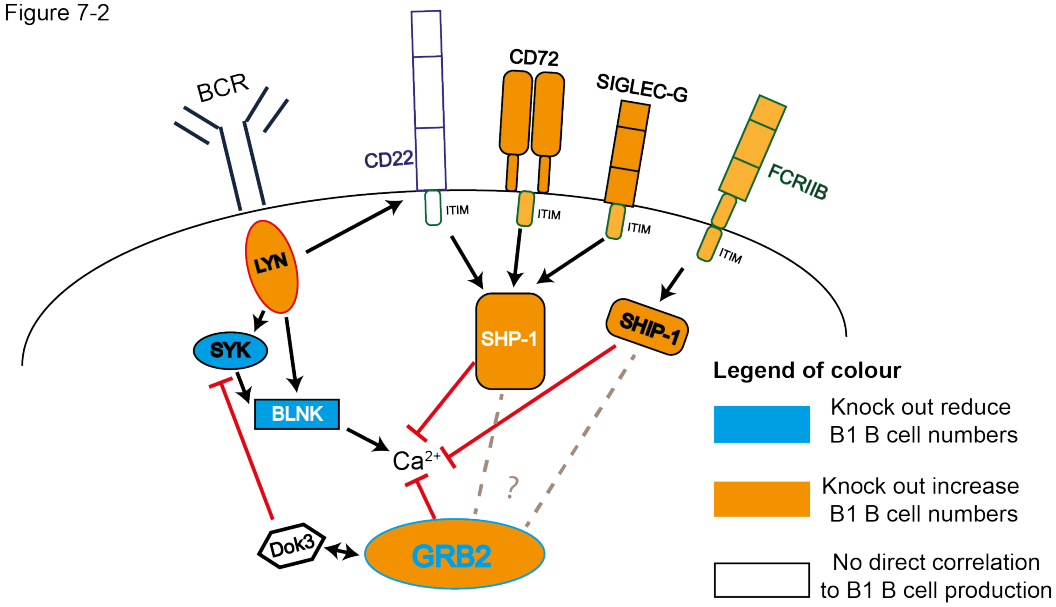

Figure 7-2 Schematic illustration summarizing the role of GRB2 in BCR signalling and its correlation with both positive and negative regulatory pathway and their association with B1 B cell generation.

This complex interplay of signalling pathways underscores the intricate balance of positive and negative signals that govern B1 B cell development. Disruption of this balance, whether by enhancing positive signals or inhibiting negative ones, appears to skew development towards the B1 B cell lineage. Further investigation into how these signals are modulated in B1 B cell development, compared to that in other B cell subsets, may provide valuable insights into the mechanisms that drive B1 B cell positive selection and maintenance.

The regulation of B1 B cell development through BCR signalling is a process wherein both the enhancement and disruption of signalling components can lead to differing outcomes. The deletion of BCR signalling molecules, such as BLNK, has been shown to impede the development of B1a B cells, highlighting its necessity in B1 B cell maturation[265]. BLNK serves as a critical scaffold in the BCR signalling complex, linking SYK kinase, PLCγ, and Vav proteins. These findings are mirrored in knockout models for VAV and PI3K, where disruption of these signalling molecules similarly leads to reduced B1 B cell populations[266, 267, 268]. These results indicate that a proper level of BCR signalling is essential for B1 B cell development.

On the other hand, the modulation of signalling strength, particularly through molecules like CD19 and BTK, might explain alternative pathways leading to B1a or B1b B cells. Inhibition or deficiency of CD19 results in the absence of B1a cells but an increase in B1b B cells[108]. The deficiency of BTK also differentially affects these B cell subsets[114]. This suggests that B1a B cells may rely more heavily on BCR signalling strength, while B1b B cells could be influenced more by alternative signalling

pathways. It is important to note that much of the research on BCR signalling has predominantly focused on B1a B cells, due to the limitations of flow cytometry gating strategies[265, 266, 267]. As a result, the impact on B1b B cells has not been as thoroughly examined, which could be crucial in understanding the nuances of B1 B cell ontogeny. Moreover, the majority of observations related to the role of BCR signalling in B1 B cell development have been made in mature B cells, which might not accurately reflect the underlying changes occurring in B cell precursors that are positively selected to become mature B1 B cells.

The observed increase in calcium mobilization upon BCR cross-linking in GRB2-deficient splenic B cells suggests that GRB2 normally acts to inhibit BCR signalling (**Figure 5-11**). Specifically, GRB2 has been identified to form a complex with DOK-3[269], which is integral to the negative feedback regulation of calcium signalling following BCR activation. DOK-3 inhibits BCR-induced activation of the SYK kinase, which is a crucial early step in BCR signalling[190]. Furthermore, the binding of GRB2 to DOK-3 through its SH2 domain suggests that GRB2 may influence BCR signalling through multiple inhibitory pathways, either directly via interactions with ITIM-bearing co-receptors or indirectly through DOK-3. GRB2 also has interactions with ITIM domains on various co-receptors, such as CD72, CD22, and FCγRIIB[260, 270, 271], which are involved in inhibitory signalling pathways. The downstream effects of these interactions likely involve SHP-1, a phosphatase that GRB2 can bind to, thereby mediating negative regulation of signalling pathways such as the STAT5 signalling pathway that was investigated in epithelial cell lines[189].

However, data on the role of GRB2 in BCR signalling, and its impact on B1 B cell generation, suggests that the situation may be more complex. In Mb1Cre-induced GRB2 KO mice, while the MAPK related pathway ERK and P38 signalling appear unaffected, there is a notable attenuation in JNK phosphorylation and an upregulation in SYK activation. At the same time, AKT signalling, downstream of PI3K, has been reported to be significantly reduced[169]. These findings suggest that GRB2 may differentially modulate specific aspects of the BCR signalling network. The discrepancies between the results from Mb1Cre-induced GRB2 KO mice and those from CD19Cre-induced GRB2 KO mice, where PLCγ2 and JNK were elevated and CD22 phosphorylation was reduced[170], highlight an inconsistency in the role of GRB2 in BCR signalling pathways, possibly due to the modifying effects of the loss of one allele of CD79α or one allele of CD19. Our observations suggest that the effects of GRB2 deficiency on proximal BCR signalling in splenic B cells are perhaps not as profound as expected, and the role of GRB2 in B cell precursors, which might be destined to become B1 B cells, has yet to be fully understood. It cannot be conclusively stated that GRB2 does not influence BCR signalling in these precursors.

Our observation that the extent of anergy in GRB2-deficient mice is reduced - at least in terms of IgM autoantibody production - may be further evidence that there is a general defect in negative selection (particularly in adult mice), or rather a shift towards positive selection. The inability of GRB2-deficient B cells to downregulate surface IgM in the presence of self-antigen hinted at a disruption in a anergic response mechanism, described by Chris Goodnow, which is associated with preventing autoimmunity (**Figure 7-3**) [111]. BCR stimulation by self-antigen leads to the

NFATC1/NFATC2 translation (and later upregulation by positive feedback)[222], thence to EGR2/EGR3 expression and the induction of ZFP318, which stabilises alternative splicing and *Ighd* expression relative to *Ighm*[223] [221]. Simultaneously, EGR2/EGR3 expression upregulates *Ztbt20*, *Zbtb32*, *Mzb1* etc, transcription and other factors associated with the inhibition of plasma cell differentiation[221, 272, 273, 274]. ID3, coincidently, a helix-loop-helix protein under the regulation of EGR2/EGR3, also functions as a negative regulator in the generation of B1b B cells[69, 275]

We considered whether GRB2-dependent regulation of EGR2/EGR3 dependent pathways including that of ZFP318 by self-antigen may be a major determinant of the balance of positive and negative selection. This also raises the possibility that these pathways might be regulated during ontogeny. Our sc-RNASeq data indicate that *Nfatc1* is still upregulated in the presence of antigen without GRB2, but *Egr3* and *Zfp318* are not, implying that GRB2 might regulate this pathway at a point post-NFATC1 activation (**Figure 5-10**). Preliminary experiments suggest that the translocation of NFATC1/NFATC2 from the cytoplasm to the nucleus is not deficient in the response of naïve GRB2 KO FO B cells upon activation with cognate antigen (data not shown); however, but this may not reflect the situation when cells are exposed to low levels of self-antigen during development. While there is no direct evidence of GRB2 interacting with EGR2/EGR3 or ZFP318, the link between GRB2 and the NFAT pathway in T cells, via CD28 to VAV signalling[276], raises the question of whether a similar or parallel mechanism exists in B cells. Further experiments are required to explore these possibilities and to quantify ZFP318 in the presence and absence of different antigens and GRB2 in the context of ontogeny.

Apart from the potential role GRB2 may have on BCR signalling, GRB2 may also regulate the metabolism of B cells and exert potential influence on B1 B cell selection. Since GRB2 is known to bind AMPK[158], which negatively regulates mTOR under conditions of metabolic stress, it stands to reason that GRB2 could be a key regulator of the metabolic state of B1 B cells. Furthermore, GRB2 also seems to modulate BAFF-R response in B cells, with the BAFF/BAFF-R signalling pathway being linked to metabolic capacity of B cells[169, 277]. If GRB2 is indeed influencing the metabolic signalling in B cells, this could have far-reaching implications for the generation of B1 B cells, which may require different metabolic conditions compared to other B cell subsets[278]. Measuring the phosphorylation levels of AMPK and MTOR in B cells from GRB2 knockout mice may provide valuable data to support or refute this hypothesis. Interestingly, AMPK may also lie upstream of EGR2/3 and these hypotheses warrant further investigation.

Figure 7-3

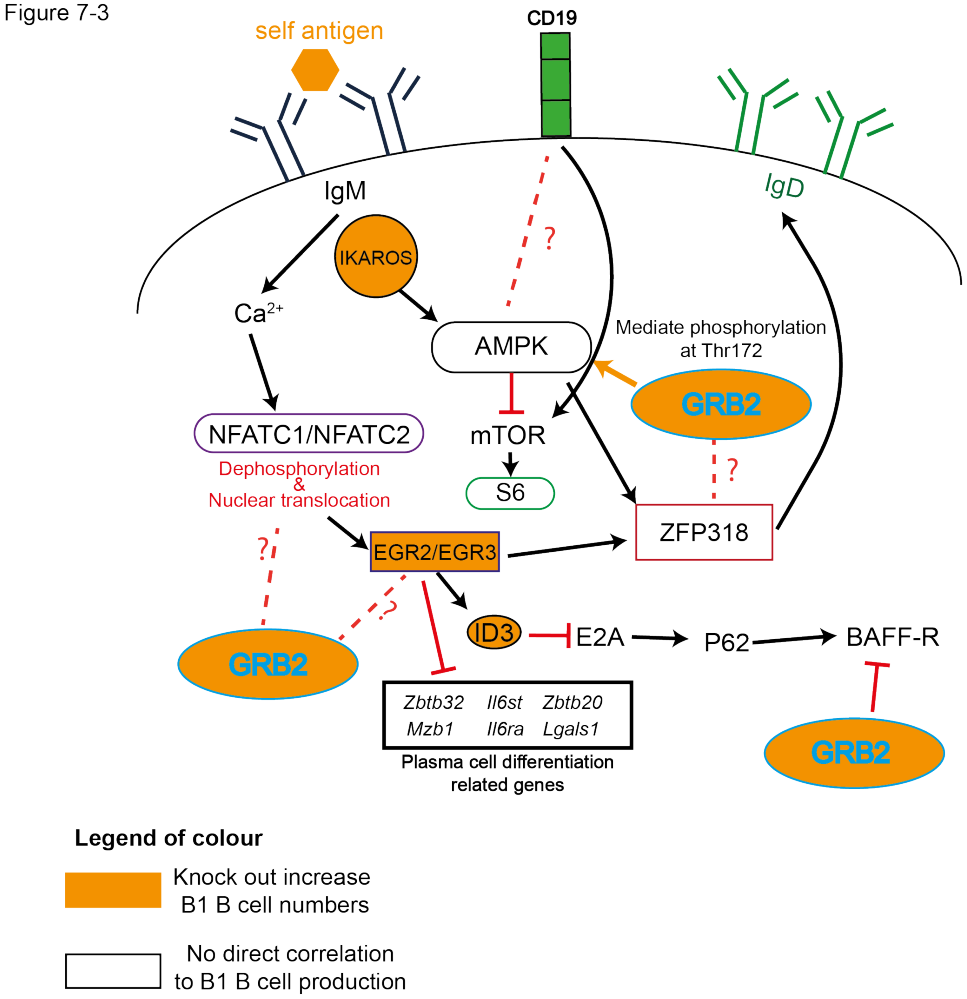

Figure 7-3 Schematic outlining the hypothesized role of GRB2 in self-antigen induced B cell anergy pathway and B cell metabolism pathway, and its potential connection with B1 B cell ontogeny.

7.6 The pathways of B1a and B1b B cell differentiation in ontogeny.

As already discussed, B1a B cells, with their tendency to be generated in early-stage tissues, and B1b B cells, which can still arise in bone marrow albeit at reduced rates, may have developmental pathways and possibly different roles within the immune system[89, 90].

It has been suggested that B1a B cells may bypass the pre-BCR stage due to early recombination of the IgK chain, something that provides an intriguing mechanistic explanation for their generation and may account for their unique characteristics[246]. The MD4 mouse model, with its engineered BCR specificity, appears to favour B1b B cell development, possibly due to the limited opportunities for light chain editing and the shorter pre-BCR stage duration.

The differential regulation of B1b B cell generation by GRB2, especially in the context of positive selection by self-antigen, suggests that GRB2 could be a crucial factor in maintaining the balance between autoimmunity and immune tolerance by selectively influencing B1b B cell generation. It is particularly interesting that the regulatory effects of GRB2 seem to target B1b B cells specifically, regardless the BCR specificity (**Figure 4-2**), which may provide insights into tailored immunological interventions that could exploit this regulatory pathway. In one scenario, wherein B1a B cells are selected by bypassing the pre-BCR checkpoint and B1b B cells are selected at a later stage where GRB2 negatively regulates the signalling, suggests a complex interplay of developmental signals that control B1 B cell maturation. Understanding these pathways could lead to novel strategies for modulating the immune response in autoimmune diseases, vaccine development, and other therapeutic areas.

7.7 The potential therapeutic applications of B1 B cells

The specialized functions of B1a and B1b B cells in the immune response may also be distinct, although reporting biases are difficult to control. For example, B1a B cells are noted for their capacity to produce IgA and secrete IL-10[75, 82, 116, 279], which is crucial for mucosal immunity and regulating inflammation, thus preventing tissue damage from excessive immune reactions. B1b B cells have been shown to be vital for defence against pathogens such as *Borrelia hermsii* and *Streptococcus pneumoniae*[76, 108], highlighting their role in pathogen-specific immune responses. The report of a role for B1b B cells in the response to the typhoid Vi polysaccharide antigen[117], points to a role in adaptive immunity; and the involvement of B1b B cells in atheroprotection suggests a link between innate immunity and chronic inflammation[69].

It has been suggested that the ability of B1 B cells to contribute to long-term memory and rapid response to pathogens could be exploited to engineer vaccines of greater effectiveness, especially in populations traditionally less responsive to TI antigens, such as the very young and the elderly[280]. The innate immune capabilities of B1 B cells could pave the way for pre-emptive strategies against common pathogens or the spread and severity of infectious diseases or atherosclerosis. Enhancing B1 B cell activity could offer a preventive measure against this chronic inflammatory condition, contributing to broader cardiovascular health strategies.

These possibilities underscore the need for more in-depth research into the ontogeny of B1 B cells and their interactions with antigens.

7.8 Human B1 B cells

Finally, the identification of B1 B cells in humans remains an area of ongoing research and debate due to the lack of consensus on specific markers that definitively distinguish this population. The expression of CD5 on B cells, which is a hallmark of murine B1a B cells, does not provide the same distinction in humans, as CD5 is present on a variable percentage of normal circulating B cells, umbilical cord blood B cells, and in pathological conditions such as chronic lymphocytic leukemia (CLL) [281], which could arise from a B1-like progenitor.

Without a set of specific markers, although remain controversial, Kaku and colleagues proposed to use following features to define the human B1 B cells : spontaneous secretion of IgM, potent stimulation of T cells, and persistent intracellular signalling[281]. Attempts to define human B1 B cells using a combination of surface markers such as CD20, CD27, CD43, and CD70 have yielded a subset that shares some of these functional characteristics[282], though this subset also shares similarities with pre-plasmablasts, complicating the distinction[283]. Additional markers like CD38 have been introduced to refine this definition[284], but a clear and distinct flow cytometry profile analogous to that found in mouse models remains elusive. Furthermore, the population of these B1-like cells and their IgM secretion capabilities appear to decline with age[285]. Despite these challenges, the protective

role of these putative human B1 B cells against pathogens like *Streptococcus pneumoniae* and their altered levels in diseases such as multiple sclerosis and lupus highlight their possible clinical relevance[286, 287, 288].

Seifert and colleagues, on the other hand, suggested a subset of human cord blood B cells should represent human B1 B cell, characterized by a mature, naïve phenotype and a highly variable yet interindividual conserved BCR clonetype. These mature $CD5^+$ ($CD5^+CD23^+CD27^-CD38^{low}IgD^+$) and $CD5^-$ ($CD5^+CD23^+CD27^-CD38^{low}IgD^+$) human cord blood B cells share several features with murine B1 B cells , including age-related decline, high surface IgM, TI response and functionally distinction from adult B cell counterparts. However, these cells lack the murine B1 cell transcriptome signatures and bias BCR usage[289], suggesting only partial similarity with murine B1 B cells. This raises the question of whether human B1 B cells need to fully mirror their murine counterparts.

Against this backdrop, the study of murine B1 B cells will continue to inform our understanding of human B1-like cells and assist in the development of new therapies based on this unique lymphocyte subset.

References

1. Hardy, R.R. & Hayakawa, K. B cell development pathways. *Annu Rev Immunol* **19**, 595-621 (2001).

2. Kondo, M., Weissman, I.L. & Akashi, K. Identification of clonogenic common lymphoid progenitors in mouse bone marrow. *Cell* **91**, 661-672 (1997).

3. Hardy, R.R. *et al.* B-cell commitment, development and selection. *Immunological Reviews* **175**, 23-32 (2000).

4. Nemazee, D. Mechanisms of central tolerance for B cells. *Nature Reviews Immunology* **17**, 281-294 (2017).

5. Clark, M.R., Mandal, M., Ochiai, K. & Singh, H. Orchestrating B cell lymphopoiesis through interplay of IL-7 receptor and pre-B cell receptor signalling. *Nat Rev Immunol* **14**, 69-80 (2014).

6. Otero, D.C. & Rickert, R.C. CD19 function in early and late B cell development. II. CD19 facilitates the pro-B/pre-B transition. *The journal of immunology* **171**, 5921-5930 (2003).

7. Karasuyama, H., Kudo, A. & Melchers, F. The proteins encoded by the VpreB and lambda 5 pre-B cell-specific genes can associate with each other and with mu heavy chain. *J Exp Med* **172**, 969-972 (1990).

8. Hendriks, R.W. & Middendorp, S. The pre-BCR checkpoint as a cell-autonomous proliferation switch. *Trends Immunol* **25**, 249-256 (2004).

9. Rickert, R.C. New insights into pre-BCR and BCR signalling with relevance to B cell malignancies. *Nature Reviews Immunology* **13**, 578-591 (2013).

10. Pieper, K., Grimbacher, B. & Eibel, H. B-cell biology and development. *J Allergy Clin Immunol* **131**, 959-971 (2013).

11. Mårtensson, I.L. & Ceredig, R. Review article: role of the surrogate light chain and the pre-B-cell receptor in mouse B-cell development. *Immunology* **101**, 435-441 (2000).

12. Rolink, A.G., Winkler, T., Melchers, F. & Andersson, J. Precursor B cell receptor-dependent B cell proliferation and differentiation does not require the bone marrow or fetal liver environment. *J Exp Med* **191**, 23-32 (2000).

13. Bannish, G., Fuentes-Pananá, E.M., Cambier, J.C., Pear, W.S. & Monroe, J.G. Ligand-independent signaling functions for the B lymphocyte antigen receptor and their role in positive selection during B lymphopoiesis. *J Exp Med* **194**, 1583-1596 (2001).

14. Bradl, H., Wittmann, J., Milius, D., Vettermann, C. & Jäck, H.M. Interaction of murine precursor B cell receptor with stroma cells is controlled by the unique tail of lambda 5 and stroma cell-associated heparan sulfate. *J Immunol* **171**, 2338-2348 (2003).

15. Gauthier, L., Rossi, B., Roux, F., Termine, E. & Schiff, C. Galectin-1 is a stromal cell ligand of the pre-B cell receptor (BCR) implicated in synapse formation between pre-B and stromal cells and in pre-BCR triggering. *Proc Natl Acad Sci U S A* **99**, 13014-13019 (2002).

16. Vettermann, C., Herrmann, K. & Jäck, H.M. Powered by pairing: the surrogate light chain amplifies immunoglobulin heavy chain signaling and pre-selects the antibody repertoire. *Semin Immunol* **18**, 44-55 (2006).

17. ten Boekel, E., Melchers, F. & Rolink, A.G. Changes in the V(H) gene repertoire of developing precursor B lymphocytes in mouse bone marrow mediated by the pre-B cell receptor. *Immunity* **7**, 357-368 (1997).

18. von Boehmer, H. & Melchers, F. Checkpoints in lymphocyte development and autoimmune disease. *Nat Immunol* **11**, 14-20 (2010).

19. Rolink, A.G., Andersson, J. & Melchers, F. Characterization of immature B cells by a novel monoclonal antibody, by turnover and by mitogen reactivity. *European journal of immunology* **28**, 3738-3748 (1998).

20. Grandien, A., Fucs, R., Nobrega, A., Andersson, J. & Coutinho, A. Negative selection of multireactive B cell clones in normal adult mice. *Eur J Immunol* **24**, 1345-1352 (1994).

21. Chen, C., Nagy, Z., Prak, E.L. & Weigert, M. Immunoglobulin heavy chain gene replacement: a mechanism of receptor editing. *Immunity* **3**, 747-755 (1995).

22. Li, H., Jiang, Y., Prak, E.L., Radic, M. & Weigert, M. Editors and editing of anti-DNA receptors. *Immunity* **15**, 947-957 (2001).

23. Tiegs, S.L., Russell, D.M. & Nemazee, D. Receptor editing in self-reactive bone marrow B cells. *J Exp Med* **177**, 1009-1020 (1993).

24. Gay, D., Saunders, T., Camper, S. & Weigert, M. Receptor editing: an approach by autoreactive B cells to escape tolerance. *J Exp Med* **177**, 999-1008 (1993).

25. Witsch, E.J., Cao, H., Fukuyama, H. & Weigert, M. Light chain editing generates polyreactive antibodies in chronic graft-versus-host reaction. *J Exp Med* **203**, 1761-1772 (2006).

26. Rolink, A.G., Andersson, J. & Melchers, F. Characterization of immature B cells by a novel monoclonal antibody, by turnover and by mitogen reactivity. *Eur J Immunol* **28**, 3738-3748 (1998).

27. Turner, M. *et al.* Syk tyrosine kinase is required for the positive selection of immature B cells into the recirculating B cell pool. *J Exp Med* **186**, 2013-2021 (1997).

28. Hachemi-Rachedi, S., Cumano, A., Drapier, A.M., Cazenave, P.A. & Sanchez, P. Does positive selection determine the B cell repertoire? *Eur J Immunol* **27**, 1069-1074 (1997).

29. Lesley, R. *et al.* Reduced competitiveness of autoantigen-engaged B cells due to increased dependence on BAFF. *Immunity* **20**, 441-453 (2004).

30. Darce, J.R., Arendt, B.K., Wu, X. & Jelinek, D.F. Regulated expression of BAFF-binding receptors during human B cell differentiation. *J Immunol* **179**, 7276-7286 (2007).

31. Thien, M. *et al.* Excess BAFF rescues self-reactive B cells from peripheral deletion and allows them to enter forbidden follicular and marginal zone niches. *Immunity* **20**, 785-798 (2004).

32. Allman, D.M., Ferguson, S.E., Lentz, V.M. & Cancro, M.P. Peripheral B cell maturation. II. Heat-stable antigen(hi) splenic B cells are an immature developmental intermediate in the production of long-lived marrow-derived B cells. *The Journal of Immunology* **151**, 4431-4444 (1993).

33. Wardemann, H. *et al.* Predominant autoantibody production by early human B cell precursors. *Science* **301**, 1374-1377 (2003).

34. Brink, R. The imperfect control of self-reactive germinal center B cells. *Curr Opin Immunol* **28**, 97-101 (2014).

35. Grawunder, U. *et al.* Down-regulation of RAG1 and RAG2 gene expression in preB cells after functional immunoglobulin heavy chain rearrangement. *Immunity* **3**, 601-608 (1995).

36. Luning Prak, E.T., Monestier, M. & Eisenberg, R.A. B cell receptor editing in tolerance and autoimmunity. *Ann N Y Acad Sci* **1217**, 96-121 (2011).

37. Usuda, S. *et al.* Immunoglobulin V gene replacement is caused by the intramolecular DNA deletion mechanism. *Embo j* **11**, 611-618 (1992).

38. Hertz, M. & Nemazee, D. BCR ligation induces receptor editing in IgM+ IgD− bone marrow B cells in vitro. *Immunity* **6**, 429-436 (1997).

39. Carsetti, R., Köhler, G. & Lamers, M.C. Transitional B cells are the target of negative selection in the B cell compartment. *J Exp Med* **181**, 2129-2140 (1995).

40. Allman, D. *et al.* Resolution of three nonproliferative immature splenic B cell subsets reveals multiple selection points during peripheral B cell maturation. *J Immunol* **167**, 6834-6840 (2001).

41. Loder, F. *et al.* B cell development in the spleen takes place in discrete steps and is determined by the quality of B cell receptor-derived signals. *J Exp Med* **190**, 75-89 (1999).

42. Allman, D. & Pillai, S. Peripheral B cell subsets. *Current Opinion in Immunology* **20**, 149-157 (2008).

43. Martin, F. & Kearney, J.F. CD21high IgMhigh splenic B cells enriched in the marginal zone: distinct phenotypes and functions. *Curr Top Microbiol Immunol* **246**, 45-50; discussion 51-42 (1999).

44. Genestier, L. *et al.* TLR agonists selectively promote terminal plasma cell differentiation of B cell subsets specialized in thymus-independent responses. *The Journal of Immunology* **178**, 7779-7786 (2007).

45. O'Connor, B.P. *et al.* BCMA is essential for the survival of long-lived bone marrow plasma cells. *The Journal of experimental medicine* **199**, 91-98 (2004).

46. Cariappa, A. *et al.* The recirculating B cell pool contains two functionally distinct, long-lived, posttransitional, follicular B cell populations. *J Immunol* **179**, 2270-2281 (2007).

47. Cinamon, G. *et al.* Sphingosine 1-phosphate receptor 1 promotes B cell localization in the splenic marginal zone. *Nature immunology* **5**, 713-720 (2004).

48. Martin, F. & Kearney, J.F. Marginal-zone B cells. *Nature Reviews Immunology* **2**, 323-335 (2002).

49. Oliver, A.M., Martin, F. & Kearney, J.F. IgMhighCD21high lymphocytes enriched in the splenic marginal zone generate effector cells more rapidly than the bulk of follicular B cells. *J Immunol* **162**, 7198-7207 (1999).

50. Hardy, R.R., Hayakawa, K., Haaijman, J. & Herzenberg, L.A. B-cell subpopulations identified by two-colour fluorescence analysis. *Nature* **297**, 589-591 (1982).

51. Hayakawa, K., Hardy, R.R., Parks, D.R. & Herzenberg, L.A. The "Ly-1 B" cell subpopulation in normal immunodefective, and autoimmune mice. *J Exp Med* **157**, 202-218 (1983).

52. Lanier, L.L., Warner, N.L., Ledbetter, J.A. & Herzenberg, L.A. Expression of Lyt-1 antigen on certain murine B cell lymphomas. *The Journal of experimental medicine* **153**, 998-1003 (1981).

53. Azzam, H.S. *et al.* CD5 Expression Is Developmentally Regulated By T Cell Receptor (TCR) Signals and TCR Avidity. *Journal of Experimental Medicine* **188**, 2301-2311 (1998).

54. Gary-Gouy, H., Harriague, J., Dalloul, A., Donnadieu, E. & Bismuth, G. CD5-negative regulation of B cell receptor signaling pathways originates from tyrosine residue Y429 outside an immunoreceptor tyrosine-based inhibitory motif. *J Immunol* **168**, 232-239 (2002).

55. Hayakawa, K., Hardy, R.R., Herzenberg, L.A. & Herzenberg, L.A. Progenitors for Ly-1 B cells are distinct from progenitors for other B cells. *J Exp Med* **161**, 1554-1568 (1985).

56. Ansel, K.M., Harris, R.B. & Cyster, J.G. CXCL13 is required for B1 cell homing, natural antibody production, and body cavity immunity. *Immunity* **16**, 67-76 (2002).

57. Krop, I. *et al.* Self-renewal of B-1 lymphocytes is dependent on CD19. *Eur J Immunol* **26**, 238-242 (1996).

58. Deenen, G.J. & Kroese, F.G. Murine peritoneal Ly-1 B cells do not turn over rapidly. *Ann N Y Acad Sci* **651**, 70-71 (1992).

59. McIntyre, T.M., Holmes, K.L., Steinberg, A.D. & Kastner, D.L. CD5+ peritoneal B cells express high levels of membrane, but not secretory, C mu mRNA. *J Immunol* **146**, 3639-3645 (1991).

60. Chace, J.H., Fleming, A.L., Gordon, J.A., Perandones, C.E. & Cowdery, J.S. Regulation of differentiation of peritoneal B-1a (CD5+) B cells. Activated peritoneal macrophages release prostaglandin E2, which inhibits IgM secretion by peritoneal B-1a cells. *The Journal of Immunology* **154**, 5630-5636 (1995).

61. Savage, H.P. *et al.* Blimp-1–dependent and –independent natural antibody production by B-1 and B-1–derived plasma cells. *Journal of Experimental Medicine* **214**, 2777-2794 (2017).

62. Morris, D.L. & Rothstein, T.L. Abnormal transcription factor induction through the surface immunoglobulin M receptor of B-1 lymphocytes. *J Exp Med* **177**, 857-861 (1993).

63. Tornberg, U.C. & Holmberg, D. B-1a, B-1b and B-2 B cells display unique VHDJH repertoires formed at different stages of ontogeny and under different selection pressures. *Embo j* **14**, 1680-1689 (1995).

64. Meyer-Bahlburg, A. B-1 cells as a source of IgA. *Ann N Y Acad Sci* **1362**, 122-131 (2015).

65. Smulski, C.R. & Eibel, H. BAFF and BAFF-Receptor in B Cell Selection and Survival. *Front Immunol* **9**, 2285 (2018).

66. Palma, J., Tokarz-Deptuła, B., Deptuła, J. & Deptuła, W. Natural antibodies - facts known and unknown. *Cent Eur J Immunol* **43**, 466-475 (2018).

67. Ayala, A., Muñoz, M.F. & Argüelles, S. Lipid peroxidation: production, metabolism, and signaling mechanisms of malondialdehyde and 4-hydroxy-2-nonenal. *Oxid Med Cell Longev* **2014**, 360438 (2014).

68. Harnett, W. & Harnett, M.M. Phosphorylcholine: friend or foe of the immune system? *Immunol Today* **20**, 125-129 (1999).

69. Rosenfeld, S.M. *et al.* B-1b Cells Secrete Atheroprotective IgM and Attenuate Atherosclerosis. *Circ Res* **117**, e28-39 (2015).

70. Shaw, P.X. *et al.* Natural antibodies with the T15 idiotype may act in atherosclerosis, apoptotic clearance, and protective immunity. *J Clin Invest* **105**, 1731-1740 (2000).

71. Rosenfeld, S.M. *et al.* B-1b cells secrete atheroprotective IgM and attenuate atherosclerosis. *Circulation research* **117**, e28-e39 (2015).

72. Boes, M., Prodeus, A.P., Schmidt, T., Carroll, M.C. & Chen, J. A critical role of natural immunoglobulin M in immediate defense against systemic bacterial infection. *J Exp Med* **188**, 2381-2386 (1998).

73. Reid, R.R. *et al.* Endotoxin shock in antibody-deficient mice: unraveling the role of natural antibody and complement in the clearance of lipopolysaccharide. *J Immunol* **159**, 970-975 (1997).

74. Rauch, P.J. *et al.* Innate response activator B cells protect against microbial sepsis. *Science* **335**, 597-601 (2012).

75. Aziz, M., Holodick, N.E., Rothstein, T.L. & Wang, P. B-1a Cells Protect Mice from Sepsis: Critical Role of CREB. *J Immunol* **199**, 750-760 (2017).

76. Alugupalli, K.R. *et al.* The resolution of relapsing fever borreliosis requires IgM and is concurrent with expansion of B1b lymphocytes. *J Immunol* **170**, 3819-3827 (2003).

77. Alugupalli, K.R. *et al.* B1b lymphocytes confer T cell-independent long-lasting immunity. *Immunity* **21**, 379-390 (2004).

78. Colombo, M.J. & Alugupalli, K.R. Complement factor H-binding protein, a putative virulence determinant of Borrelia hermsii, is an antigenic target for protective B1b lymphocytes. *J Immunol* **180**, 4858-4864 (2008).

79. Cole, L.E. *et al.* Antigen-specific B-1a antibodies induced by Francisella tularensis LPS provide long-term protection against F. tularensis LVS challenge. *Proc Natl Acad Sci U S A* **106**, 4343-4348 (2009).

80. Yang, Y. *et al.* Antigen-specific memory in B-1a and its relationship to natural immunity. *Proc Natl Acad Sci U S A* **109**, 5388-5393 (2012).

81. Ordoñez, C. *et al.* Both B-1a and B-1b cells exposed to Mycobacterium tuberculosis lipids differentiate into IgM antibody-secreting cells. *Immunology* **154**, 613-623 (2018).

82. Leech, J.M., Lacey, K.A., Mulcahy, M.E., Medina, E. & McLoughlin, R.M. IL-10 Plays Opposing Roles during Staphylococcus aureus Systemic and Localized Infections. *J Immunol* **198**, 2352-2365 (2017).

83. Choi, Y.S. & Baumgarth, N. Dual role for B-1a cells in immunity to influenza virus infection. *J Exp Med* **205**, 3053-3064 (2008).

84. Waffarn, E.E. *et al.* Infection-induced type I interferons activate CD11b on B-1 cells for subsequent lymph node accumulation. *Nat Commun* **6**, 8991 (2015).

85. Popi, A.F., Lopes, J.D. & Mariano, M. Interleukin-10 secreted by B-1 cells modulates the phagocytic activity of murine macrophages in vitro. *Immunology* **113**, 348-354 (2004).

86. Wu, L. *et al.* IL-10–producing B cells are enriched in murine pericardial adipose tissues and ameliorate the outcome of acute myocardial infarction. *Proceedings of the National Academy of Sciences* **116**, 21673-21684 (2019).

87. Geherin, S.A. *et al.* IL-10+ Innate-like B Cells Are Part of the Skin Immune System and Require α4β1 Integrin To Migrate between the Peritoneum and Inflamed Skin. *J Immunol* **196**, 2514-2525 (2016).

88. Baumgarth, N. The double life of a B-1 cell: self-reactivity selects for protective effector functions. *Nature Reviews Immunology* **11**, 34-46 (2011).

89. Herzenberg, L.A. & Tung, J.W. B cell lineages: documented at last! *Nature Immunology* **7**, 225-226 (2006).

90. Montecino-Rodriguez, E., Leathers, H. & Dorshkind, K. Identification of a B-1 B cell–specified progenitor. *Nature Immunology* **7**, 293-301 (2006).

91. Godin, I.E., Garcia-Porrero, J.A., Coutinho, A., Dieterlen-Lièvre, F. & Marcos, M.A. Para-aortic splanchnopleura from early mouse embryos contains B1a cell progenitors. *Nature* **364**, 67-70 (1993).

92. Yuan, J., Nguyen, C.K., Liu, X., Kanellopoulou, C. & Muljo, S.A. Lin28b reprograms adult bone marrow hematopoietic progenitors to mediate fetal-like lymphopoiesis. *Science* **335**, 1195-1200 (2012).

93. Hayakawa, K. *et al.* Crucial Role of Increased Arid3a at the Pre-B and Immature B Cell Stages for B1a Cell Generation. *Front Immunol* **10**, 457 (2019).

94. Kreslavsky, T. *et al.* Essential role for the transcription factor Bhlhe41 in regulating the development, self-renewal and BCR repertoire of B-1a cells. *Nat Immunol* **18**, 442-455 (2017).

95. Kristiansen, T.A. *et al.* Cellular Barcoding Links B-1a B Cell Potential to a Fetal Hematopoietic Stem Cell State at the Single-Cell Level. *Immunity* **45**, 346-357 (2016).

96. Zhou, Y. *et al.* Lin28b promotes fetal B lymphopoiesis through the transcription factor Arid3a. *J Exp Med* **212**, 569-580 (2015).

97. New, J.S. *et al.* Neonatal Exposure to Commensal-Bacteria-Derived Antigens Directs Polysaccharide-Specific B-1 B Cell Repertoire Development. *Immunity* **53**, 172-186.e176 (2020).

98. Vergani, S. *et al.* A self-sustaining layer of early-life-origin B cells drives steady-state IgA responses in the adult gut. *Immunity* **55**, 1829-1842.e1826 (2022).

99. Graf, R. *et al.* BCR-dependent lineage plasticity in mature B cells. *Science* **363**, 748-753 (2019).

100. Hayakawa, K. *et al.* Positive selection of natural autoreactive B cells. *Science* **285**, 113-116 (1999).

101. Arnold, L.W., Pennell, C.A., McCray, S.K. & Clarke, S.H. Development of B-1 cells: segregation of phosphatidyl choline-specific B cells to the B-1 population occurs after immunoglobulin gene expression. *Journal of Experimental Medicine* **179**, 1585-1595 (1994).

102. Ferry, H., Crockford, T.L., Leung, J.C. & Cornall, R.J. Signals from a self-antigen induce positive selection in early B cell ontogeny but are tolerogenic in adults. *The Journal of Immunology* **176**, 7402-7411 (2006).

103. Ferry, H., Jones, M., Vaux, D.J., Roberts, I.S. & Cornall, R.J. The cellular location of self-antigen determines the positive and negative selection of autoreactive B cells. *J Exp Med* **198**, 1415-1425 (2003).

104. Pao, L.I. *et al.* B cell-specific deletion of protein-tyrosine phosphatase Shp1 promotes B-1a cell development and causes systemic autoimmunity. *Immunity* **27**, 35-48 (2007).

105. Nishizumi, H. *et al.* Impaired proliferation of peripheral B cells and indication of autoimmune disease in lyn-deficient mice. *Immunity* **3**, 549-560 (1995).

106. Lamagna, C., Hu, Y., DeFranco, A.L. & Lowell, C.A. B Cell–Specific Loss of Lyn Kinase Leads to Autoimmunity. *The Journal of Immunology* **192**, 919-928 (2014).

107. Getahun, A., Beavers, N.A., Larson, S.R., Shlomchik, M.J. & Cambier, J.C. Continuous inhibitory signaling by both SHP-1 and SHIP-1 pathways is required to maintain unresponsiveness of anergic B cells. *J Exp Med* **213**, 751-769 (2016).

108. Haas, K.M., Poe, J.C., Steeber, D.A. & Tedder, T.F. B-1a and B-1b cells exhibit distinct developmental requirements and have unique functional roles in innate and adaptive immunity to S. pneumoniae. *Immunity* **23**, 7-18 (2005).

109. Xu, X. *et al.* An ontogenetic switch drives the positive and negative selection of B cells. *Proceedings of the National Academy of Sciences* **117**, 3718-3727 (2020).

110. Ferry, H. *et al.* Increased Positive Selection of B1 Cells and Reduced B Cell Tolerance to Intracellular Antigens in c1q-Deficient Mice1. *The Journal of Immunology* **178**, 2916-2922 (2007).

111. Goodnow, C.C. *et al.* Altered immunoglobulin expression and functional silencing of self-reactive B lymphocytes in transgenic mice. *Nature* **334**, 676-682 (1988).

112. Hippen, K.L., Tze, L.E. & Behrens, T.W. CD5 maintains tolerance in anergic B cells. *J Exp Med* **191**, 883-890 (2000).

113. Stall, A.M., Adams, S., Herzenberg, L.A. & Kantor, A.B. Characteristics and development of the murine B-1b (Ly-1 B sister) cell population. *Ann N Y Acad Sci* **651**, 33-43 (1992).

114. Riggs, J. *et al.* X-chromosome-linked immune-deficient mice have B-1b cells. *Immunology* **108**, 440-451 (2003).

115. Tornberg, U.C. & Holmberg, D. B-1a, B-1b and B-2 B cells display unique VHDJH repertoires formed at different stages of ontogeny and under different selection pressures. *The EMBO Journal* **14**, 1680-1689 (1995).

116. Rosado, M.M. *et al.* From the fetal liver to spleen and gut: the highway to natural antibody. *Mucosal Immunology* **2**, 351-361 (2009).

117. Marshall, J.L. *et al.* The Capsular Polysaccharide Vi from Salmonella Typhi Is a B1b Antigen. *The Journal of Immunology* **189**, 5527-5532 (2012).

118. Kyaw, T., Tipping, P., Bobik, A. & Toh, B.-H. Protective Role of Natural IgM-Producing B1a Cells in Atherosclerosis. *Trends in Cardiovascular Medicine* **22**, 48-53 (2012).

119. Martin, F. & Kearney, J.F. B-cell subsets and the mature -preimmune repertoire. Marginal zone and B1 B cells as part of a "natural immune memory". *Immunological Reviews* **175**, 70-79 (2000).

120. Won, W.-J. *et al.* Fc Receptor Homolog 3 Is a Novel Immunoregulatory Marker of Marginal Zone and B1 B Cells1. *The Journal of Immunology* **177**, 6815-6823 (2006).

121. Won, W.-J. & Kearney, J.F. CD9 Is a Unique Marker for Marginal Zone B Cells, B1 Cells, and Plasma Cells in Mice1. *The Journal of Immunology* **168**, 5605-5611 (2002).

122. Martin, F., Oliver, A.M. & Kearney, J.F. Marginal zone and B1 B cells unite in the early response against T-independent blood-borne particulate antigens. *Immunity* **14**, 617-629 (2001).

123. Kaminski, D.A. & Stavnezer, J. Enhanced IgA Class Switching in Marginal Zone and B1 B Cells Relative to Follicular/B2 B Cells1. *The Journal of Immunology* **177**, 6025-6029 (2006).

124. Baumgarth, N. The double life of a B-1 cell: self-reactivity selects for protective effector functions. *Nat Rev Immunol* **11**, 34-46 (2011).

125. Chen, X., Martin, F., Forbush, K.A., Perlmutter, R.M. & Kearney, J.F. Evidence for selection of a population of multi-reactive B cells into the splenic marginal zone. *Int Immunol* **9**, 27-41 (1997).

126. Martin, F. & Kearney, J.F. Positive selection from newly formed to marginal zone B cells depends on the rate of clonal production, CD19, and btk. *Immunity* **12**, 39-49 (2000).

127. Wen, L. *et al.* Evidence of marginal-zone B cell-positive selection in spleen. *Immunity* **23**, 297-308 (2005).

128. Mackay, F. & Schneider, P. Cracking the BAFF code. *Nat Rev Immunol* **9**, 491-502 (2009).

129. Schiemann, B. *et al.* An Essential Role for BAFF in the Normal Development of B Cells Through a BCMA-Independent Pathway. *Science* **293**, 2111-2114 (2001).

130. Xue, L. *et al.* Defective development and function of Bcl10-deficient follicular, marginal zone and B1 B cells. *Nature Immunology* **4**, 857-865 (2003).

131. Witt, C.M., Hurez, V., Swindle, C.S., Hamada, Y. & Klug, C.A. Activated Notch2 potentiates CD8 lineage maturation and promotes the selective development of B1 B cells. *Mol Cell Biol* **23**, 8637-8650 (2003).

132. Cuenca, M., Romero, X., Sintes, J., Terhorst, C. & Engel, P. Targeting of Ly9 (CD229) Disrupts Marginal Zone and B1 B Cell Homeostasis and Antibody Responses. *The Journal of Immunology* **196**, 726-737 (2016).

133. Kretschmer, K. *et al.* The Selection of Marginal Zone B Cells Differs from That of B-1a Cells 1. *The Journal of Immunology* **171**, 6495-6501 (2003).

134. Monroe, J.G. ITAM-mediated tonic signalling through pre-BCR and BCR complexes. *Nature Reviews Immunology* **6**, 283-294 (2006).

135. Parnes, J.R. & Pan, C. CD72, a negative regulator of B-cell responsiveness. *Immunol Rev* **176**, 75-85 (2000).

136. Pan, C., Baumgarth, N. & Parnes, J.R. CD72-deficient mice reveal nonredundant roles of CD72 in B cell development and activation. *Immunity* **11**, 495-506 (1999).

137. Hoffmann, A. *et al.* Siglec-G is a B1 cell–inhibitory receptor that controls expansion and calcium signaling of the B1 cell population. *Nature Immunology* **8**, 695-704 (2007).

138. Sato, S. *et al.* CD22 is both a positive and negative regulator of B lymphocyte antigen receptor signal transduction: altered signaling in CD22-deficient mice. *Immunity* **5**, 551-562 (1996).

139. Lajaunias, F.d.r. *et al.* Differentially Regulated Expression and Function of CD22 in Activated B-1 and B-2 Lymphocytes1. *The Journal of Immunology* **168**, 6078-6083 (2002).

140. Jellusova, J., Wellmann, U., Amann, K., Winkler, T.H. & Nitschke, L. CD22 × Siglec-G Double-Deficient Mice Have Massively Increased B1 Cell Numbers and Develop Systemic Autoimmunity. *The Journal of Immunology* **184**, 3618-3627 (2010).

141. Ochi, H. *et al.* Regulation of B-1 cell activation and its autoantibody production by Lyn kinase-regulated signallings. *Immunology* **98**, 595-603 (1999).

142. Xu, Y., Harder, K.W., Huntington, N.D., Hibbs, M.L. & Tarlinton, D.M. Lyn Tyrosine Kinase: Accentuating the Positive and the Negative. *Immunity* **22**, 9-18 (2005).

143. Dal Porto, J.M., Burke, K. & Cambier, J.C. Regulation of BCR signal transduction in B-1 cells requires the expression of the Src family kinase Lck. *Immunity* **21**, 443-453 (2004).

144. Liu, S.K. & McGlade, C.J. Gads is a novel SH2 and SH3 domain-containing adaptor protein that binds to tyrosine-phosphorylated Shc. *Oncogene* **17**, 3073-3082 (1998).

145. Feng, G.-S. *et al.* Grap Is a Novel SH3-SH2-SH3 Adaptor Protein That Couples Tyrosine Kinases to the Ras Pathway (∗). *Journal of Biological Chemistry* **271**, 12129-12132 (1996).

146. Chen, D., Waters, S.B., Holt, K.H. & Pessin, J.E. SOS Phosphorylation and Disassociation of the Grb2-SOS Complex by the ERK and JNK Signaling Pathways (∗). *Journal of Biological Chemistry* **271**, 6328-6332 (1996).

147. Li, W. *et al.* A new function for a phosphotyrosine phosphatase: linking GRB2-Sos to a receptor tyrosine kinase. *Molecular and cellular biology* (1994).

148. Li, N. *et al.* Guanine-nucleotide-releasing factor hSos1 binds to Grb2 and links receptor tyrosine kinases to Ras signalling. *Nature* **363**, 85-88 (1993).

149. Batzer, A.G., Rotin, D., Ureña, J.M., Skolnik, E.Y. & Schlessinger, J. Hierarchy of binding sites for Grb2 and Shc on the epidermal growth factor receptor. *Mol Cell Biol* **14**, 5192-5201 (1994).

150. Tari, A.M. & Lopez-Berestein, G. GRB2: a pivotal protein in signal transduction. *Semin Oncol* **28**, 142-147 (2001).

151. Honma, M. *et al.* Dok-3 sequesters Grb2 and inhibits the Ras-Erk pathway downstream of protein-tyrosine kinases. *Genes to Cells* **11**, 143-151 (2006).

152. Lowenstein, E.J. *et al.* The SH2 and SH3 domain-containing protein GRB2 links receptor tyrosine kinases to ras signaling. *Cell* **70**, 431-442 (1992).

153. Buday, L. & Downward, J. Epidermal growth factor regulates p21ras through the formation of a complex of receptor, Grb2 adapter protein, and Sos nucleotide exchange factor. *Cell* **73**, 611-620 (1993).

154. Gale, N.W., Kaplan, S., Lowenstein, E.J., Schlessinger, J. & Bar-Sagi, D. Grb2 mediates the EGF-dependent activation of guanine nucleotide exchange on Ras. *Nature* **363**, 88-92 (1993).

155. Xie, Y. *et al.* FGF/FGFR signaling in health and disease. *Signal Transduction and Targeted Therapy* **5**, 181 (2020).

156. Ahmed, Z. *et al.* Grb2 controls phosphorylation of FGFR2 by inhibiting receptor kinase and Shp2 phosphatase activity. *Journal of Cell Biology* **200**, 493-504 (2013).

157. Lin, C.C. *et al.* Inhibition of basal FGF receptor signaling by dimeric Grb2. *Cell* **149**, 1514-1524 (2012).

158. Pan, Z. *et al.* The function study on the interaction between Grb2 and AMPK. *Mol Cell Biochem* **307**, 121-127 (2008).

159. Cheng, A.M. *et al.* Mammalian Grb2 regulates multiple steps in embryonic development and malignant transformation. *Cell* **95**, 793-803 (1998).

160. Radtke, D. *et al.* Grb2 Is Important for T Cell Development, Th Cell Differentiation, and Induction of Experimental Autoimmune Encephalomyelitis. *The Journal of Immunology* **196**, 2995-3005 (2016).

161. Jang, I.K. *et al.* Grb2 functions at the top of the T-cell antigen receptor-induced tyrosine kinase cascade to control thymic selection. *Proc Natl Acad Sci U S A* **107**, 10620-10625 (2010).

162. Gong, Q. *et al.* Disruption of T cell signaling networks and development by Grb2 haploid insufficiency. *Nat Immunol* **2**, 29-36 (2001).

163. Jang, I.K. *et al.* Grb2 functions at the top of the T-cell antigen receptor–induced tyrosine kinase cascade to control thymic selection. *Proceedings of the National Academy of Sciences* **107**, 10620-10625 (2010).

164. Sieh, M., Batzer, A., Schlessinger, J. & Weiss, A. GRB2 and phospholipase C-gamma 1 associate with a 36- to 38-kilodalton phosphotyrosine protein after T-cell receptor stimulation. *Mol Cell Biol* **14**, 4435-4442 (1994).

165. Linsley, P.S. & Ledbetter, J.A. The role of the CD28 receptor during T cell responses to antigen. *Annu Rev Immunol* **11**, 191-212 (1993).

166. Schneider, H. & Rudd, C.E. CD28 and Grb-2, relative to Gads or Grap, preferentially co-operate with Vav1 in the activation of NFAT/AP-1 transcription. *Biochem Biophys Res Commun* **369**, 616-621 (2008).

167. Schneider, H., Cai, Y.C., Prasad, K.V., Shoelson, S.E. & Rudd, C.E. T cell antigen CD28 binds to the GRB-2/SOS complex, regulators of p21ras. *Eur J Immunol* **25**, 1044-1050 (1995).

168. Stork, B. *et al.* Grb2 and the non-T cell activation linker NTAL constitute a Ca(2+)-regulating signal circuit in B lymphocytes. *Immunity* **21**, 681-691 (2004).

169. Ackermann, J.A., Radtke, D., Maurberger, A., Winkler, T.H. & Nitschke, L. Grb2 regulates B-cell maturation, B-cell memory responses and inhibits B-cell Ca2+ signalling. *The EMBO Journal* **30**, 1621-1633 (2011).

170. Jang, I.K. *et al.* Growth-factor receptor-bound protein-2 (Grb2) signaling in B cells controls lymphoid follicle organization and germinal center reaction. *Proceedings of the National Academy of Sciences* **108**, 7926-7931 (2011).

171. Brooks, S.R., Li, X., Volanakis, E.J. & Carter, R.H. Systematic Analysis of the Role of CD19 Cytoplasmic Tyrosines in Enhancement of Activation in Daudi Human B Cells: Clustering of Phospholipase C and Vav and of Grb2 and Sos with Different CD19 Tyrosines1. *The Journal of Immunology* **164**, 3123-3131 (2000).

172. Carter, R.H., Wang, Y. & Brooks, S. Role of CD19 signal transduction in B cell biology. *Immunologic Research* **26**, 45-54 (2002).

173. Li, X. & Carter, R.H. CD19 signal transduction in normal human B cells: linkage to downstream pathways requires phosphatidylinositol 3-kinase, protein kinase C and Ca2+. *European Journal of Immunology* **30**, 1576-1586 (2000).

174. Heathcote, H.R. *et al.* Protein kinase C phosphorylates AMP-activated protein kinase α1 Ser487. *Biochem J* **473**, 4681-4697 (2016).

175. Hobeika, E. *et al.* Testing gene function early in the B cell lineage in mb1-cre mice. *Proc Natl Acad Sci U S A* **103**, 13789-13794 (2006).

176. Mombaerts, P. *et al.* RAG-1-deficient mice have no mature B and T lymphocytes. *Cell* **68**, 869-877 (1992).

177. Lambe, T. *et al.* CD4 T Cell-Dependent Autoimmunity against a Melanocyte Neoantigen Induces Spontaneous Vitiligo and Depends upon Fas-Fas Ligand Interactions1. *The Journal of Immunology* **177**, 3055-3062 (2006).

178. Goodnow, C.C., Crosbie, J., Jorgensen, H., Brink, R.A. & Basten, A. Induction of self-tolerance in mature peripheral B lymphocytes. *Nature* **342**, 385-391 (1989).

179. Hao, Y. *et al.* Integrated analysis of multimodal single-cell data. *Cell* **184**, 3573-3587.e3529 (2021).

180. Bunis, D.G., Andrews, J., Fragiadakis, G.K., Burt, T.D. & Sirota, M. dittoSeq: universal user-friendly single-cell and bulk RNA sequencing visualization toolkit. *Bioinformatics* **36**, 5535-5536 (2021).

181. Yu, G., Wang, L.G., Han, Y. & He, Q.Y. clusterProfiler: an R package for comparing biological themes among gene clusters. *Omics* **16**, 284-287 (2012).

182. Carlson, M. org. Hs. eg. db: Genome Wide Annotation for Human. R package version 3.2. 3. 2019.

183. Yu, G. & He, Q.-Y. ReactomePA: an R/Bioconductor package for reactome pathway analysis and visualization. *Molecular BioSystems* **12**, 477-479 (2016).

184. Carlson, M. org. Mm. eg. db: Genome wide annotation for Mouse. R package version 3.8. 2. *Bioconductor. London, United Kingdom: Genome Biology (BMC)* (2019).

185. Kowalczyk, M.S. *et al.* Single-cell RNA-seq reveals changes in cell cycle and differentiation programs upon aging of hematopoietic stem cells. *Genome Res* **25**, 1860-1872 (2015).

186. Cao, J. *et al.* The single-cell transcriptional landscape of mammalian organogenesis. *Nature* **566**, 496-502 (2019).

187. Yang, Y., Tung, J.W., Ghosn, E.E., Herzenberg, L.A. & Herzenberg, L.A. Division and differentiation of natural antibody-producing cells in mouse spleen. *Proceedings of the National Academy of Sciences* **104**, 4542-4546 (2007).

188. Ahmed, Z. *et al.* Grb2 monomer–dimer equilibrium determines normal versus oncogenic function. *Nature Communications* **6**, 7354 (2015).

189. Minoo, P., Zadeh, M.M., Rottapel, R., Lebrun, J.-J. & Ali, S. A novel SHP-1/Grb2–dependent mechanism of negative regulation of cytokine-receptor signaling: contribution of SHP-1 C-terminal tyrosines in cytokine signaling. *Blood* **103**, 1398-1407 (2004).

190. Lösing, M. *et al.* The Dok-3/Grb2 protein signal module attenuates Lyn kinase-dependent activation of Syk kinase in B cell antigen receptor microclusters. *Journal of Biological Chemistry* **288**, 2303-2313 (2013).

191. Cerutti, A., Cols, M. & Puga, I. Marginal zone B cells: virtues of innate-like antibody-producing lymphocytes. *Nature Reviews Immunology* **13**, 118-132 (2013).

192. Dorshkind, K. & Montecino-Rodriguez, E. Fetal B-cell lymphopoiesis and the emergence of B-1-cell potential. *Nature Reviews Immunology* **7**, 213-219 (2007).

193. Montecino-Rodriguez, E., Leathers, H. & Dorshkind, K. Identification of a B-1 B cell-specified progenitor. *Nat Immunol* **7**, 293-301 (2006).

194. Graf, R. *et al.* BCR-dependent lineage plasticity in mature B cells. *Science* **363**, 748-753 (2019).

195. Goodnow, C.C. *et al.* Altered immunoglobulin expression and functional silencing of self-reactive B lymphocytes in transgenic mice. *Nature* **334**, 676-682 (1988).

196. Braun, U., Rajewsky, K. & Pelanda, R. Different sensitivity to receptor editing of B cells from mice hemizygous or homozygous for targeted Ig transgenes. *Proc Natl Acad Sci U S A* **97**, 7429-7434 (2000).

197. Hayakawa, K. *et al.* Positive Selection of Natural Autoreactive B Cells. *Science* **285**, 113-116 (1999).

198. Arnold, L.W., Pennell, C.A., McCray, S.K. & Clarke, S.H. Development of B-1 cells: segregation of phosphatidyl choline-specific B cells to the B-1 population occurs after immunoglobulin gene expression. *J Exp Med* **179**, 1585-1595 (1994).

199. Hartley, S.B. *et al.* Elimination from peripheral lymphoid tissues of self-reactive B lymphocytes recognizing membrane-bound antigens. *Nature* **353**, 765-769 (1991).

200. Frasca, D. *et al.* Hematopoietic reconstitution after lethal irradiation and bone marrow transplantation: effects of different hematopoietic cytokines on the recovery of thymus, spleen and blood cells. *Bone Marrow Transplantation* **25**, 427-433 (2000).

201. Xu, X. Investigating the positive and negative selection of B cell development. University of Oxford, 2018.

202. Walter, J.E. *et al.* Expansion of immunoglobulin-secreting cells and defects in B cell tolerance in Rag-dependent immunodeficiency. *Journal of Experimental Medicine* **207**, 1541-1554 (2010).

203. Phan, T.G. *et al.* B cell receptor-independent stimuli trigger immunoglobulin (Ig) class switch recombination and production of IgG autoantibodies by anergic self-reactive B cells. *J Exp Med* **197**, 845-860 (2003).

204. Tumang, J.R., Francés, R., Yeo, S.G. & Rothstein, T.L. Spontaneously Ig-secreting B-1 cells violate the accepted paradigm for expression of differentiation-associated transcription factors. *J Immunol* **174**, 3173-3177 (2005).

205. Oliver, A.M., Martin, F., Gartland, G.L., Carter, R.H. & Kearney, J.F. Marginal zone B cells exhibit unique activation, proliferative and immunoglobulin secretory responses. *European Journal of Immunology* **27**, 2366-2374 (1997).

206. Tedoldi, S. *et al.* Jaw1/LRMP, a germinal centre-associated marker for the immunohistological study of B-cell lymphomas. *J Pathol* **209**, 454-463 (2006).

207. Huber, C., Mårtensson, A., Bokoch, G.M., Nemazee, D. & Gavin, A.L. FGD2, a CDC42-specific exchange factor expressed by antigen-presenting cells, localizes to early endosomes and active membrane ruffles. *J Biol Chem* **283**, 34002-34012 (2008).

208. Taguchi, T., Kiyokawa, N., Sato, N., Saito, M. & Fujimoto, J. Characteristic expression of Hck in human B-cell precursors. *Exp Hematol* **28**, 55-64 (2000).

209. He, C. *et al.* CD36 and LC3B initiated autophagy in B cells regulates the humoral immune response. *Autophagy* **17**, 3577-3591 (2021).

210. Tumanov, A. *et al.* Distinct role of surface lymphotoxin expressed by B cells in the organization of secondary lymphoid tissues. *Immunity* **17**, 239-250 (2002).

211. Bourdon, J.C., Renzing, J., Robertson, P.L., Fernandes, K.N. & Lane, D.P. Scotin, a novel p53-inducible proapoptotic protein located in the ER and the nuclear membrane. *J Cell Biol* **158**, 235-246 (2002).

212. Kim, H.-R., Park, J.-S., Karabulut, H., Yasmin, F. & Jun, C.-D. Transgelin-2: A Double-Edged Sword in Immunity and Cancer Metastasis. *Frontiers in Cell and Developmental Biology* **9** (2021).

213. Hanson, C.H. *et al.* CD62L expression marks a functionally distinct subset of memory B cells. *Cell Rep* **42**, 113542 (2023).

214. Morrison, V.L., Barr, T.A., Brown, S. & Gray, D. TLR-mediated loss of CD62L focuses B cell traffic to the spleen during Salmonella typhimurium infection. *J Immunol* **185**, 2737-2746 (2010).

215. Kiso, K. *et al.* Transgelin-2 is upregulated on activated B-cells and expressed in hyperplastic follicles in lupus erythematosus patients. *PLoS One* **12**, e0184738 (2017).

216. Tsui, C. *et al.* Dynamic reorganisation of intermediate filaments coordinates early B-cell activation. *Life Sci Alliance* **1**, e201800060 (2018).

217. Matza, D. *et al.* A scaffold protein, AHNAK1, is required for calcium signaling during T cell activation. *Immunity* **28**, 64-74 (2008).

218. Lauzurica, P. *et al.* Phenotypic and functional characteristics of hematopoietic cell lineages in CD69-deficient mice. *Blood* **95**, 2312-2320 (2000).

219. Krzyzak, L. *et al.* CD83 Modulates B Cell Activation and Germinal Center Responses. *J Immunol* **196**, 3581-3594 (2016).

220. Heng, T.S. & Painter, M.W. The Immunological Genome Project: networks of gene expression in immune cells. *Nat Immunol* **9**, 1091-1094 (2008).

221. Masle-Farquhar, E. *et al.* Uncontrolled CD21low age-associated and B1 B cell accumulation caused by failure of an EGR2/3 tolerance checkpoint. *Cell Reports* **38**, 110259 (2022).

222. Healy, J.I. *et al.* Different nuclear signals are activated by the B cell receptor during positive versus negative signaling. *Immunity* **6**, 419-428 (1997).

223. Sabouri, Z. *et al.* IgD attenuates the IgM-induced anergy response in transitional and mature B cells. *Nature Communications* **7**, 13381 (2016).

224. Rengarajan, J. *et al.* Sequential Involvement of NFAT and Egr Transcription Factors in FasL Regulation. *Immunity* **12**, 293-300 (2000).

225. Li, S. *et al.* The transcription factors Egr2 and Egr3 are essential for the control of inflammation and antigen-induced proliferation of B and T cells. *Immunity* **37**, 685-696 (2012).

226. Enders, A. *et al.* Zinc-finger protein ZFP318 is essential for expression of IgD, the alternatively spliced Igh product made by mature B lymphocytes. *Proc Natl Acad Sci U S A* **111**, 4513-4518 (2014).

227. Cornall, R.J. *et al.* Polygenic autoimmune traits: Lyn, CD22, and SHP-1 are limiting elements of a biochemical pathway regulating BCR signaling and selection. *Immunity* **8**, 497-508 (1998).

228. Ng, C.H., Xu, S. & Lam, K.P. Dok-3 plays a nonredundant role in negative regulation of B-cell activation. *Blood* **110**, 259-266 (2007).

229. Poe, J.C., Fujimoto, M., Jansen, P.J., Miller, A.S. & Tedder, T.F. CD22 forms a quaternary complex with SHIP, Grb2, and Shc. A pathway for regulation of B lymphocyte antigen receptor-induced calcium flux. *J Biol Chem* **275**, 17420-17427 (2000).

230. Berry, C.T. *et al.* BCR-Induced Ca(2+) Signals Dynamically Tune Survival, Metabolic Reprogramming, and Proliferation of Naive B Cells. *Cell Rep* **31**, 107474 (2020).

231. Alhabbab, R. *et al.* Galectin-1 is required for the regulatory function of B cells. *Scientific Reports* **8**, 2725 (2018).

232. West, L.C. & Cresswell, P. Expanding roles for GILT in immunity. *Curr Opin Immunol* **25**, 103-108 (2013).

233. Smulski, C. & Eibel, H. BAFF and BAFF-receptor in B cell selection and survival. Front Immunol 9: 2285. 2018.

234. Medvinsky, A. & Dzierzak, E. Definitive hematopoiesis is autonomously initiated by the AGM region. *Cell* **86**, 897-906 (1996).

235. Chang, K.T., Šefc, L., Pšenák, O., Vokurka, M. & Nečas, E. Early Fetal Liver Readily Repopulates B Lymphopoiesis in Adult Bone Marrow. *Stem Cells* **23**, 230-239 (2005).

236. Kikuchi, K. & Kondo, M. Developmental switch of mouse hematopoietic stem cells from fetal to adult type occurs in bone marrow after birth. *Proc Natl Acad Sci U S A* **103**, 17852-17857 (2006).

237. Nutt, S.L., Urbánek, P., Rolink, A. & Busslinger, M. Essential functions of Pax5 (BSAP) in pro-B cell development: difference between fetal and adult B lymphopoiesis and reduced V-to-DJ recombination at the IgH locus. *Genes Dev* **11**, 476-491 (1997).

238. Holodick, N.E., Repetny, K., Zhong, X. & Rothstein, T.L. Adult BM generates CD5+ B1 cells containing abundant N-region additions. *Eur J Immunol* **39**, 2383-2394 (2009).

239. Düber, S. *et al.* Induction of B-cell development in adult mice reveals the ability of bone marrow to produce B-1a cells. *Blood* **114**, 4960-4967 (2009).

240. Kobayashi, M. & Yoshimoto, M. Multiple waves of fetal‐derived immune cells constitute adult immune system. *Immunological Reviews* **315**, 11-30 (2023).

241. Li, Y.S., Hayakawa, K. & Hardy, R.R. The regulated expression of B lineage associated genes during B cell differentiation in bone marrow and fetal liver. *J Exp Med* **178**, 951-960 (1993).

242. Benedict, C.L. & Kearney, J.F. Increased junctional diversity in fetal B cells results in a loss of protective anti-phosphorylcholine antibodies in adult mice. *Immunity* **10**, 607-617 (1999).

243. Korsunsky, I. *et al.* Fast, sensitive and accurate integration of single-cell data with Harmony. *Nature Methods* **16**, 1289-1296 (2019).

244. Lee, R.D. *et al.* Single-cell analysis identifies dynamic gene expression networks that govern B cell development and transformation. *Nature Communications* **12**, 6843 (2021).

245. Wong, J.B. *et al.* B-1a cells acquire their unique characteristics by bypassing the pre-BCR selection stage. *Nat Commun* **10**, 4768 (2019).

246. Wong, J.B. *et al.* B-1a cells acquire their unique characteristics by bypassing the pre-BCR selection stage. *Nature Communications* **10**, 4768 (2019).

247. Trapnell, C. *et al.* The dynamics and regulators of cell fate decisions are revealed by pseudotemporal ordering of single cells. *Nature Biotechnology* **32**, 381-386 (2014).

248. Luo, Y. *et al.* Single-cell genomics identifies distinct B1 cell developmental pathways and reveals aging-related changes in the B-cell receptor repertoire. *Cell & Bioscience* **12**, 57 (2022).

249. Hartley, S.B. *et al.* Elimination of self-reactive B lymphocytes proceeds in two stages: arrested development and cell death. *Cell* **72**, 325-335 (1993).

250. Esplin, B.L., Welner, R.S., Zhang, Q., Borghesi, L.A. & Kincade, P.W. A differentiation pathway for B1 cells in adult bone marrow. *Proc Natl Acad Sci U S A* **106**, 5773-5778 (2009).

251. Carvalho, T.L., Mota-Santos, T., Cumano, A., Demengeot, J. & Vieira, P. Arrested B Lymphopoiesis and Persistence of Activated B Cells in Adult Interleukin 7−/− Mice. *Journal of Experimental Medicine* **194**, 1141-1150 (2001).

252. Yoshimoto, M. *et al.* Embryonic day 9 yolk sac and intra-embryonic hemogenic endothelium independently generate a B-1 and marginal zone progenitor lacking B-2 potential. *Proc Natl Acad Sci U S A* **108**, 1468-1473 (2011).

253. Hao, Z. & Rajewsky, K. Homeostasis of Peripheral B Cells in the Absence of B Cell Influx from the Bone Marrow. *Journal of Experimental Medicine* **194**, 1151-1164 (2001).

254. Nitschke, L. & Tsubata, T. Molecular interactions regulate BCR signal inhibition by CD22 and CD72. *Trends Immunol* **25**, 543-550 (2004).

255. Jellusova, J. *et al.* Siglec-G Regulates B1 Cell Survival and Selection. *The Journal of Immunology* **185**, 3277-3284 (2010).

256. Brenner, S. *et al.* A hypomorphic IgH-chain allele affects development of B-cell subsets and favours receptor editing. *The EMBO Journal* **30**, 2705-2718 (2011).

257. Nitschke, L., Carsetti, R., Ocker, B., Köhler, G. & Lamers, M.C. CD22 is a negative regulator of B-cell receptor signalling. *Curr Biol* **7**, 133-143 (1997).

258. Doody, G.M. *et al.* A role in B cell activation for CD22 and the protein tyrosine phosphatase SHP. *Science* **269**, 242-244 (1995).

259. Pfrengle, F., Macauley, M.S., Kawasaki, N. & Paulson, J.C. Copresentation of antigen and ligands of Siglec-G induces B cell tolerance independent of CD22. *J Immunol* **191**, 1724-1731 (2013).

260. Wu, Y. *et al.* The B-cell transmembrane protein CD72 binds to and is an in vivo substrate of the protein tyrosine phosphatase SHP-1. *Curr Biol* **8**, 1009-1017 (1998).

261. Poe, J.C., Fujimoto, M., Jansen, P.J., Miller, A.S. & Tedder, T.F. CD22 forms a quaternary complex with SHIP, Grb2, and Shc: a pathway for regulation of B lymphocyte antigen receptor-induced calcium flux. *Journal of Biological Chemistry* **275**, 17420-17427 (2000).

262. Amezcua Vesely, M.C. *et al.* FcγRIIb and BAFF Differentially Regulate Peritoneal B1 Cell Survival. *The Journal of Immunology* **188**, 4792-4800 (2012).

263. Lamagna, C., Hu, Y., DeFranco, A.L. & Lowell, C.A. B cell-specific loss of Lyn kinase leads to autoimmunity. *J Immunol* **192**, 919-928 (2014).

264. Chan, V.W., Meng, F., Soriano, P., DeFranco, A.L. & Lowell, C.A. Characterization of the B lymphocyte populations in Lyn-deficient mice and the role of Lyn in signal initiation and down-regulation. *Immunity* **7**, 69-81 (1997).

265. Xu, S. *et al.* B cell development and activation defects resulting in xid-like immunodeficiency in BLNK/SLP-65-deficient mice. *International Immunology* **12**, 397-404 (2000).

266. Zhang, R., Alt, F.W., Davidson, L., Orkin, S.H. & Swat, W. Defective signalling through the T- and B-cell antigen receptors in lymphoid cells lacking the vav proto-oncogene. *Nature* **374**, 470-473 (1995).

267. Fruman, D.A. *et al.* Impaired B cell development and proliferation in absence of phosphoinositide 3-kinase p85alpha. *Science* **283**, 393-397 (1999).

268. Tedford, K. *et al.* Compensation between Vav-1 and Vav-2 in B cell development and antigen receptor signaling. *Nature Immunology* **2**, 548-555 (2001).

269. Stork, B. *et al.* Subcellular localization of Grb2 by the adaptor protein Dok-3 restricts the intensity of Ca2+ signaling in B cells. *The EMBO journal* **26**, 1140-1149 (2007).

270. Otipoby, K.L., Draves, K.E. & Clark, E.A. CD22 regulates B cell receptor-mediated signals via two domains that independently recruit Grb2 and SHP-1. *J Biol Chem* **276**, 44315-44322 (2001).

271. Neumann, K., Oellerich, T., Heine, I., Urlaub, H. & Engelke, M. Fc gamma receptor IIb modulates the molecular Grb2 interaction network in activated B cells. *Cell Signal* **23**, 893-900 (2011).

272. Chevrier, S. *et al.* The BTB-ZF transcription factor Zbtb20 is driven by Irf4 to promote plasma cell differentiation and longevity. *Journal of Experimental Medicine* **211**, 827-840 (2014).

273. Yoon, H.S. *et al.* ZBTB32 is an early repressor of the CIITA and MHC class II gene expression during B cell differentiation to plasma cells. *The Journal of Immunology* **189**, 2393-2403 (2012).

274. Andreani, V. *et al.* Cochaperone Mzb1 is a key effector of Blimp1 in plasma cell differentiation and β1-integrin function. *Proceedings of the National Academy of Sciences* **115**, E9630-E9639 (2018).

275. Miao, T. *et al.* Egr2 and 3 control adaptive immune responses by temporally uncoupling expansion from T cell differentiation. *Journal of Experimental Medicine* **214**, 1787-1808 (2017).

276. Schneider, H. & Rudd, C.E. CD28 and Grb-2, relative to Gads or Grap, preferentially co-operate with Vav1 in the activation of NFAT/AP-1 transcription. *Biochemical and Biophysical Research Communications* **369**, 616-621 (2008).

277. Caro-Maldonado, A. *et al.* Metabolic reprogramming is required for antibody production that is suppressed in anergic but exaggerated in chronically BAFF-exposed B cells. *The Journal of Immunology* **192**, 3626-3636 (2014).

278. Clarke, A.J., Riffelmacher, T., Braas, D., Cornall, R.J. & Simon, A.K. B1a B cells require autophagy for metabolic homeostasis and self-renewal. *J Exp Med* **215**, 399-413 (2018).

279. O'garra, A. *et al.* Ly-1 B (B-1) cells are the main source of B cell-derived interleukin 10. *European Journal of Immunology* **22**, 711-717 (1992).

280. Lesinski, G.B. & Westerink, M.A.J. Novel vaccine strategies to T-independent antigens. *Journal of Microbiological Methods* **47**, 135-149 (2001).

281. Rothstein, T.L., Griffin, D.O., Holodick, N.E., Quach, T.D. & Kaku, H. Human B-1 cells take the stage. *Ann N Y Acad Sci* **1285**, 97-114 (2013).

282. Griffin, D.O. & Rothstein, T.L. Human b1 cell frequency: isolation and analysis of human b1 cells. *Frontiers in immunology* **3**, 122 (2012).

283. Covens, K. *et al.* Characterization of proposed human B-1 cells reveals pre-plasmablast phenotype. *Blood, The Journal of the American Society of Hematology* **121**, 5176-5183 (2013).

284. Quách, T.D. *et al.* Distinctions among Circulating Antibody-Secreting Cell Populations, Including B-1 Cells, in Human Adult Peripheral Blood. *The Journal of Immunology* **196**, 1060-1069 (2016).

285. Rodriguez-Zhurbenko, N., Quach, T.D., Hopkins, T.J., Rothstein, T.L. & Hernandez, A.M. Human B-1 cells and B-1 cell antibodies change with advancing age. *Frontiers in immunology* **10**, 483 (2019).

286. Verbinnen, B., Covens, K., Moens, L., Meyts, I. & Bossuyt, X. Human CD20+ CD43+ CD27+ CD5− B cells generate antibodies to capsular polysaccharides of Streptococcus pneumoniae. *Journal of allergy and clinical immunology* **130**, 272-275 (2012).

287. Tørring, C. *et al.* The B1-cell subpopulation is diminished in patients with relapsing-remitting multiple sclerosis. *J Neuroimmunol* **262**, 92-99 (2013).

288. Griffin, D.O. & Rothstein, T.L. A small CD11b+ human B1 cell subpopulation stimulates T cells and is expanded in lupus. *Journal of Experimental Medicine* **208**, 2591-2598 (2011).

289. Budeus, B. *et al.* Human Cord Blood B Cells Differ from the Adult Counterpart by Conserved Ig Repertoires and Accelerated Response Dynamics. *The Journal of Immunology* **206**, 2839-2851 (2021).

Appendix

P value	Average log2FC	P value adjusted	Cluster	Gene symbol
0	2.15476324	0	0_IgM^{low}Fr.F	Iglc2
0	2.0369237	0	0_IgM^{low}Fr.F	Ly6a
0	1.69901225	0	0_IgM^{low}Fr.F	Fcer2a
0	1.62855972	0	0_IgM^{low}Fr.F	Shisa5
0	1.43640716	0	0_IgM^{low}Fr.F	Ltb
0	1.31343144	0	0_IgM^{low}Fr.F	H2-Aa
0	1.29669175	0	0_IgM^{low}Fr.F	Gimap6
0	1.29468773	0	0_IgM^{low}Fr.F	Cd55
0	1.21031212	0	0_IgM^{low}Fr.F	Gimap3
0	1.21008944	0	0_IgM^{low}Fr.F	H2-Eb1
0	1.90799303	0	1_Fr.E	Ifi30
0	1.64039536	0	1_Fr.E	Ms4a1
0	1.61469502	0	1_Fr.E	Iglc1
0	1.38471871	0	1_Fr.E	Hck
0	1.32084238	0	1_Fr.E	2010309G21Rik
0	1.30328933	0	1_Fr.E	Vpreb3
0	1.24149044	0	1_Fr.E	Fam129c
0	1.16375437	0	1_Fr.E	Spib
0	1.10047177	0	1_Fr.E	Cd79b

0	1.08624885	0	1_Fr.E	Ighv3-8
0	5.14474176	0	1_Fr.E	Hist1h2ap
0	4.17196155	0	1_Fr.E	Hist1h2ae
0	4.15104741	0	2_CD93^{hi}Fr.C	Hist1h1b
0	3.8774254	0	2_CD93^{hi}Fr.C	H2afx
0	3.79740365	0	2_CD93^{hi}Fr.C	Hist1h1a
0	3.67037281	0	2_CD93^{hi}Fr.C	Hist1h1e
0	3.63917906	0	2_CD93^{hi}Fr.C	Hist1h2ao
0	3.56938556	0	2_CD93^{hi}Fr.C	Hist1h1d
0	3.49967468	0	2_CD93^{hi}Fr.C	Tuba1b
0	3.4565066	0	2_CD93^{hi}Fr.C	Hmgb2
0	2.18235873	0	3_Early Fr.E	Myl4
0	2.12424417	0	3_Early Fr.E	Rsph1
0	1.5905008	0	3_Early Fr.E	Cd72
0	1.5627599	0	3_Early Fr.E	Vpreb3
0	1.46495391	0	3_Early Fr.E	Lrmp
0	1.42515155	0	3_Early Fr.E	Cd24a
0	1.25502535	0	3_Early Fr.E	Tmprss3
0	1.2470396	0	3_Early Fr.E	Emid1
0	1.23903091	0	3_Early Fr.E	Chchd10
0	1.20118326	0	3_Early Fr.E	Sox4
0	4.43990524	0	4_Fr.A	Cox6a2
0	4.31802204	0	4_Fr.A	Tyrobp

0	4.17005916	0	4_Fr.A	Bst2
0	4.01859741	0	4_Fr.A	Ly6c2
0	4.01764419	0	4_Fr.A	Siglech
0	3.53829712	0	4_Fr.A	Ctsb
0	3.4342025	0	4_Fr.A	Ctsl
0	3.40428165	0	4_Fr.A	Gm34680
0	3.38457554	0	4_Fr.A	Cd7
0	3.31441937	0	4_Fr.A	Psap
0	3.39420906	0	5_Pax5^{hi}Fr.F	Gm26917
3.46E-248	2.54195361	1.12E-243	5_Pax5^{hi}Fr.F	Maml2
0	2.53014499	0	5_Pax5^{hi}Fr.F	Prkce
0	2.49355386	0	5_Pax5^{hi}Fr.F	Arhgap15
0	2.48791045	0	5_Pax5^{hi}Fr.F	Aff3
1.87E-148	2.42145858	6.05E-144	5_Pax5^{hi}Fr.F	Immp2l
0	2.32686421	0	5_Pax5^{hi}Fr.F	Dock2
0	2.30846954	0	5_Pax5^{hi}Fr.F	Bank1
0	2.25088989	0	5_Pax5^{hi}Fr.F	Runx1
0	2.23780061	0	5_Pax5^{hi}Fr.F	Elmo1
0	2.58798324	0	6_SLC^{hi}Fr.C	Igll1
0	2.43526805	0	6_SLC^{hi}Fr.C	Pclaf
0	2.41944637	0	6_SLC^{hi}Fr.C	Dut
0	2.28478004	0	6_SLC^{hi}Fr.C	Mcm6
0	2.26390621	0	6_SLC^{hi}Fr.C	Vpreb1

0	2.21013486	0	6_SLC^{hi}Fr.C	Hells
0	2.16663107	0	6_SLC^{hi}Fr.C	Mcm3
0	2.14640742	0	6_SLC^{hi}Fr.C	Cdca7
0	2.13804835	0	6_SLC^{hi}Fr.C	Hmgb2
0	2.12561476	0	6_SLC^{hi}Fr.C	H2afz
0	5.40894444	0	7_NK	Ccl5
0	5.02908057	0	7_NK	Gzma
0	4.63131032	0	7_NK	Nkg7
0	4.02888101	0	7_NK	AW112010
0	3.88439749	0	7_NK	Ms4a4b
0	3.61843421	0	7_NK	Il2rb
0	3.53451764	0	7_NK	Ncr1
0	3.34098573	0	7_NK	Klra8
0	3.28212582	0	7_NK	Klra4
0	3.23420058	0	7_NK	Klrb1c
3.02E-126	2.22793009	9.76E-122	8_Ly6a^{hi}Fr.F	Hbb-bs
0	2.01476511	0	8_Ly6a^{hi}Fr.F	Hmox1
0	1.25795866	0	8_Ly6a^{hi}Fr.F	C1qb
1.98E-106	1.23309142	6.40E-102	8_Ly6a^{hi}Fr.F	Apoe
4.62E-34	1.13013801	1.49E-29	8_Ly6a^{hi}Fr.F	Ftl1
0	1.11928638	0	8_Ly6a^{hi}Fr.F	C1qc
1.52E-33	0.91992287	4.92E-29	8_Ly6a^{hi}Fr.F	Grik3
1.20E-41	0.88641695	3.86E-37	8_Ly6a^{hi}Fr.F	Ly6a

1.28E-36	0.86112533	4.12E-32	8_Ly6a^{hi}Fr.F	Selenop
1.35E-57	0.85390704	4.37E-53	8_Ly6a^{hi}Fr.F	Iglc2
2.84E-08	1.19125923	0.00091702	9_IgKc^{hi}MZb1^{hi}Fr.F	Igkc
1.18E-14	1.01150414	3.80E-10	9_IgKc^{hi}MZb1^{hi}Fr.F	S100a6
7.88E-10	0.83687	2.54E-05	9_IgKc^{hi}MZb1^{hi}Fr.F	Mzb1
1.37E-72	0.77396506	4.44E-68	9_IgKc^{hi}MZb1^{hi}Fr.F	Clec2g
2.35E-34	0.72388185	7.57E-30	9_IgKc^{hi}MZb1^{hi}Fr.F	Iglc2
3.85E-56	0.71523531	1.24E-51	9_IgKc^{hi}MZb1^{hi}Fr.F	Gm15987
5.92E-20	0.63389153	1.91E-15	9_IgKc^{hi}MZb1^{hi}Fr.F	Tmtc2
1.89E-47	0.6055345	6.11E-43	9_IgKc^{hi}MZb1^{hi}Fr.F	Iglc1
3.62E-36	0.58045831	1.17E-31	9_IgKc^{hi}MZb1^{hi}Fr.F	Ly6a
4.36E-14	0.55292885	1.41E-09	9_IgKc^{hi}MZb1^{hi}Fr.F	Pdia4
0	4.23035821	0	10_G2/M Fr.C	Ube2c
0	3.40424164	0	10_G2/M Fr.C	Cenpf
9.71E-292	3.23386185	3.13E-287	10_G2/M Fr.C	Tuba1c
0	3.17691771	0	10_G2/M Fr.C	Kpna2
0	2.99959095	0	10_G2/M Fr.C	Cdc20
1.03E-186	2.98810136	3.32E-182	10_G2/M Fr.C	Tubb4b
1.37E-170	2.98079567	4.43E-166	10_G2/M Fr.C	Hmgb2
0	2.89746925	0	10_G2/M Fr.C	Cks2
0	2.8933255	0	10_G2/M Fr.C	Ccnb1
0	2.77740178	0	10_G2/M Fr.C	Cenpa
3.52E-168	2.60852846	1.14E-163	11_Rag1^{hi}Fr.D	Atp1b1

3.13E-101	2.47672198	1.01E-96	11_Rag1^{hi}Fr.D	Dnajc7
3.60E-168	2.28038249	1.16E-163	11_Rag1^{hi}Fr.D	Agbl1
1.74E-101	2.04136925	5.63E-97	11_Rag1^{hi}Fr.D	Coq7
8.37E-98	1.97945717	2.70E-93	11_Rag1^{hi}Fr.D	Arl5c
2.17E-78	1.9708011	6.99E-74	11_Rag1^{hi}Fr.D	Smarca4
1.27E-110	1.8742142	4.11E-106	11_Rag1^{hi}Fr.D	Tifa
1.86E-90	1.87038934	5.99E-86	11_Rag1^{hi}Fr.D	Cecr2
0	1.86265331	0	11_Rag1^{hi}Fr.D	Rag1
8.70E-96	1.84707762	2.81E-91	11_Rag1^{hi}Fr.D	Il7r
2.97E-272	3.43963372	9.58E-268	12_Il7ra^{hi}FrB/FrC	Mki67
1.63E-147	3.42942658	5.27E-143	12_Il7ra^{hi}FrB/FrC	Kcnq5
2.09E-140	3.04569235	6.76E-136	12_Il7ra^{hi}FrB/FrC	Gm26917
1.10E-129	3.0020607	3.55E-125	12_Il7ra^{hi}FrB/FrC	Tmem108
6.92E-265	2.93730142	2.23E-260	12_Il7ra^{hi}FrB/FrC	Gfra1
7.68E-197	2.87512798	2.48E-192	12_Il7ra^{hi}FrB/FrC	Pola1
7.36E-119	2.82695107	2.38E-114	12_Il7ra^{hi}FrB/FrC	Bach2
1.15E-113	2.82463676	3.71E-109	12_Il7ra^{hi}FrB/FrC	Gm42047
0	2.80248492	0	12_Il7ra^{hi}FrB/FrC	Diaph3
3.30E-178	2.71835199	1.06E-173	12_Il7ra^{hi}FrB/FrC	Gm4258
1.57E-12	1.10754957	5.07E-08	13_Mito^{hi}FrF	Zc3h7a
0.00179882	0.92613454	1	13_Mito^{hi}FrF	AY036118
3.99E-25	0.82506258	1.29E-20	13_Mito^{hi}FrF	mt-Co3
7.45E-11	0.82229913	2.41E-06	13_Mito^{hi}FrF	mt-Nd1

2.39E-09	0.75801395	7.70E-05	13_Mito^{hi}FrF	mt-Nd2
8.10E-21	0.74755675	2.62E-16	13_Mito^{hi}FrF	mt-Cytb
0.00024079	0.73320473	1	13_Mito^{hi}FrF	mt-Nd5
9.36E-09	0.69557266	0.00030215	13_Mito^{hi}FrF	mt-Nd4l
3.22E-09	0.67766551	0.00010401	13_Mito^{hi}FrF	mt-Atp8
3.22E-14	0.6584965	1.04E-09	13_Mito^{hi}FrF	mt-Co2
3.94E-244	5.21342275	1.27E-239	14_Tcf4^{hi}Fr.A	Runx2
2.28E-77	4.89290246	7.36E-73	14_Tcf4^{hi}Fr.A	Tcf4
3.39E-85	4.22195641	1.09E-80	14_Tcf4^{hi}Fr.A	Mctp2
1.74E-80	4.09863623	5.63E-76	14_Tcf4^{hi}Fr.A	Rnf220
8.26E-273	4.01562987	2.67E-268	14_Tcf4^{hi}Fr.A	Tex2
0	3.98138069	0	14_Tcf4^{hi}Fr.A	Apba1
0	3.91540298	0	14_Tcf4^{hi}Fr.A	Tbc1d8
2.67E-192	3.89354898	8.63E-188	14_Tcf4^{hi}Fr.A	Slc9a9
3.62E-230	3.85305382	1.17E-225	14_Tcf4^{hi}Fr.A	Phactr2
0	3.77375857	0	14_Tcf4^{hi}Fr.A	Siglech
3.41E-71	9.36832426	1.10E-66	15_GN	S100a8
4.64E-64	9.29278842	1.50E-59	15_GN	S100a9
2.45E-302	7.53578595	7.92E-298	15_GN	Camp
1.58E-298	7.43818685	5.10E-294	15_GN	Ngp
0	6.7431072	0	15_GN	Lyz2
0	5.70523989	0	15_GN	Lcn2
0	5.43905852	0	15_GN	Ltf

0	4.33689817	0	15_GN	Ifitm3
1.17E-31	4.29363784	3.78E-27	15_GN	Wfdc21
0	4.2226922	0	15_GN	Chil3

Appendix table A Top DE genes of each cluster of total B cells in BM mixed chimera sc-RNASeq experiment

P value	Average log2FC	P value adjusted	Cluster	Gene symbol
1.47E-194	0.66028444	4.74E-190	IM0	Ifi30
3.71E-137	0.61029422	1.20E-132	IM0	Fgd2
2.61E-13	0.52977923	8.41E-09	IM0	Lars2
5.14E-213	0.49526037	1.66E-208	IM0	Ms4a1
6.81E-98	0.48849209	2.20E-93	IM0	Hck
1.96E-25	0.45954458	6.34E-21	IM0	Wfdc21
1.02E-42	0.45066283	3.29E-38	IM0	2010309G21Rik
1.71E-127	0.42156117	5.53E-123	IM0	Cd52
1.80E-62	0.38955724	5.81E-58	IM0	Sp140
7.95E-64	0.37355415	2.57E-59	IM0	Pld4
0	1.45857718	0	IM1	Myl4
0	1.38839415	0	IM1	Rsph1
0	1.30951686	0	IM1	Cd72
0	1.26573742	0	IM1	Lrmp
0	1.03480581	0	IM1	Emid1
2.16E-214	0.96063308	6.97E-210	IM1	Nrgn

2.85E-267	0.90416396	9.20E-263	IM1	Tmprss3
0	0.89858052	0	IM1	Vpreb3
1.72E-171	0.87195738	5.55E-167	IM1	Rpgrip1
9.49E-168	0.80413187	3.07E-163	IM1	Cd93
0	1.7445668	0	IM2	Ltb
0	1.56138864	0	IM2	Shisa5
1.05E-155	1.24309332	3.40E-151	IM2	Iglc2
7.59E-131	1.12376356	2.45E-126	IM2	Tagln2
1.15E-262	1.12329296	3.71E-258	IM2	Fcer2a
3.78E-286	1.09524543	1.22E-281	IM2	Sell
2.11E-305	1.09115728	6.82E-301	IM2	Gm15987
0	1.08335083	0	IM2	Ms4a4c
5.49E-160	1.0137971	1.77E-155	IM2	Ly6a
3.54E-199	0.96526622	1.14E-194	IM2	Cd55
5.66E-302	1.53268888	1.83E-297	IM3	Stat1
1.52E-261	1.40436722	4.92E-257	IM3	Trim30a
0	1.34408967	0	IM3	Rtp4
5.83E-190	1.28885763	1.88E-185	IM3	Ifi27l2a
6.72E-191	1.16412228	2.17E-186	IM3	Ifi47
2.00E-168	1.16347553	6.46E-164	IM3	Bst2
1.43E-184	1.11911431	4.60E-180	IM3	Slfn2
5.06E-190	1.08744965	1.63E-185	IM3	Tor3a
4.63E-169	1.08712928	1.49E-164	IM3	Rnf213

3.73E-193	1.07244317	1.20E-188	IM3	Phf11b
3.99E-176	3.46112443	1.29E-171	IM4	Hmgb2
0	2.73499352	0	IM4	Hmgn2
1.12E-253	2.52581911	3.63E-249	IM4	H2afz
5.23E-238	2.14943936	1.69E-233	IM4	Hmgb1
0	2.13834966	0	IM4	Ccnb2
0	2.11733892	0	IM4	Mki67
2.31E-293	2.01876642	7.45E-289	IM4	Hist1h2bc
5.58E-228	1.99059321	1.80E-223	IM4	Myl4
6.13E-217	1.84380823	1.98E-212	IM4	Cenpa
4.10E-184	1.83505189	1.32E-179	IM4	Lgals1
1.17E-12	3.93335561	3.79E-08	IM5	Iglv1
2.04E-182	2.7588911	6.60E-178	IM5	Atp1b1
1.52E-84	2.03742616	4.90E-80	IM5	Dnajc7
2.51E-72	1.9261378	8.10E-68	IM5	Agbl1
0	1.84250735	0	IM5	Rag1
1.88E-102	1.8369542	6.07E-98	IM5	Il7r
3.84E-59	1.81130135	1.24E-54	IM5	Smarca4
1.23E-61	1.65821204	3.97E-57	IM5	Coq7
2.57E-57	1.61347516	8.30E-53	IM5	Cecr2
4.10E-60	1.59993873	1.33E-55	IM5	Xrcc6
2.71E-64	3.40438276	8.75E-60	IM6	S100a6
3.10E-157	2.96127823	1.00E-152	IM6	Ly6a

0	2.21982061	0	IM6	Gimap4
6.40E-83	2.20161008	2.06E-78	IM6	Iglc2
1.05E-67	2.1952715	3.38E-63	IM6	Man1a
2.56E-118	1.91815849	8.26E-114	IM6	Apoe
7.98E-53	1.80371044	2.58E-48	IM6	Inpp4b
1.54E-50	1.78531319	4.97E-46	IM6	Gm15987
3.01E-103	1.73399633	9.72E-99	IM6	Gimap3
7.32E-104	1.66169532	2.36E-99	IM6	Fxyd5
0	6.9558975	0	IM7	Jchain
1.85E-83	6.92287293	5.96E-79	IM7	Igha
9.35E-06	2.52284076	0.30174008	IM7	Igkc
4.72E-10	2.03393198	1.52E-05	IM7	Mzb1
1.35E-06	1.90796395	0.04350443	IM7	Hsp90b1
4.45E-16	1.86636697	1.44E-11	IM7	Creld2
3.05E-15	1.76027252	9.84E-11	IM7	Iglc2
8.48E-08	1.70364033	0.00273769	IM7	Iglv1
1.87E-05	1.67651596	0.60250264	IM7	Ssr4
9.60E-12	1.66743676	3.10E-07	IM7	Rexo2
5.64E-24	3.24560035	1.82E-19	IM8	Gm42047
3.53E-16	2.07501077	1.14E-11	IM8	Bax
0.00014702	2.01394069	1	IM8	Fcer2a
6.01E-16	2.00032744	1.94E-11	IM8	Ccng1
5.73E-117	1.84285195	1.85E-112	IM8	Pvt1

0	1.80851446	0	IM8	Phlda3
4.46E-09	1.76185852	0.00014389	IM8	Gm15987
4.62E-12	1.72377047	1.49E-07	IM8	Clec2g
8.22E-12	1.7165307	2.65E-07	IM8	Rps27l
1.42E-45	1.67174174	4.57E-41	IM8	Snhg15

Appendix table B Top DE genes of each cluster within immature B cells in BM mixed chimera sc-RNASeq experiment

P value	Average log2FC	P value adjusted	Cluster	Gene symbol
0	0.64644615	0	M0	Rps24
0	0.64311287	0	M0	Uba52
0	0.63099346	0	M0	Rps27
0	0.62235838	0	M0	Rps15a
0	0.62211075	0	M0	Fau
0	0.61959992	0	M0	Rpl18a
8.20E-246	0.61918444	2.65E-241	M0	Iglc3
0	0.61784483	0	M0	Rps16
5.51E-303	0.61379344	1.78E-298	M0	Rpl9-ps6
7.14E-307	0.6089619	2.31E-302	M0	Rpl36
0	2.14384597	0	M1	Tagln2
0	2.0694449	0	M1	Vim
0	1.51217537	0	M1	Myadm
2.52E-277	1.26470181	8.13E-273	M1	Ahnak

1.50E-206	1.15906249	4.84E-202	M1	Adgre5
7.76E-261	1.14248477	2.51E-256	M1	Jund
2.92E-141	0.97004537	9.43E-137	M1	Cd2
2.84E-161	0.9600032	9.16E-157	M1	Stt3b
6.63E-123	0.8838276	2.14E-118	M1	Cd69
3.03E-81	0.85362383	9.77E-77	M1	Emp3
3.23E-223	3.30517418	1.04E-218	M2	Gm26917
5.34E-194	2.40395326	1.73E-189	M2	Maml2
2.19E-128	2.23360449	7.07E-124	M2	Immp2l
6.98E-186	2.20569419	2.25E-181	M2	Lncpint
0	2.15276978	0	M2	Aff3
0	2.1436026	0	M2	Arhgap15
1.38E-225	2.08822895	4.45E-221	M2	Prkce
9.07E-283	2.07509244	2.93E-278	M2	Dock2
3.41E-204	2.03587248	1.10E-199	M2	Runx1
7.87E-214	2.01284113	2.54E-209	M2	Elmo1
6.53E-142	2.17153846	2.11E-137	M3	Ifi27l2a
2.88E-118	1.68674145	9.29E-114	M3	Stat1
0	1.66082669	0	M3	Rtp4
2.70E-256	1.5789153	8.71E-252	M3	Irf7
4.55E-93	1.41792058	1.47E-88	M3	Ifi47
1.41E-128	1.41339055	4.57E-124	M3	Slfn5
9.23E-155	1.34888709	2.98E-150	M3	Ifi208

5.32E-76	1.33086437	1.72E-71	M3	Bst2
2.88E-138	1.3291636	9.30E-134	M3	Isg15
1.61E-86	1.29772761	5.20E-82	M3	Trim30a
1.71E-206	3.28226323	5.52E-202	M4	Hdac9
1.66E-240	3.13052596	5.36E-236	M4	Zeb2
3.07E-263	3.08913036	9.92E-259	M4	Fhit
1.09E-233	3.08432156	3.51E-229	M4	Cux1
6.38E-182	2.84578189	2.06E-177	M4	Ebf1
3.16E-186	2.71449969	1.02E-181	M4	Ptprj
8.69E-175	2.70140092	2.81E-170	M4	Bach2
2.42E-196	2.68234217	7.82E-192	M4	Sox5
8.54E-261	2.62964673	2.76E-256	M4	Ppm1e
1.18E-160	2.6158391	3.81E-156	M4	Prkce
0	2.19002063	0	M5	Hmox1
7.19E-66	1.61756671	2.32E-61	M5	Ftl1
0	1.56221803	0	M5	C1qb
1.38E-55	1.42171108	4.47E-51	M5	Ctsb
0	1.40845604	0	M5	C1qc
1.27E-44	1.36265716	4.10E-40	M5	Grik3
0	1.33785652	0	M5	Vcam1
1.49E-59	1.26028489	4.80E-55	M5	Ctsd
1.75E-83	1.23738856	5.66E-79	M5	Selenop
0	1.211883	0	M5	C1qa

6.36E-63	2.38458753	2.05E-58	M6	S100a6
2.41E-49	1.63720647	7.78E-45	M6	Apoe
1.27E-40	1.12895131	4.11E-36	M6	Plac8
3.57E-77	1.12309353	1.15E-72	M6	Sox5
6.41E-193	1.08295485	2.07E-188	M6	Ptpn22
8.85E-87	1.01832945	2.86E-82	M6	Cacna1e
1.96E-104	0.97648299	6.33E-100	M6	Atxn1
4.22E-36	0.92219931	1.36E-31	M6	Nfatc1
3.83E-251	0.87981582	1.24E-246	M6	Cd9
0	0.85356332	0	M6	Nid1
8.00E-37	1.27557039	2.58E-32	M7	Vpreb3
2.50E-48	1.23858166	8.08E-44	M7	Cd24a
4.31E-53	1.21436472	1.39E-48	M7	Ifi30
1.64E-96	1.08693425	5.31E-92	M7	Fam129c
3.39E-27	0.96202574	1.09E-22	M7	Ifi27l2a
2.59E-38	0.96199569	8.37E-34	M7	Plac8
2.51E-42	0.94035069	8.10E-38	M7	Iglc1
3.34E-43	0.89192808	1.08E-38	M7	Ucp2
1.54E-48	0.86436072	4.96E-44	M7	Ms4a1
4.42E-239	0.85006914	1.43E-234	M7	Wfdc21
0	3.7375449	0	M8	Hbb-bs
0	2.90890426	0	M8	Hbb-bt
0	1.98015087	0	M8	Hba-a1

1.26E-05	0.47776753	0.40764196	M8	Atpif1
0.00422983	0.40358067	1	M8	Blvrb
0.00020684	0.38049336	1	M8	Scp2
3.73E-05	0.34476977	1	M8	Gpx4
0.00019546	0.3076983	1	M8	Ran
0.00080354	0.3026211	1	M8	Tuba1b
0.00127481	0.29719104	1	M8	BC028528
6.72E-51	3.07411002	2.17E-46	M9	Hist1h2ap
3.16E-106	2.78558241	1.02E-101	M9	Hist1h2af
1.21E-85	2.40460037	3.90E-81	M9	Mki67
3.24E-23	2.29982226	1.05E-18	M9	Hist1h1e
2.36E-25	2.29689542	7.61E-21	M9	Hmgb2
5.43E-33	2.2502807	1.75E-28	M9	Hist1h2ab
3.72E-34	2.23446331	1.20E-29	M9	Hist1h1b
6.64E-29	2.18576807	2.14E-24	M9	Hist1h1d
3.05E-69	2.13512382	9.86E-65	M9	Top2a
5.97E-19	1.86153883	1.93E-14	M9	Hist1h1c
8.01E-81	7.111428	2.58E-76	M10	Igha
0	6.87500615	0	M10	Jchain
1.74E-15	3.52300338	5.62E-11	M10	Igkc
5.53E-35	2.88858357	1.79E-30	M10	Iglv1
2.92E-08	2.5212893	0.0009439	M10	Hsp90b1
4.30E-06	2.32182349	0.1387237	M10	Mzb1

5.93E-12	1.96348666	1.92E-07	M10	Xbp1
7.99E-17	1.93935404	2.58E-12	M10	Creld2
0.00027143	1.80837298	1	M10	Manf
0.00023593	1.79231257	1	M10	Ssr4

Appendix table C Top DE genes of each cluster within mature B cells in BM mixed chimera sc-RNASeq experiment